

## **APPENDIX D**

### **TESTING AT WILMINGTON, NORTH CAROLINA**

#### **INTRODUCTION**

The project on which the NCHRP pile group was tested consisted of a design phase foundation load test program for a planned new bridge over the Northeast Cape Fear River on US 17 in Wilmington, North Carolina. A primary objective of the program was lateral load testing since the design of future bridge foundations is heavily influenced by lateral loading. Both conventional static load tests as well as Statnamic lateral load tests were performed as part of the program, both on individual steel pipe piles and on a group of 12 steel pipe piles. The NCHRP pipe piles (13 total) had an external diameter of 273 mm and a wall thickness of 15 mm, were closed at the ends and had a nominal length of 12.2 meters. All 13 piles had been previously instrumented with strain gauges, six with 14 gauges each and the rest with 6 gauges each.

The testing program was divided into two geographic areas designated as Test Area 1 and Test Area 2. Test Area 1 was located toward the west side of the Cape Fear River and has been referred to as the Ratt Island location. Test Area 2 was located on the east side of the Cape Fear River. A total of four Statnamic tests, each at increasing load amplitudes, were carried out on the group of 12 piles at both test areas. In addition, a static lateral load test was carried out on the 12 pile group at Test Area 1 (Ratt Island), and static lateral tests were also carried out on single piles at both locations.

## SOIL CONDITIONS

The geotechnical exploration at the site was performed by the North Carolina Department of Transportation. Figure D-1 and Figure D-2 represent subsurface conditions at Test Areas 1 and 2, respectively. The soil profile at Test Area 1 (Ratt Island) consists of an upper 2.5 meters of soft organic clay underlain by a 7.5-meter-thick layer of alluvial, loose sandy silts and silty sands. Beneath this layer was a thin layer of very soft alluvial clay just above the top of a dense silty sand comprising a formation known locally as the "Peedee Formation." The test piles were entirely within the organic clay and alluvial sand. Standard penetration test values in the upper 6 meters were generally 0, with 11 to 12 blows per 30 cm (bpf) in the lower portions of the alluvial sand. Cone penetration (CPT) tip resistance in the organic clay was close to 0 (at the lower limit of the instrument), around 3 to 5 MPa in the 3 to 7 m depth range, and above 10 MPa below 7 m. Some pressuremeter tests (PMT) were performed at this location, and these data indicate a modulus of deformation of around 2 to 3 MPa in the upper 2.5 m, around 20 MPa for the alluvial sand at the 3 to 5 m depths, and around 60 MPa for the lower portion of the alluvial sand.

Subsurface conditions at Test Area 2 (east side of river) consisted of 2 meters of water depth at high tide and 0.3 to 0.6 meters of depth at low tide. The upper 13.5 meters consisted of alluvial loose silty sands and loose to dense sands. The top of the Peedee Formation was encountered around elevation -15.5 meters. The piles were entirely within the alluvial sands. These sands had SPT values of 0 to 4 blows per 30 cm (bpf) in the -2 m to -7 m elevation range, and in the range of 10 to 20 blows per 30 cm (bpf) below. CPT tip resistance was less than 1 MPa above elevation -6 m and rose steadily to a value of around 15 MPa at a depth of around -9 m. PMT modulus was 3 to 4 MPa in the 5 tests performed above elevation -7 m, increasing to around 65 MPa at elevation -9 m.

Dilatometer modulus values ranged from 1 to 10 MPa above elevation -7 m, and ranged from 50 to 130 MPa below.

## **FOUNDATION INSTRUMENTATION**

The instrumentation scheme was designed to obtain very specific information from the test program. This section briefly describes the equipment used to measure response, while specific details as to instrumentation setup on a test by test basis are described later.

### **Strain Gauges**

Each of the 13 pipe piles was instrumented with full bridge strain gauges positioned in pairs on opposite faces of the inside of the piles at various depths. Piles marked 1 through 7 were instrumented at 3 levels (6 gauges total), at depths of 2.591, 3.048 and 3.962 meters (8.5, 10 and 13 feet) from the top of the piles. Piles marked 8 through 13 had additional strain gauge pairs at depths of 4.877, 5.791, 6.706 and 7.620 meters (16, 19, 22 and 25 feet) from the pile top (head) for a total of 14 strain gauges per pile.

### **External Accelerometers**

Piezoelectric ICP<sup>®</sup> type accelerometers manufactured by PCB Piezotronics were mounted on the steel frame built around the pile group using magnetic mounting bases. The accelerometers were used primarily to augment LVDT deflection data, to measure rocking and torsion in the cap, and also to provide a means of estimating inertial forces developed in the system during Statnamic testing.

### **Linear Potentiometers**

These have also been referred to loosely as LVDTs. These are resistance-based mechanical displacement measuring devices with 300 mm (12 inches) of travel. The linear potentiometers were used to measure the displacement response of the system during both static and dynamic loading.

## **Load Cells**

Various load cells were used during the testing sequence. The load cells use resistance-based strain gauges to respond to a fast load application. A Geokon 4.5 MN capacity cell was used for all static load testing as well as Statnamic testing on the NCHRP pile group.

## **Hydraulic Jack**

A 1.785 MN capacity double acting jack was used for all static testing. The maximum stroke was 1.34 meters with a safe limit of 1.0 meters (to avoid of possible damage due to bending). The jack was manufactured by Elgood-Mayo Corporation of Lancaster, Pennsylvania.

## **Megadac Data Acquisition System**

The system is manufactured by Optim, Inc. The core consists of the primary data acquisition module (ADC-5616) which can be supplemented by additional expansion modules. Plug-in types of analog to digital data cards (AD-808FB1) were used with this system to monitor various analog devices. The ADC-5616 module allows sampling at the desired rate of 1.0 to 2.0 KHz for Statnamic tests. For static tests, data were typically sampled at 2 to 10 second intervals for the duration of the test. The Megadac system was controlled by a laptop computer using the Test Control Software (TCS) and an IEEE-488 data interface. Test data saved by TCS were exported to various formats like ASCII and Matlab for further analysis.

## **STATNAMIC LOAD TESTING**

The Statnamic load test provides a method for generating large axial or lateral loads on foundations by "launching" a heavy reaction mass away from the foundation at an acceleration approaching 20 g's. Figure D-3 illustrates the test setup. The energy for the test is generated by



burning special fuel pellets in a combustion chamber inside the Statnamic device, and allowing the resulting high pressure gas to vent at a controlled rate, which in turn controls the rate at which the foundation is loaded. The reaction mass is initially set up against the side of the foundation and imparts a load that ramps up to its maximum value in a finite amount of time, usually between 0.1 and 0.3 seconds, and then gradually decreases as the mass is propelled away from the foundation and physical contact between the foundation and the reaction mass ceases. The load is not a sharp impact, but is similar to the case where a moving barge might impact a bridge foundation, even though the ramp time for the latter case may be several times larger depending on the mass of the barge and the speed at which it was moving. The primary advantages of the Statnamic test are that it is quick, it provides energy in a frequency band close to the fundamental frequency of the foundation, and it produces significant inertial forces in the system, which allows the determination of dynamic system properties. The Statnamic testing system is manufactured by Berminghammer Foundation Equipment of Hamilton, Ontario.

## **INSTALLATION OF THE NCHRP PILES**

The NCHRP pipe piles were driven to toe penetrations of 9.4 m at Test Area 1 and 8.2 m at Test Area 2 by the McLean Contracting Company using a Delmag model D22 open-end diesel impact hammer. While installing the pile group the two middle piles (innermost) were driven first, then the two middle rows. The middle part of the frame was then tightened around the two middle rows, and this was followed by the driving of the two outer rows and the tightening of the rest of the frame around the entire group. For the most part, the piles were installed by dry firing the hammer, while only the last meter or two of penetration required that the hammer actually be run. Driving records were not kept since the installation objective was to achieve the specified penetration only.

At Test Area 1 (Ratt Island) the blow count needed was about 20 blows per meter for the last 2 meters, while it took between 10 and 15 blows for the piles to achieve their last 1 meter of penetration at Test Area 2 (east side of river).

### **STATIC TEST ON PILE GROUP, TEST AREA 1 (RATT ISLAND)**

The static load test was carried out by pulling the NCHRP pile group and a group of nearby drilled shafts towards each other using steel cables and a hydraulic jack. The load cell, displacement transducers and strain gauges were monitored using the Megadac data acquisition system, recording a total of 144 channels, which included the strain gauges in the 2 drilled shafts reactions (not discussed in this report). The test took approximately 93 minutes to complete. 560 data points per channel were recorded with a sampling period of 10.010 seconds.

The NCHRP pile group included a total of 12 piles, arrayed in 4 rows of 3 piles each, 7 of which were instrumented with 6 strain gauges while 5 were instrumented with 14 strain gauges. The piles were spaced 0.819 meters apart (3 diameters), center to center, both laterally and along the direction of loading, and were structurally connected together using a steel framework that served as the cap for the group. The elevations at the top of the piles and the base of the frame were approximately 2.79 meters and 1.07 meters, respectively, above the ground surface. Figure D-4 is a schematic diagram illustrating the layout of individual piles in the group as well as the displacement transducers and the accelerometers, the latter being used during the Statnamic tests only. Figure D-5 shows the elevation of a single pile on the trailing row, and indicates the levels of attachment of the frame to the pile (load points) and the placement of the LVDTs.

### **Generalized Displacement Response**

A total of 4 horizontally aligned displacement transducers were used to record the lateral

movement of the frame. The transducers were placed at the 4 corners in a grid pattern, which enabled the measurement of the rocking and torsional movement as well. Figure D-6 is a plot of the load vs mean displacement (average of the 4 transducers). The foundation group was loaded to a maximum load of 1064 kN, which resulted in a total lateral displacement of just under 140 mm. The maximum load was achieved using 13 load steps, and the load was then allowed to return to zero using 2 steps. The load jack was seen to relax slightly after the initial load was achieved at each step, and the foundation was also seen to creep slightly between successive load steps. The foundation exhibited a permanent or plastic set of 52 mm when the load was released fully. In addition to the lateral displacement, the rotational movement of the pile frame was also monitored. Rocking (rotation of the frame in the vertical plane of loading) was computed as the difference in lateral movement between 2 transducers along a vertical line divided by the distance between them. Two measures for rocking rotation were thus obtained, along the north and south edges of the frame. Figure D-7 shows the mean rocking rotation (average of the 2 edges) of the frame as a function of applied load. The maximum recorded mean rocking was seen to be 0.0119 rad, with the upper edge of the frame being the leading edge. Figure D-7 also includes the plot showing the load vs. torsional movement (yaw) of the frame. Torsional movement is defined as the rotation of the frame about a vertical axis. Torsional movement was computed at the top and bottom edges by taking the difference in the transducer readings and dividing by the horizontal distance between them. The maximum torsion recorded was 0.0019 rad, anticlockwise when looking down on the frame from above. Finally, Figure D-8 is a plot of the individual response histories indicated by the 4 displacement transducers. Gauges 92 and 95 located at the top of the frame indicated greater displacements than gauges 87 and 86 located along the bottom which shows that the upper edge of the frame was the leading edge.

## Strains, Bending Moments, and Load Distribution

A total of 112 strain gauges were used to monitor strains in the 12 piles. Piles 8 through 12 were fully instrumented with 14 gauges each, 7 along each face at the following depths: 2591, 3048, 3962, 4877, 5791, 6706, and 7620 mm from the top of the pile (8.5, 10, 13, 16, 19, 22, and 25 ft), while Piles 1 through 7 were instrumented with 6 gauges each, 3 along each face at depths of 2591, 3048 and 3962 mm (8.5, 10, and 13 ft) from the pile top. The distance from the top of the pile to the base of the frame was 1.73 m. Therefore, the top gauge level was above the mudline at a distance of 0.86 m below the bottom of the frame. Bending moments and axial forces in each pile were derived at each time step using the following formulas, after the strain data had been corrected using the calibration factors presented in Appendix F:

$$Ax = AE(s1 + s2)/2 \quad , \quad \text{and}$$

$$Bm = EI(s1 - s2)/(2y) \quad ,$$

where

$Ax$  = axial load at a particular depth at a particular load/time step,

$Bm$  = bending moment at that depth at that time step,

$A$  = pile cross sectional area = 0.0103875 m<sup>2</sup>,

$E$  = modulus of elasticity of pile material = 1.9996E+08 kPa,

$I$  = moment of inertia of pile cross section = 8.8214E+07 mm<sup>4</sup>,

$s1, s2$  = strains indicated by the gauges on opposite faces at a given depth, and

$y$  = distance from centroidal axis of the pile to the centerline of the gauge = 111.125 mm.

The axial load was thus based on the mean axial strain in the pile, while the bending moment was based on the difference of the 2 strain gauge readings. The Matlab software was used to process the strain data in a batch mode, and several programs ("m" files) were written using the Matlab

programming language specifically for this task. Matlab was also used to prepare, display and annotate all the graphics for presentation in this report.

All in all, the strain gauges appeared to provide excellent data, although a few gauges did not function reliably. Those that did not appear to record a reliable signal were assigned values estimated from the records of the gauges above and below them. The estimates were checked by deriving axial load and bending moment profiles (as a function of depth at specific times) and studying these to see if they appeared reasonable. The bending moment time history was analyzed for each pile at each gauge location.

Figure D-9 gives the measured bending moment response of Pile 11 at all 7 gauge levels (1 through 7 from top to bottom), presented here as an example. The maximum values of bending moment for each of the 5 fully instrumented piles is presented in Table D-1. The second column in the table refers to the maximum value of bending moment measured below the ground surface, while column 3 indicates the gauge level from the top of the pile at which this moment was measured. The fourth column indicates the maximum value of moment at the bottom load point (1.73 m from pile top) where the frame was connected to the piles. This moment was derived by extrapolating the linear top portion of the moment vs. depth relationship for each pile at the instant of peak load. In most cases the absolute maximum moment in the pile was seen to occur at the base of the frame (negative moment). It is also interesting to note that the peak subsurface moments recorded for the lead piles (8 and 9) occurred at a shallower depth than the corresponding peak moments for the trailing piles (10, 11 and 12).

Each of the 12 piles was further analyzed to provide bending moment as a function of depth along the pile at different values of time/load. Figure D-10 through Figure D-14 are plots of bending moment vs depth for Piles 8 through 12, respectively. Each figure presents 2 "time slices," the first



at 2192 seconds when the applied load was 570 kN, and the second at 4045 seconds when the applied load was at its peak value of 1064 kN. Each bending moment point on the graph is actually the average of 11 points spaced equally about the time of interest. This averaging was done to negate the effects of spurious variations in the digitized data from point to point which can sometimes occur with digital sampling.

The bending moment vs. depth relationship was also used to derive the shear at the pile head at these 2 points in time. The shear force at the pile head was computed as the slope of the initial portion of the bending moment curve ( $dM/dZ$ ). This allows a study of the load distribution among all of the piles in the group. Table D-2 shows the distribution of pile-head shear at loads of 570 and 1064 kN obtained in this way.

Figure D-15 illustrates the head shear distribution profile graphically. It plots the distribution on a pile by pile basis as well as on a row by row basis. The leading row (bottommost) carries the maximum shear (about 29 %), rows 2 and 3 carry progressively less (about 25 % and 21 %, respectively), while the shear in the trailing row (number 4) increases again to about 25 % and carries more shear load than row 3. It is also interesting to note that the percent distribution of load remains practically the same at both 570 and 1064 kN, with the individual rows carrying shear proportionally.

A study of the load transfer diagram also reveals that Piles 1, 4 and 6 (rows 1, 2 and 3, right hand side) carry significantly lower shear than their counterparts on the left hand side (5, 3 and 2, respectively). It is not known exactly why this happened, but it appears to be related to a significant variation in soil properties between the left and the right sides of the pile group. This discrepancy in shear transfer between the 2 sides is also evident from an analysis of the Statnamic test results on the same group, which show a similar skewed resistance pattern (discussed in a later section).

There is a discrepancy between the applied load and the sum of all the pile head shears in the

group. At an applied load of 570 kN the total computed pile head shear is 334 kN, while at a load of 1064 kN the sum is 654 kN. This appears to be beyond the scope of simple round-off errors and appears in spite of the raw strain readings having been corrected prior to extracting bending moment profiles. It should be noted that the computation of pile-head shear is very subjective (done graphically by hand), and the slope of the line chosen to represent the load transferred to a pile is extremely sensitive to the smallest variation in choosing the end points for the line. In fact, the slope of the line chosen to represent the best fit may vary by as much as 30 % and still be considered reasonable. Figure D-16 presents the bending moment profile for Pile 10 at a load of 1064 kN. Two estimates for the shear load transferred to Pile 10 have been shown. Fit 1 indicates a slope of 70.1 kN (kN-m/m), as reported in Figure D-15, while Fit 2, which graphically appears very similar to Fit 1, indicates a slope of 92.5 kN, which is 29 % larger than Fit 1. Since the resolution of points on the bending moment profile is limited by the number of strain gauges used and their spacing, it is hard to tell just from the Figure which fit is best. However, based on the knowledge that the sum of all pile head shears must equal the total applied load, it appears that Fit 2 may be more reasonable in this particular case. It is noted that Fit 1 was used in deriving the values in Table D-2. In conclusion, it must be said that with the current spacing of strain gauges the accuracy with which the loads transferred to individual piles may be determined is suspect. However, if one were to be consistent in the approach to determining the best fit line, the relative proportions of load transferred to every pile would remain the same and provide an accurate picture of the distribution of load through the group.

#### **STATNOMIC TEST ON PILE GROUP, TEST AREA 1 (RATT ISLAND)**

A total of 4 Statnamic tests at increasing load levels, with a lapse of about one hour between

each Statnamic load application, were conducted on the pile group at the Ratt Island location. Each test recorded a total of 121 channels of data sampled at a rate of 2000 Hz. The test included the following instrumentation:

- 1 Load Cell,
- 4 Displacement Transducers (LVDTs),
- 112 Strain Gauges, and
- 4 Accelerometers.

The instrumentation layout has been discussed in an earlier section of this appendix dealing with the static load test on the pile group at Test Area 1 (Figure D-4). The only difference is the fact that 4 accelerometers were added to the receiver array, which were not needed for the static test. The load time histories for all 4 tests have been plotted in Figure D-17. The peak values of load achieved for tests 1 through 4 are 323, 513, 874 and 1209 kN, respectively. The loading impulse ranged between 0.15 and 0.30 seconds, with the bigger loads ramping up faster. The post-event load signals are also cleaner than the corresponding load signals recorded at Test Area 2.

### **Generalized Displacement Response**

As before, the lateral displacement response was monitored at each of the 4 corners of the pile group frame using linear potentiometers. The mean lateral displacement response for all the tests have been plotted in Figure D-18, while Figures D-19 and D-20 present the mean rocking and torsional rotation response time histories. A summary of the results is presented in Table D-3.

The pile group exhibited substantially higher stiffness at this location compared to the Statnamic tests conducted at Test Area 2. This is evident when one compares the damped frequency of oscillation exhibited at the 2 sites. The pile group at the east side location (Test Area 2) was founded in deep water, while in this case (Test Area 1) the group was founded on land; hence, the

piles were able to achieve significantly higher lateral resistance. The peak lateral displacements ranged from 28 to 108 mm, while the mean plastic set increased from 6.1 to 11.1 mm from the first test to the last. The period of oscillation was also seen to increase from 0.28 to 0.35 seconds with increasing load levels and increasing nonlinearity in the system. Another interesting fact can be noted when the displacement time histories are studied in detail. The amplitude of oscillation decreases in a roughly exponential fashion from the start to about 1.5 seconds, but the decay pattern changes slightly beyond this time, indicating that the reference beams from which the displacement transducers were mounted were effected by the shock wave propagating through the earth as a result of the Statnamic event. This adds a small spurious component to the signal and has to be taken into account when trying to back calculate system properties such as damping ratio.

Note also that the stiffness and permanent set of the initial test load, and perhaps even the second test load, is likely to have been affected by the prior static loading in the opposite direction.

### **Strains, Bending Moments and Load Distribution**

A total of 112 strain gauges were monitored for the tests, and most of the gauges appeared to work well. After the strain signals had been corrected using the derived calibration factors, the bending moment and axial load time histories were extracted using Matlab routines. Figure D-21 is the bending moment response of Pile 11 at all 7 gauge levels (1 through 7 from top to bottom), presented here as a representative sample.

The maximum values of bending moment for each of the 5 fully instrumented piles are presented in Table D-4. The second column in Table D-4 shows the maximum subsurface bending moment recorded for each pile at the gauge level specified in column 3. Column 4 shows the estimated moment at the base of the frame computed by extrapolation of the initial linear part of the measured moment vs. depth function at peak load.

The 12 piles were further analyzed to provide bending moment as a function of depth. Figures D-22, D-23, D-24 and D-25 describe the bending moment profiles for Piles 8 through 12 for tests 1, 2, 3 and 4 respectively. The times at which the profiles are plotted correspond to times at which the bending moment reached its peak value:

Test 1 - 0.613 seconds

Test 2 - 0.587 seconds

Test 3 - 0.549 seconds

Test 4 - 0.539 seconds

It is noted that peak bending moments do not as a rule occur at the same instant for all the piles, there is usually a small phase difference for peak response from pile to pile. As before, every point on each of the graphs representing a bending moment value is actually the average of 11 points spaced equally about the time of interest.

Shear load distribution to individual piles was also derived for each Statnamic test at the times specified. Table D-5 shows the actual distribution of pile head shear at these points in time. Figure D-26 shows the load distribution profile graphically. Rows are numbered 1 through 4, top to bottom, with row 1 being the leading row in this case. Just as for the load distribution profile for the static load test conducted on the same pile group (Figure D-15), Piles 1, 4 and 6 carry significantly lower load than their counterparts on the left hand side, namely, Piles 5, 3 and 2 respectively. The load distribution to the rows is also strikingly similar to that seen for the Static Load Test. The leading row (row 1) carries the highest proportion of the load (between 32 and 33 %, which is more than that carried by the leading row for the Static Test, which was seen to be about 28 - 29 %), rows 2 and 3 carry substantially lower proportions, while the load carried by the trailing row (row 4, bottommost) is a little more than that carried by row 3. It should be noted that the static load test and



the Statnamic tests loaded the pile group in opposite directions.

### **Pile-Head Acceleration Response**

The acceleration response was monitored using 4 accelerometers, 3 of which were aligned horizontally to record the lateral response of the group, while one was aligned vertically to record the axial response. The signals recorded were clean and relatively noise free for tests 1, 2 and 3, while 2 of the accelerometers failed to respond correctly during test 4. Table D-6 summarizes the acceleration results.

The peak average acceleration was computed for each test by averaging the 3 lateral acceleration signals except for test 4, where only one lateral channel was available. Time refers to the time at which the peak response was recorded (averaged signals). The primary frequency of oscillation was determined by computing the discrete Fourier Transform of the averaged lateral acceleration response. Figure D-27 plots the averaged lateral acceleration time history for test 1 along with the magnitude part of its Fourier Transform.

### **STATNAMIC TEST ON PILE GROUP - TEST AREA 2 (EAST SIDE OF RIVER)**

A series of 4 Statnamic tests, with approximately a one-hour delay between tests, was conducted on the pile group located on the east bank of the river. 121 channels of data were recorded during each test at a sampling rate of 2000 Hz. The test included the following instrumentation:

- 1 Load Cell.
- 4 Displacement Transducers (LVDTs),
- 112 Strain Gauges, and
- 4 Accelerometers.

The instrumentation layout is described in Figure D-28, while the elevation of a single pile

on the trailing row is shown in Figure D-29. Due to a connection problem at the load cell, the load time history could not be monitored for the first test. The problem was rectified for the next 3 tests by using a different load cell. The load time histories for tests 2, 3 and 4 are presented in Figure D-30. Maximum loads achieved were 216, 334 and 488 kN respectively. The times of the loading events ranged between 0.2 and 0.4 seconds, with the higher loads ramping up faster. Some of the traces also indicate some post-event oscillations felt by the load cell, possibly as a result of the movement of the frame system used to support the piston part of the Statnamic device.

### **Generalized Displacement Response**

As in the case of the static pull test, displacements were monitored at each of the 4 corners of the pile group frame, which enabled the determination of lateral translation as well as rocking and torsional rotations. The signals from the 4 displacement transducers were averaged to give the mean lateral displacement response, which have been shown in Figure D-31 (tests 3 and 4). Figure D-32 shows the mean rocking and torsional rotation time histories for the same tests. A summary of the results for Test Area 2 is provided in Table D-7, which also provides the damped frequency of oscillation of the system (post-load, free vibration part). The damped natural frequency was obtained by computing the Discrete Fourier Transform (DFT) of the mean displacement time histories and plotting the magnitude parts of the signal vs. frequency. The period of oscillation (reciprocal of frequency) is seen to elongate with increasing levels of load. This behavior is expected, as the degree of nonlinearity increases with increasing load and displacement levels. The mean set refers to the average plastic deformation recorded by each displacement transducer at the end of the test and is computed as the difference in displacement values at the beginning and end of the signals.

Note that the rocking rotations are much larger than at Test Area 1, undoubtedly due to the larger clear distance to the mudline. The large permanent rotation after load 4 may suggest that some

piles had permanent axial displacements.

### **Strains, Bending Moments, and Load Distribution**

A total of 112 strain gauges were monitored during the test. These included 5 fully instrumented piles (8 through 12) with 14 gauges each, and 7 partially instrumented piles (1 through 7) with 6 gauges each. The bending moment and axial load time histories were extracted using Matlab, as described in a previous section of the report (static pull test). Other than Pile 3, where 3 of the 6 gauges did not work (possibly due to faulty connections at the STB terminal block), the results obtained from the strain gauge data appear to be good. Figure D-33 is the bending moment response of Pile 11 at all 7 gauge levels (1 through 7 from top to bottom), presented here as a representative example. The maximum values of bending moment (below the ground surface) and the moment at the base of the frame for each of the 5 fully instrumented piles are presented in Table D-8. It is of interest to compare the results in Table D-8 (Test Area 2) with those in Table D-4 (Test Area 1). In Test Area 1, the absolute values of the moments at the base of the frame (simulated cap) were approximately equal to the absolute values of the maximum moments below the ground surface, whereas the frame-base moments were much smaller relative to the below-ground moments in Test Area 1. This suggests that the group was much more flexible in rotation (softer axial pile load response) in Test Area 2, allowing the "fixing" moments at the base of the frame, which are high in Test Area 1, to diminish to a small magnitude. This observation indicates the importance of considering the axial response of piles in modeling lateral pile group response.

Each of the 12 piles was further analyzed to provide bending moment as a function of depth. Figures D-34, D-35 and D-36 describe the bending moment profiles for Piles 8 through 12 for tests 2, 3 and 4, respectively. The times at which the profiles are plotted correspond to the times at which the load reached its peak value, which are:

Test 2 - 0.667 seconds

Test 3 - 0.638 seconds

Test 4 - 0.617 seconds

It should be noted again that peak bending moments do not as a rule occur at the same instant for all the piles, there is usually a small phase difference for peak response from pile to pile. As before, every point on the graphs representing a bending moment value is actually the average of 11 points spaced equally about the time of interest.

The bending moment vs depth relationship was also used to derive the shear at the pile head at these instances in time. Table D-9 shows the interpreted distribution of pile-head shear for Statnamic Tests 2, 3 and 4, respectively, derived at the instant of peak load for each test. Note that these values appear much more reliable and less subject to interpretation than at Test Area 1 because of the large distance between the frame and mudline. This distance provided multiple gauge levels within the straight line portion of the moment vs. depth relation.

Figure D-37 illustrates the load distribution profile graphically. It plots the distribution on a pile by pile and a row by row basis. Only the distribution profiles for Statnamic tests 3 and 4 have been shown. The rows are numbered 1 through 4, top to bottom (lead to trail), respectively, with row 1 being the leading row. For test 3, row 1 carries 24 % of the load, row 2 carries the smallest amount (18 %), row 3 the largest (30 %), while the load transferred to row 4 is slightly smaller than that transferred to row 3 (28 %). The distribution pattern changes significantly however at the next load level (test 4), where rows 1 and 2 carry significantly larger proportions of the total load, while the contribution of row 4 drops to 23 %. The contribution of row 4 remains fixed at 30 %.

## **STATIC TEST ON SINGLE PILE - TEST AREA 1**

A static load test was conducted on Pile 13 at Test Area 1 (Ratt Island). The following instruments were used to monitor the response:

- 1 Load Cell,
- 14 Strain Gauges on Pile 13, and
- 4 Displacement Transducers (LVDTs).

The test setup is shown in Figure D-38. The displacement response on the test pile was monitored using 2 LVDTs, while 2 more were used to measure the response of the reaction pile. Their locations were as shown in the figure. The maximum average displacement recorded was 0.106 meters at a maximum load of 40.1 kN. Figure D-39 is a plot of the load-displacement response of the test pile.

The bending moments and axial stresses in the piles were extracted from the corrected strain data. The maximum value of bending moment recorded for the pile was 100.6 kN.m at gauge elevation 3. Figure D-40 shows the bending moment vs. depth profile at 3 values of applied lateral load : 14.2, 27.1, and 39.5 kN. The bending moment profiles were also used to compute shear at the pile head for these 3 values of applied shear by calculating the slope of the initial portion of the bending moment curves. The values of shear recorded for shear loads 1, 2 and 3 are as shown in the figure as 14.08 kN, 28.08 kN, and 38.69 kN, which correspond very closely to the applied pile-head loads and validate the moment diagram slope method for evaluating pile-head shears..

## **STATIC TEST ON SINGLE PILE - TEST AREA 2**

The static load test conducted on Pile 13 at Test Area 2 (east side of Cape Fear River) used the same instrumentation as that used at Test Area 1. Displacement response of the test pile and the



reaction pile were monitored using 2 LVDTs each. The test setup has been illustrated in Figure D-41. The maximum average displacement recorded was 0.197 meters at a load of 38.9 kN, while the maximum load achieved was 40.1 kN. Figure D-42 shows the load-displacement response.

As before, the bending moments and axial stresses in the test pile were computed once the raw strain readings had been corrected using the appropriate correction factors discussed in Appendix F. The maximum value of recorded bending moment was 110.6 kN.m at gauge elevation 5. The measured bending moment vs. depth relationship is plotted in Figure D-43 for loads of 10.4, 37.0, and 18.5 kN. The shear at the pile head was computed using the bending moment profiles (at loads of 8.4, 31.9 and 16.1 kN, respectively) and are shown in the same figure. The computed pile-head shears are not as close to the actual applied loads as was seen for Pile 13 in Test Area 1.

## **ANALYZING FOUNDATION RESPONSE USING AN EQUIVALENT SINGLE DEGREE OF FREEDOM MODEL**

The dynamic response of each foundation group tested has been modeled using an equivalent single-degree-of-freedom (SDOF) system. The dynamic response of an SDOF system is governed by the following differential equation:

$$Mu'' + Cu' + Ku = F(t) \quad , \quad (D-1)$$

where  $u''$ ,  $u'$ , and  $u$  represent the acceleration, velocity and displacement of the system, respectively, that define the physical state of the system at any instant of time,  $t$ .  $F(t)$  represents the forcing function vector.  $M$ ,  $C$  and  $K$  are the generalized mass, damping and stiffness coefficients of the SDOF system that may or may not change over time, with frequency of motion or with amplitude of motion. The mass and the damping coefficient were considered constant during a single loading event. Because soil load-displacement response to lateral loading at large strains is known to be

highly nonlinear, the stiffness coefficient  $K$  was modeled as a nonlinear term that decreases as a function of displacement,  $u$  within a single loading event. Equation D.1 may also be expressed as follows:

$$F_{\text{inertia}} + F_{\text{damping}} + F_{\text{static}} = F_{\text{statnamic}} \quad (D-2)$$

where

$F_{\text{inertia}}$  = inertial resistance from effective mass of the foundation,

$F_{\text{damping}}$  = effective viscous damping resistance,

$F_{\text{static}}$  = effective static soil resistance, and

$F_{\text{statnamic}}$  = measured force on the Statnamic load cell.

The Newmark- $\beta$  integration algorithm was used to solve the dynamic equation of motion numerically. Assuming the acceleration varied linearly between consecutive time steps, the response at any time could be computed using a total force balance and the state of the system at the previous step. The solution was implemented using a Matlab program with a graphic user interface whose input consisted of the measured Statnamic load vector  $F(t)$  and the values of the system parameters  $M$ ,  $C$  and  $K$ . The response of the system was obtained by interactively changing the values of  $M$ ,  $C$  and  $K$  until a good match was noted between the measured displacement time history (signals from the displacement transducers), and the simulated response (computed for the SDOF model). The goodness of match between the model response and the measured response was judged by eye by plotting the time histories simultaneously on the same graph. In most cases it was possible to arrive at a good match between the measured and computed time histories with a relatively small number of trials. The procedure used for signal matching can be broadly divided into the following steps:

1. Determine the mass coefficient by computing the mass of the foundation above the ground line. The actual participating mass may vary slightly from this number, and  $M$  may be

changed slightly ( $\pm 5\%$ , but usually slightly more) during the trials to establish a better match.

2. Estimate the lateral static stiffness of the foundation and use this value as a starting point for the stiffness parameter  $K$ . Compare the first peak in the computed displacement response with the first peak in the measured response and determine if  $K$  appears reasonable. Increase or decrease  $K$  until a good match is achieved for the amplitude of the first peak. It may also be necessary to vary the mass parameter  $M$  slightly to match the phase of the simulated response to the measured response where the displacement ramps up to its first peak. If  $M$  is chosen too large, the computed displacement response will lag the measured response.
3. Finally, adjust the value of the damping coefficient by changing the damping ratio until the post loading free vibration parts of the measured and computed displacement response are in good agreement. The measured response may be affected by significant permanent deformations, but this cannot be simulated using the simplified SDOF model. The objective, however, is to estimate the amount of damping present in the system, and this can be done by comparing the amplitude decay pattern and the damped frequency of free vibration.

The effective mass  $M$  is comprised of the total mass of the pile cap and portions of individual piles that contribute inertially to the response. The latter is usually restricted to the mass of the piles above the mud line, but may vary slightly depending on the magnitude of displacement and the degree of nonlinearity of the system. As such, this is the parameter that is easiest to define for SDOF analysis. The mass term effects the amplitude and form of the forced vibration part of the response (duration of Statnamic load), and the frequency of oscillation for the post-loading event, where the system undergoes damped free vibration.

The numerical value of the viscous damping constant ("dashpot"),  $C$ , has relatively little

effect on the response magnitude during the actual loading event, but is significant in determining the amplitude of decay and the damped free vibration frequency for post-loading response. In order to relate  $C$  more meaningfully to a system damping parameter, the damping constant may also be expressed as a percent of the critical damping constant  $C_c$  as follows:

$$\xi = C/C_c = C/[2(KM)^{1/2}] ,$$

where  $\xi$  is termed the "damping ratio" and

$$F_{\text{damping}} = 2 \xi (KM)^{1/2} u' .$$

The magnitude of the first peak in the simulated displacement time history is sensitive to the value of the effective stiffness parameter chosen,  $K$ . The stiffness term also effects the frequency of damped free vibration at the end of the Statnamic loading event.  $K$  is also used to back calculate a derived static load-displacement response, which may be compared to the load-displacement function obtained from a conventional static test.

### **Modeling the Pile and Shaft Group at Pascagoula**

The Matlab program *sdnon.m* was used to model the response of the test foundations at Pascagoula, Mississippi. Table D-10 summarizes the results for all load cases. Appendix C describes the test pile group but not the shaft group that is referred to in Table D-10. In the table headings,  $K$ ,  $C$  and  $M$  represent the model system parameters - equivalent static stiffness, equivalent damping coefficient and equivalent mass, respectively, that provided the optimum fit to the measured data.  $AFd@$  denotes the damped frequency of free vibration, while  $U_{\text{max}}$  and  $Fs_{\text{max}}$  represent the peak values of lateral displacement and static lateral resistance force generated within the system.

The upper plate in Figure D-44 compares the measured and computed (model) load-deflection response for a Statnamic loading case, called load case 2, for the pile group, while the lower panel in Figure D-44 shows the static, damping and inertial components of force that were

generated within the computational SDOF model system for that time history analysis. The equivalent static force vector is the product of the equivalent static stiffness,  $K$  and the computed displacement vector,  $u$ , the damping vector the product of  $C$  and  $u'$ , and the inertial force component the product of  $M$  and  $u''$ .

## **Discussion of Results, Pascagoula**

### *Mass Contribution*

The pile cap had a mass of a little over 163000 Kg, while the mass of the six piles supporting the cap was about 51000 Kg for every 6.1 m run. The unsupported length of the piles was about 12.2 m above the mud line. As an estimate for the mass term it was assumed that this length of piling contributed inertially to the response, plus a small amount to include some contribution of soil. The inertial contribution was also seen to vary with the amplitude of the forcing function. The mass term was observed to effect the magnitude and shape of the forced vibration part of the response and the frequency of free vibration following the loading event.

### *Damping*

The damping had relatively little effect on the response amplitude during the loading event, but it controlled the exponential decay envelope and the frequency of the post-loading free vibration response.

### *Static Stiffness*

As shown in Table D-10, the equivalent static stiffness  $K$  decreased for both groups (piles and drilled shaft) with increasing amplitude of lateral load. This is expected behavior, as soil is a strain softening material, and its stiffness is a nonlinear function of displacement. The first test conducted on the pile group indicated an anomalous value of  $K$  (slightly lower than  $K$  for the next case). A static load test conducted earlier in the opposite direction had resulted in some permanent as



displacement and had caused an apparent reduction of the stiffness term for the first Statnamic loading.

#### *Static and Dynamic Forces of Resistance*

The SDOF model provided estimates for the components of force generated within the system during the dynamic event. This information was used to predict the response of the system to a conventional static load test. Each Statnamic test provides one data point that describes the static response at a particular load level. The peaks of the equivalent static force vectors were plotted as function of the peaks of the displacement vectors, which in effect describes the static load-deflection behavior of the foundation. This can be done because the peak static resistance occurs when the displacement of the system is at its maximum and the damping force is zero. This concept can be taken further to include the total dynamic resistance of the system by considering the effects of damping. The total resistance offered by the system at any time is the sum of the static and the damping components ( $K[u]+C[u']$ ). Figure D-45 shows the derived static load-deflection curves for both foundations along with the derived peak total resistance and the measured static load-deflection response. Overall, the derived static curves are seen to match the measured static curves quite well, although the measured response is slightly softer than the computed response at large lateral displacements. The system was also seen to achieve its peak total resistance just ahead of the peak displacement, i. e., the static component lagged the total force component slightly because of damping.

#### *Damped Frequency*

The damped natural frequency of the system can be estimated from the post-loading free vibration response. The period of free vibration (inverse of the frequency) was seen to elongate significantly with increasing magnitude of load and level of nonlinearity in the system. This is

because as the level of nonlinearity in the system increases, the static stiffness decreases and the damping ratio increases, causing the period to elongate. The damped frequency has been plotted as a function of maximum lateral displacement in the upper panel in Figure D-46. The frequency decreased from 4.23 Hz to 3.61 Hz in a linear manner for the pile group as the peak displacement increased. For the shaft group the frequency decreased from 3.84 Hz to 2.75 Hz in a somewhat nonlinear fashion.

### *Damping Ratio*

The damping ratio changed both as a function of the foundation type and the applied load amplitude. The results plotted in the lower panel of Figure D-46 indicate significantly higher amounts of damping in the shaft group compared to the pile group. The shaft group, which consisted of two vertical drilled shafts, provided most of its resistance to Statnamic load by mobilizing lateral soil resistance, whereas the pile group, which contained batter piles did so by mobilizing significantly higher proportions of axial soil resistance (side friction) and end bearing in the batter piles. Being more massive and offering a larger contact area to soil made it easier for the shafts to dissipate energy imparted to the foundation. The shafts may also have dissipated more energy within the concrete material than the piles because the shafts were not prestressed and hence more prone to cracking under lateral loading than the piles, which were prestressed and therefore less prone to dissipate energy internally. For the pile group, the damping ratio increased somewhat uniformly from 16.8% to 19.4% with increasing amplitude of load. For the shaft group, the damping ratio increased from 22.6% to 29.3% over the first three tests, but then decreased slightly for the last two. This may be due to gapping between the shafts and the surrounding soil near the mud line at the higher loads which reduced the contact area and the hence the ability of soil to dissipate energy by radiation and internal damping (hysteresis).

Overall, the simple mathematical model described above provided good results when predicting response during the actual loading event, which depends largely on the mass and stiffness characteristics, but it is unable to fully capture the post-load damping behavior. The free vibration response for both foundations indicated that the damping was not completely viscous. The decay of amplitude from peak to peak was not defined by an exponential envelope, nor did the period of vibration remain constant from cycle to cycle. This may be due to several reasons: (a) nonlinear behavior of the soil and foundation elements, (b) participation of higher modes which a SDOF model cannot capture, and finally (c) energy dissipation in forms other than viscous damping.

#### **SDOF Model of Pile Group, Test Area 1**

The displacement response of the pile group at Test Area 1 (Ratt Island) was highly nonlinear. For this reason the equivalent foundation stiffness was modeled as a nonlinear function of displacement, i. e., the stiffness  $K$  decreased as an exponential function of displacement, starting from an initial value, and was limited by bounds that could be changed within the analysis. The analysis itself was designed to simulate each Statnamic test in sequential order, from the lowest to the highest load amplitude. The solution for each test (except for the first one) was based upon the previous load and deflection history of the system, and the foundation stiffness  $K$  at the beginning of each test was initialized to the stiffness value at the end of the previous test. The damping ratio was assumed to remain constant for all four tests. The primary objective of this analysis was to derive the equivalent static load-deflection curve for the system and match it to the measured static response of the group recorded at the same location. Since it is known that the first peak in the simulated displacement response is particularly sensitive to  $K$ , the model parameters were adjusted by trial and error until a good match was observed between the measured and computed first peaks for all four tests. The match was also influenced by the frequency of the computed free vibration

response and how closely it matched the frequency of the measured signal. No attempt was made to model the inelastic deformation observed in the real system. This was done in an effort to keep the model as mathematically simple as possible and not introduce another set of complex parameters that would influence the simulated behavior.

Figure D-47 shows the match between the measured and computed displacement response for all four Statnamic tests conducted on the pile group at Test Area 1. The terms LC1...LC4 refer to Statnamic load cases 1 through 4, respectively. The abscissa represents the time axis, while the ordinate represents lateral displacement in meters. Figure D-48 is a plot of the nonlinear stiffness time history for all four tests. The system begins with an initial lateral stiffness of 14.0 MN/m, and degrades to a lateral stiffness of roughly 9.4 MN/m at the end of the final test. The other system parameters were defined as follows:

Mass (M)	25000 Kg
Damping Ratio ( $\xi$ )	0.20
Stiffness Degradation Parameter ( $\alpha$ )	0.40
Reference Diameter for Pile	10.0 meters
Time Step	0.004 seconds

The static resistance is modeled as a function of displacement,  $x$ , using a spring with stiffness  $k_s$ . Because the soil response for lateral loading at large soil strains is known to be highly nonlinear, this spring is modeled as a nonlinear stiffness that decreases as a function of displacement. For the

analyses in this project, stiffness has been presumed to decay exponentially from an initial value of  $k_i$  at  $x = 0$  to a value  $k = \alpha k_i$  at a displacement of 5% of some reference pile diameter (10% of its radius,  $r$ ). Because the analyses here are for a group of piles, this reference diameter is of no physical significance and serves only to define a point on the lateral stiffness vs. displacement curve. Thus, the static resistance is modeled using two constants,  $k_i$  and  $\alpha$ , according to:

$$F_{\text{static}} = x \exp\{\ln k_i + \ln[\alpha(0.1 r)]\}$$

A simple computational model of the Statnamic loading is thus established, involving the effective mass, damping ratio and stiffness constants  $k_i$  and  $\alpha$ . Figure D-49 shows an excellent match between the measured and the derived static response. The derived static load displacement relationship was calculated using the parameters defined in Table D-11.  $F_s$  is the peak equivalent static force and is computed as the product of the peak computed displacement  $U_s$  and the value of the equivalent static stiffness  $K$  at that particular time step. Figure D-49 also plots the total (dynamic) derived soil resistance  $F_d$  as a function of the displacement  $U_d$  at which it occurs.  $F_d$  is computed as the sum of the equivalent static and damping force vectors, where the damping force vector is the product of the scalar damping coefficient and the velocity vector computed by the model.  $F_d$  is thus a function of the time rate at which the foundation is loaded. The peak static force was seen to lag the peak total force for all four load cases, with the phase difference increasing with increasing applied loads and damping forces in the system.

### **SDOF Model of Pile Group, Test Area 2**

The dynamic response of the pile group was modeled using an equivalent SDOF system for tests 2 through 4. The first test could not be modeled because the load cell did not work and had to be replaced. The lateral displacement response computed by the SDOF model was compared to the measured displacement response recorded during the series of Statnamic tests. Using the measured



Statnamic force record as the forcing function input to the model and changing the system parameters (mass, stiffness and damping), it was possible to arrive at a good match for the lateral response. Using the modeling results also enabled the back-calculation of the static and total soil response curves for the pile group. For this series of Statnamic tests, the static stiffness  $K$  was assumed to remain constant during each test but was adjusted from test to test. Table D-12 summarizes the results obtained.

The equivalent static force was computed as the product of the static stiffness and the computed deflection and the total soil resistance as the vector sum of the equivalent static force vector and the computed velocity vector multiplied by the damping coefficient. The peak total soil resistance was seen to occur slightly before (to lead) the peak static resistance.

Figure D-50 shows the match between the measured and computed lateral response for the second Statnamic test on the pile group. The objective was to model the behavior for the first two oscillations (2 peaks). The first peak is dependent largely on the static stiffness, and the relationship of the second peak to the first is influenced by the amount of damping in the system. The response is also affected by the mass, as larger loads increase the mass participation, but this change is small and not easy to quantify with precision. The latter part of the free vibration response does not match exactly with the computed response, but this part of the record is effected by strong nonlinearities like gapping and nonviscous damping in the system which cannot be modeled easily using the simplified SDOF model. The measured response may also have been affected by the movement of the reference beams used to mount the displacement transducers, but this movement was not significant considering the substantial movements recorded for the pile group.

The amount of damping increased from 20 to 28% and the damped natural frequency decreased from 2.698 Hz to 2.294 Hz from the second to the fourth test. Figure D-51 plots the

derived static and total soil resistance as functions of peak recorded displacement. The peak static and total resistances are relatively close at the smaller load (test 2), but the amount of damping increases significantly for tests 3 and 4 and the peak static resistance starts to lag the peak total resistance by larger amounts.

### Modeling Rate Effects using a Single Degree of Freedom System

The SDOF model can be used to derive a rate effect parameter to predict the dynamic resistance of the foundation to loading that causes the foundation to react at a different rate. The equivalent static and total soil resistance functions computed by the model, along with the average velocity of the foundation during the loading event may be used as follows:

1. Compute the effective static stiffness of the foundation,  $K_s$ .

$$K_s = F_s \div U_s.$$

2. Compute the effective total stiffness of the foundation,  $K_t$ .

$$K_t = F_d \div U_d.$$

3. Compute the average rate of displacement of the foundation during the loading event,  $V$

$$V = U_s \div t_s$$

where  $t_s$  = total time for displacement to go from 0 to  $U_s$

4. Plot the ratio  $K_t/K_s$  as function of  $V$  for each Statnamic test.

The terms  $F_s$ ,  $U_s$ ,  $F_d$  and  $U_d$  have been defined earlier. The effective static stiffness  $K_s$  is computed at the time the foundation reaches its maximum displacement,  $U_s$ . The effective total stiffness  $K_t$  is computed as the ratio of the peak total resistance (static + damping) to the displacement at which it occurs. It should be noted that the peak total resistance and the peak static resistance usually do not occur at the same time.

The rate parameter accounts for the influence of damping resistance offered by the

foundation during dynamic loading and is a function of both the peak displacement  $U_s$  and the average rate of displacement,  $V$ . It is not meant to be an exact representation of the dynamic foundation resistance, but is meant to serve as a guideline for estimating the resistance that might be mobilized by a forcing function that induces the system to react at a different rate. The rate parameter function was derived for the Statnamic tests on the pile and shaft groups at Pascagoula, and the NCHRP group at Test Areas 1 and 2 in Wilmington. These have been shown in Figures D-52 (Pascagoula results) and D-53 (Wilmington results). Each graph presents the results for the last three Statnamic tests, which have been indicated by the peak displacement. The peak total resistance mobilized by the pile group at Pascagoula for the last test is about 1.15 times the peak static resistance, and for the shaft group it is almost 1.37 times the peak static resistance. The shaft group mobilized significantly higher damping forces in the soil, and may have experienced higher material damping within the foundation elements, than the pile group. This accounts for the higher effective total stiffness and the larger rate factor.

As an example of where such a rate effect parameter might be used, consider the case of a barge impacting the shaft group. Assuming the impact causes the foundation to deflect by 0.1 meters (peak), and that it takes the foundation 3 seconds to reach this deflection, the average rate of displacement is computed to be 0.033 meters/sec. Referring to Figure D-52, the corresponding rate factor lies within 1.03 and 1.05, which indicates that under these conditions, the total soil resistance mobilized is about 3 to 5 % more than the effective static resistance. In other words, a slowly moving barge impacting a similar foundation would not mobilize significant damping resistance forces in the soil, and the load deflection response of the foundation would be very similar to a static loading condition.

## MODELING THE RESPONSE USING FINITE ELEMENTS

The NCHRP pile group tested at the Ratt Island location (Test Area 1) at Wilmington, NC, was modeled using finite elements. The program "Florida Pier" (FLPIER, Appendix C) was used because it can account for load distribution within groups and reduced efficiencies due to group effects when the group is loaded statically.

When a group of piles are loaded laterally, the resistance offered by the group is usually not equal to the sum of the resistances of each pile acting alone, in isolation. The group resistance is a function of pile location within the group and pile spacing. One way to account for group effects is to scale the p-ordinates of the computed p-y curves. Every p-y curve on every pile in a particular row is scaled using the same factor, using the findings set forth in Brown, Morrison, and Reese, [1] and Brown, Reese, and O'Neill [2].

Florida Pier uses p-multipliers to scale the ordinates of computed p-y curves on a row by row basis (Appendix A, Appendix C). For a pile group with four rows of piles, the default p-multipliers used by the program are as described in Table D-13. These multipliers represent an overall group efficiency of 70 - 75 % for 3D spacing and about 95 % for 5D spacing, where D is the pile diameter or equivalent diameter. The p-multipliers may also be defined explicitly for each row by the user. For example, Appendix A suggests that the row-by-row p-multipliers will be different for bored and driven piles in predominantly cohesionless soil.

The pile group at Test Area 1 consisted of twelve, 12.19-m- (40-foot-) long steel pipe piles with an outer diameter of 273 mm (10.75 inches) and a wall thickness of 12.7mm (0.5 inches). The piles were driven at a spacing of 0.819m (32.25 inches, or 3 times the pile diameter) in a group of  $4 \times 3$ , with the longer dimension being along the direction of loading. The pile heads were bound together using a steel frame that, as closely as possible, fixed the piles into the frame with moment

connections at the pile heads. The group was tested statically up to a peak lateral load of 1068 kN. In addition to the static test conducted on the group, a lateral static load test was conducted on a similar single reference steel pile driven adjacent to the group, in a manner similar to the Chaiyi tests described in Appendix A. The peak lateral load applied to the reference pile was approximately 40 kN. The results of these tests have been described earlier in this appendix.

#### **Lateral Load Test on Single Pile**



Before starting with the analysis of the pile group, the lateral soil model was verified using the results from the static test on the single reference pile (NCHRP Pile 13). The pile/soil interaction was modeled using both the Florida Pier (Appendix C) and the SeaStar (CAP) [3] finite element packages. This enabled modeling of the tests using two independent programs and also allowed for the comparison of the two programs.

The finite element model used by SeaStar for the single pile is shown in Figure D-54. The freestanding (unstressed) portion of the pile extends from nodes 1 to 3, and nodes 2 and 4 represent the locations of the displacement transducers recording lateral movement at the pile head. The lateral load was applied at node 3, and the structural connection between the loading frame and the pile was modeled as a hinged connection that allowed the transfer of lateral load but no moments. The loading point was located 1.55 m above the ground line. The pile below the load point was modeled using thirty one elastic beam elements, each having a length of 0.358 m. The model used for analysis by Florida Pier was very similar to the one used by SeaStar. SeaStar allows the user greater control in setting up the finite element model, in terms of defining node locations and the number and length of elements. Florida Pier sets up the model by itself, given the basic pile and soil stratification information, and does not allow the user to change the number of elements used to model individual piles. Florida Pier modeled the reference pile using a total of sixteen elements, and the resulting mesh was coarser than the one used by SeaStar.

The soil parameters used to generate p-y curves in both cases were identical, as shown in Table D-14. In that table E50 refers to the strain at 50 % failure stress in an unconfined compression test. The p-y curves for the clay layer were formulated using Matlock's criteria for soft clays below the water table [4]. The p-y curves for the sand layer used the criteria recommended by Reese, Cox

and Koop [5].

The lateral load-displacement response at the load point computed by SeaStar and Florida Pier (FLPIER) are shown in Figure D-55, along with the measured response. The responses predicted by both programs are seen to be similar and close to the measured load-displacement relation. Florida Pier predicted the initial part of the response (from 0 to 15 kN) more accurately but over-predicted the displacements at higher loads, while SeaStar provided a better match above 25 kN but over-predicted deflections at lower loads. It should be noted that only the lateral soil model could be established using the single pile test since no axial load tests had been conducted on the reference pile.

The bending moment profile computed by Florida Pier along the length of the reference pile at a lateral load of 35.58 kN (8 Kips) is shown in Figure D-56 along with the moment profile at the same load derived from measured strain data. The profiles are seen to be in good agreement even though the magnitude of the peak moment does not match exactly.

### **Lateral Load Test on Pile Group**

The static load test on the pile group was modeled using FLPIER only, since the program SeaStar currently has no provision for using P-multipliers for individual rows. The finite element model used by Florida Pier is shown in Figure D-57. Each pile was modeled using sixteen linear beam elements, each element having a length of 0.626m. The steel frame holding the twelve piles together as a group was designed to transfer applied lateral loads to the individual piles at two levels. For the model, the elevation of the pile cap was set at 1.067m (the level of the attachment of the frame to the piles at the lower point, which was also the lower load point for each pile). The pile cap was modeled using shell elements, each 0.276m in thickness and with an elastic modulus of steel,

to account for the total mass of the frame and the pile lengths above 1.067m. The resulting flexural stiffness of the cap was roughly equal to that of a concrete cap 0.53m (21 inches) thick. The static lateral load was simulated by a combination of equivalent lateral loads and moments applied at the heads of the three piles along the left face (shorter dimension) of the group. The moments were included in the forcing function to account for the offset of the upper load points relative to the elevation of the pile cap used in the model. The piles were modeled as fixed to the cap (full moment connection).

The input parameters for the lateral soil model (p-y curves) were fixed at the values derived from the analysis of the single pile test described previously. The input parameters for the axial soil model (t-z curves) were varied within reasonable bounds, and the computed response of the pile group, both load vs. displacement at the level of the pile cap and bending moment profiles down the lengths of selected piles, were compared for each trial set of t-z curves. These t-z curves (unit axial load transfer curves) are computed in FLPIER using the model referenced in Appendix A. The final axial soil model parameters that produced the best estimates for displacement and moment response of the pile group overall are provided in Table D-15.

#### *Static Response of Ratt Island 12 Pile Group*

The p-multipliers used for the analysis were the default values recommended by Florida Pier for a pile group with four rows. The p-multipliers used were 0.3, 0.2, 0.4, and 0.8, starting with the trailing row and ending with the leading row.

The computed lateral load displacement response at the level of the cap is shown in Figure D-58 for the optimum set of t-z curves (Table D-15) and the default p-multipliers. The computed lateral displacement at the pile-head elevation is in excellent agreement with the measured response

out to very large displacements, and the computed rotation is seen to be near the measured rotation, as well. Also shown on Figure D-58 is a plot of pile group response using the FLPIER model with all piles having a common p-multiplier of 0.425. This value represents the weighted average of all the p-multipliers for all 12 piles according to row position. This model appears to capture the overall foundation response approximately as well as the more detailed (row-wise p-multiplier) model.

Figure D-59 provides a plot of the computed and measured bending moments as a function of depth for two piles. Pile 12 is the middle pile in the trailing row, while Pile 8 is the middle pile in the leading row. The bending moments have been plotted at a lateral load of 712 kN. The agreement between the measured and computed bending moment profiles is not as good as was noted for the single pile model. However, these profiles are still close in terms of shape, and both predict the peak moment location quite well. Note also that the computed moment vs. depth profile using a uniform p-multiplier of 0.425 is also reasonable.

The axial load vs. depth relationship for the piles on the leading and trailing rows have been plotted in Figure D-60 at the same load level (712 kN), along with the axial load profile computed by FLPIER. The measured values are seen to be somewhat erratic, owing to both random variations in soil response and measurement errors; it is difficult to measure accurately axial force in a pipe with two strain sensors when large bending moments are superposed on the pipe. Nevertheless, the model appears to provide reasonable estimates of the maximum axial forces indicated by these measurements.

The pile-head shear distribution at a lateral load of 712 kN is shown in Figure D-61. The arrangement of individual piles in the group has been shown along with the shear values computed for each pile and the shear contribution of the rows along the direction of loading. The percent load

transferred to each row was computed to be 21%, 19%, 26% and 34 % (left to right), which is in approximate agreement with the measured row-wise shear distribution of 24%, 20%, 25%, and 30 %, again from left to right or trailing to leading row. Figure D-62 shows the computed and measured pile-head axial loads for every pile in the group at a lateral load of 712 kN. A negative value for axial load indicates tension, and a positive value indicates compression. The agreement between the measured and computed values are fair to good for the outer leading and trailing rows which carry the maximum compression and tension, respectively. The model tends to overpredict the axial loads on the middle two rows, which carry significantly smaller loads than the other rows. A study of the strain data on which the measured axial load profiles were based indicates that some of the piles may have moved vertically or slipped relative to the frame during the unload phase just after the peak lateral load was reached. In particular, the strain data for Piles 4, 6 and 9 seem to indicate this quite strongly. Slippage relative to the frame would also have affected the axial loads derived from the strain measurements significantly and may have resulted in the less-than-perfect match between the model response and the measured axial response.

#### *Scaling p-multipliers to Account for Rate Effects*

In an attempt to account for dynamic rate effects using the static model, the default p-multipliers recommended by FLPIER were scaled using a scale factor ranging from 1.0 (static case) to 1.7 (high viscous rate effect). The scale factor was applied identically to the p-multiplier for each row in the model, a static analysis was conducted on the model with the scaled p-multipliers, and the derived static load-deflection curve was plotted against the total soil resistance curve derived from the equivalent SDOF model described previously. A total of ten load cases were analyzed with the scale factors shown in Table D-16.



The results are plotted in Figure D-63. The total resistance function (static + damping from the SDOF analysis) has been plotted using circles, and the derived static load-deflection curves for load cases 1 to 10 have also been shown. The effect of increasing the scale factor is to stiffen the foundation and has been indicated by the arrow.

Figure D-63 shows that the dynamic effects are very much more significant at the large rate of loads associated with the large displacement events. The larger loads are applied at a much higher velocity and therefore may mobilize much higher viscous damping resistance within the system, even though the damping ratio does not change significantly. However, it is also possible that the increased damping at higher displacement amplitudes is due to increased hysteresis in the soil and not exclusively to rate of loading. However, it appears that it would be difficult for design purposes to capture the dynamic effects by using a static model with a p-multiplier rate factor applied to the static p-multipliers since the rate factor is not known until the rate (average velocity) is known. On the other hand, the static model can provide the static stiffness for use with the SDOF model, and one can estimate the percent damping for design.

#### *Dynamic Response Using FLPIER*

In order to evaluate the dynamic version of FLPIER, the final static p-y curves (using the adjusted p-multipliers as outlined above) and the Statnamic force measurements from the load cell were sent to the computational research team at the University of Florida. Their computations were returned in the form of the FLPIER output files compared with the plots provided in this section of the report that were generated by the experimental research team members at Auburn University.

The pile-group model setup was identical to the static pile-group model test setup, except that the load time history was provided as input. The University of Florida team specified no viscous

damping for the p-y curves (although as shown in Appendix C, the use of viscous damping is an option in FLPEIR), but their model did track hysteresis in the p-y curves (calibrated by comparison with single-pile static behavior). Structural (proportional, or Rayleigh) damping was provided as follows: in the pile cap —  $0.015 * \text{cap mass} + 0.01 * \text{cap stiffness}$ ; in the piles —  $0.01 * \text{pile mass} + 0.01 * \text{pile stiffness}$ . Default static p-multipliers were used (0.8, 0.4, 0.4, and 0.3, respectively from leading row to back row). Presented on Figure D-64 are the computed and measured displacement time histories for the 12-pile group at Test Area 1 (Ratt Island). The initial computed peak displacement is fairly close to the measured value for all four Statnamic loadings. However, the model appears to have a frequency response that is somewhat too high after the initial peak. Note that the measured oscillations from the LVDT measurements are thought to be the result of measurement errors related to vibration of the reference beam. Although the reference system was founded on piles, the ground was so soft that movements of this system could be visibly detected; the integrated accelerometer measurements are shown to indicate fairly high damping of the test foundation.

#### **Summary - FEM Analysis of Pile Group at Test Area 1**

1. Group effects were substantial for lateral loading.
2. The default p-multipliers used by FLPIER seem reasonable and capture the general behavior of the group. The use of a weighted average P-multiplier uniformly applied to all piles in the group provides a reasonable approximation of the overall behavior.
3. There was a substantial amount of variability in pile response within the group due to (random) spatial variation in soil resistance that appears unrelated to group effects.
4. The static response function derived from the Statnamic tests using the simple SDOF model

appears to match closely with the measured static response.

5. Damping adds significant additional resistance in these soils, but the static stiffness is dominant.
6. The lateral stiffness and rotation of the cap were sensitive to the axial behavior of the piles.
7. The dynamic version of FLPIER appears to capture the initial peak displacement response reasonably for all four Statnamic loadings at Test Site 1, but the subsequent frequency response is somewhat high. The damping used in the FLPIER analysis appears reasonable, judging from the integrated accelerometer measurements of displacement.

## REFERENCES

1. Brown, D. A., Reese, L. C., and O'Neill, M. W., "Cyclic Lateral Loading of a Large-Scale Pile Group," *Journal of Geotechnical Engineering*, ASCE, Vol. 113, No. 11 (1987).
2. Brown, D. A., Morrison, C., and Reese, L. C., "Lateral Load Behavior of Pile Group in Sand," *Journal of Geotechnical Engineering*, ASCE, Vol. 114, No. 11 (1988).
3. PMB Engineering, Inc., "SeaStar P3.20: Offshore Analysis and Design Software," *User's Manual*, San Francisco, California (April, 1984).
4. Matlock, H., "Correlations for Design of Laterally Loaded Piles in Soft Clay," Offshore Technology Conference, Proceedings, Vol. 1 (1970), Paper No. 1204, Houston, Texas.
5. Reese, L. C., Cox, W. R., and Koop, F. D., "Analysis of Laterally Loaded Piles in Sand," Offshore Technology Conference, Proceedings, Vol. II (1974), Paper No. 2080, Houston, Texas.

<i>Table D-1. Maximum Bending Moments - Static Pull Test</i>			
Pile Number	Maximum B.M. (N.m)	Gauge Level from Top	B.M. at Connection (N.m)
12	8.62e+04	7	-8.40e+04
11	8.25e+04	6	-9.50e+04
10	6.72e+04	6	-1.10e+05
9	9.28e+04	5	-1.24e+05
8	9.69e+04	5	-1.25e+05

<i>Table D-2. Pile-Head Load Distribution - Static Load Test</i>		
Pile Number	Shear @ Load = 570 (kN)	Shear @ Load = 1064 (kN)
1	20	38
2	30	55
3	34	65
4	19	36
5	34	75
6	16	31
7	34	54
8	38	77
9	29	62
10	30	70
11	25	50
12	24	43



<i>Table D-3 : Displacement Response - Statnamic Test on Pile Group - Test Area 1</i>				
Test Number	1	2	3	4
Maximum Displacement (mm)	27.9	47.3	82.8	107.8
Maximum Rocking (rad)	0.0031	0.0048	0.0100	0.0166
Maximum Torsional Rotation (rad)	0.0013	0.0013	0.0023	0.0022
Mean Set (mm)	6.1	6.2	10.6	11.1
Damped Frequency (Hz)	3.55	3.10	2.88	2.86

*Table D-4. Maximum Bending Moments - Statnamic Tests - Test Area 1*

Pile Number	Maximum B.M. (N.m)	Gauge Level from Top	B.M. at Connection (N.m)
Test 1			
8	-3.169E+04	5	4.30E+04
9	-2.891E+04	5	3.70E+04
10	-1.929E+04	5	4.50E+04
11	-2.326E+04	5	3.40E+04
12	-2.562E+04	5	3.50E+04
Test 2			
8	-5.483E+04	5	7.00E+04
9	-4.950E+04	5	6.50E+04
10	-3.395E+04	5	7.80E+04
11	-4.179E+04	6	5.80E+04
12	-4.603E+04	5	6.00E+04
Test 3			
8	-9.308E+04	5	9.20E+04
9	-8.480E+04	5	8.90E+04
10	-5.960E+04	6	1.21E+05
11	-7.178E+04	6	9.50E+04
12	-8.149E+04	6	9.70E+04
Test 4			
8	-1.206E+05	5	9.90E+04
9	-1.083E+05	5	8.10E+04
10	-8.058E+04	6	1.47E+05
11	-9.663E+04	5	1.25E+05
12	-1.091E+05	5	1.15E+05

<i>Table D-5. Pile Head Load Distribution - Statnamic, Test Area 1</i>			
Pile Number	Shear - Test 2 (kN)	Shear - Test 3 (kN)	Shear - Test 4 (kN)
1	-24	-29	-40
2	-39	-58	-70
3	-41	-62	-82
4	-20	-24	-34
5	-42	-56	-71
6	-21	-34	-48
7	-43	-70	-89
8	-40	-51	-66
9	-34	-38	-55
10	-44	-73	-91
11	-30	-51	-67
12	-32	-56	-67

<i>Table D-6. Acceleration Results - Statnamic Tests, Test Area 1</i>			
Test Number	Peak Average Acceleration (g's)	Time(sec)	Primary Frequency (Hz)
1	1.014	0.662	3.33
2	2.073	0.606	3.54
3	4.882	0.559	3.32
4	6.305	0.543	3.11

<i>Table D-7. Displacement Response - Statnamic Test on Pile Group - East Side</i>			
Test Number	2	3	4
Maximum Displacement (mm)	58.6	102.8	137.9
Maximum Rocking Rotation (rad)	0.0062	0.0145	0.0268
Maximum Torsional Rotation (rad)	0.0013	0.0022	0.0052
Mean Set (mm)	4.4	0.8	12.9
Damped Frequency (Hz)	2.25	1.82	1.81



Table D-8. Maximum Moments - Statnamic Test, Test Area 2			
Pile Number	Maximum B.M. (N.m)	Gauge Level from Top	B.M. at Connection (N.m)
Test 2			
8	5.096E+04	5	-2.20E+04
9	4.555E+04	5	7.00E+03
10	4.663E+04	6	-1.40E+04
11	5.254E+04	5	-4.10E+04
12	4.599E+04	5	-2.30E+04
Test 3			
8	7.945E+04	5	-2.30E+04
9	7.642E+04	5	1.10E+04
10	7.414E+04	6	-1.70E+04
11	8.011E+04	5	-4.30E+04
12	7.392E+04	6	-3.30E+04
Test 4			
8	1.030E+05	5	-2.00E+04
9	1.026E+05	5	8.00E+03
10	9.853E+04	6	-2.10E+04
11	1.054E+05	5	-6.40E+04
12	9.885E+04	6	-5.10E+04

<i>Table D-9. Pile-Head Load Distribution - Statnamic, Test Area 2</i>			
Pile Number	Shear - Test 2 (kN)	Shear - Test 3 (kN)	Shear - Test 4 (kN)
1	15	25	35
2	26	40	53
3	Not Available		
4	31	40	37
5	34	49	60
6	30	42	44
7	32	42	49
8	21	27	30
9	12	18	26
10	17	20	25
11	30	39	53
12	20	27	38

*Table D-10. Results From SDOF Modeling, Pascagoula*

<b>Pile Group</b>							
	K (N/m)	C (N.s/m)	M (Kg)	Damping Ratio (%)	Fd (Hz)	U_max (m)	Fs_max (N)
PEW1	1.82E+08	2.27E+06	2.50E+05	1.6830E+01	4.2330E+00	9.2000E-03	1.6595E+06
PEW2	1.88E+08	2.50E+06	2.75E+05	1.7380E+01	4.0980E+00	1.5300E-02	2.8789E+06
PEW3	1.66E+08	2.35E+06	2.56E+05	1.8020E+01	3.9864E+00	2.1800E-02	3.5989E+06
PEW4	1.48E+08	2.20E+06	2.45E+05	1.8270E+01	3.8459E+00	3.0900E-02	4.5678E+06
PEW5	1.28E+08	2.15E+06	2.40E+05	1.9400E+01	3.6057E+00	4.3600E-02	5.6018E+06
<b>Shaft Group</b>							
	K(N/m)	C(N.s/m)	M (Kg)	Damping Ratio (%)	Fd (Hz)	U_max (m)	Fs_max (N)
SEW1	1.70E+08	3.10E+06	2.77E+05	2.2590E+01	3.8409E+00	8.2000E-03	1.4101E+06
SEW2	1.41E+08	3.35E+06	2.82E+05	2.6560E+01	3.4310E+00	1.9500E-02	2.7611E+06
SEW3	1.15E+08	3.35E+06	2.85E+05	2.9260E+01	3.0571E+00	3.0000E-02	3.6477E+06
SEW4	9.70E+07	2.70E+06	2.75E+05	2.6140E+01	2.8852E+00	4.4400E-02	4.5040E+06
SEW5	8.80E+07	2.60E+06	2.75E+05	2.6430E+01	2.7458E+00	5.5800E-02	5.0134E+06

<i>Table D-11. SDOF Model Results for Pile Group - Test Area 1</i>				
Computed Response				
Load Case	$U_s$ (mm)	$F_s$ (KN)	$U_d$ (mm)	$F_d$ (KN)
Test 1	2.93E+01	3.53E+02	2.88E+01	3.62E+02
Test 2	5.03E+01	5.50E+02	4.79E+01	5.87E+02
Test 3	8.08E+01	7.99E+02	7.27E+01	8.98E+02
Test 4	1.01E+02	9.46E+02	8.78E+01	1.09E+03

Table D-12. SDOF Model Results for Pile Group - Test Area 2

System Properties Fitted to Model				
Load Case	Mass (Kg)	Stiffness (N/m)	Damping (%)	Freq (Hz)
Test 2	1.42E+04	4.25E+06	20.00	2.698
Test 3	1.46E+04	3.80E+06	22.00	2.505
Test 4	1.42E+04	3.20E+06	28.00	2.294
Computed Response				
Load Case	$U_s$ (m)	$F_s$ (N)	$U_d$ (m)	$F_d$ (N)
Test 2	5.8800E-02	2.4537E+05	5.7500E-02	2.5212E+05
Test 3	1.0220E-01	3.7675E+05	9.6300E-02	4.0430E+05
Test 4	1.3810E-01	3.9929E+05	1.1910E-01	4.6996E+05

$U_s$  = peak lateral displacement

$F_s$  = peak equivalent static force =  $K [U_s]$

$U_d$  = displacement at peak total soil resistance

$F_d$  = peak total soil resistance =  $K [U] + C [V]$

$U$  = computed lateral displacement vector

$C$  = damping coefficient

$V$  = computed lateral velocity vector



*Table D-13. Default P-multipliers - Florida Pier*

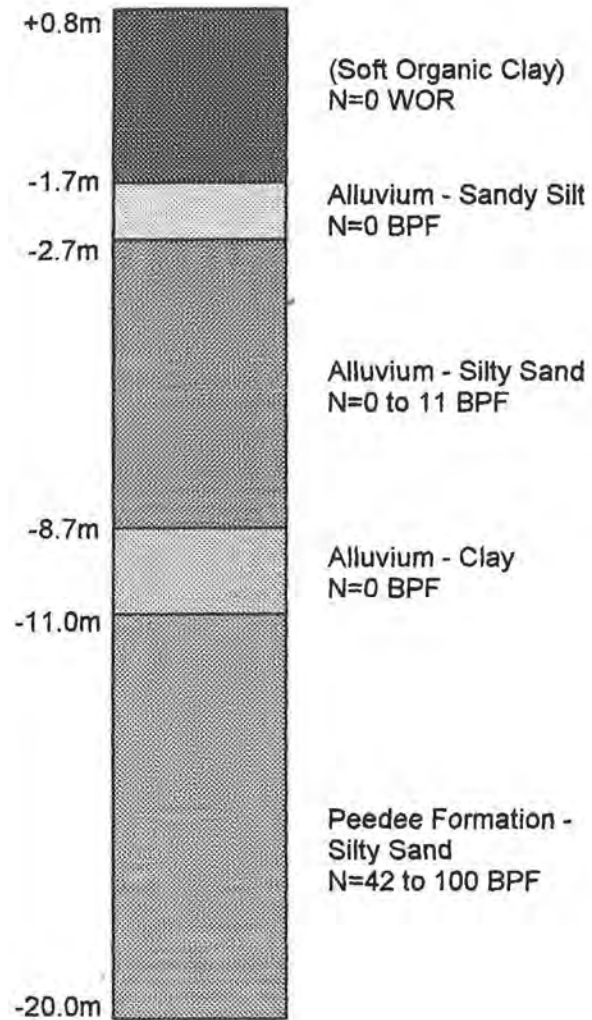
Row	P-multiplier Spacing = 3 diameters	P-multiplier Spacing = 5 diameters
Leading	0.80	1.00
2nd	0.40	0.85
3rd	0.20	0.70
Trailing	0.30	0.70

*Table D-14. Soil Model, Test Area 1, Wilmington*

Depth (m)	Submerged Unit Weight (kN/m <sup>3</sup> )	Soil Type	Undrained Shear Strength (kPa)	Angle of Friction	$\epsilon_{50}$	Subgrade Modulus (kN/m <sup>3</sup> )
0.00	4.072	Soft Clay	6.895		0.02	
2.54	4.072	Soft Clay	13.790		0.02	
2.54	8.143	Sand		30		54287
15.24	15.240	Sand		30		54287

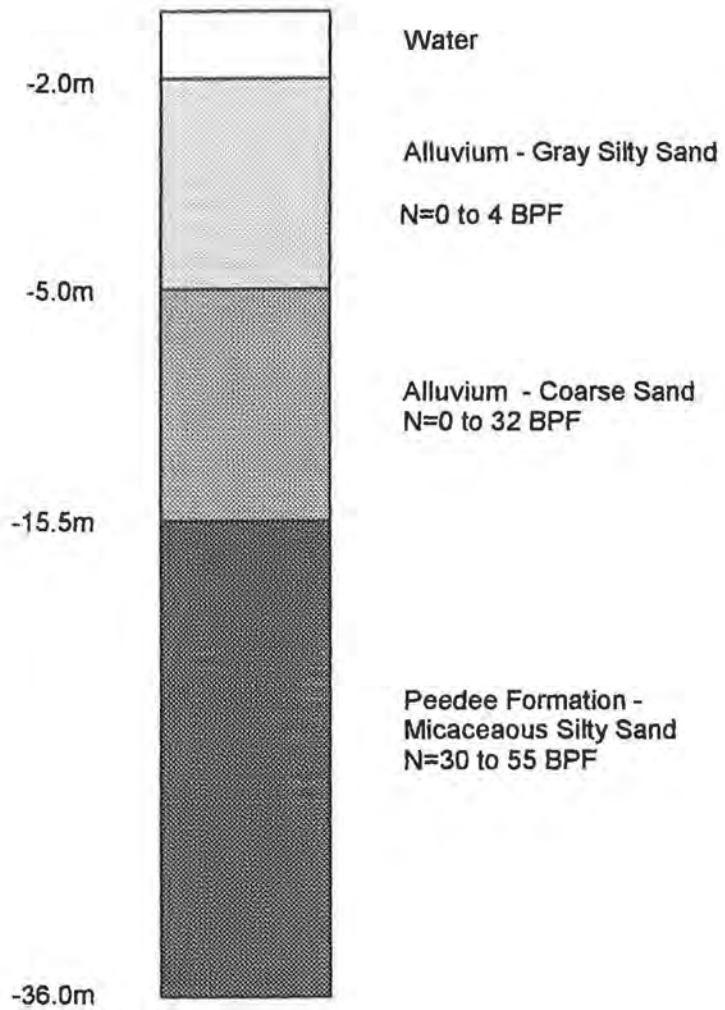
<i>Table D-15. Axial Soil Model, Test Area 1, Wilmington</i>			
Depth (m)	Shear Modulus (kPa)	Poisson's Ratio	$\tau_{\max}$ (kPa)
0.00	414	0.3	13.9
2.54	724	0.3	24.1
2.54	1241	0.3	414
15.24	10341	0.3	414

<i>Table D-16. P-multiplier Scaling Factor</i>			
Load Case	Scale Factor	Load Case	Scale Factor
1 (static)	1.00	6	1.30
2	1.10	7	1.40
3	1.15	8	1.50
4	1.20	9	1.60
5	1.25	10	1.70

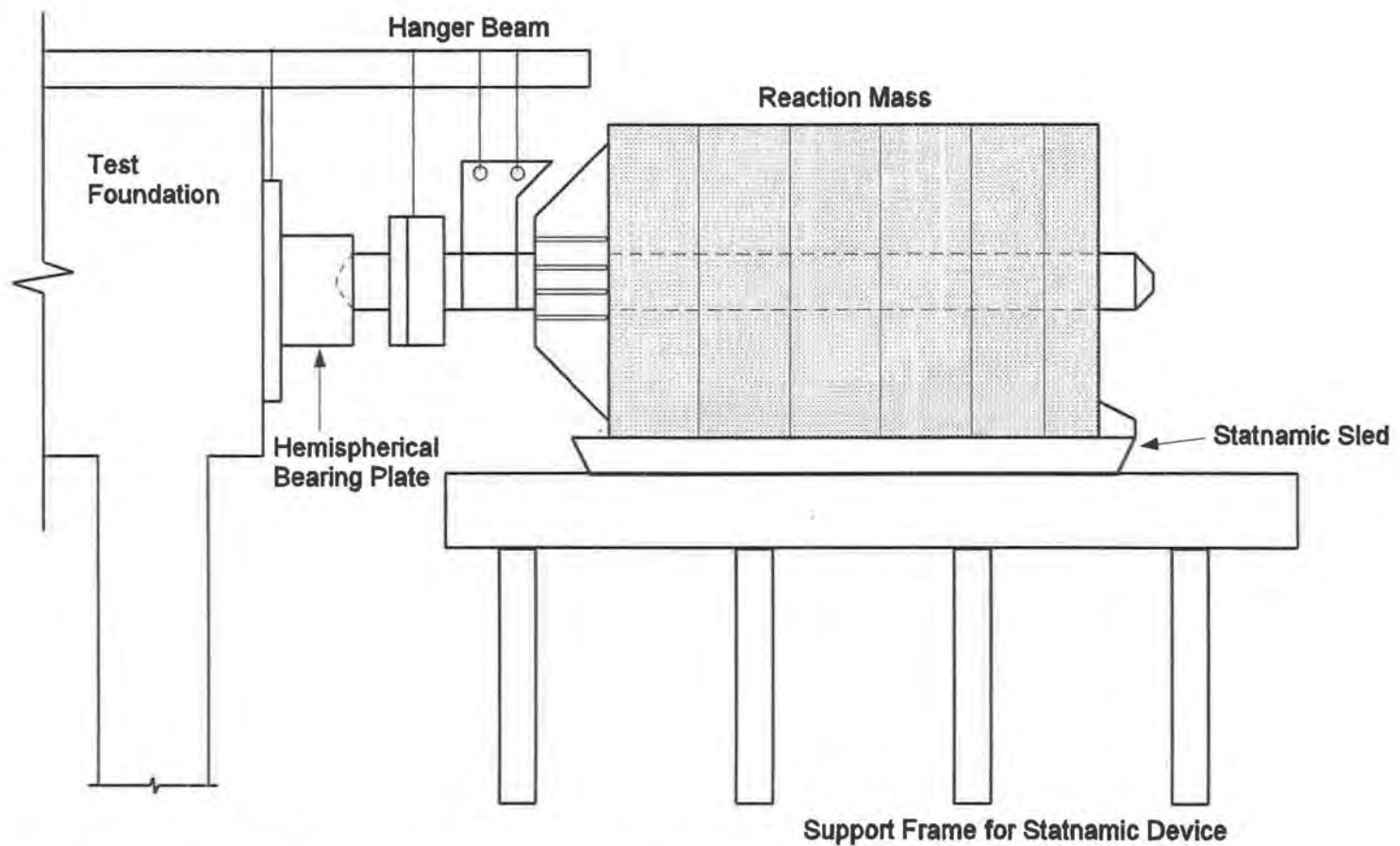


*Figure D-1. Soil Profile, Test Area 1*





*Figure D-2. Soil Profile, Test Area 2*



1. Statnamic device is placed against test foundation
2. Pelletized fuel inside piston is ignited
3. Expanding gases push reaction mass away from foundation imparting equal and opposite thrust on the foundation

*Figure D-3. Schematic of Statnamic Load Test*

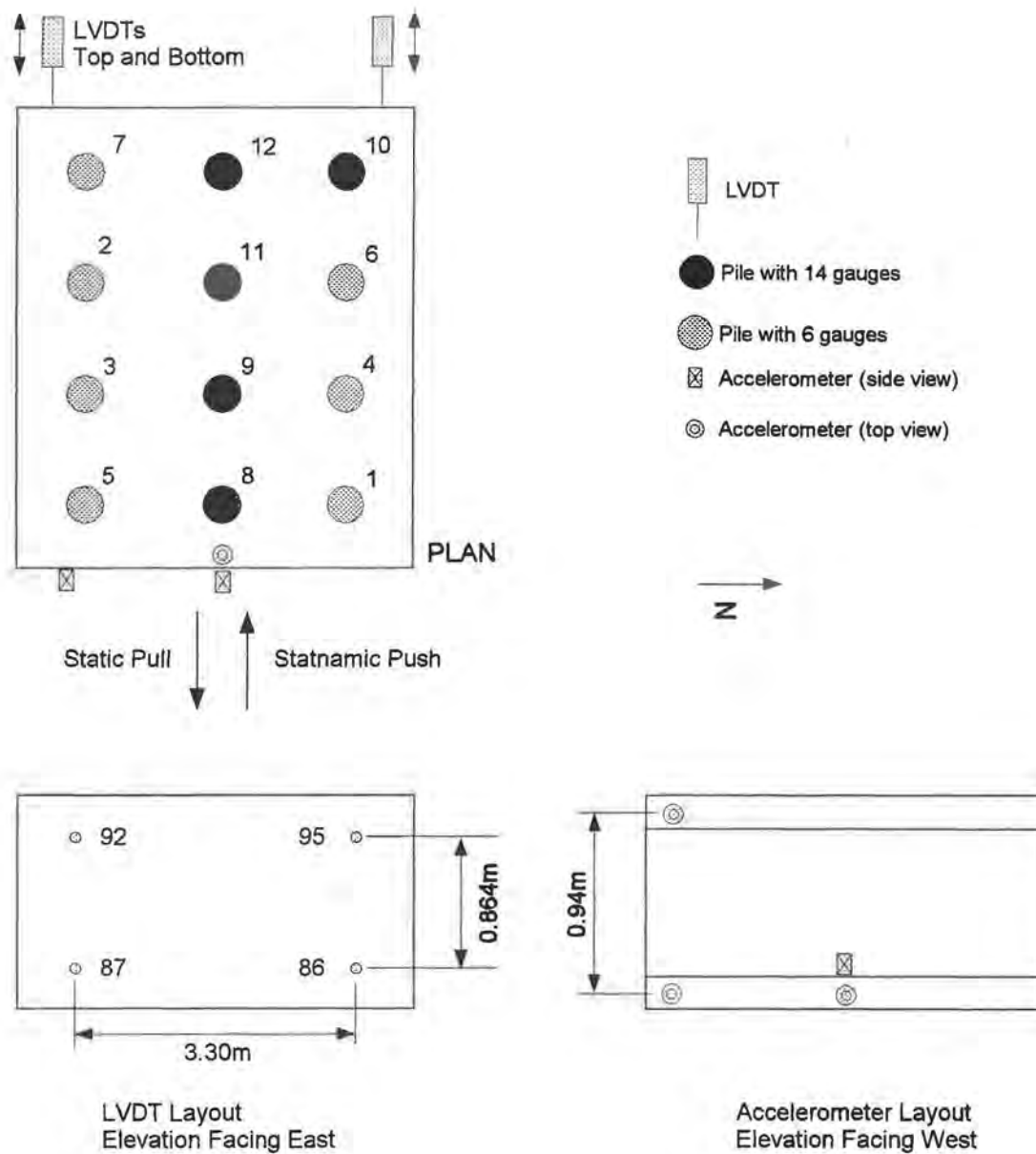


Figure D-4. Instrumentation - Pile Group, Test Area 1

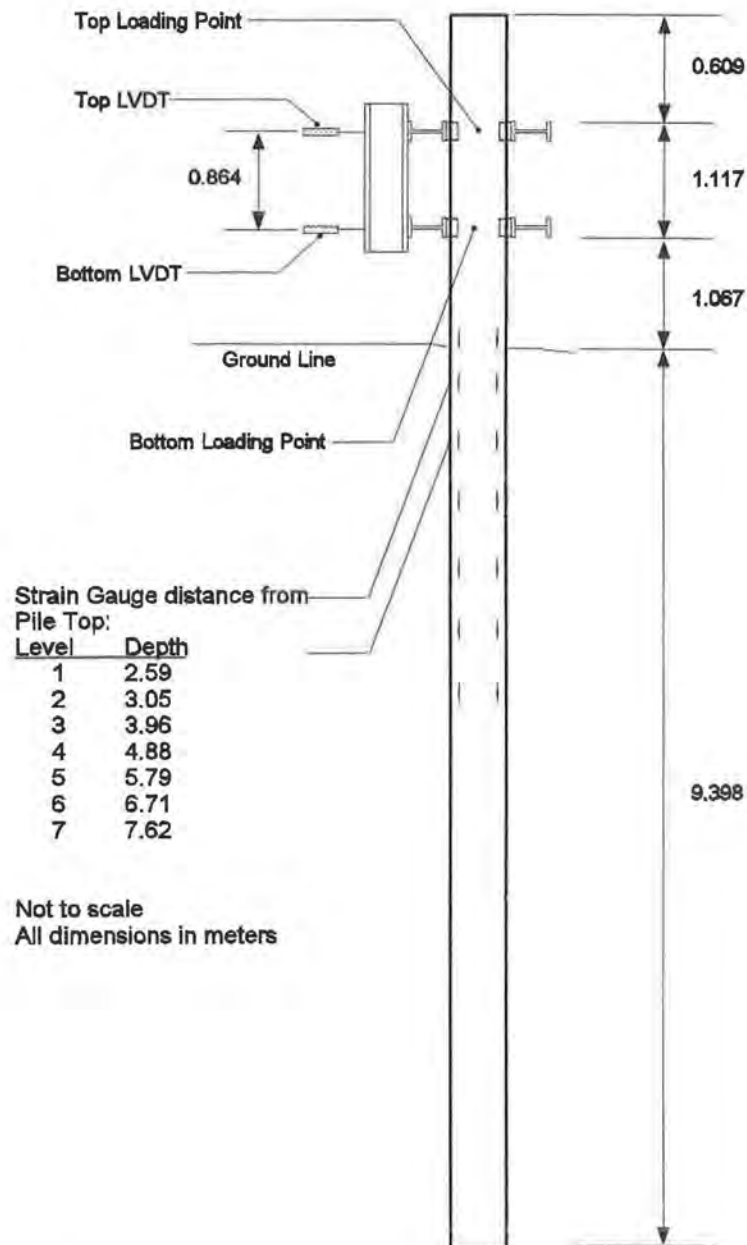
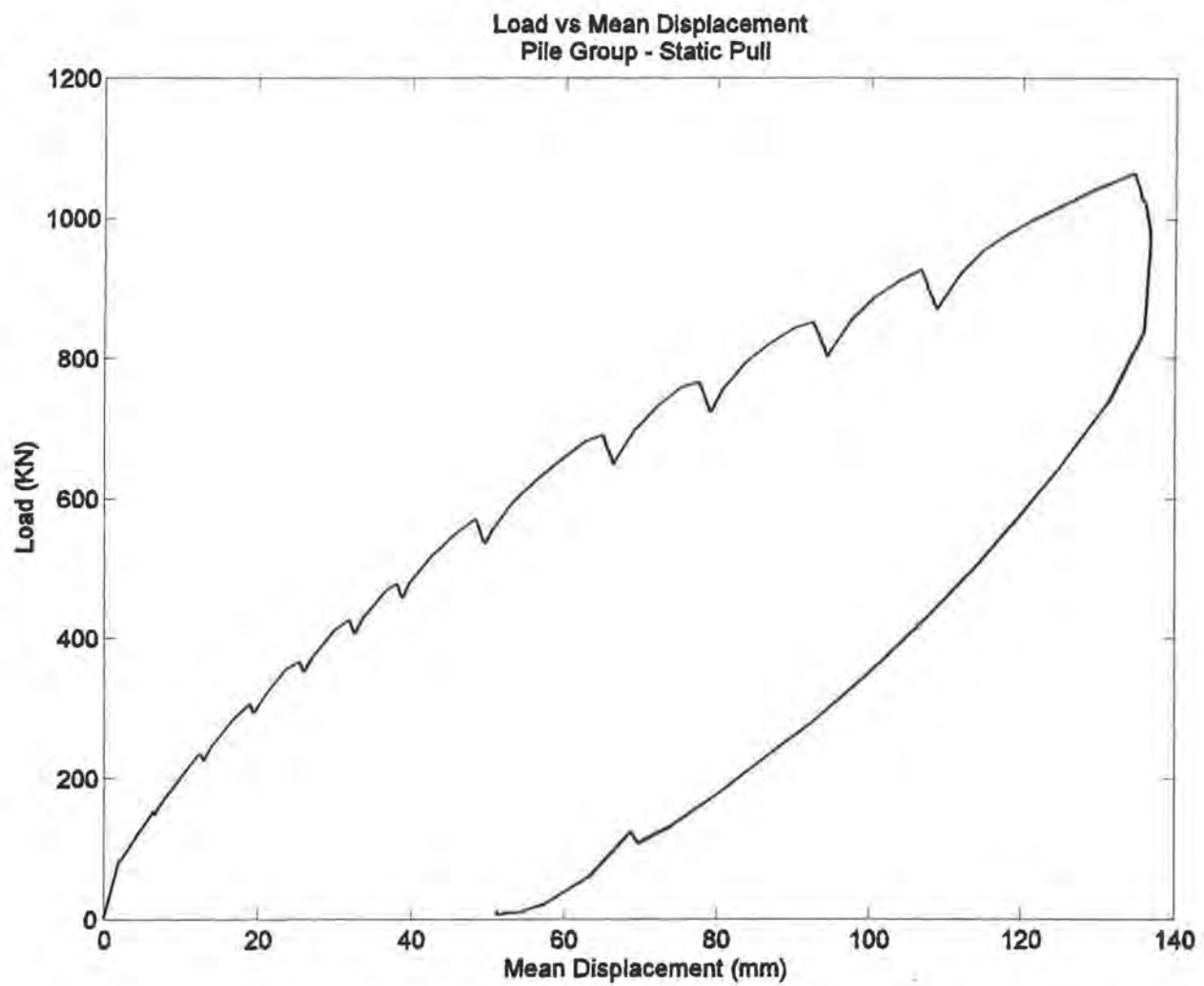
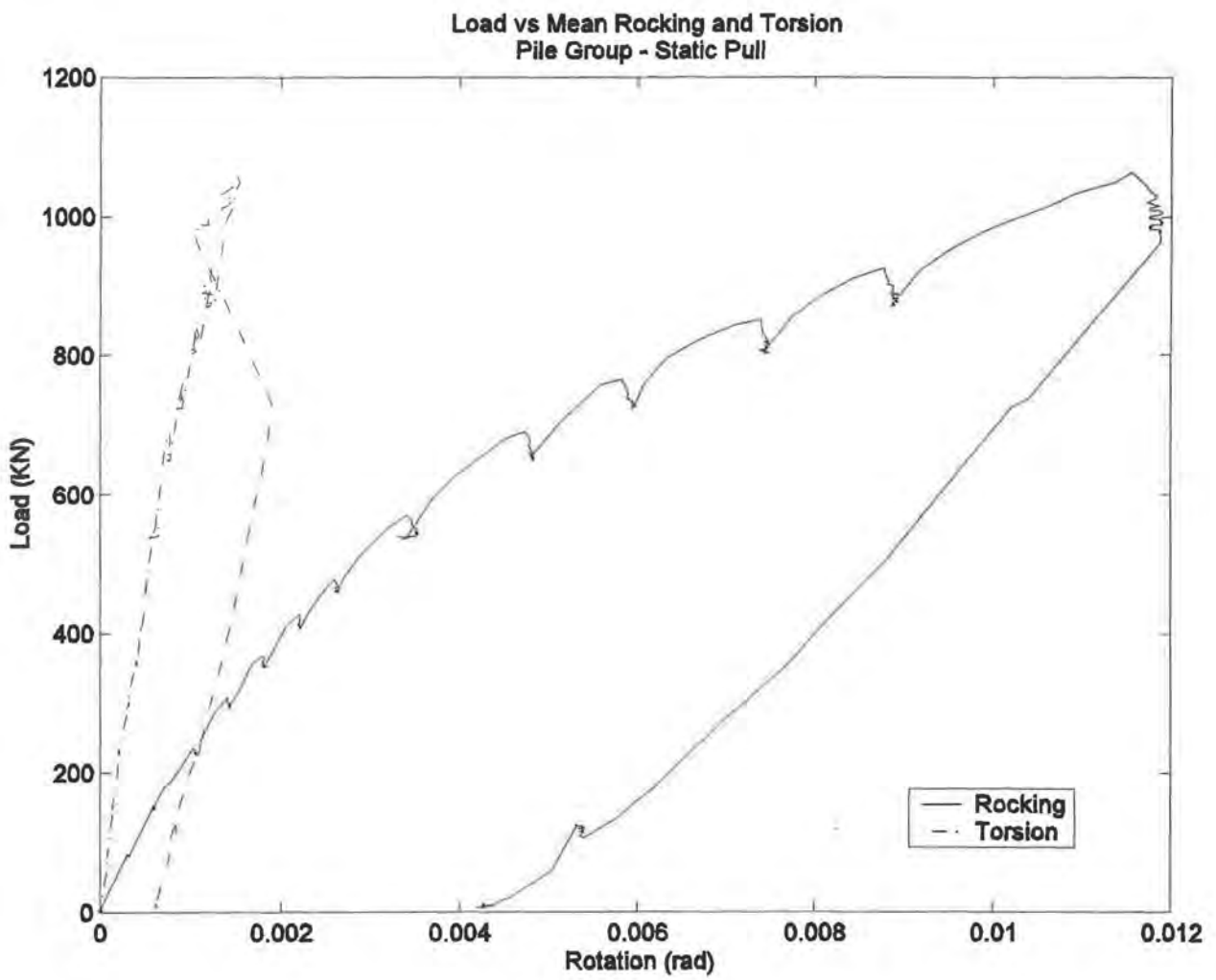


Figure D-5. Load Transfer Setup, Pile Group, Test Area 1

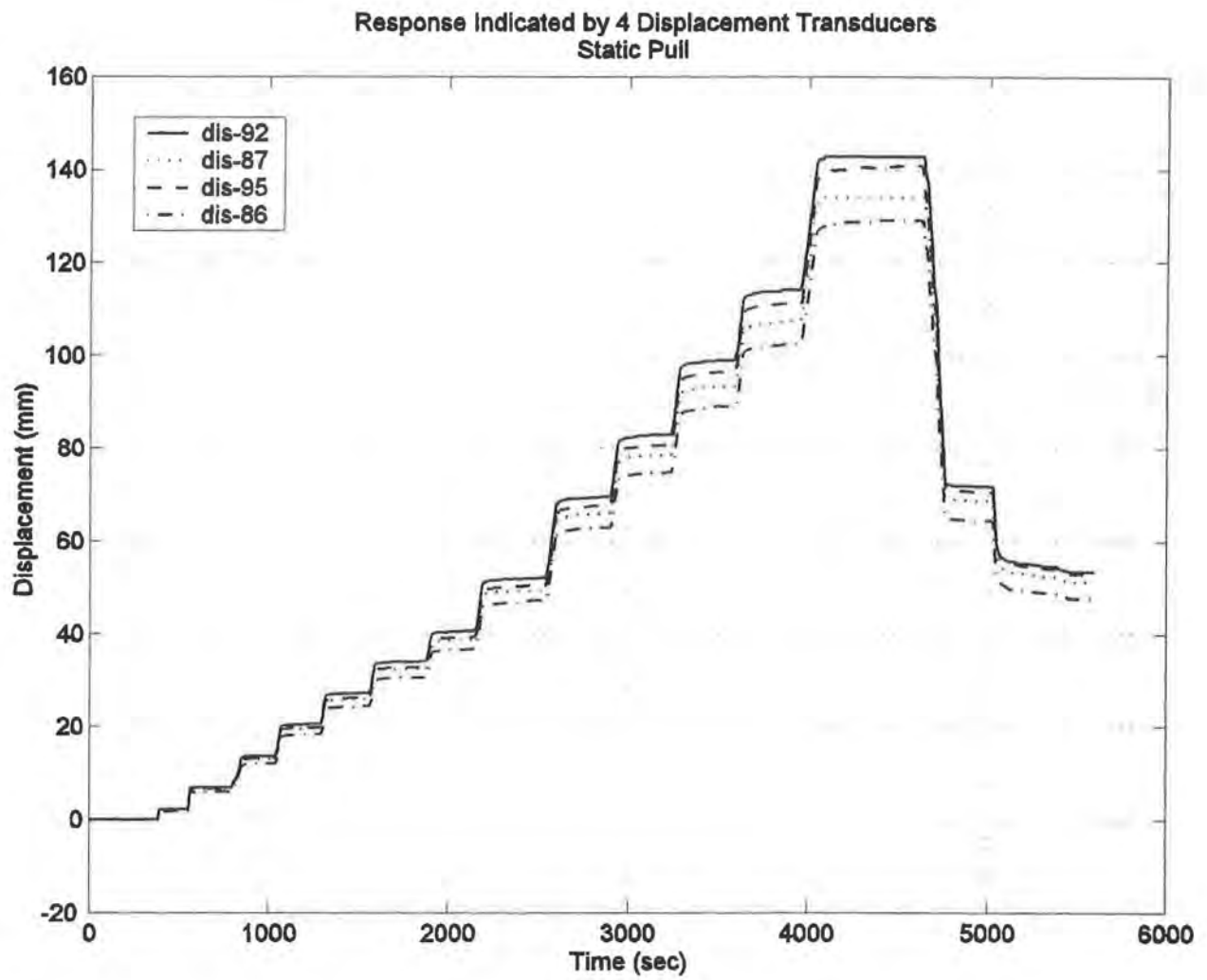


*Figure D-6. Load vs Mean Displacement, Pile Group, Static Load Test*





*Figure D-7. Load vs. Mean Rocking and Torsional Rotation, Static Load Test*



*Figure D-8. Displacement Response of 4 LVDTs, Static Load Test*

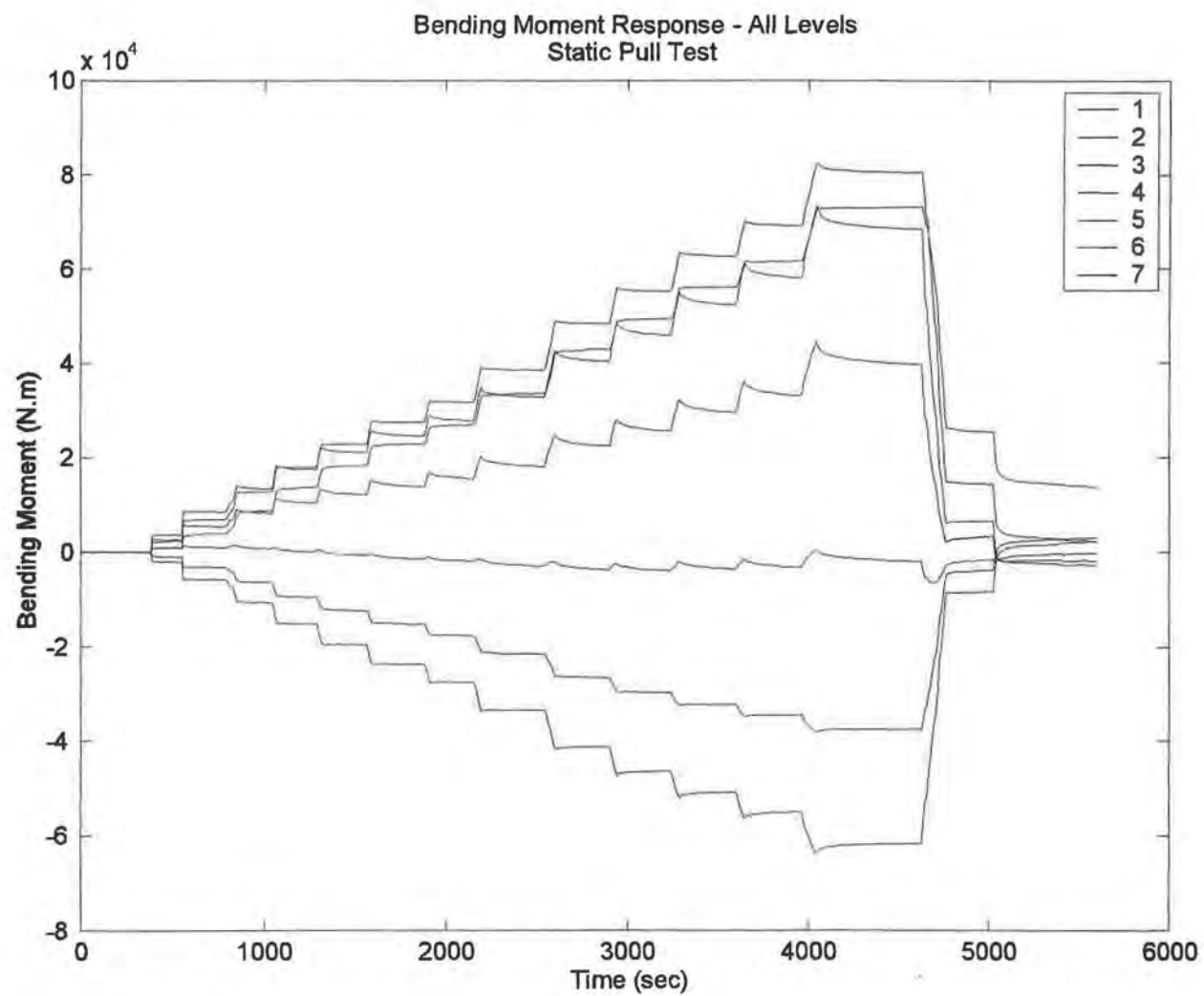


Figure D-9. Bending Moment Response, Pile 11, Static Load Test

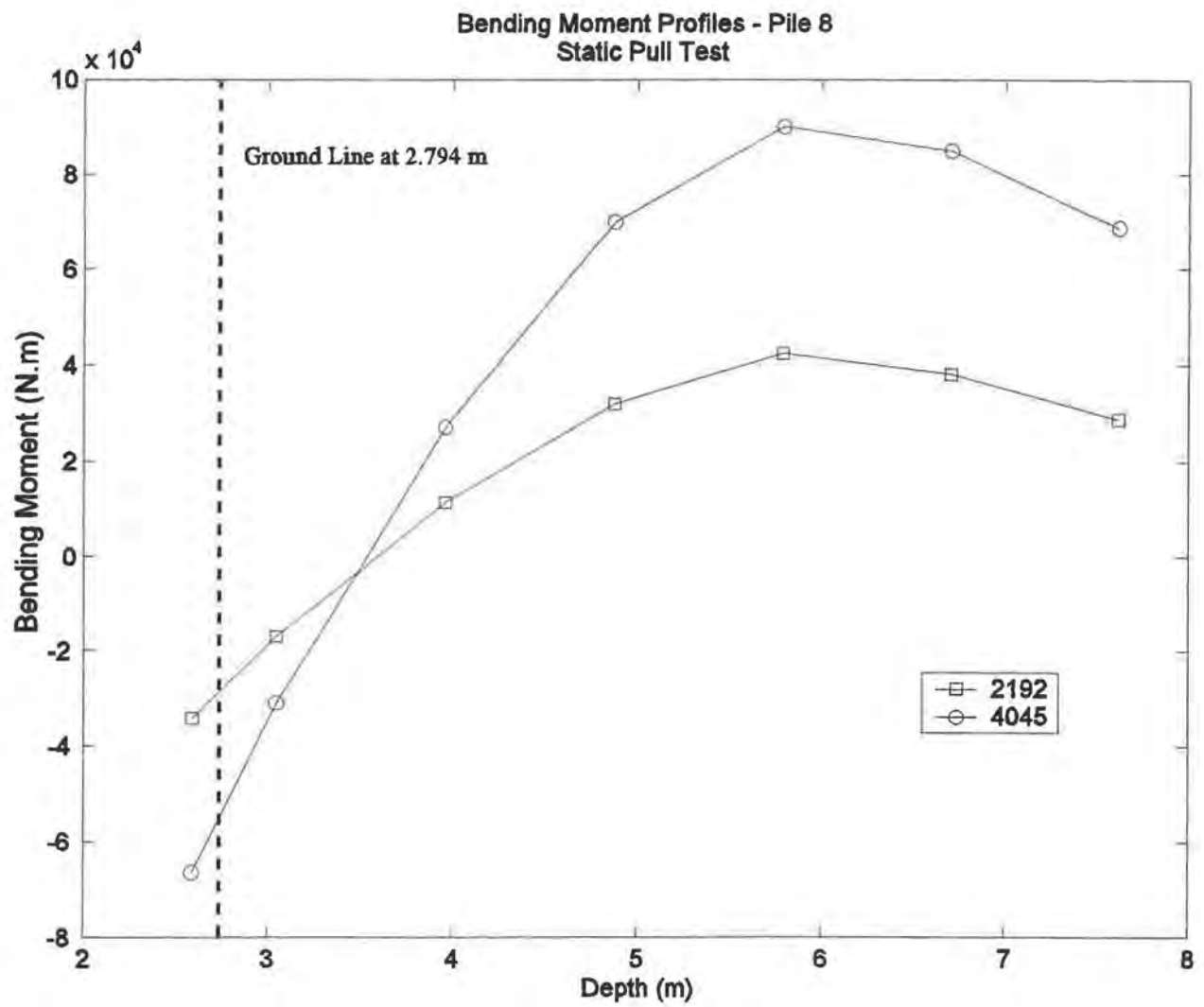
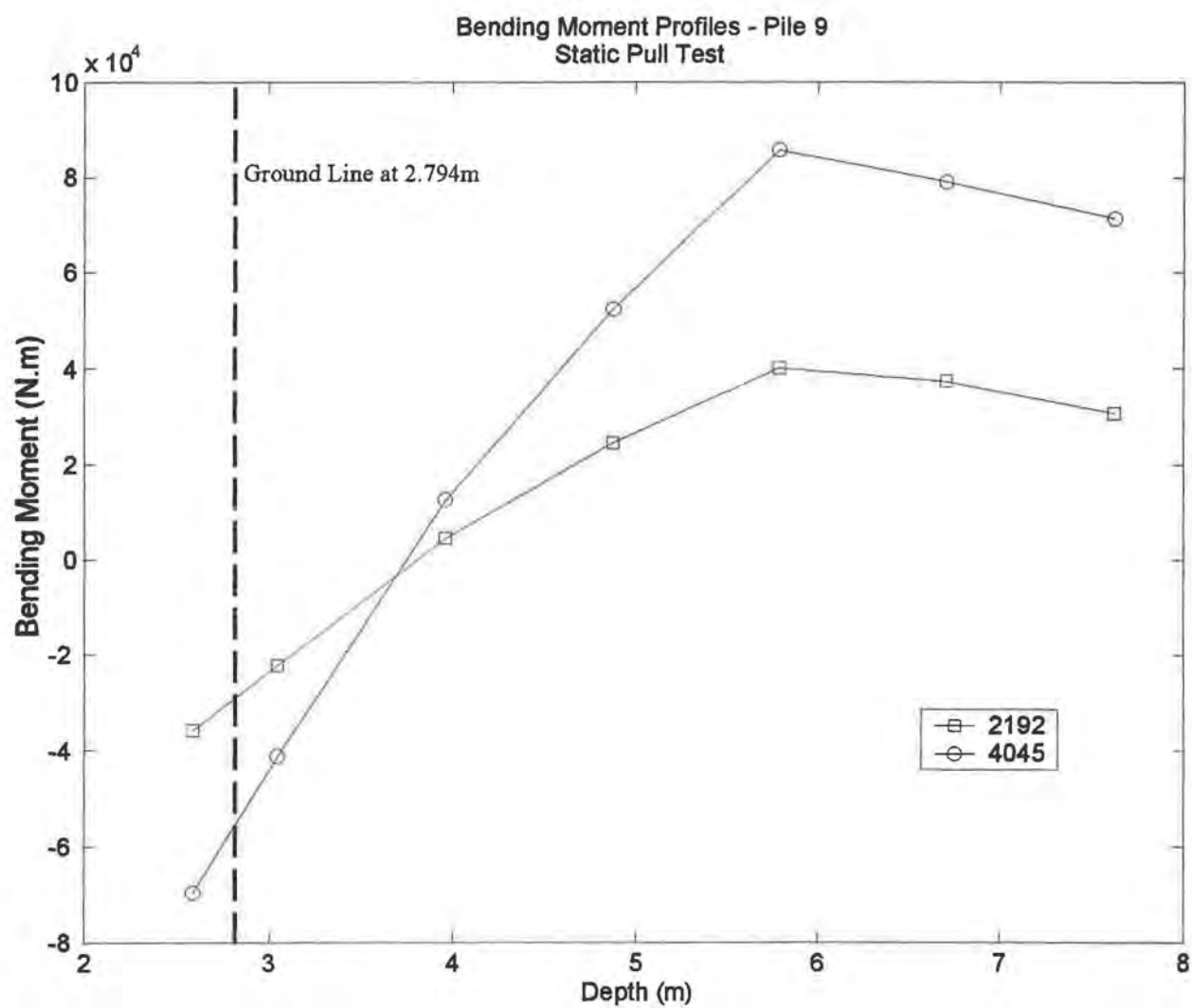
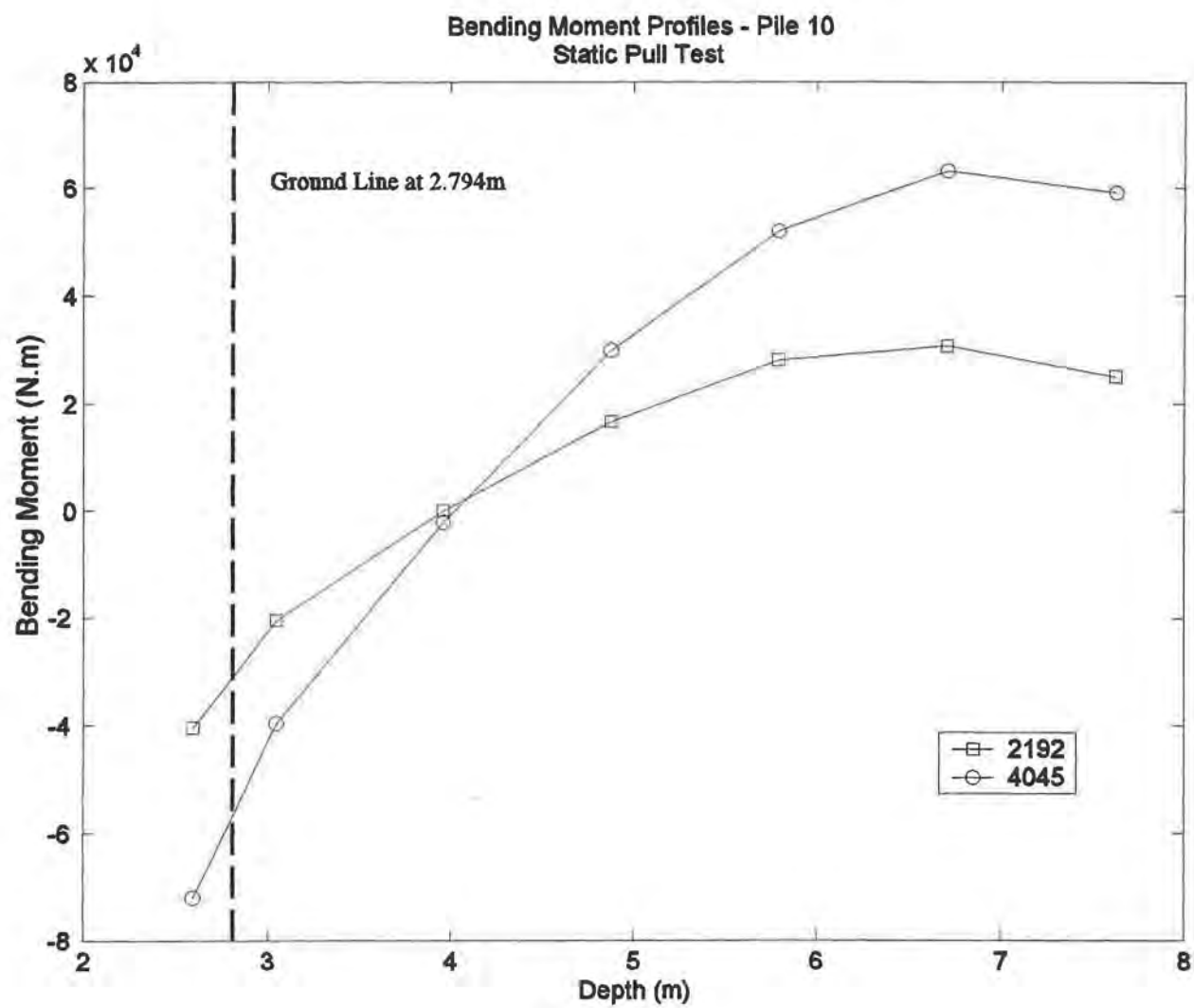


Figure D-10. Bending Moment Profiles, Pile 8, Static Load Test



*Figure D-11. Bending Moment Profiles, Pile 9, Static Load Test*



*Figure D-12. Bending Moment Profiles, Pile 10, Static Load Test*



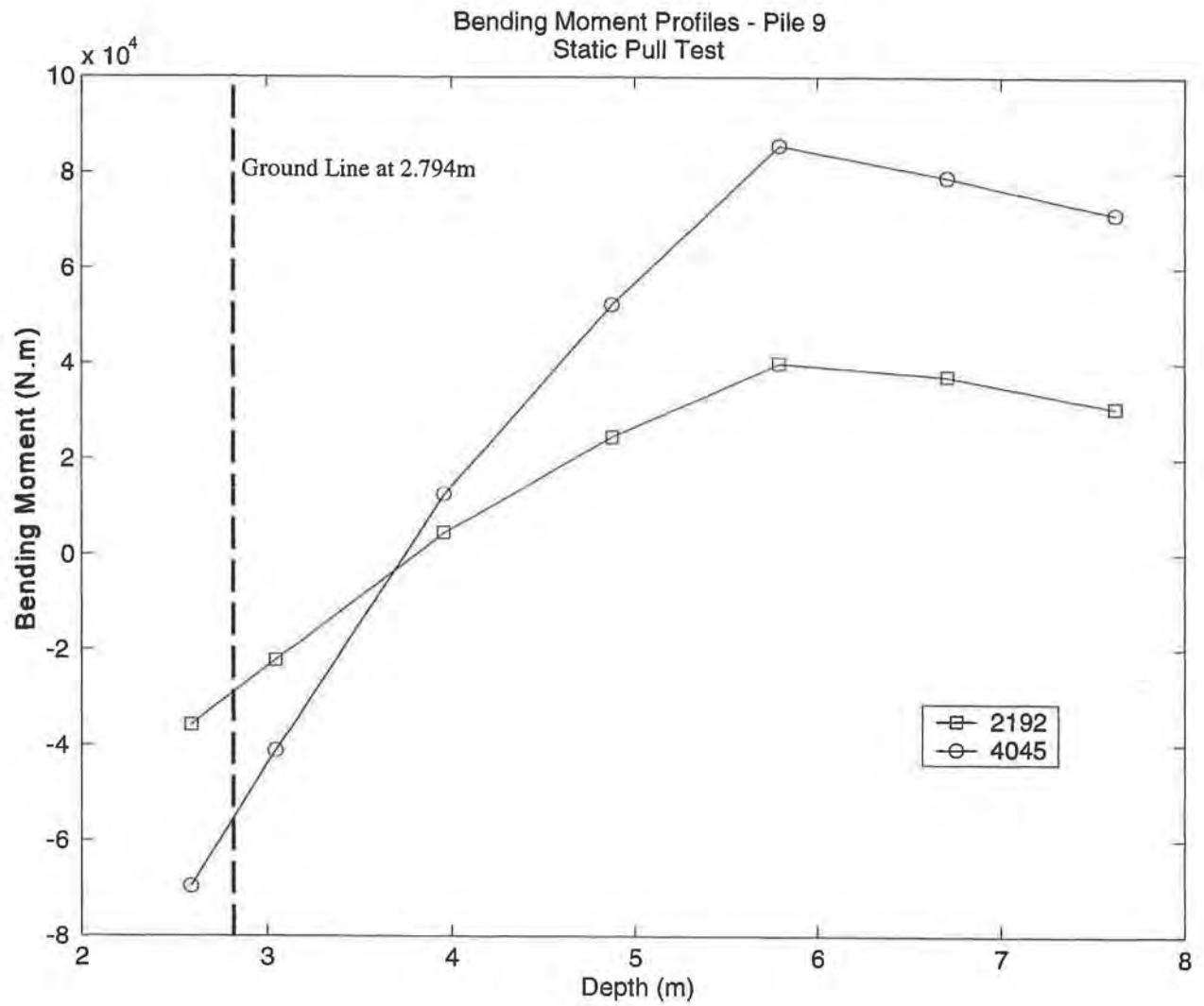


Figure D-11. Bending Moment Profiles, Pile 9, Static Load Test

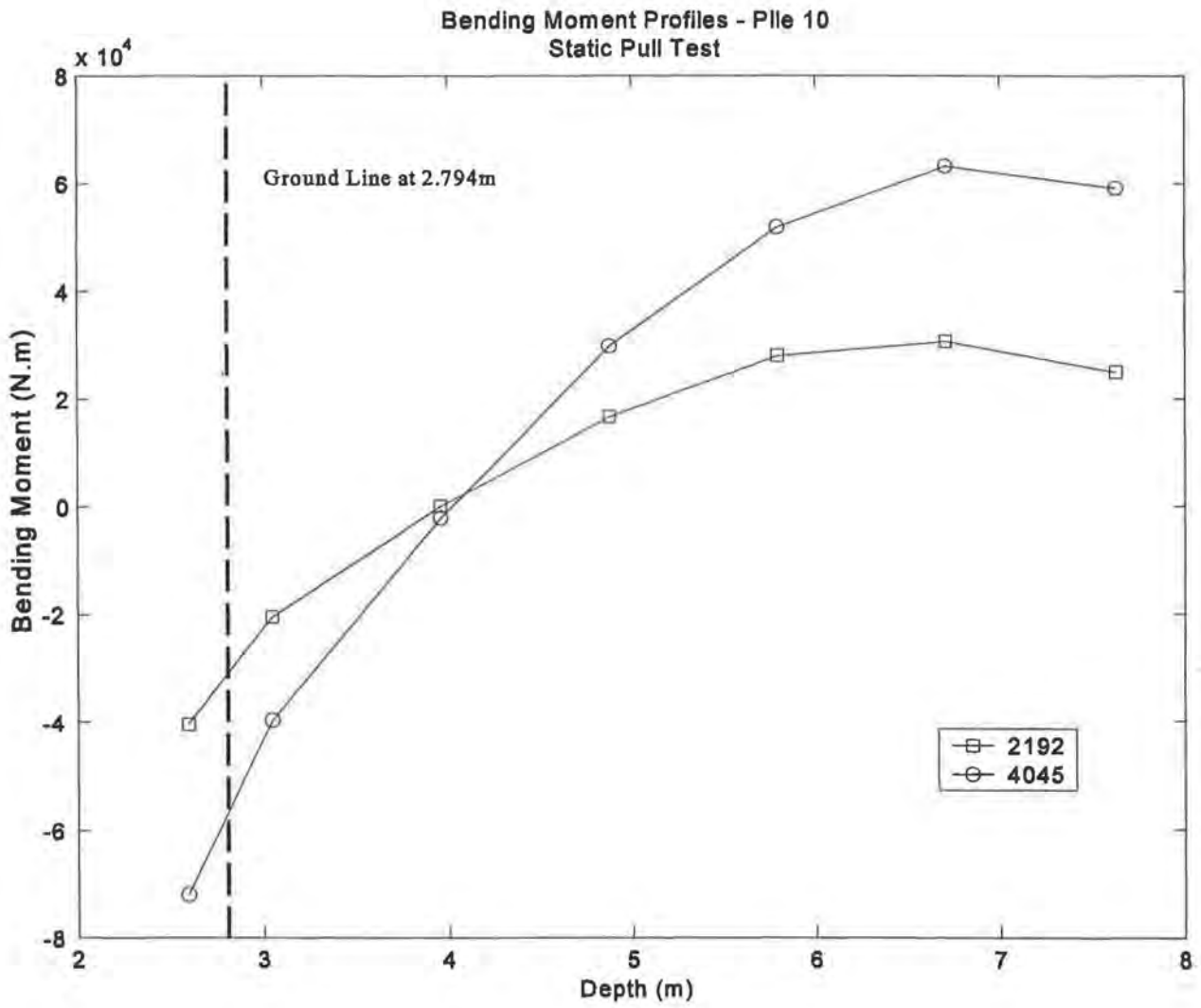
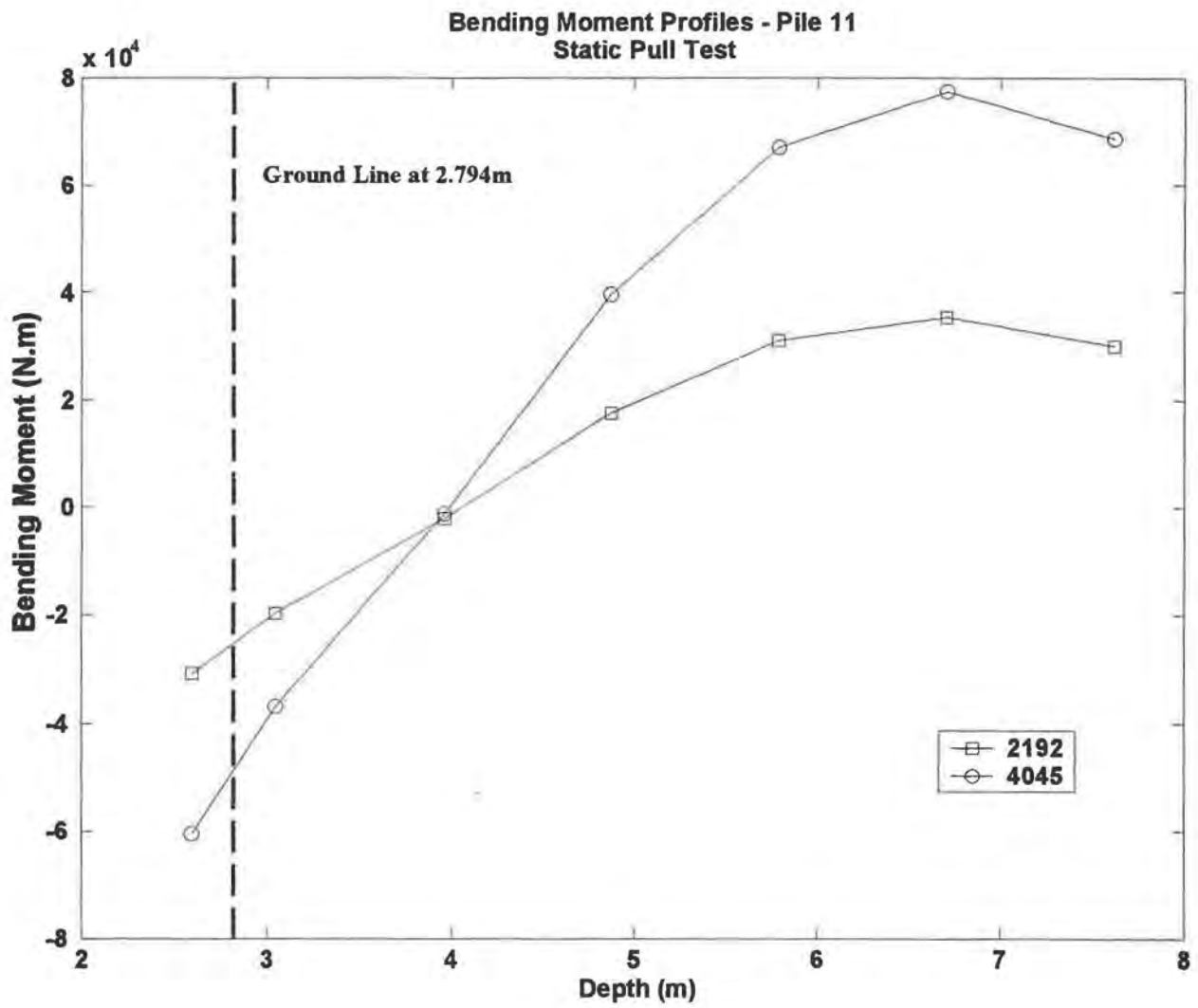


Figure D-12. Bending Moment Profiles, Pile 10, Static Load Test



*Figure D-13. Bending Moment Profiles, Pile 11, Static Load Test*

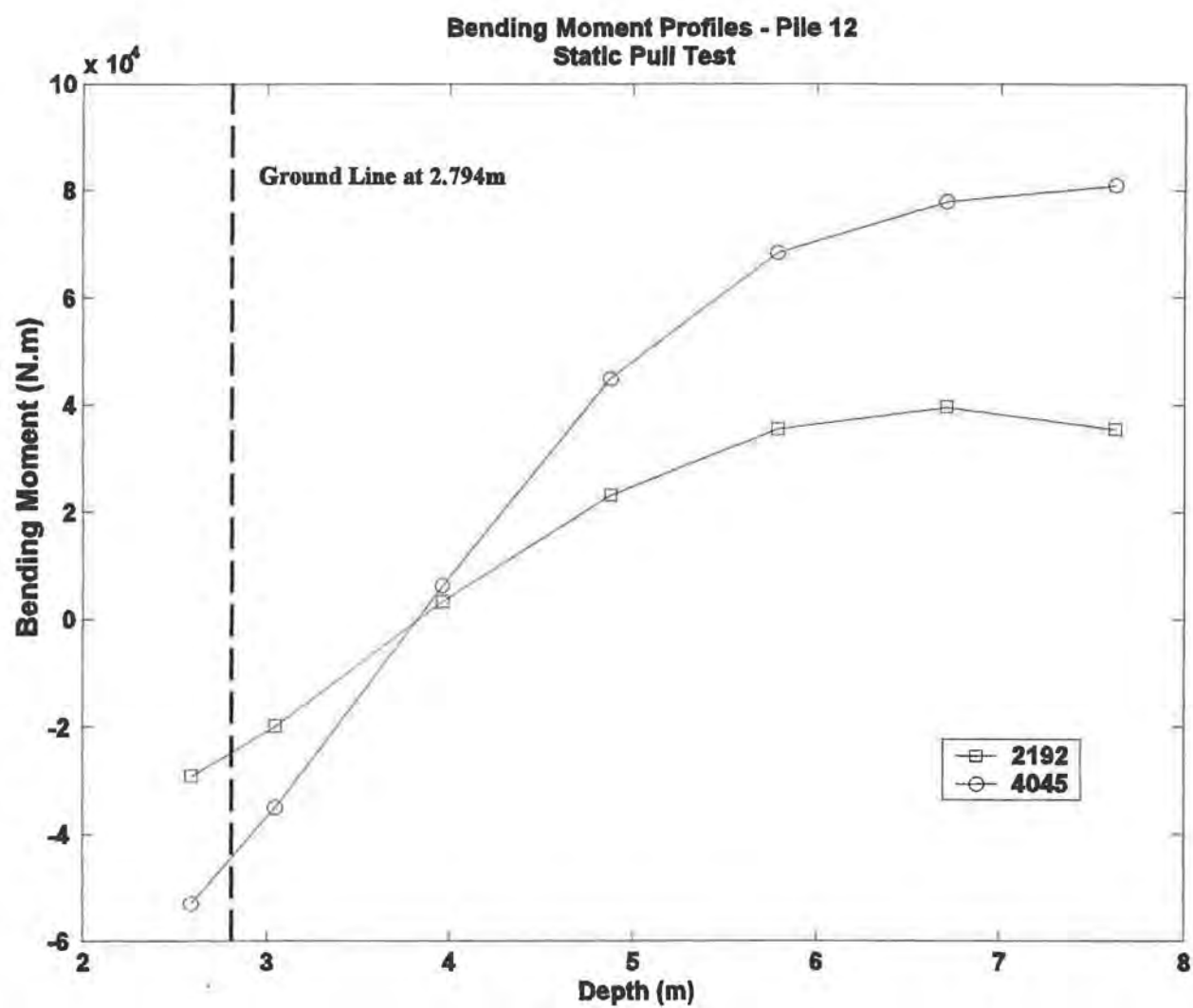



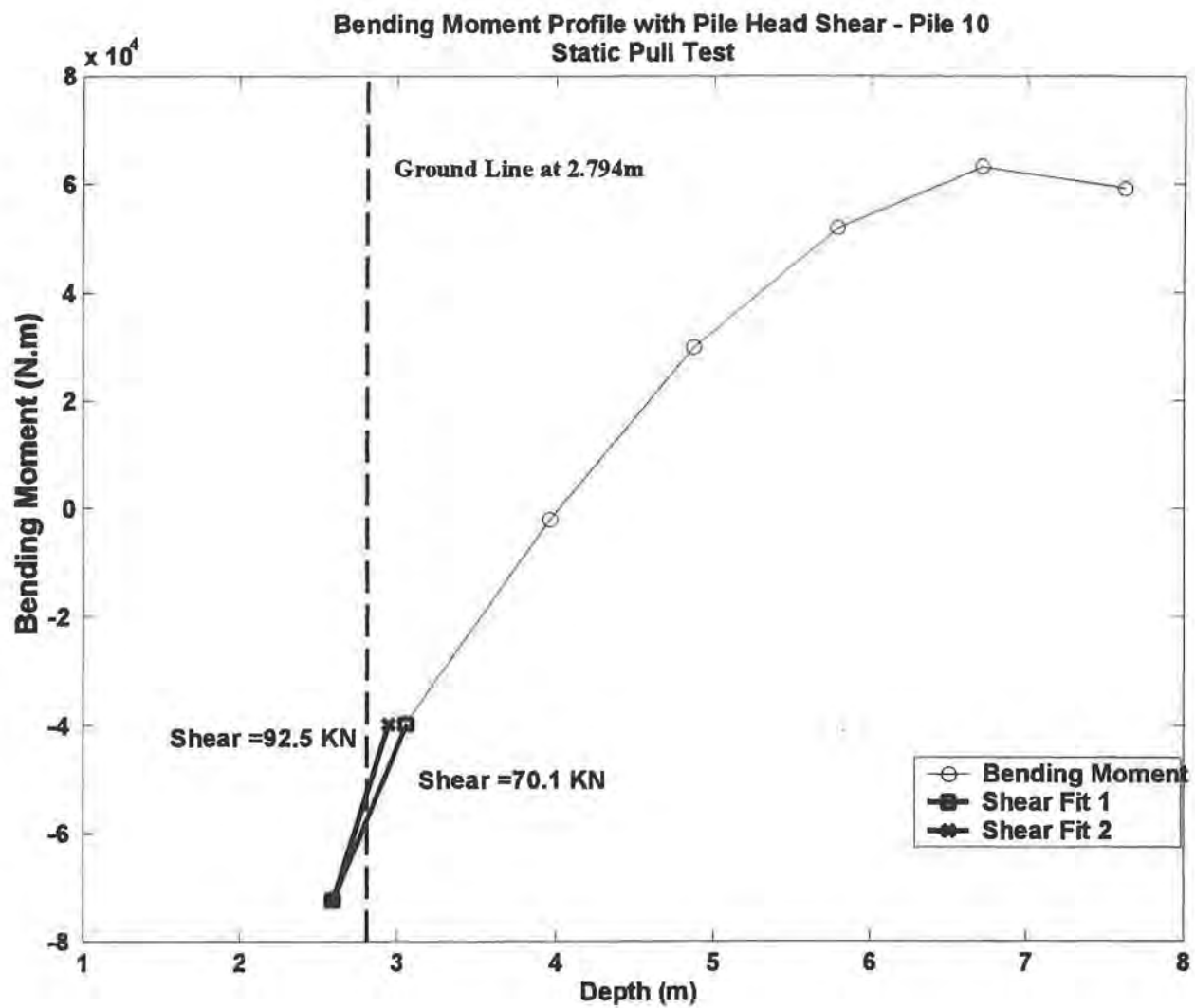
Figure D-14. Bending Moment Profiles, Pile 12, Static Load Test

Load Transferred to Individual Piles (KN)			Load Transferred To Row (KN)	% Load Transferred
<div>7</div> <div>[53.6,33.7]</div>	<div>12</div> <div>[42.7,24.4]</div>	<div>10</div> <div>[70.1,30.2]</div>	[166.4,88.3]	[25 / 26]
<div>2</div> <div>[55.2,29.7]</div>	<div>11</div> <div>[50.2,24.7]</div>	<div>6</div> <div>[30.8,16.0]</div>	[136.2,70.4]	[21 / 21]
<div>3</div> <div>[64.6,34.3]</div>	<div>9</div> <div>[61.6,29.5]</div>	<div>4</div> <div>[35.5,19.2]</div>	[161.7,83.0]	[25 / 25]
<div>5</div> <div>[74.5,33.8]</div>	<div>8</div> <div>[77.4,37.6]</div>	<div>1</div> <div>[37.7,20.4]</div>	[189.6, 91.8]	[29 / 28]


 Direction of Static Load

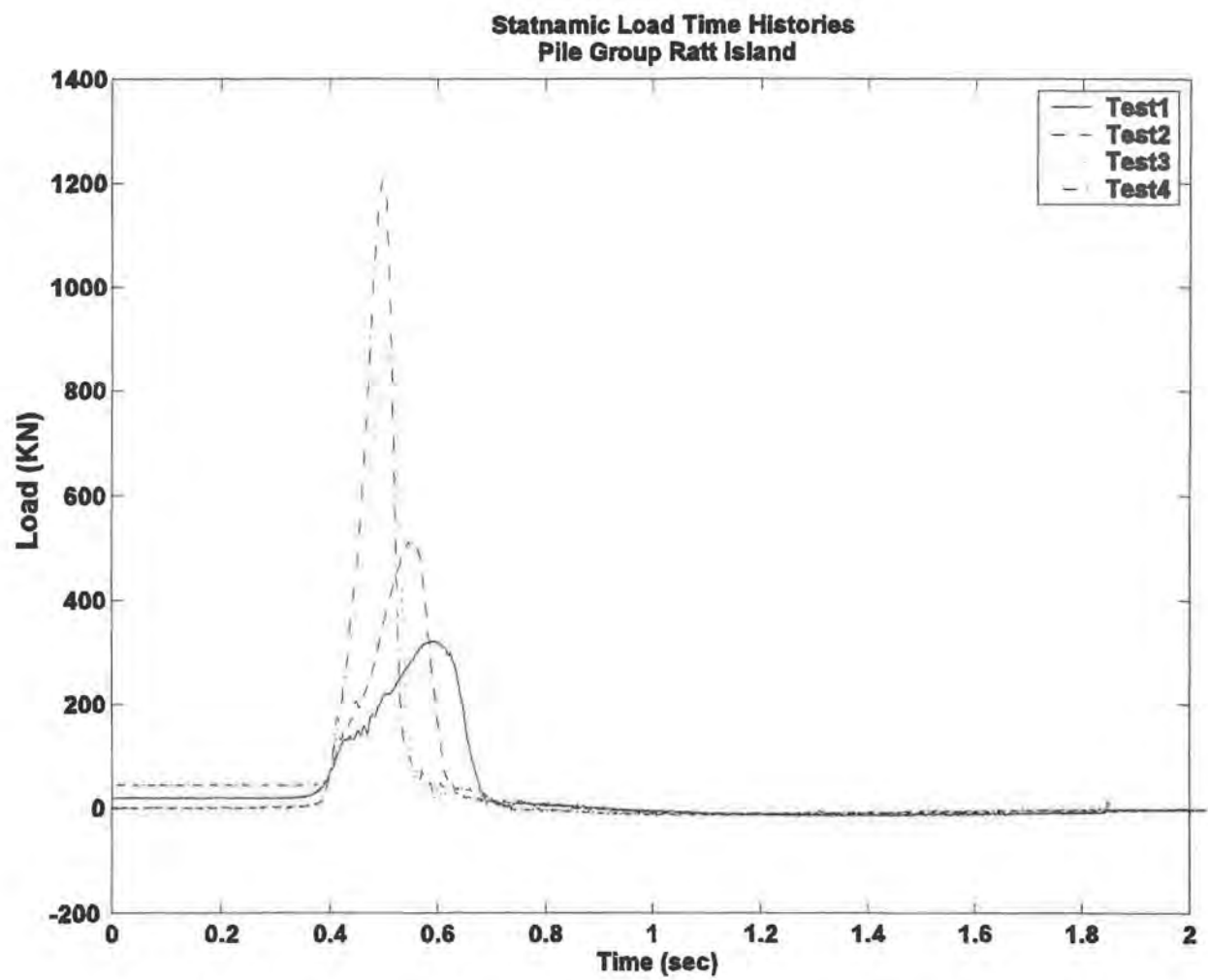
- Every circle represents one pile in the group
- The number within the circle represents the pile number
- The 2 numbers immediately to the right of a pile represent the pile head shear at loads of 1064 and 570 KN respectively
- The rightmost column of numbers indicates the total lateral load transferred to that particular row for that particular load

*Figure D-15. Static Pile-Head Shear Distribution, Test Area 1*



*Figure D-16. Pile Head Shear, Pile 10, Static Load Test*





*Figure D-17. Load Time Histories, Statnamic Tests, Test Area 1*

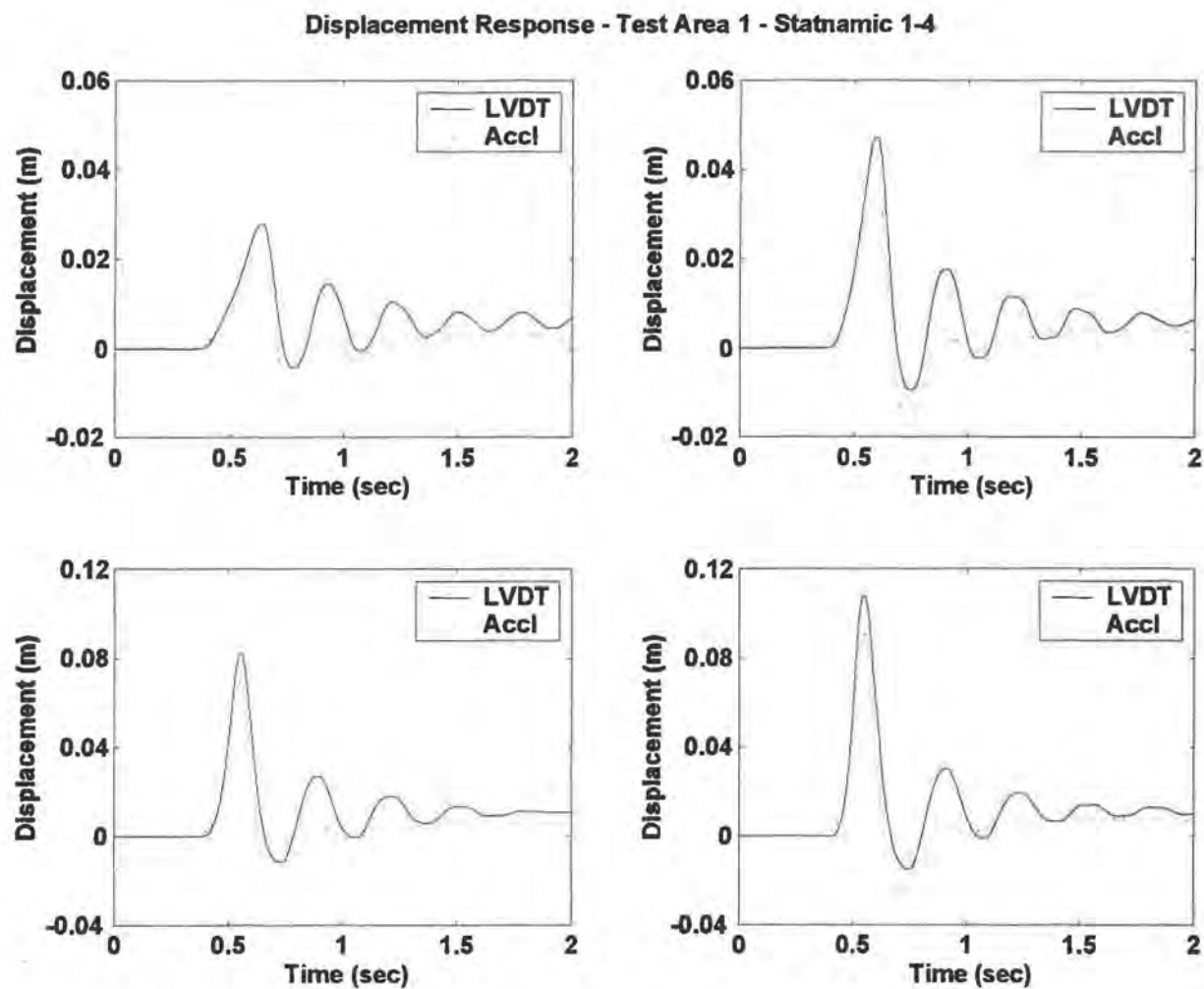
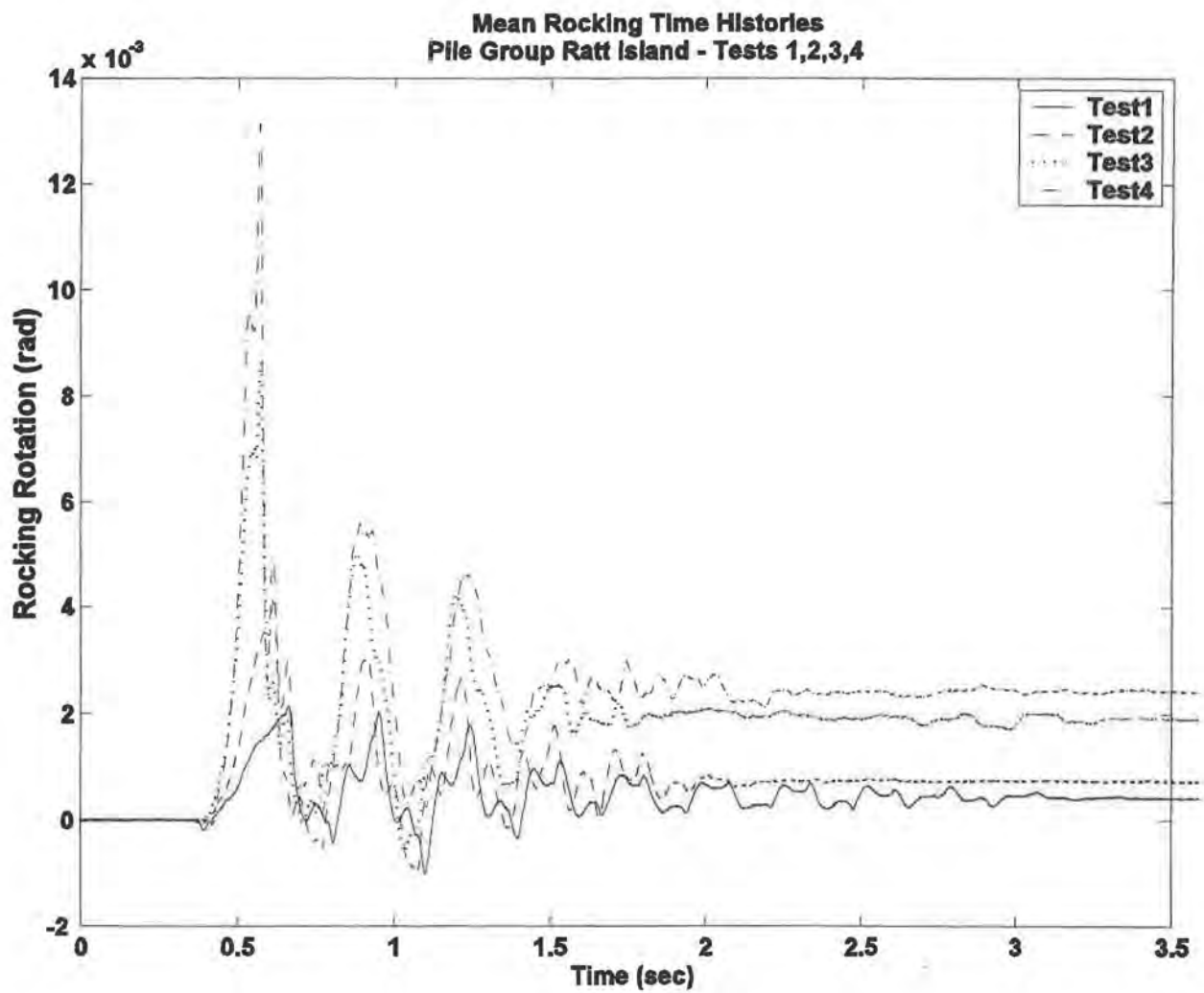
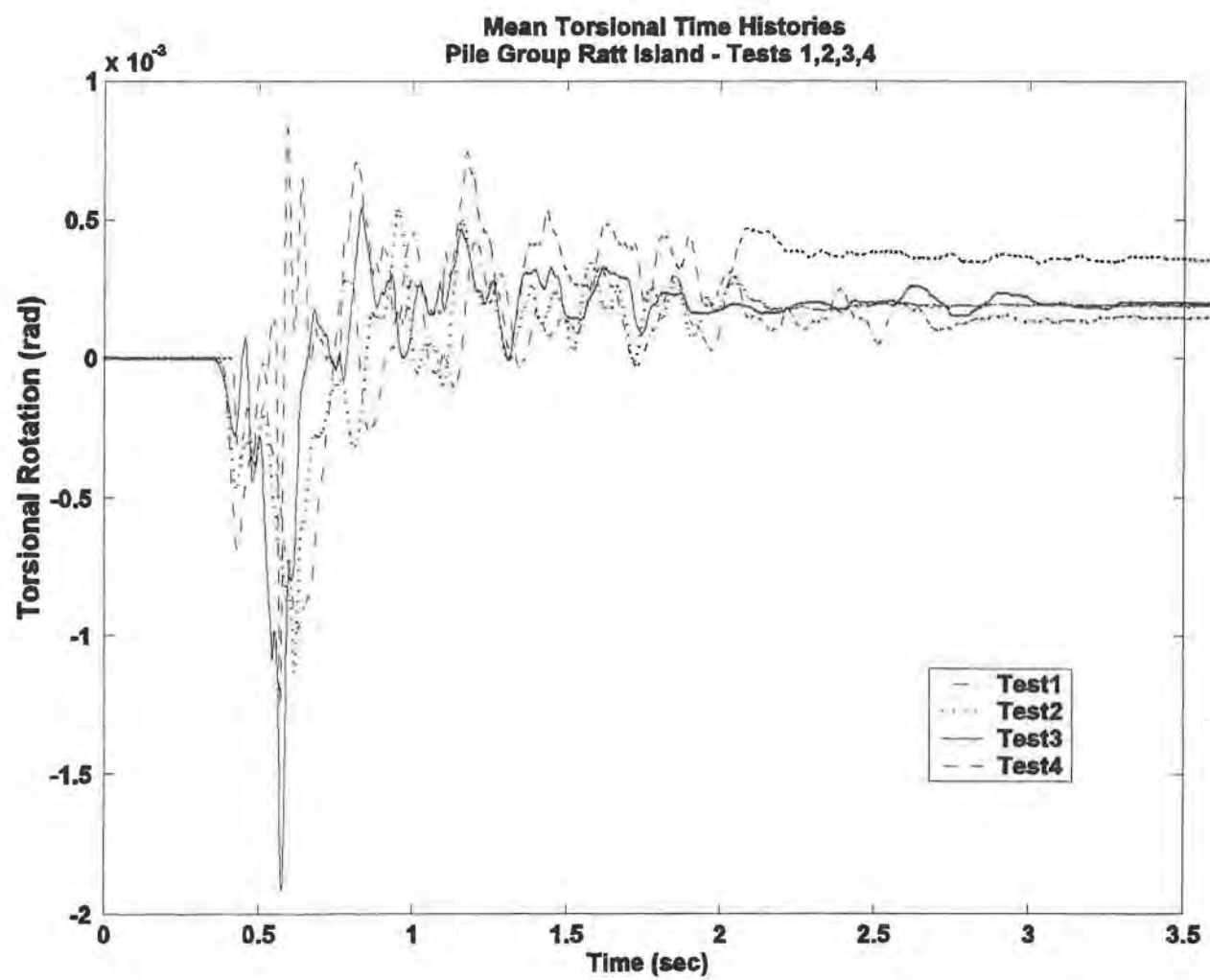


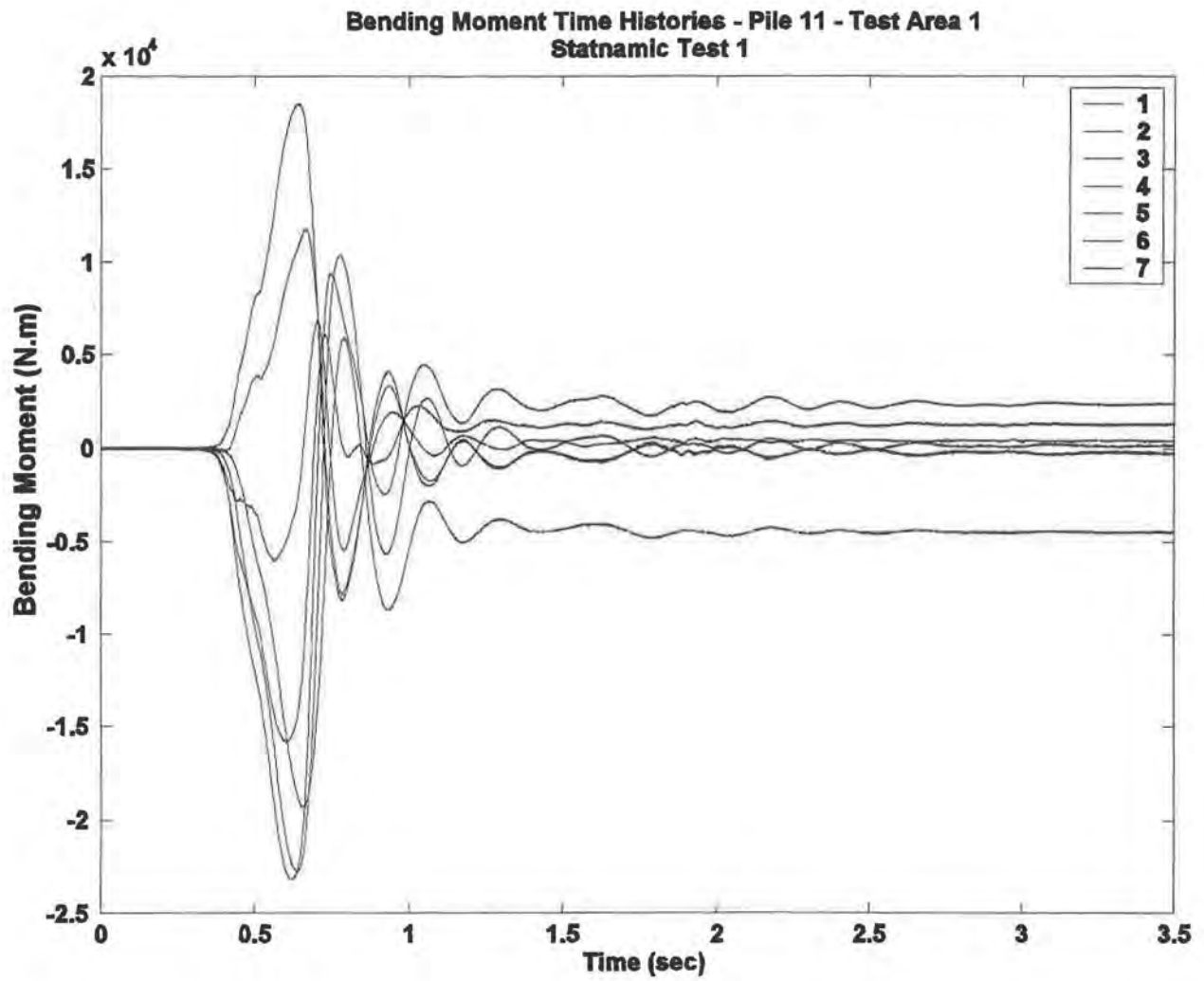
Figure D-18. Displacement Time Histories, Statnamic Tests, Test Area 1



*Figure D-19. Rocking Time Histories, Statnamic Tests, Test Area 1*



*Figure D-20. Torsional Rotation Time Histories, Statnamic Tests, Test Area 1*



*Figure D-21. Bending Moment Response, Pile 11, Statnamic 1, Test Area 1*

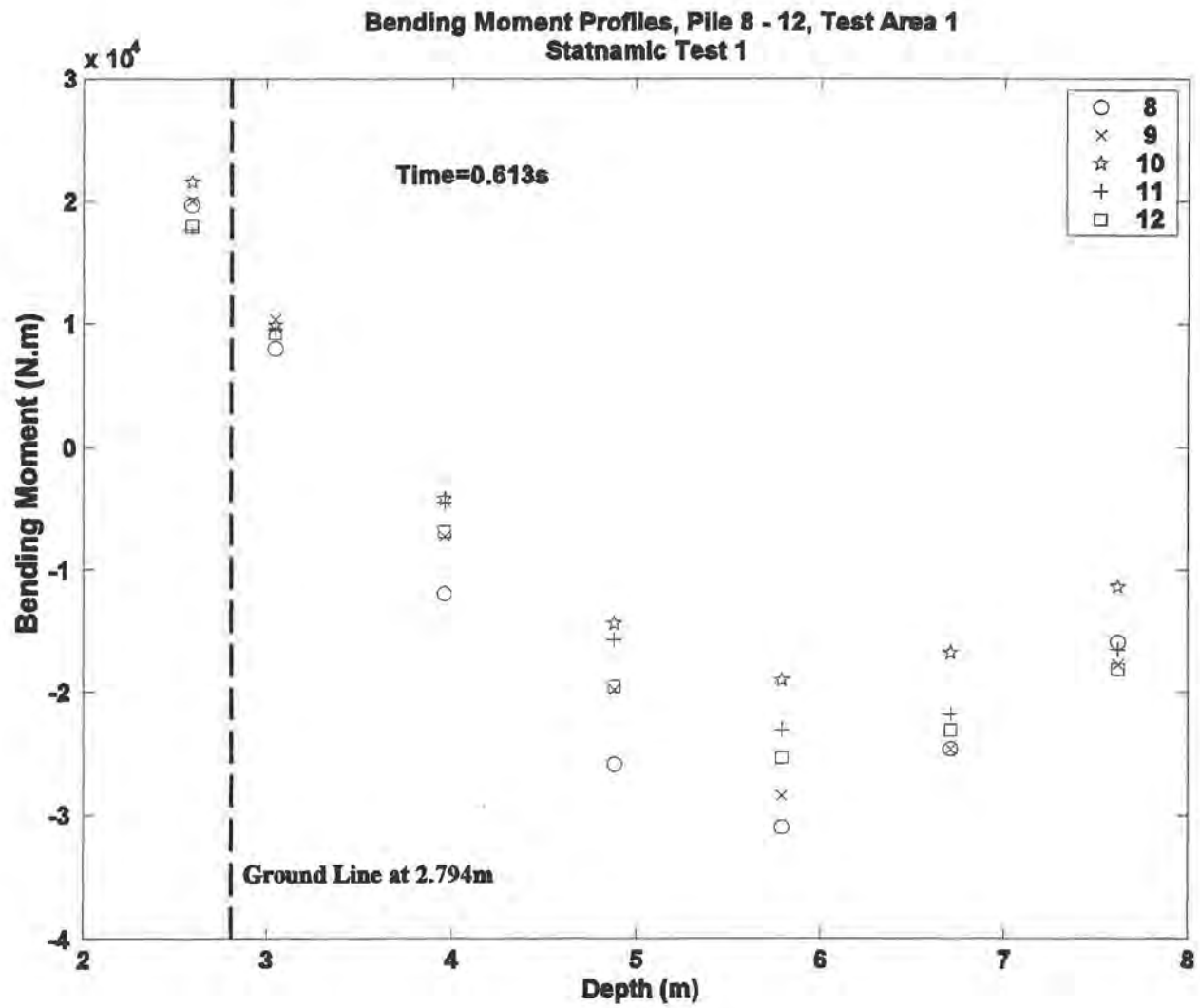
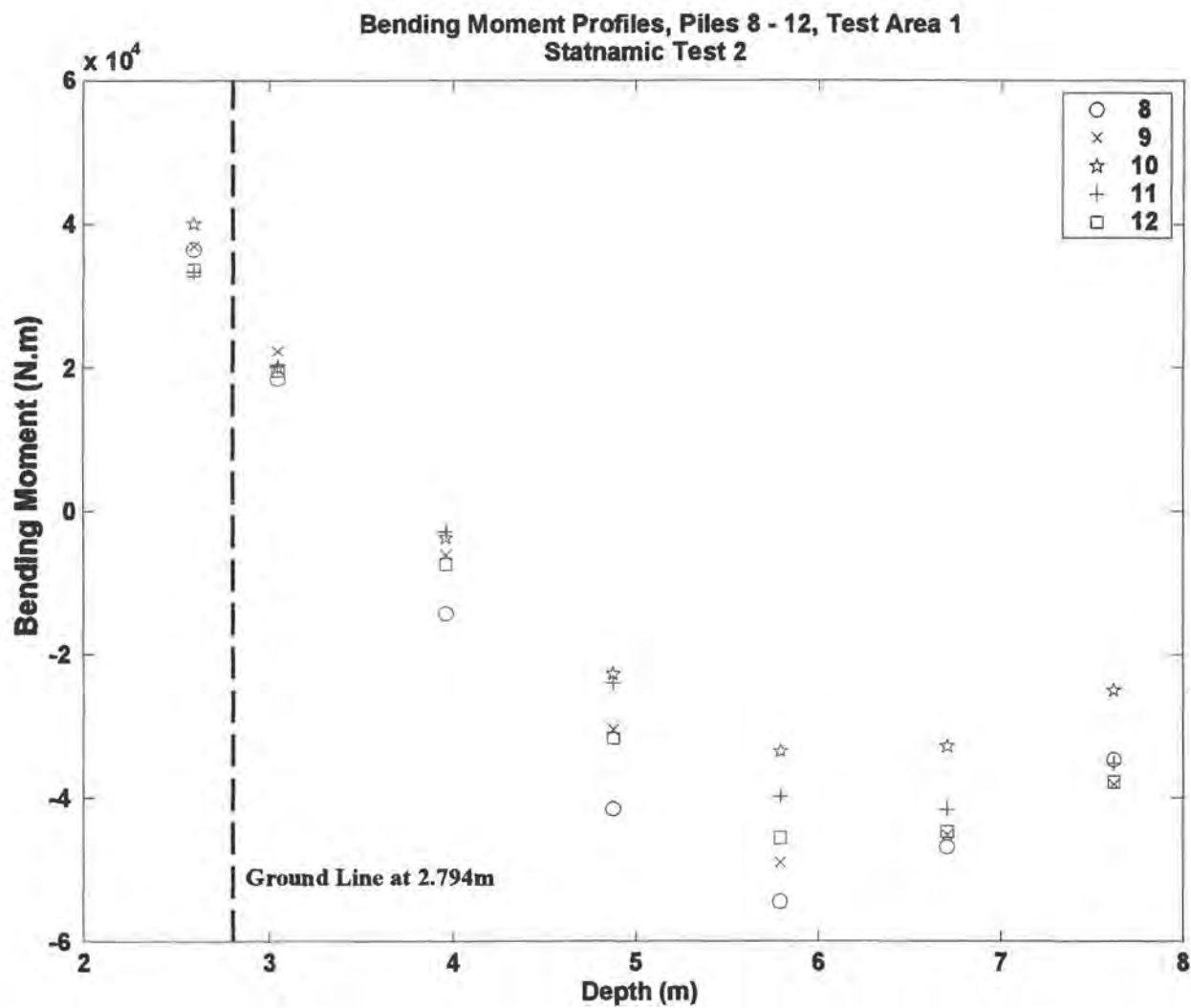


Figure D-22. Bending Moment Profiles, Statnamic 1, Test Area 1



*Figure D-23. Bending Moment Profiles, Statnamic 2, Test Area 1*



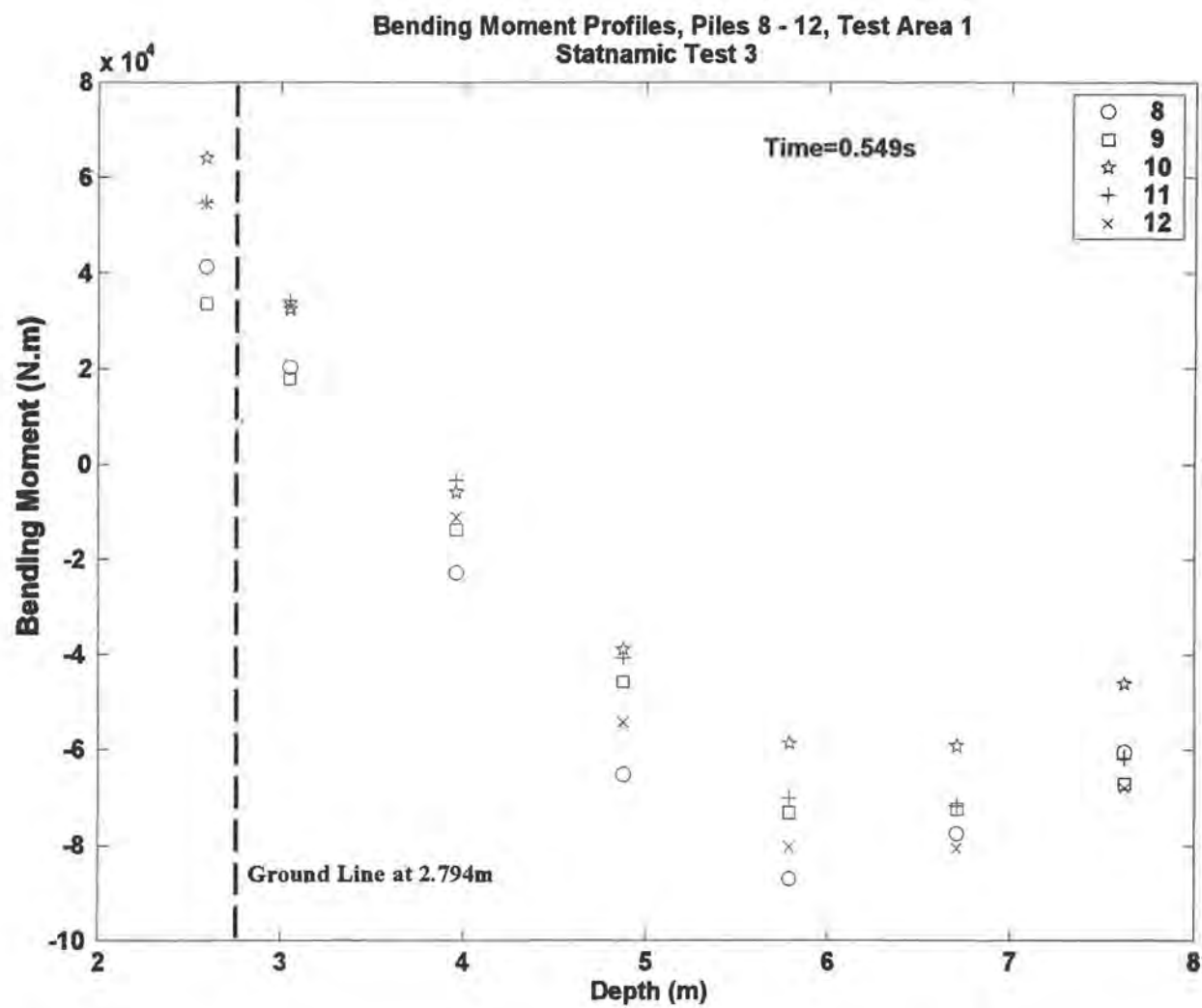


Figure D-24. Bending Moment Profiles, Statnamic 3, Test Area 1

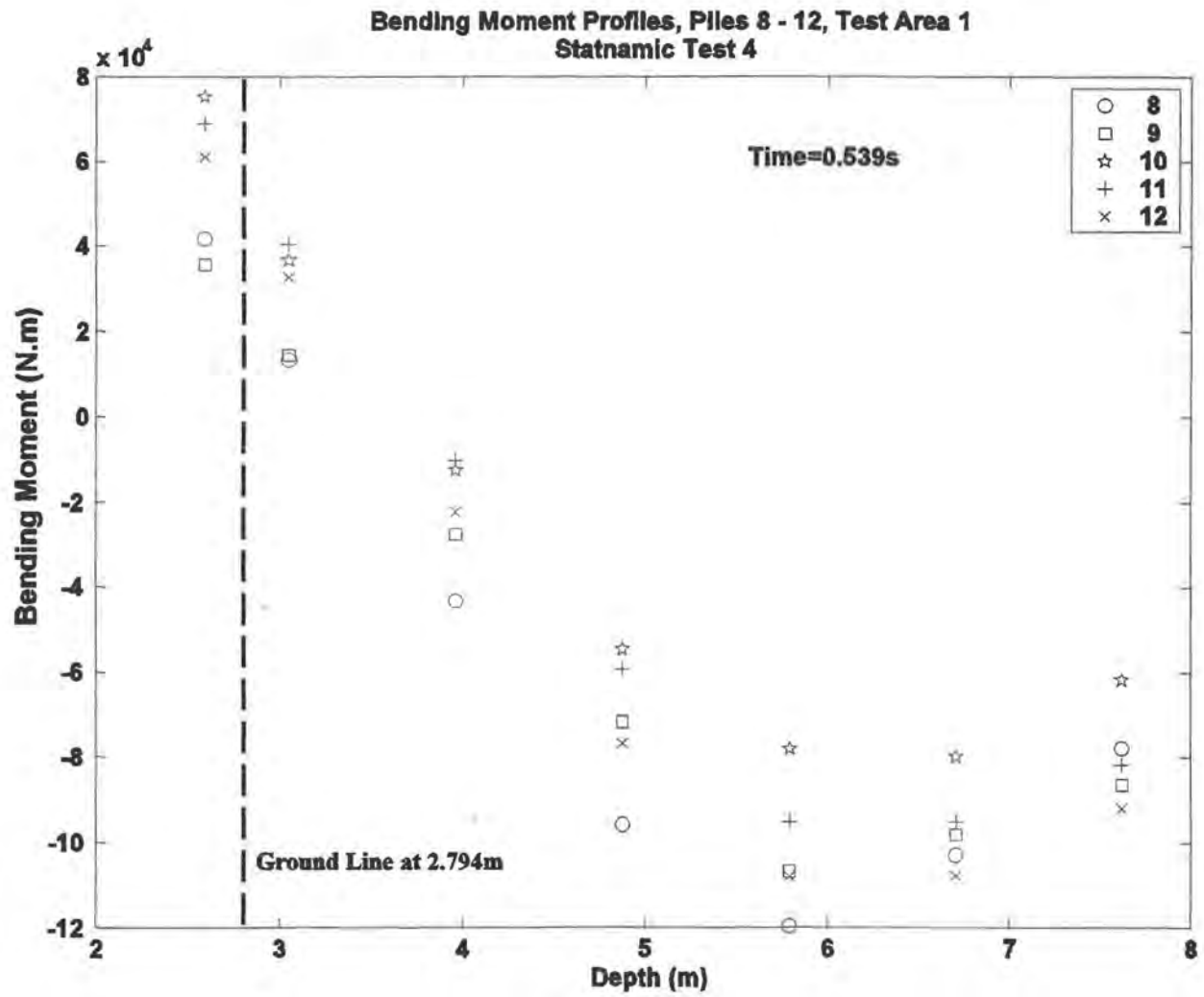


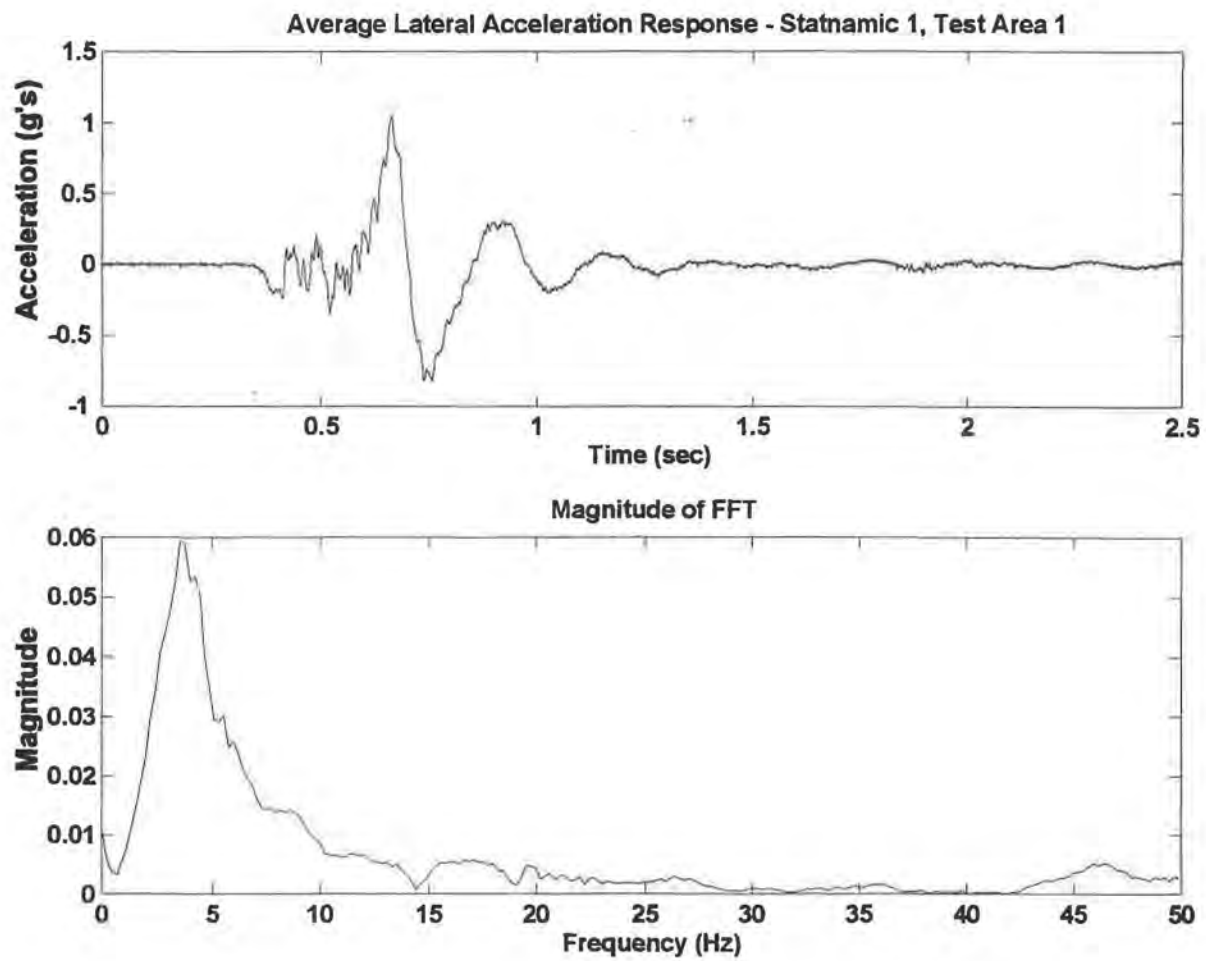
Figure D-25. Bending Moment Profiles, Statnamic 4, Test Area 1

Loads Transferred to Individual Piles (KN)			Load Transferred to Row (KN)	% Load Transferred
7 [69.6,89.5]	12 [56.1,66.5]	10 [72.9,91.5]	[198.6 ,247.5]	[33 / 32]
2 [57.9,70.2]	11 [50.7,66.7]	6 [34.2,47.7]	[142.8,184.6]	[23 / 24]
3 [62.3,82.1]	9 [37.9,54.7]	4 [23.6,34.5]	[123.8,171.3]	[21 / 22]
5 [56.2,70.9]	8 [51.2,66.0]	1 [28.8,39.7]	[136.2,176.6]	[23 / 22]

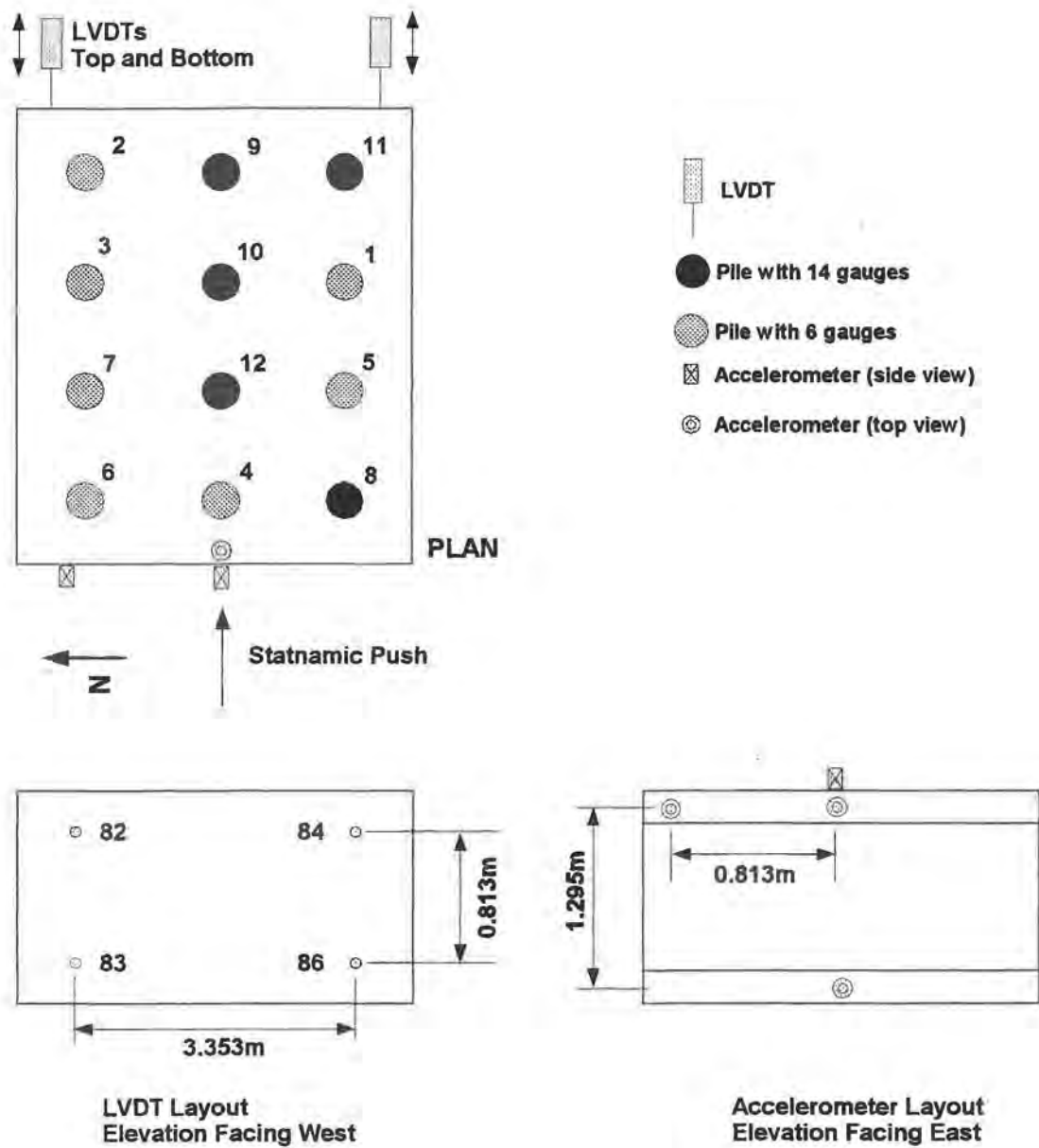

 Direction of Statnamic Load

- Every circle represents one pile in the group
- The number within the circle represents the pile number
- The 2 numbers immediately to the right of a pile represents the pile head shear at peak bending moments for tests 3 and 4 respectively
- The rightmost column of numbers indicates the total lateral load transferred to that particular row for that particular load

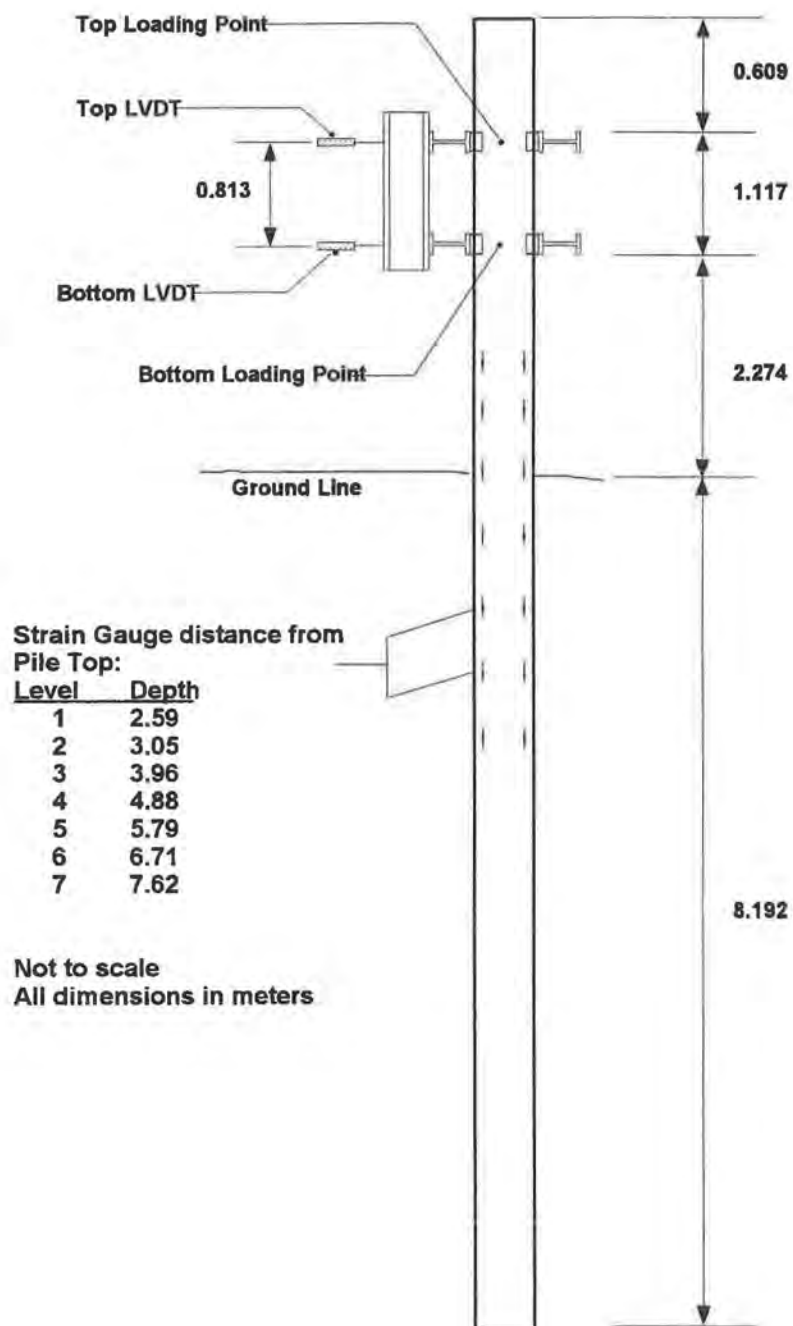
*Figure D-26. Pile Head Shear Distribution, Statnamic 3-4, Test Area 1*



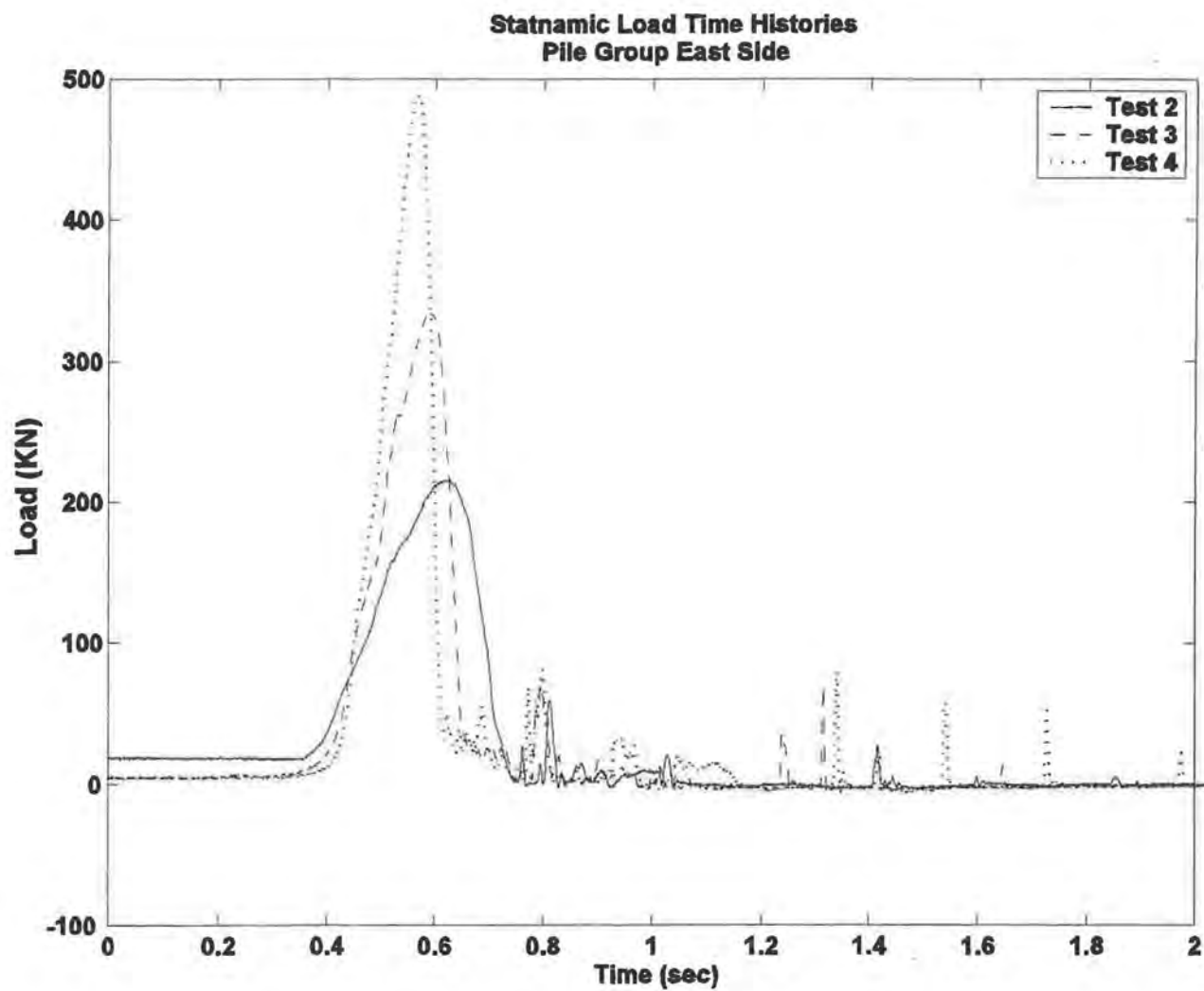
*Figure D-27. Acceleration Response, Time and Frequency, Test 1, Ratt Island*



**Figure D-28. Instrumentation - Pile Group, Test Area 2**

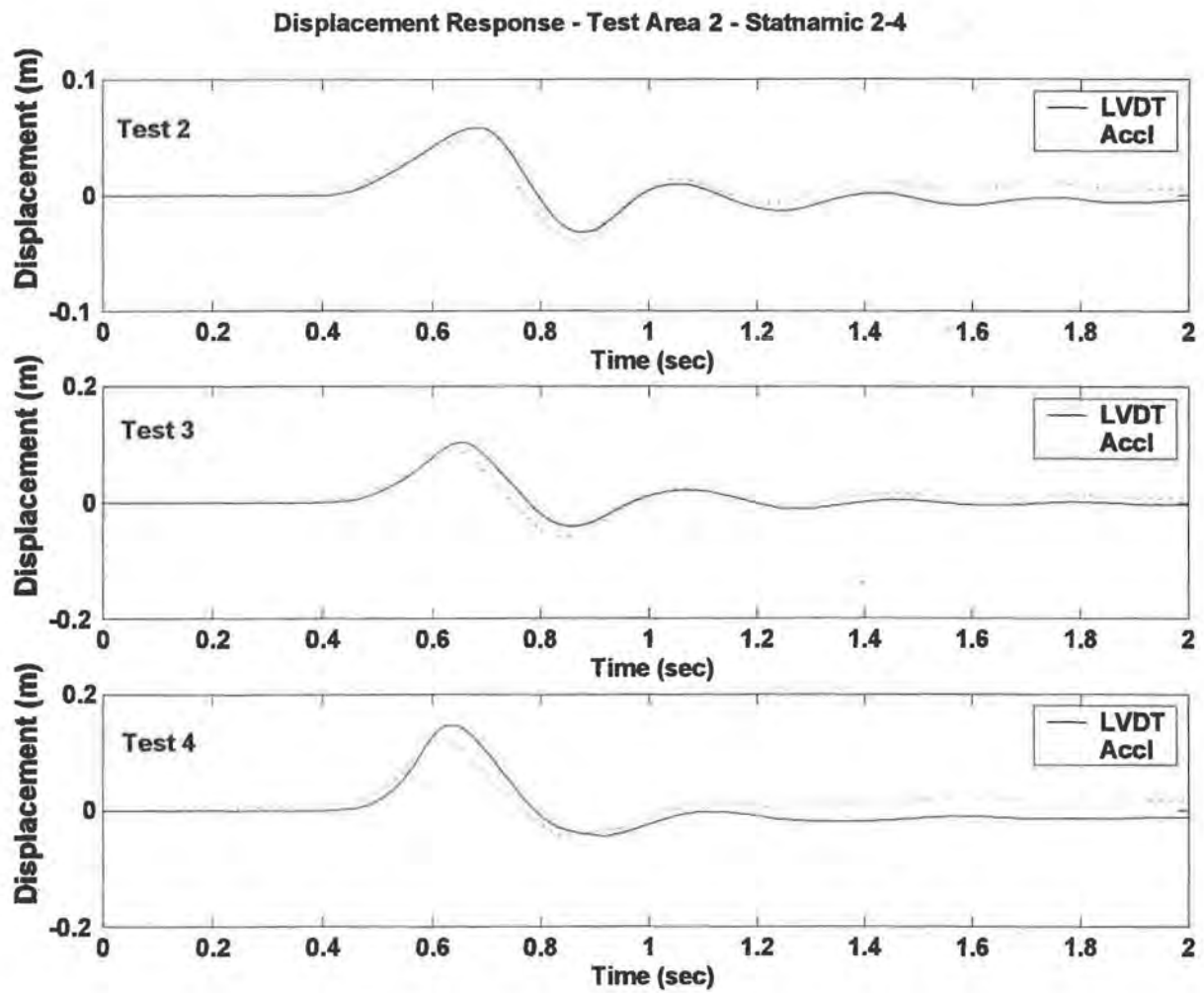


**Figure D-29. Load Transfer Setup, Pile Group, Test Area 2**



*Figure D-30. Statnamic Load Time Histories, Test Area 2*





*Figure D-31. Lateral Displacement Response, Statnamic, Test Area 2*

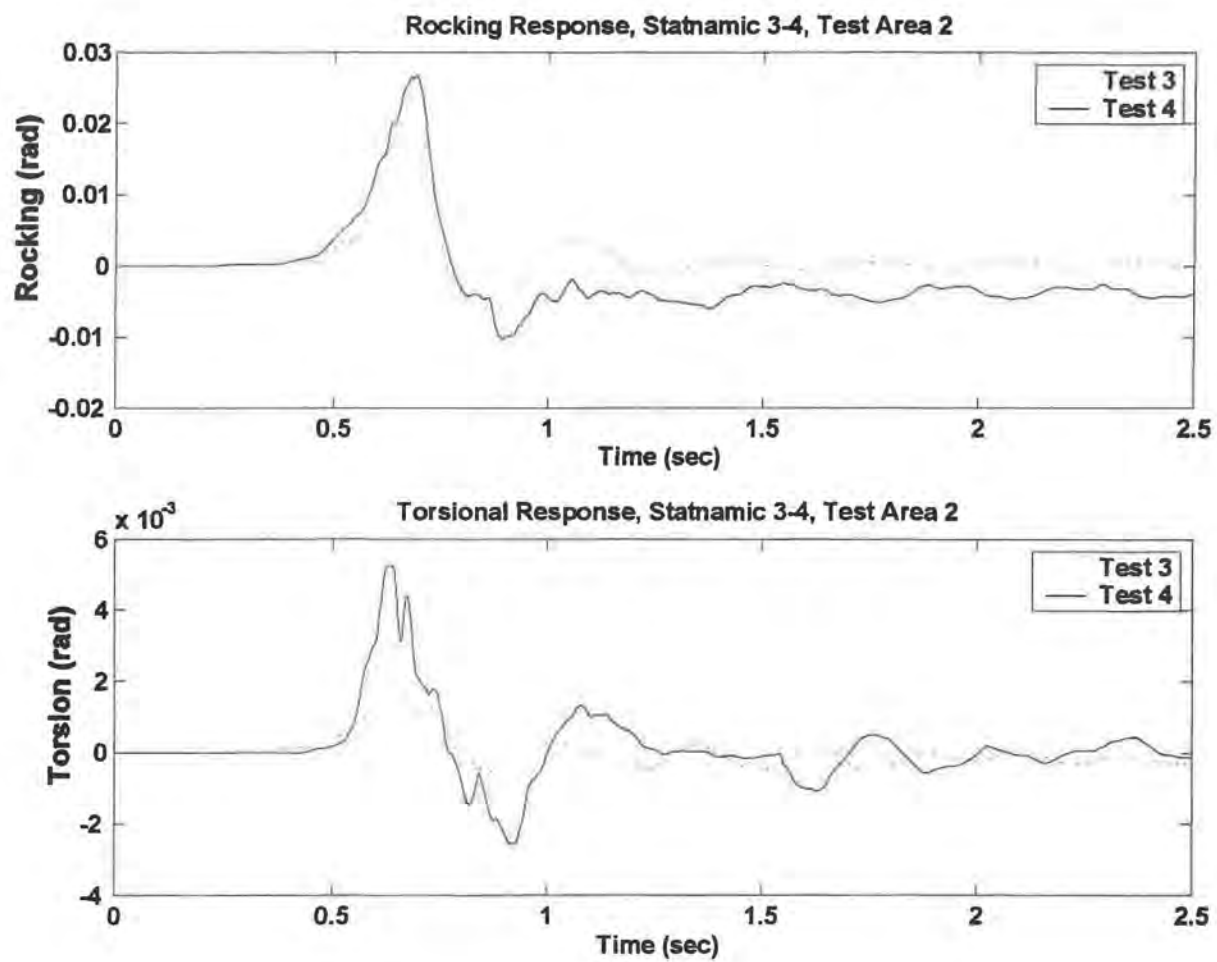
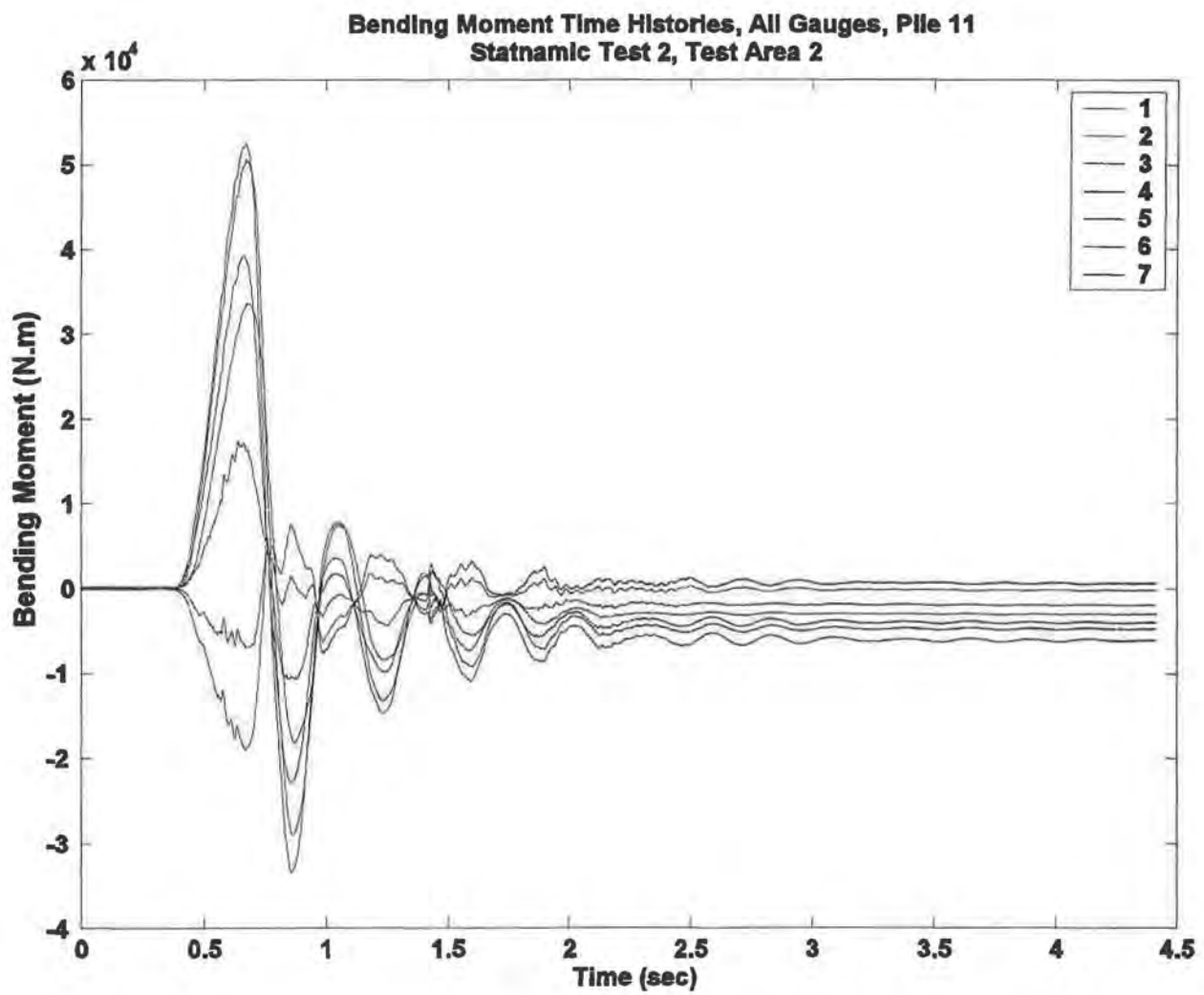


Figure D-32. Rocking and Torsional Rotational Response, Statnamic, Test Area 2



*Figure D-33. Bending Moment Response, Pile 11, Statnamic 2, Test Area 2*

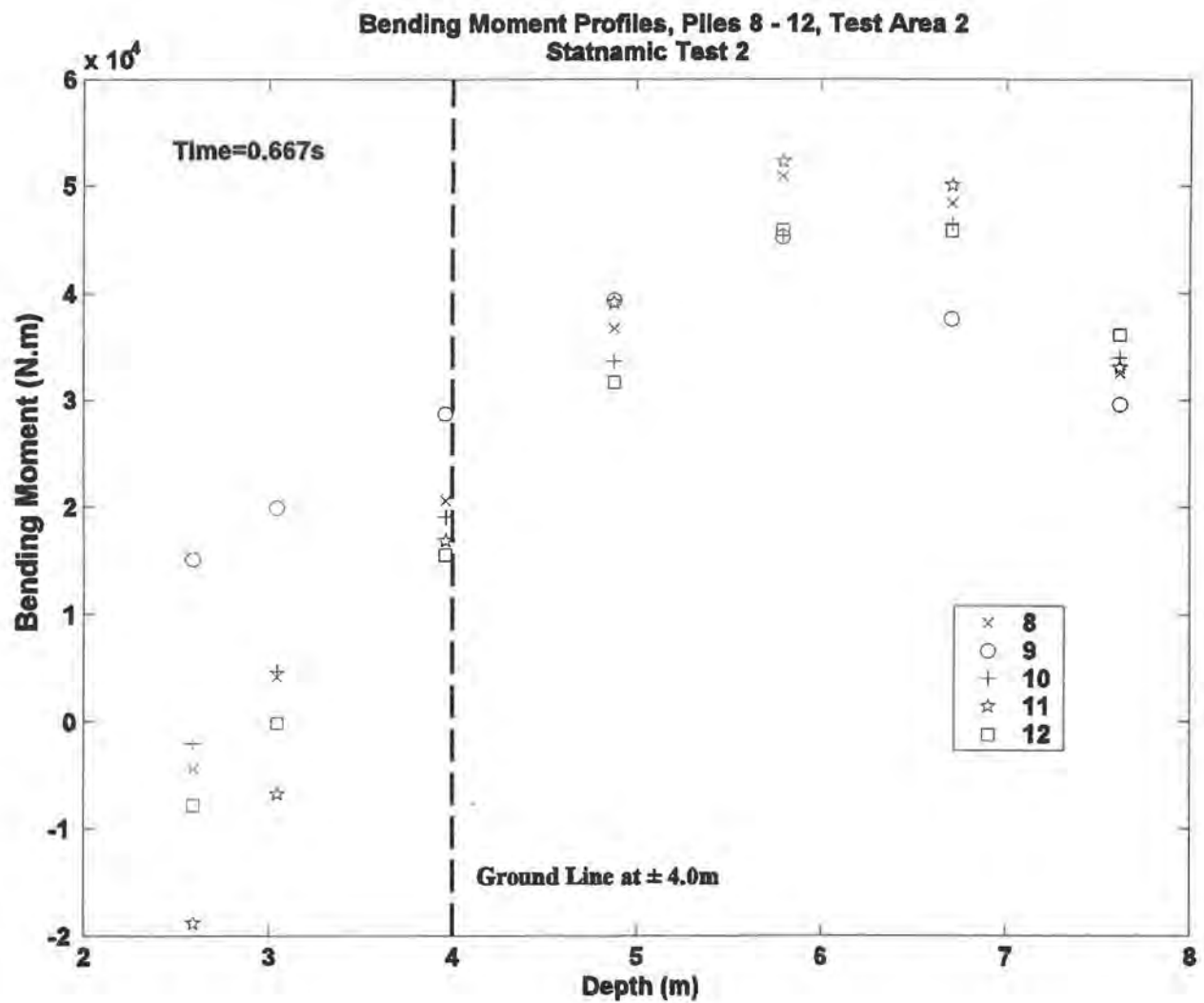


Figure D-34. Bending Moment Profiles, Statnamic 2, Test Area 2

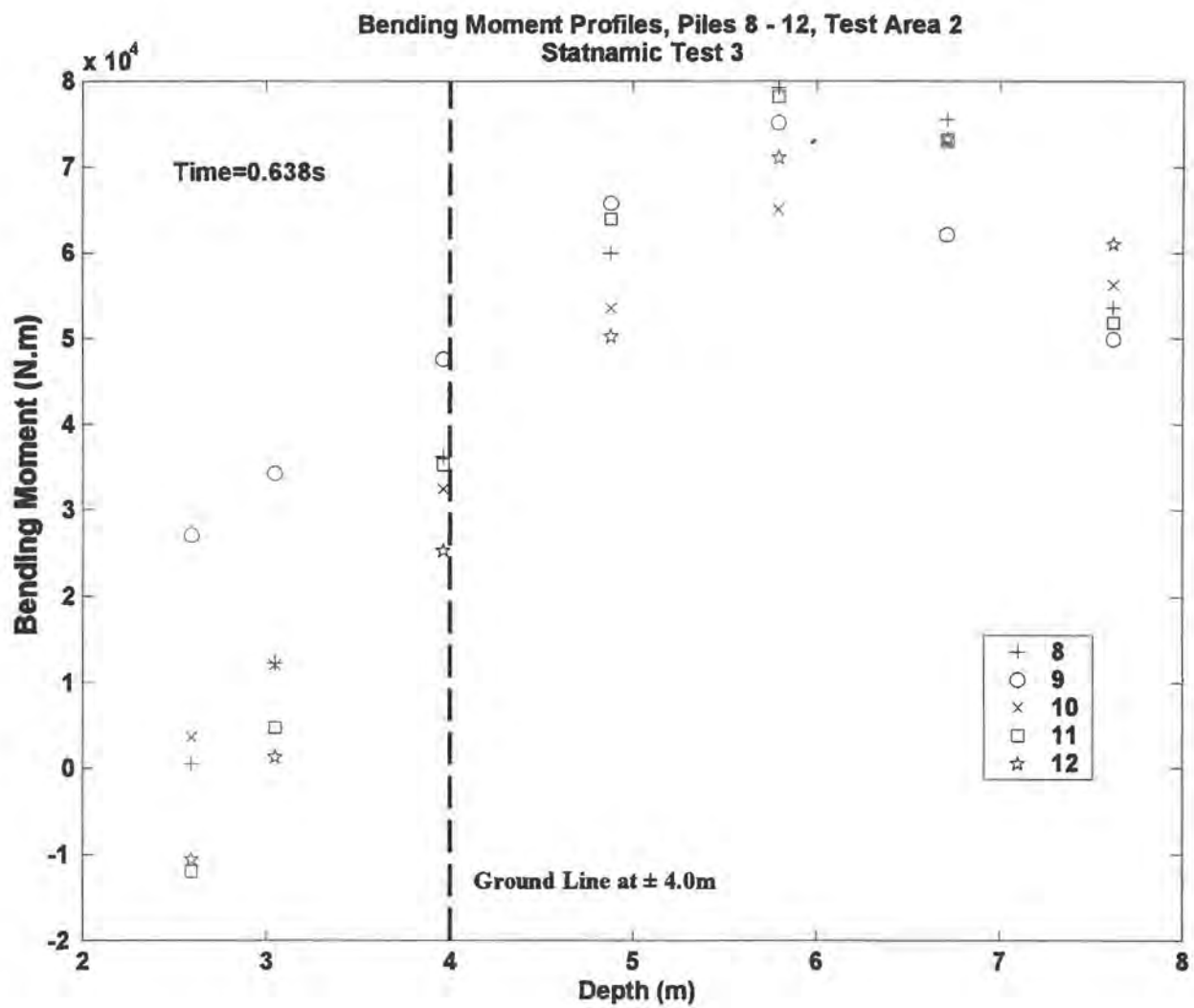


Figure D-35. Bending Moment Profiles, Statnamic 3, Test Area 2

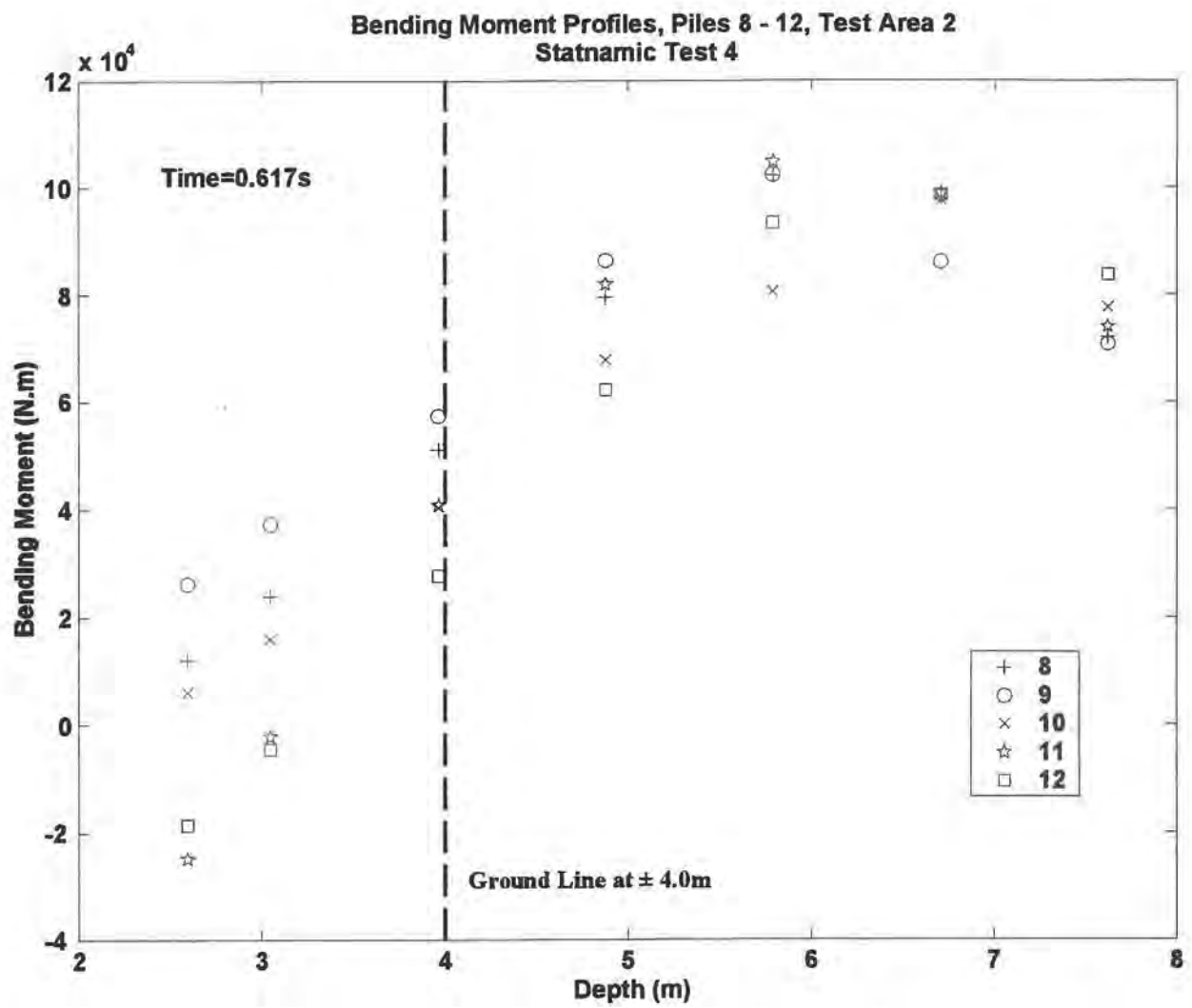


Figure D-36. Bending Moment Profiles, Statnamic 4, Test Area 2

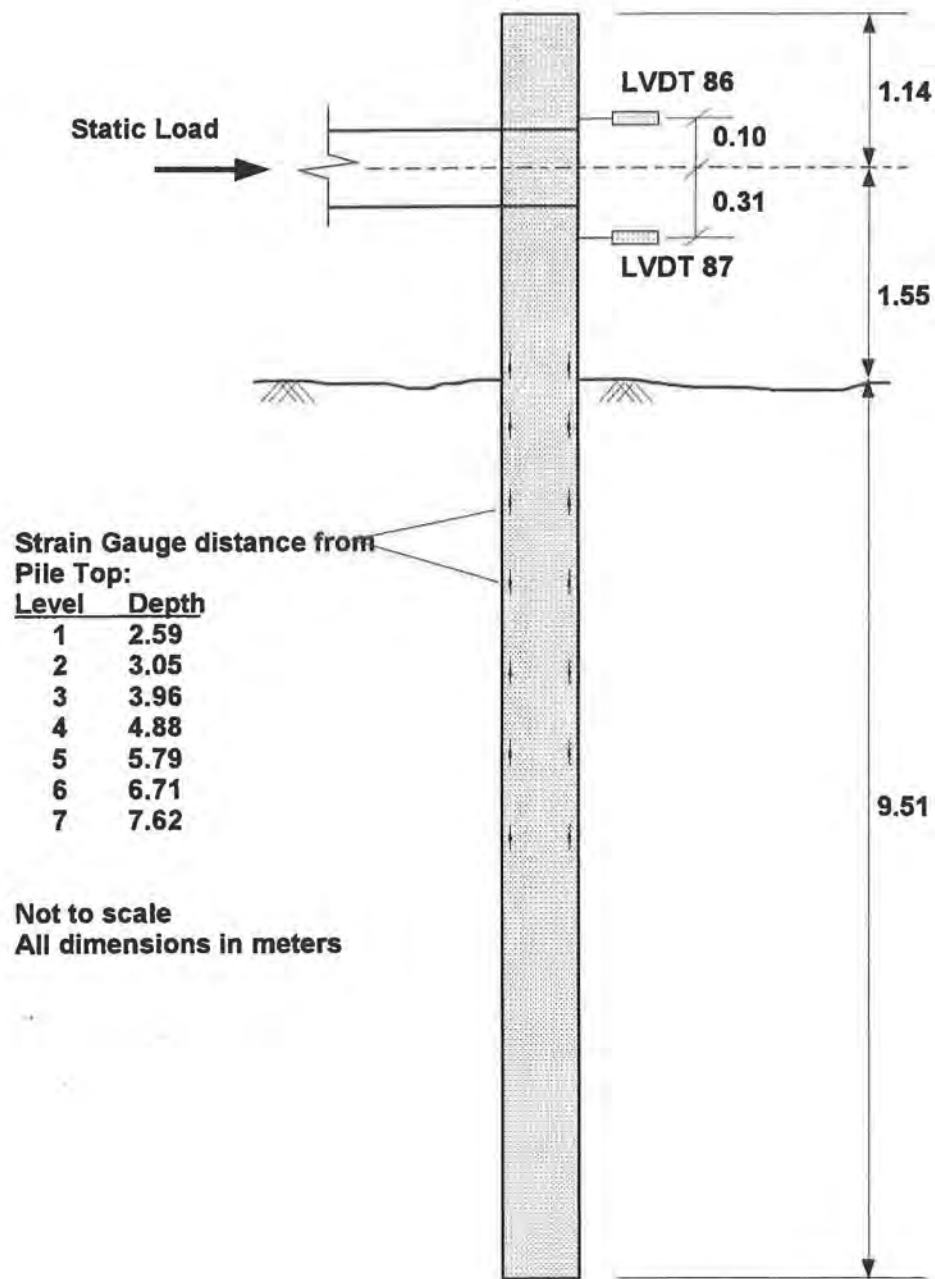
Loads transferred to individual piles (KN)			Load transferred to row (KN)	% Load Transferred
2 [39.9,52.6]	9 [17.5,26.3]	11 [38.8,53.0]	[96.2,131.9]	[24 / 27]
3 [?, ?]	10 [20.4,25.4]	1 [24.9,35.1]	[70.2,95.6]	[18 / 20]
7 [41.8,49.0]	12 [27.2,37.7]	5 [49.1,59.6]	[118.1,146.3]	[30 / 30]
6 [42.4,43.8]	4 [39.7,36.9]	8 [26.8,29.5]	[108.9,110.2]	[28 / 23]

  
 Direction of Statnamic Load

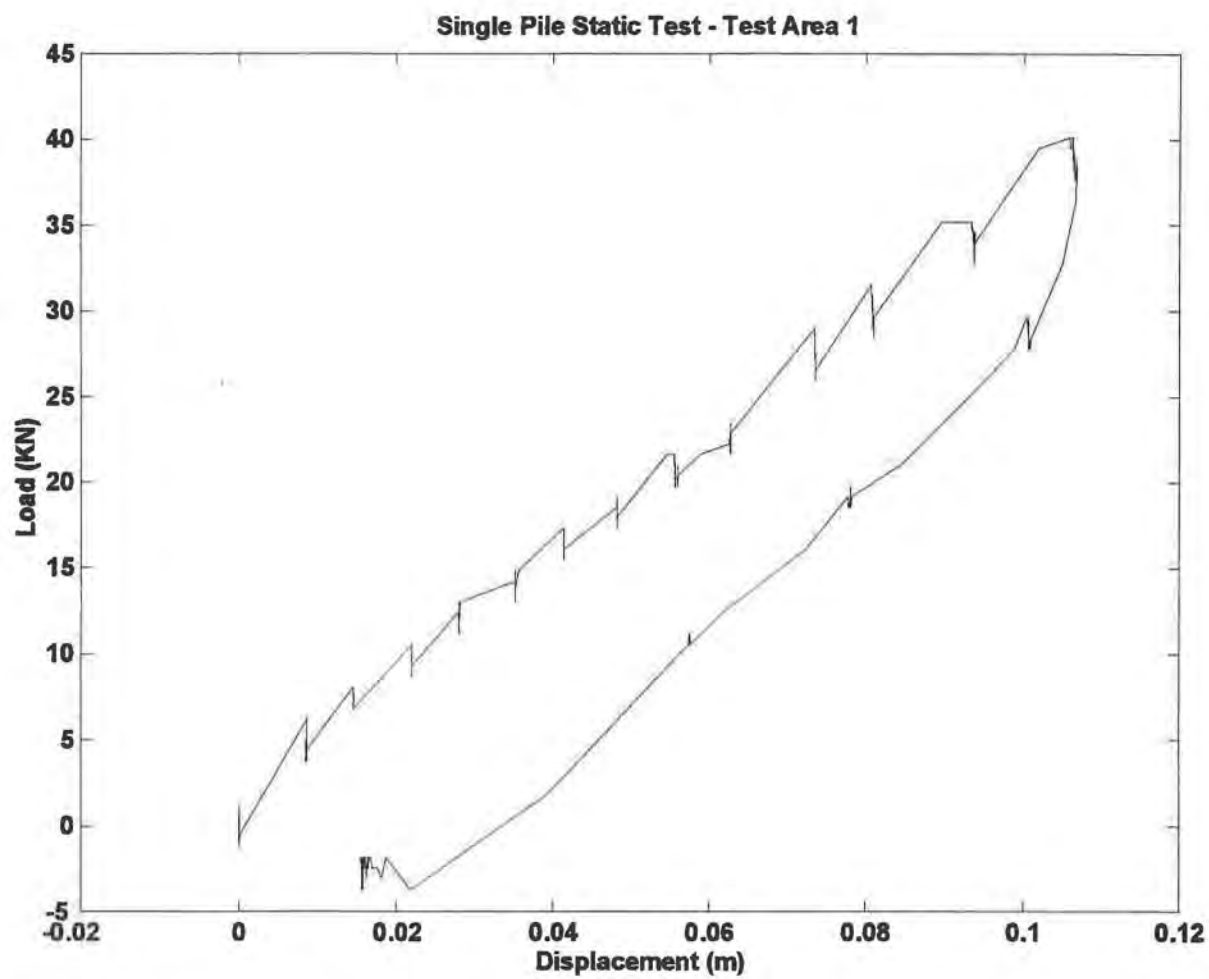
- Every circle represents one pile in the group
- The number within the circle represents the pile number
- The 2 numbers immediately to the right of a pile represents the pile head shear at peak load for tests 3 and 4 respectively
- The rightmost column of numbers indicates the total lateral load transferred to that particular row for that particular load

*Figure D-37. Pile Head Shear Distribution, Statnamic, Test Area 2*





**Figure D-38. Test Setup, Single Pile, Test Area 1**



*Figure D-39. Load-Displacement Response, Single Pile, Test Area 1*

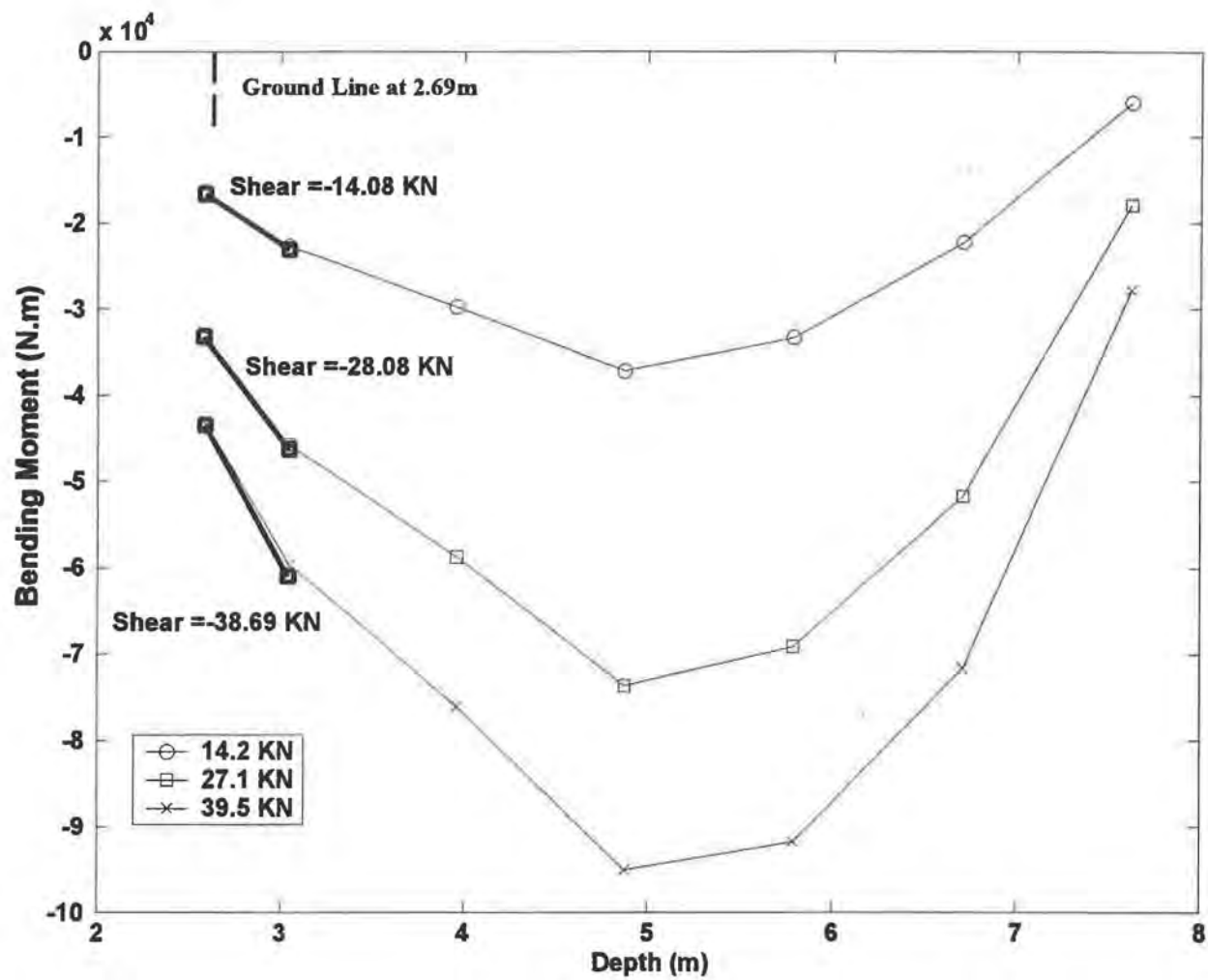


Figure D-40. Bending Moment vs. Depth, Single Pile Static, Test Area 1

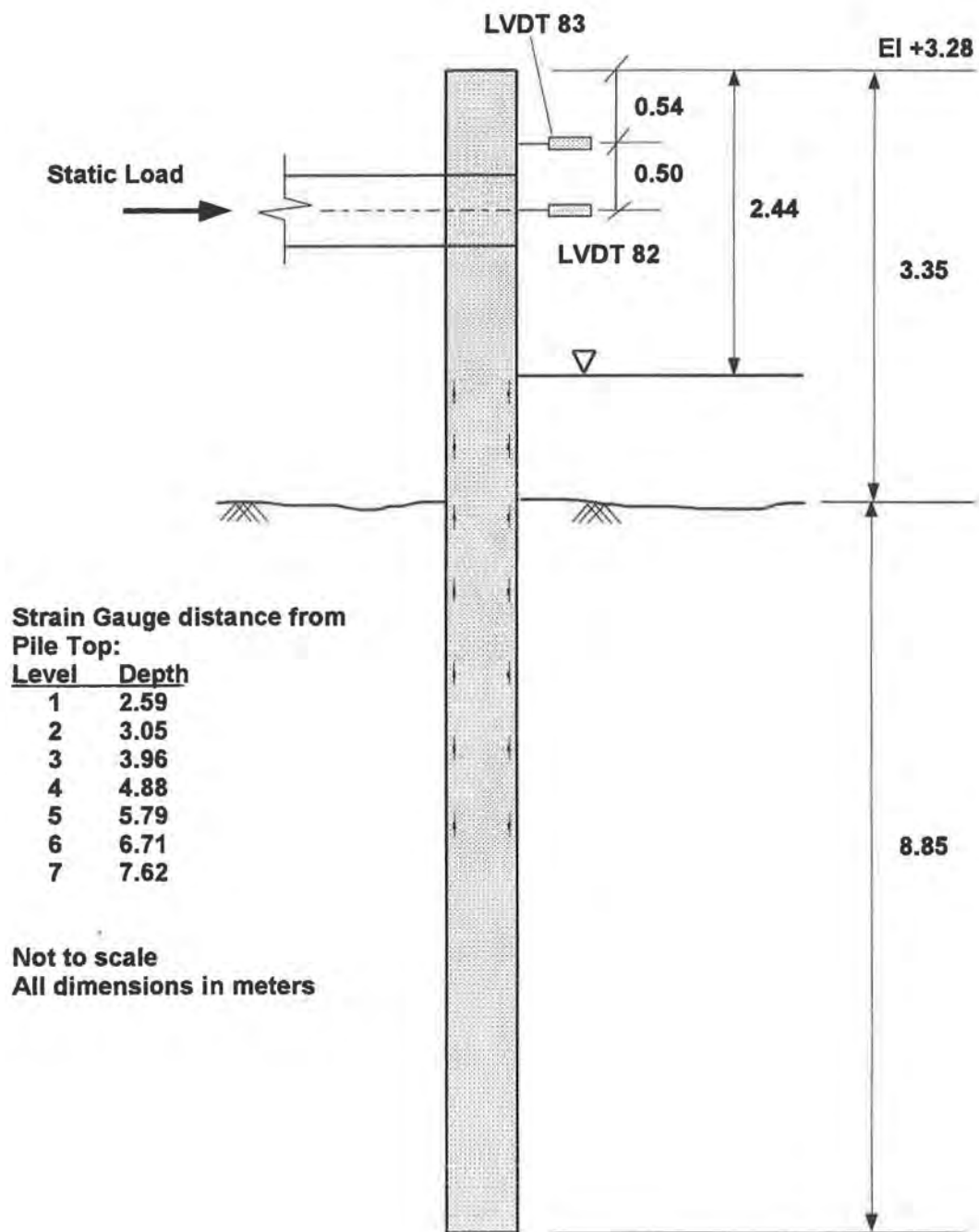
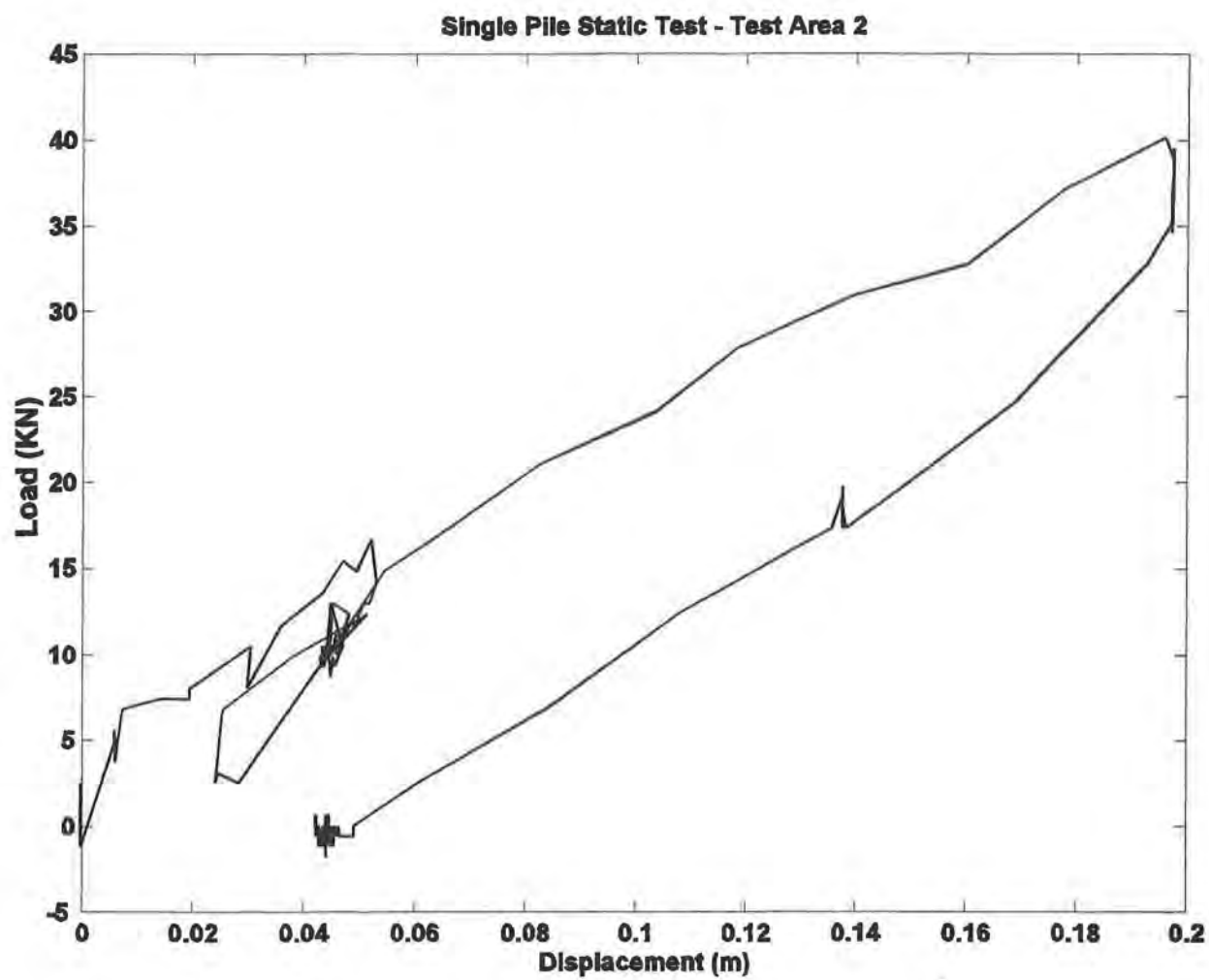


Figure D-41. Test Setup, Single Pile, Test Area 2



*Figure D-42. Load Displacement Response, Single Pile, Test Area 2*

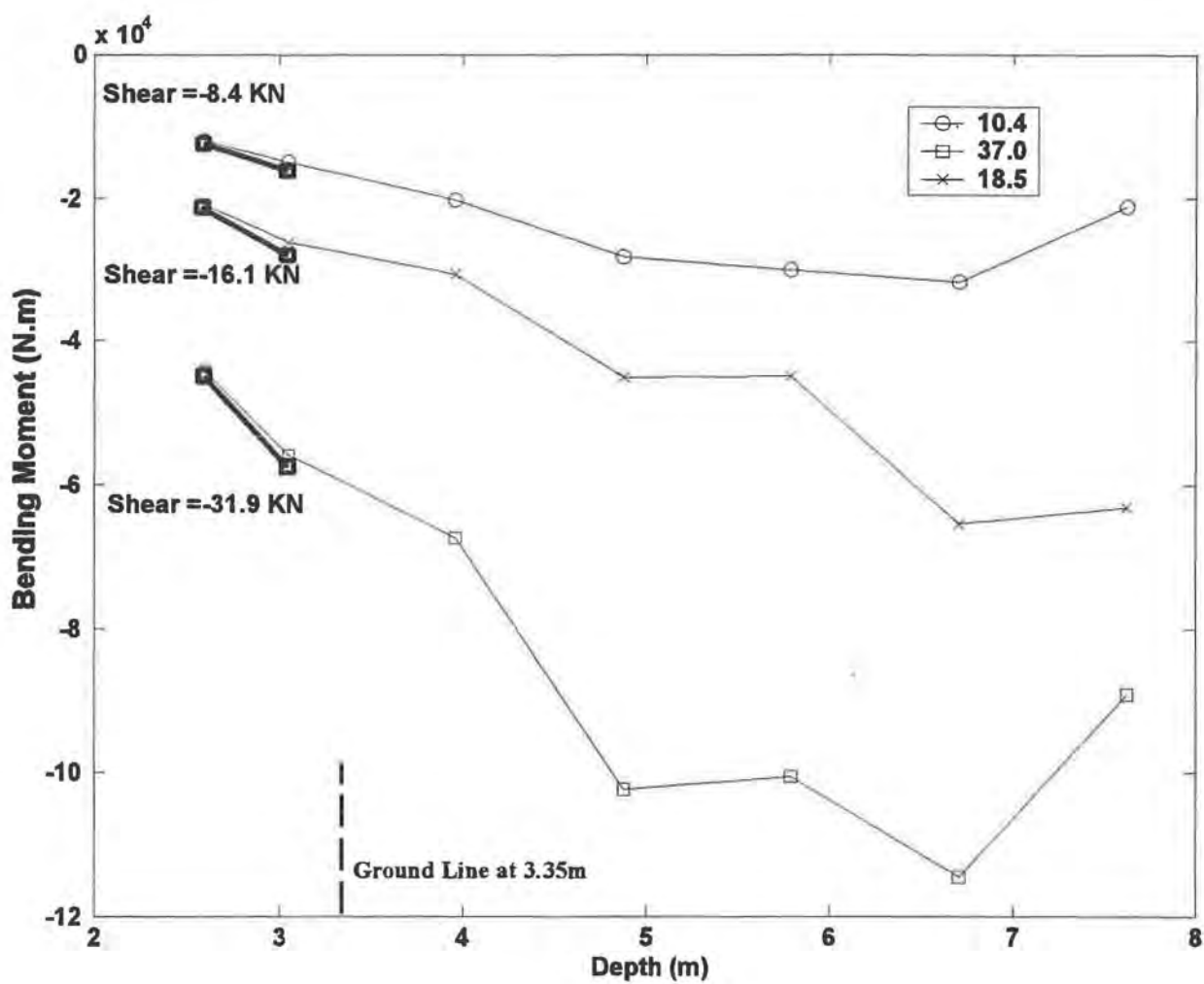


Figure D-43. Bending Moment vs. Depth, Single Pile Static, Test Area 2

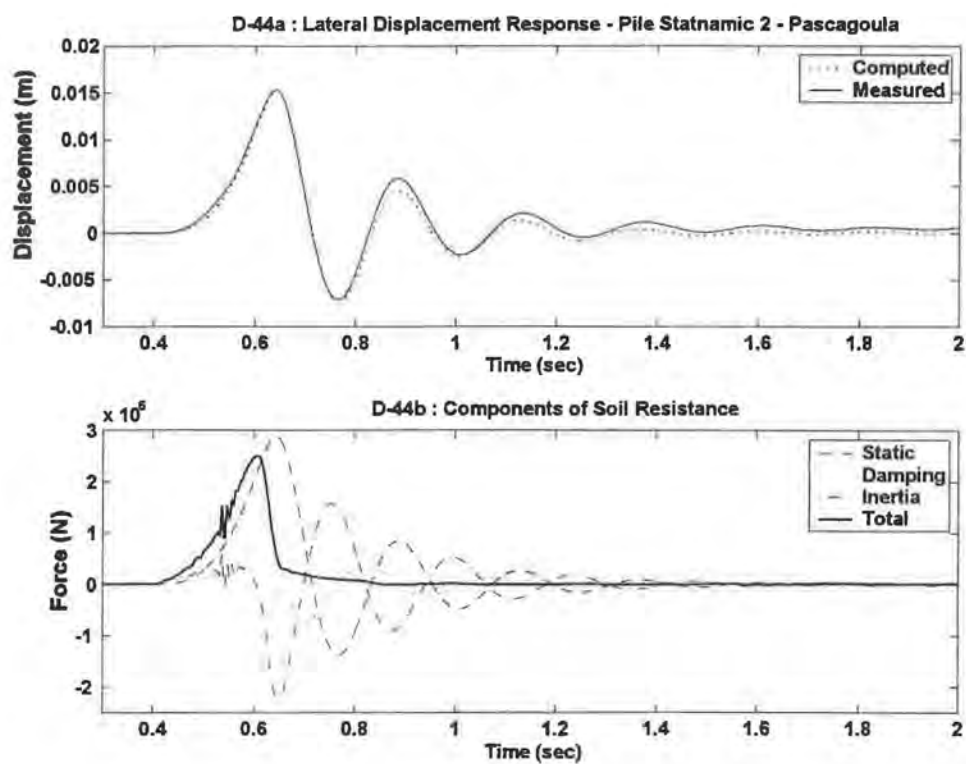


Figure D-44. Computed vs. Measured Lateral Response, Pile Statnamic 2, Pascagoula



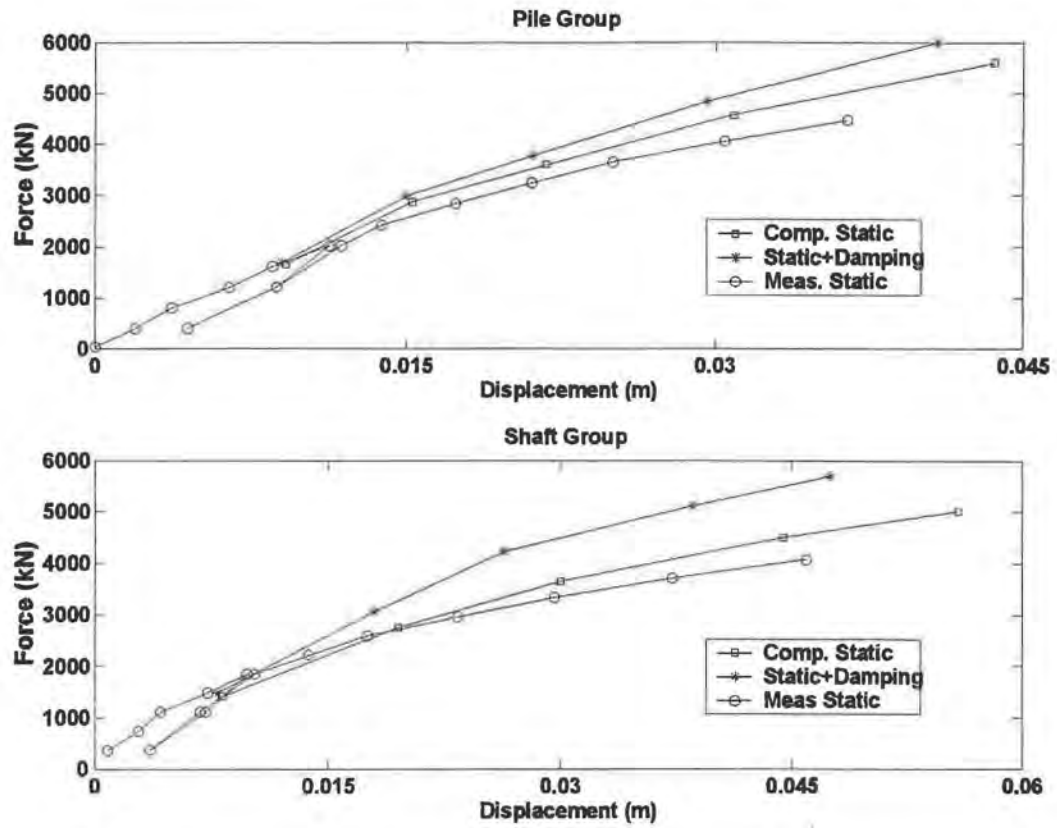


Figure D-45. Derived Static Load Deflection Response, Pascagoula

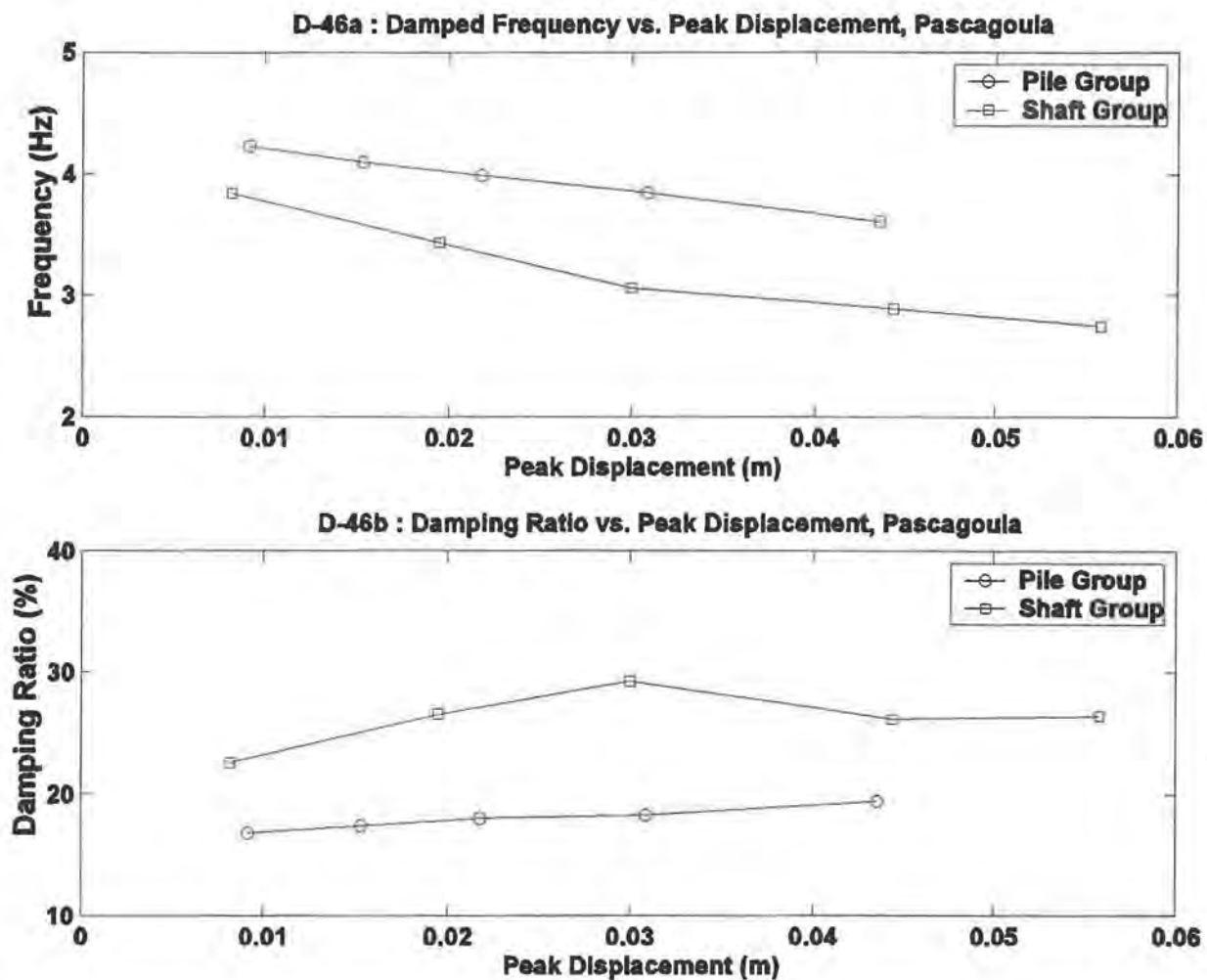


Figure D-46. Frequency and Damping Ratio vs. Peak Displacement, Pascagoula

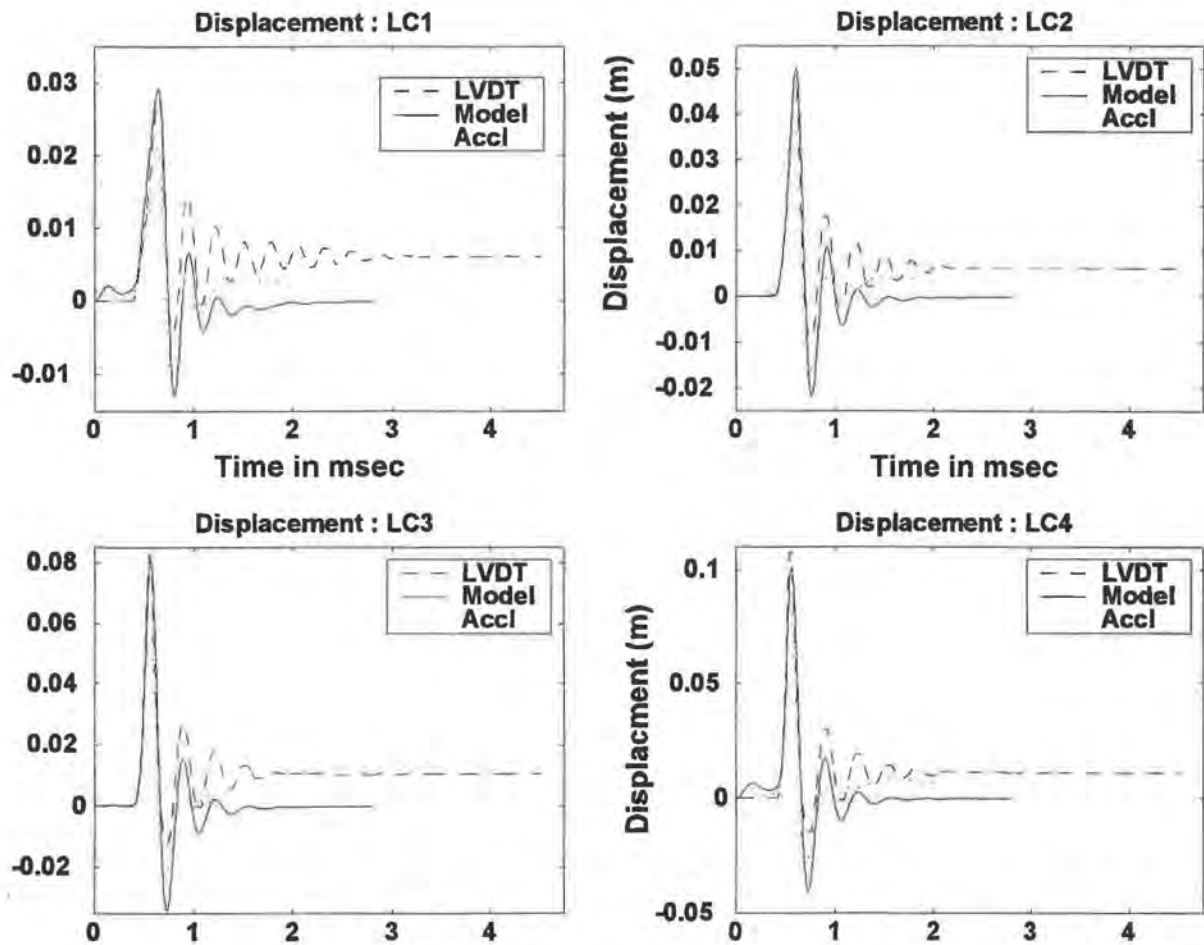
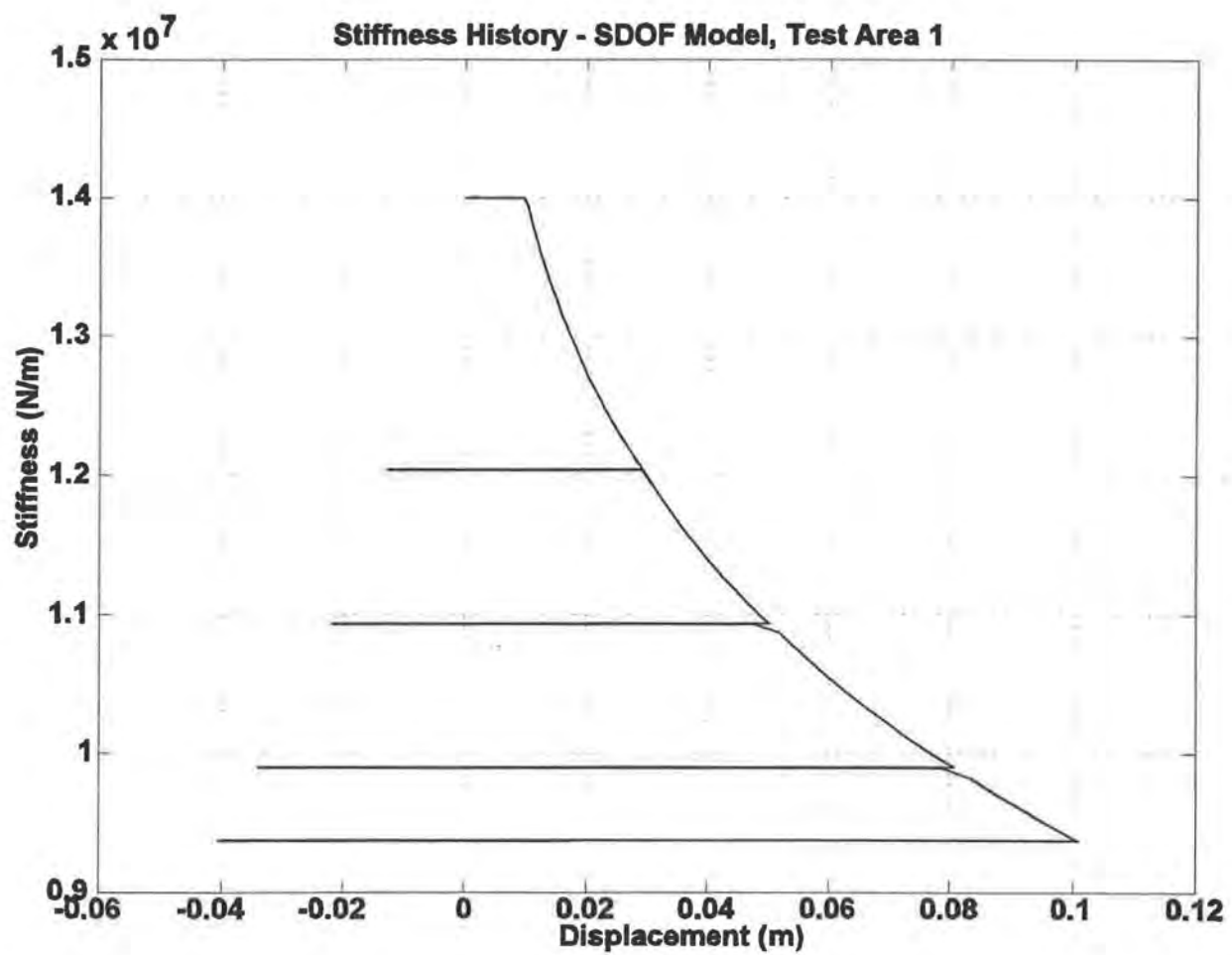
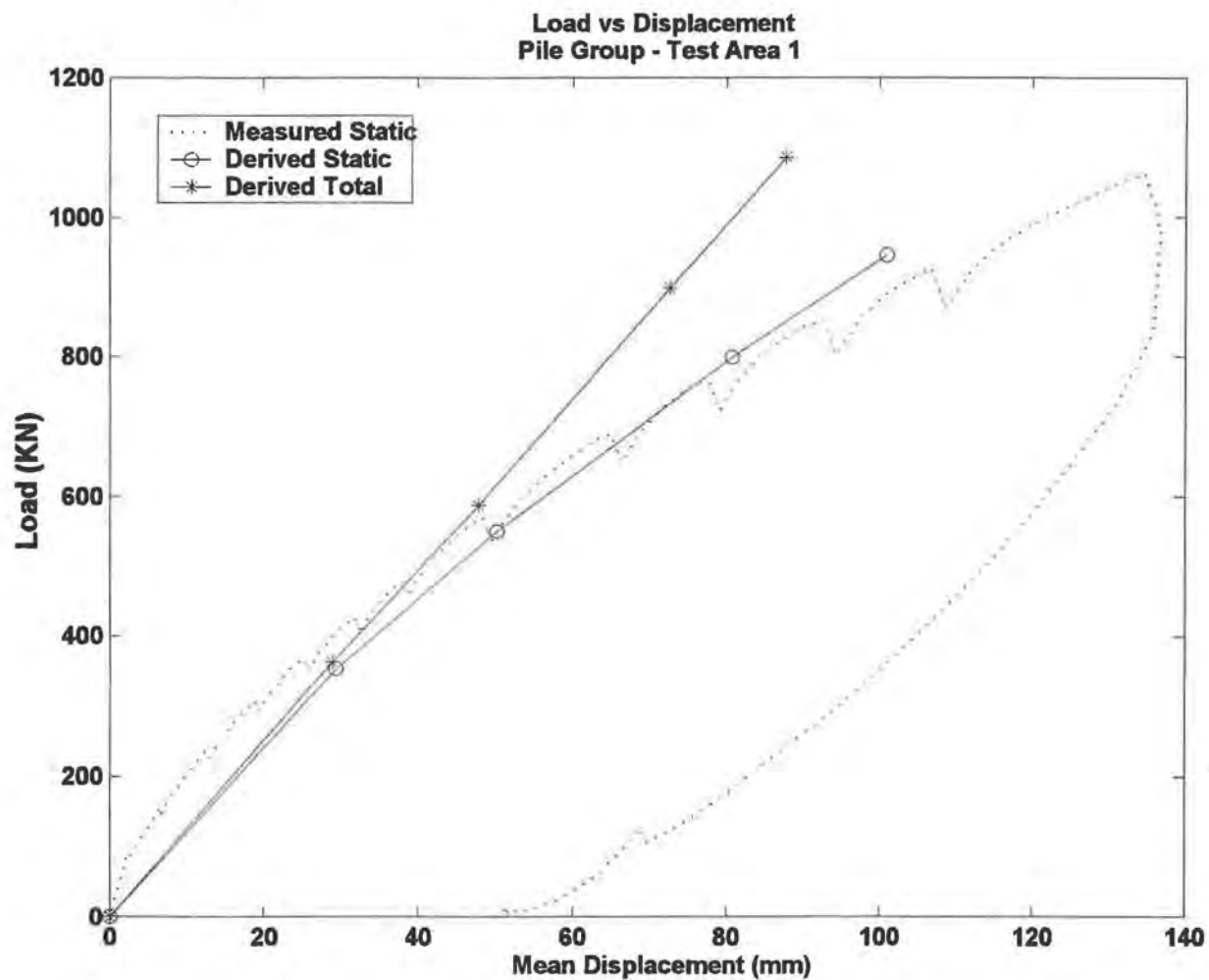


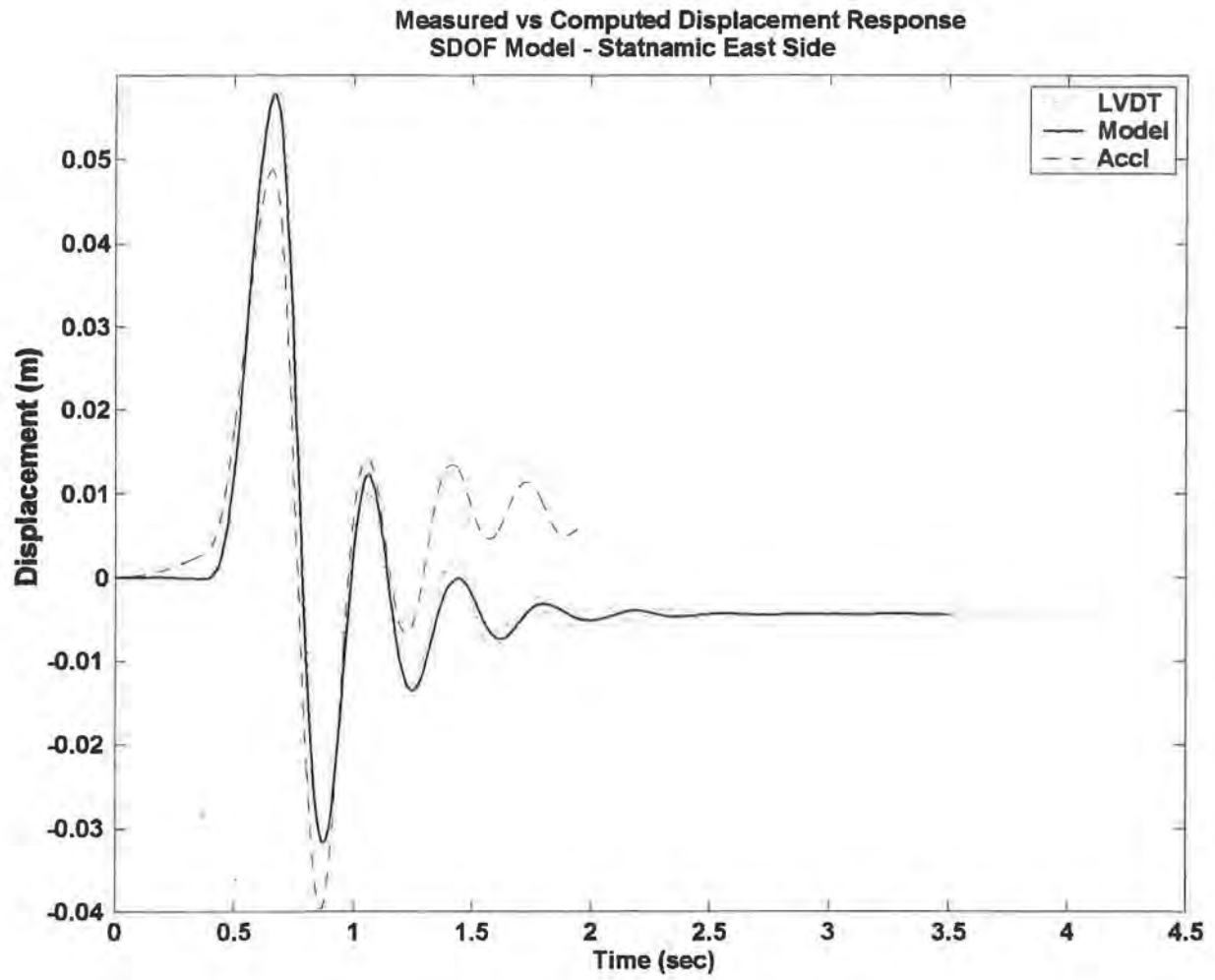
Figure D-47. Computed vs. Measured Lateral Group Response, Test Area 1



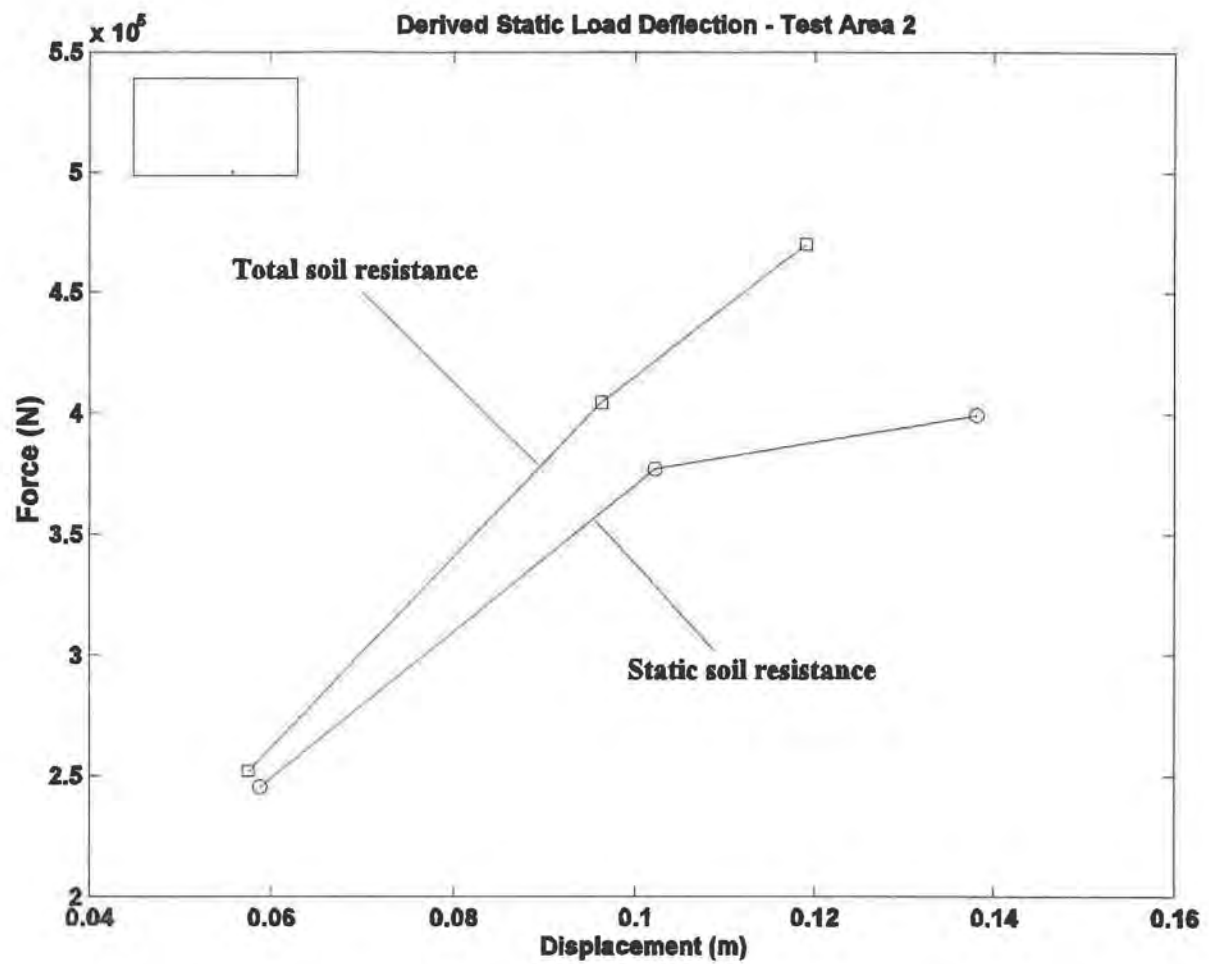
*Figure D-48. Stiffness History - SDOF Model, Test Area 1*



*Figure D-49. Derived Static Load Deflection Response, Test Area 1*



*Figure D-50. Computed vs. Measured Lateral Response, Statnamic 2, Test Area 2*



*Figure D-51. Derived Static Load Deflection Response, Test Area 2*

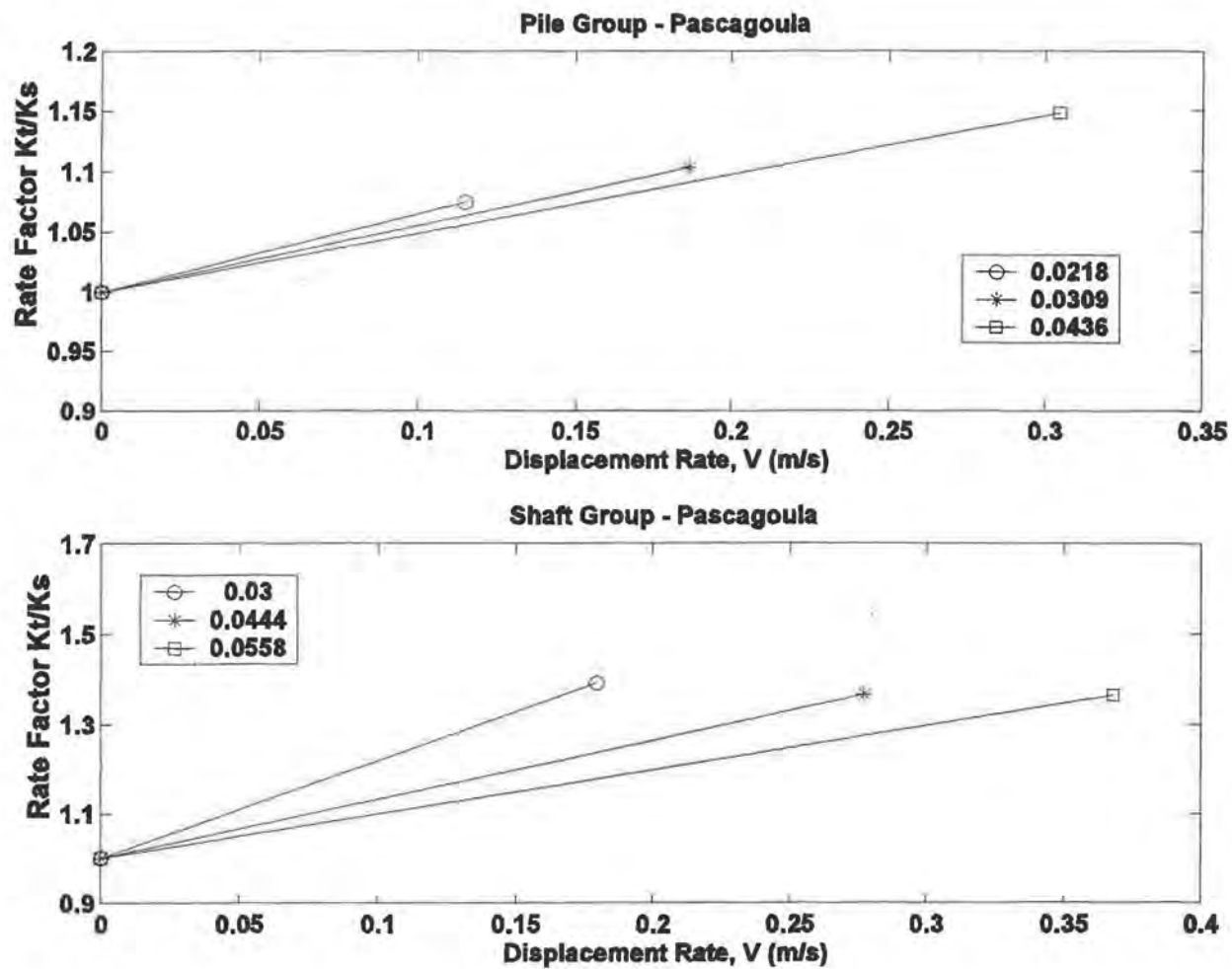
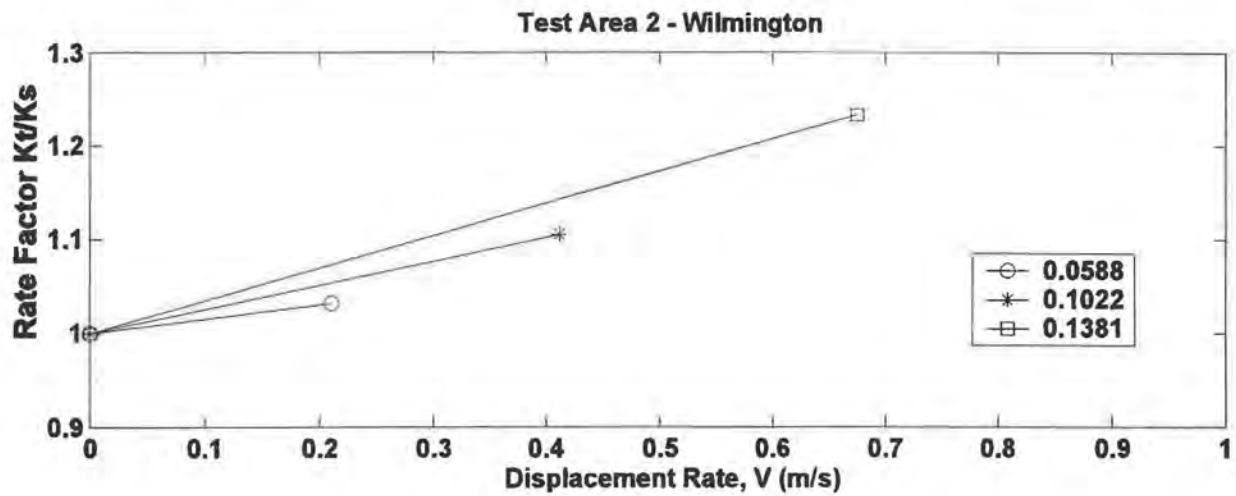
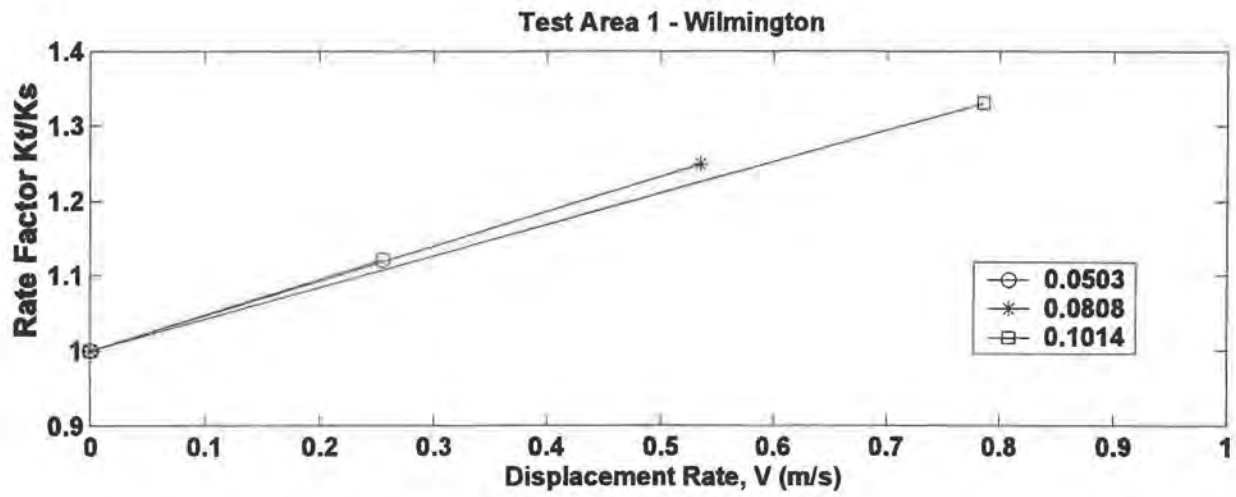
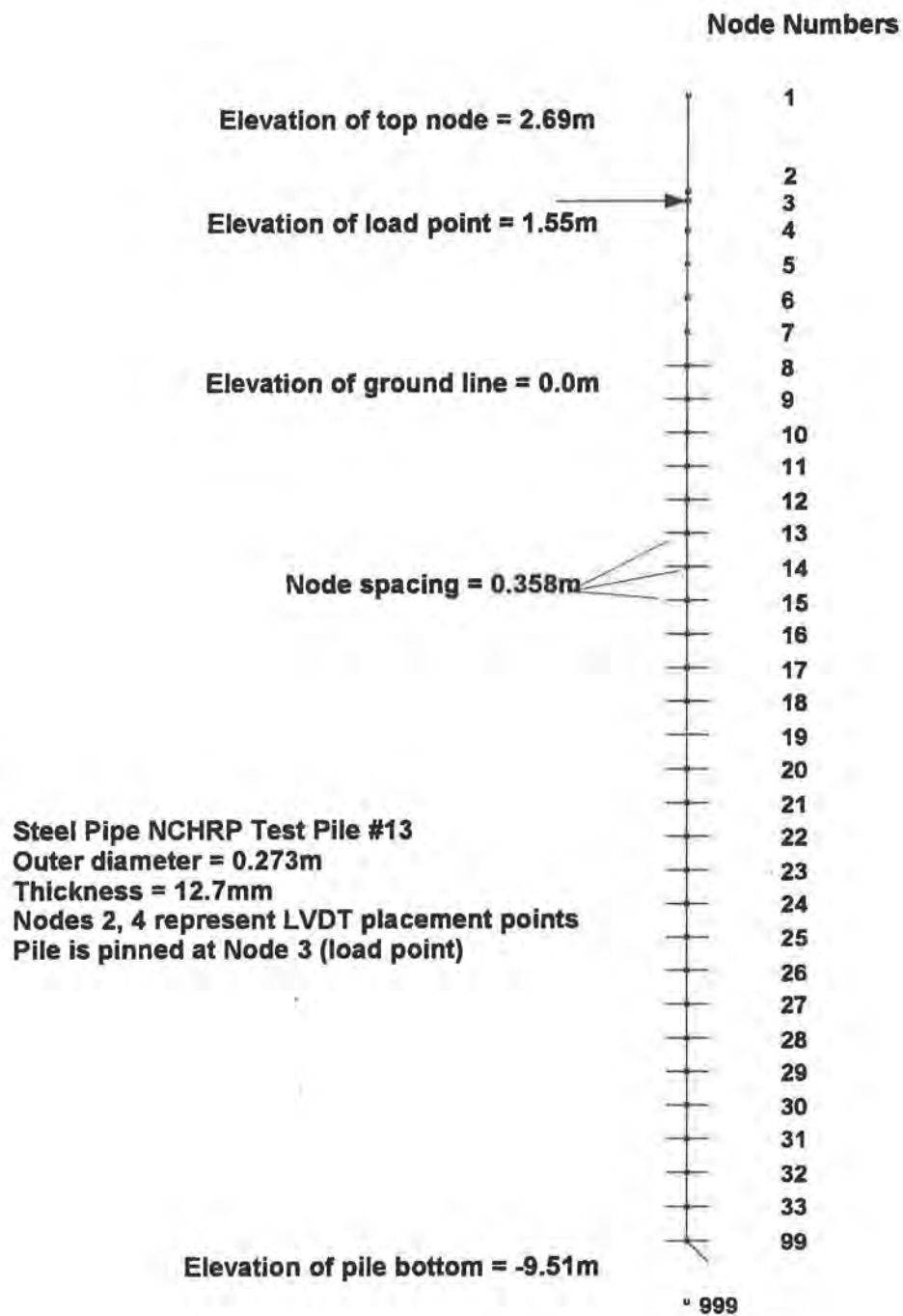


Figure D-52. Rate Factors, Pascagoula

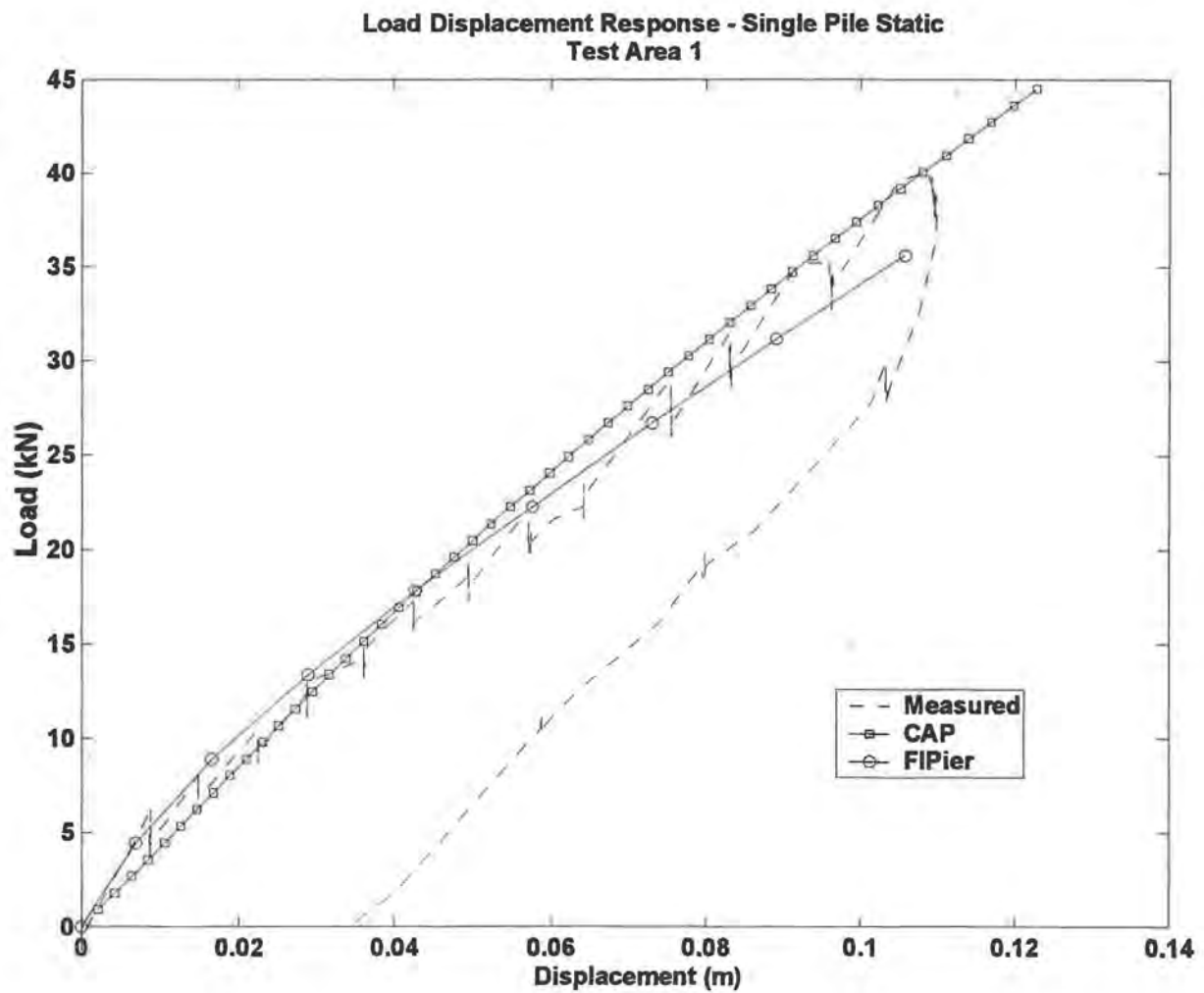




*Figure D-53. Rate Factors, Wilmington*



*Figure D-54. Finite Element Model, Single Pile Static, Test Area 1*



*Figure D-55. Load-Displacement Response, Single Pile Static, Test Area 1*

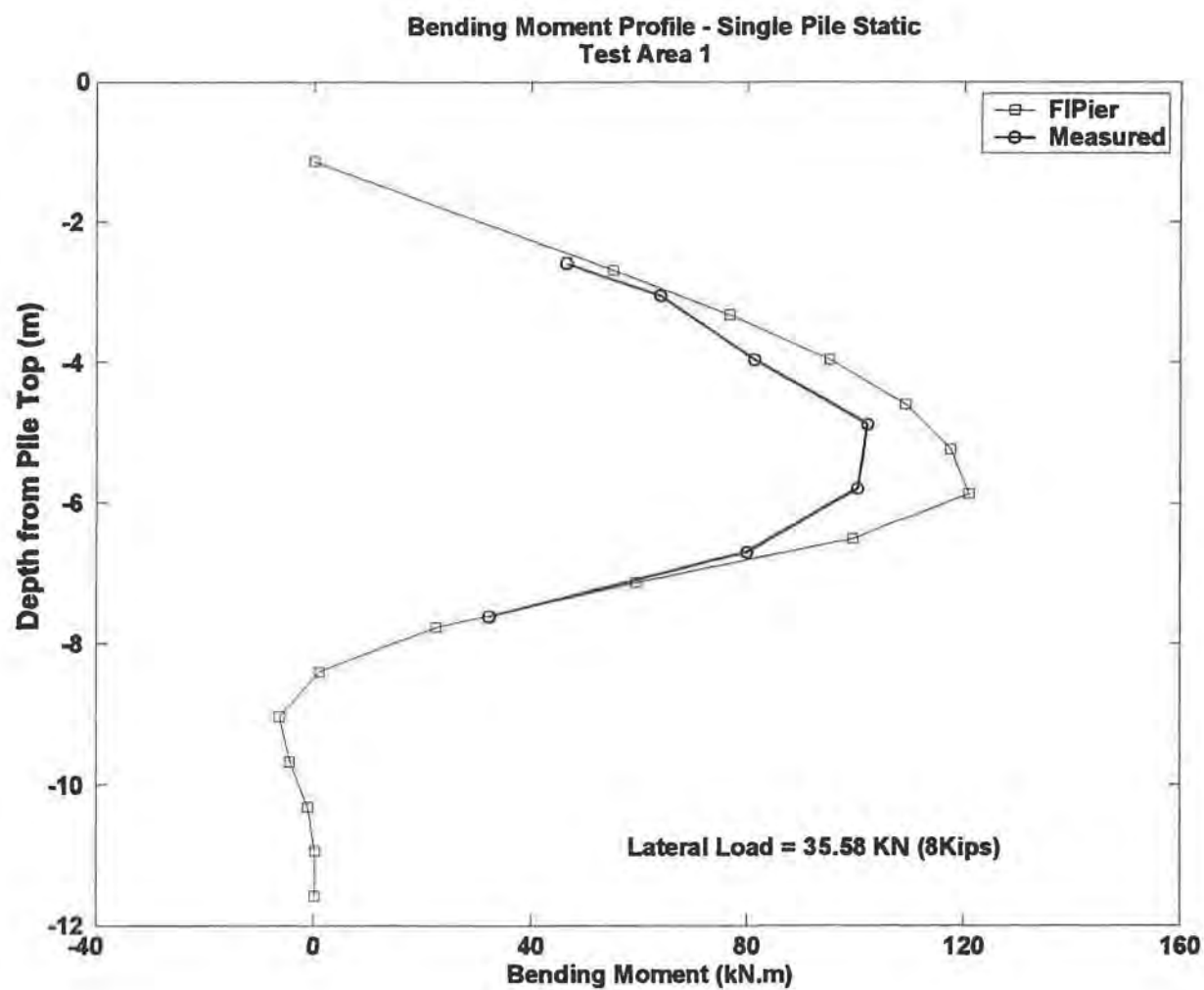
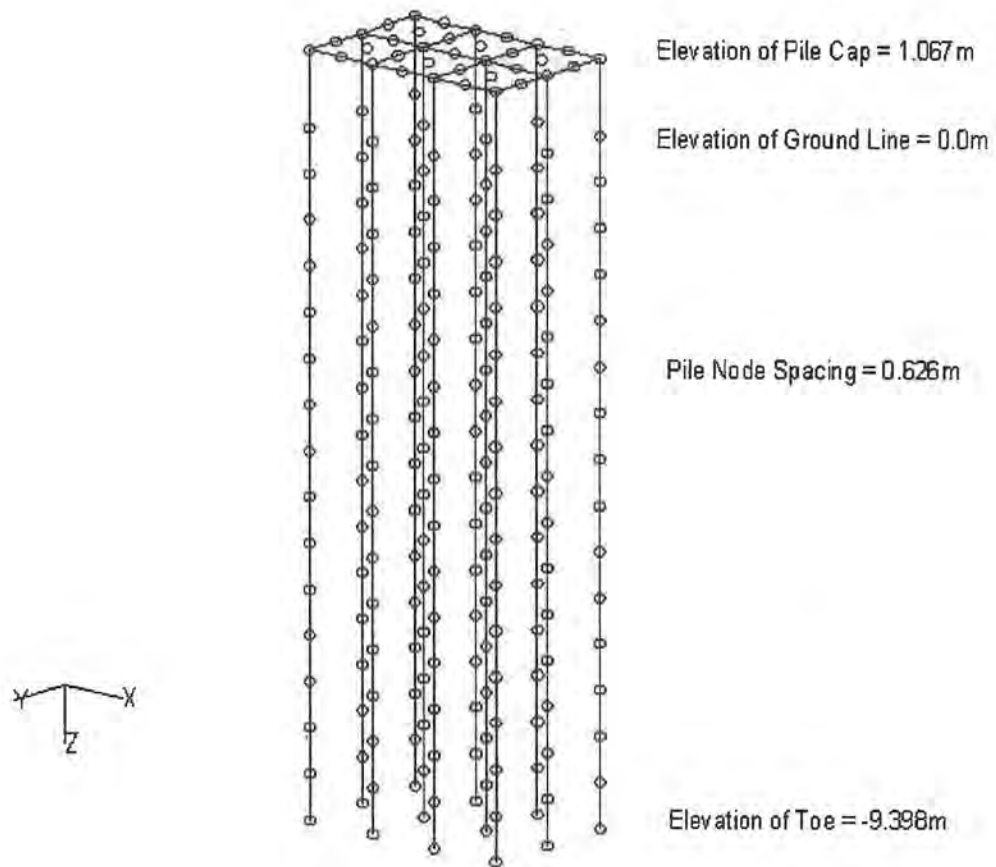


Figure D-56. Bending Moment Profile, Single Pile Static, Test Area 1

The Pile Cap was modeled using Plate Elements 0.273m thick



*Figure D-57. Finite Element Model - FLPIER, Pile Group, Test Area 1*

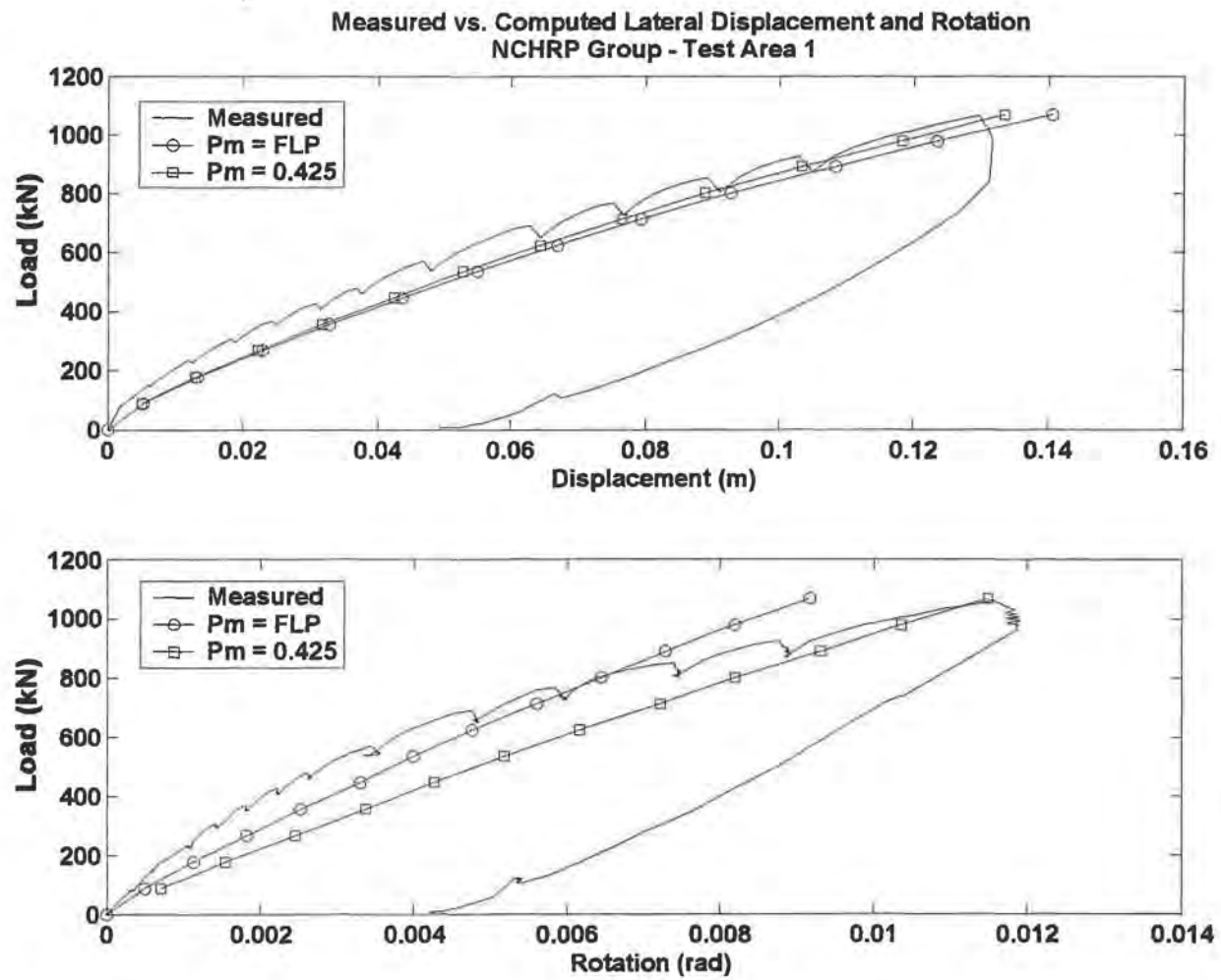


Figure D-58. Load Displacement Response, Group Static, Test Area 1

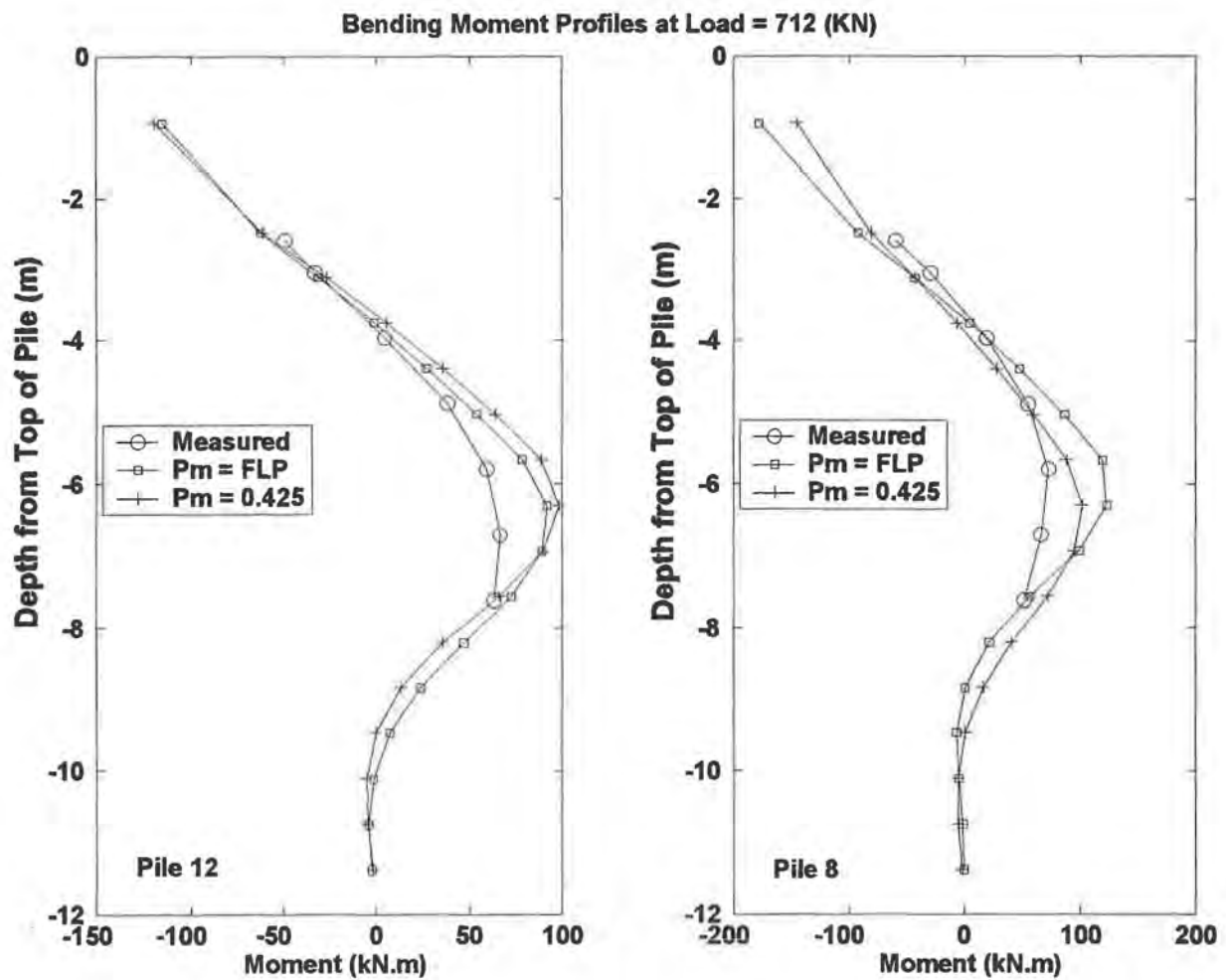
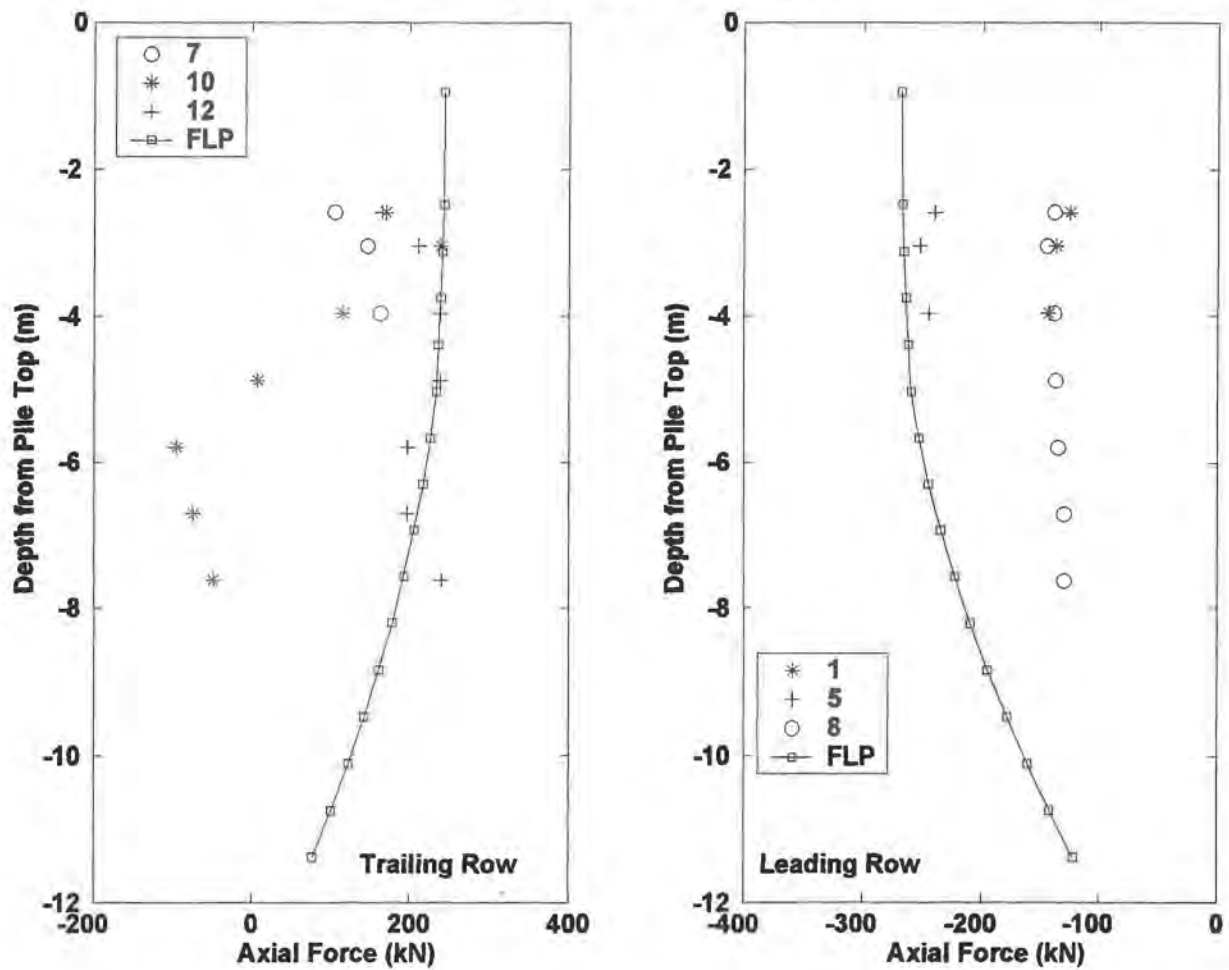


Figure D-59. Bending Moment Profile, Piles 12 and 8, Test Area 1

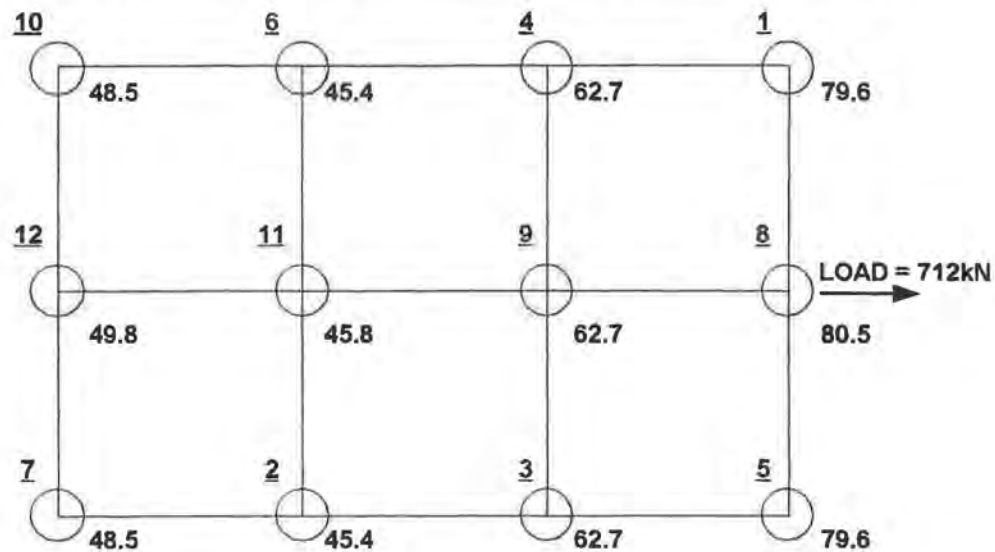
**Axial Load Profile at Load = 712 kN**



*Figure D-60. Axial Load Profile, Leading and Trailing Rows, Test Area 1*



Total Lateral Load = 712 kN 8th load step in FI-Pier, 292nd load step in the measured data			
P-Multipliers used:			
0.3	0.2	0.4	0.8



Row Sums (kN, computed):			
146.8	136.6	188.1	239.7
% Load Transferred to Row (computed):			
20.6	19.2	26.4	33.7
% Load Transferred to Row (measured):			
24.1	20.4	25.4	30.1

**Notes:**

All loads in kN

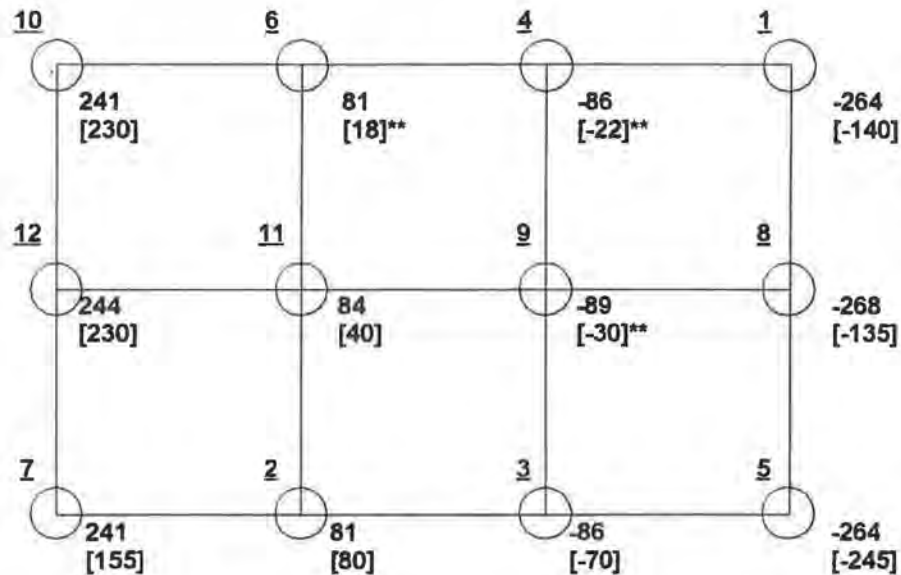
Underlined numbers denote original pile numbering

Numbers immediately to the right and below a pile

represents the computed pile head shear at a load of 1068 k N

**Figure D-61. Pile Head Shear Distribution, Group Static, Test Area 1**

Total Lateral Load = 712 kN 8th load step in FI-Pier, 292nd load step in the measured data			
P-Multipliers used:			
0.3	0.2	0.4	0.8



**Notes :**

Numbers to the right and just below the pile are the computed pile head axial loads in kN

Numbers in brackets [nn] are the measured pile head axial loads in kN

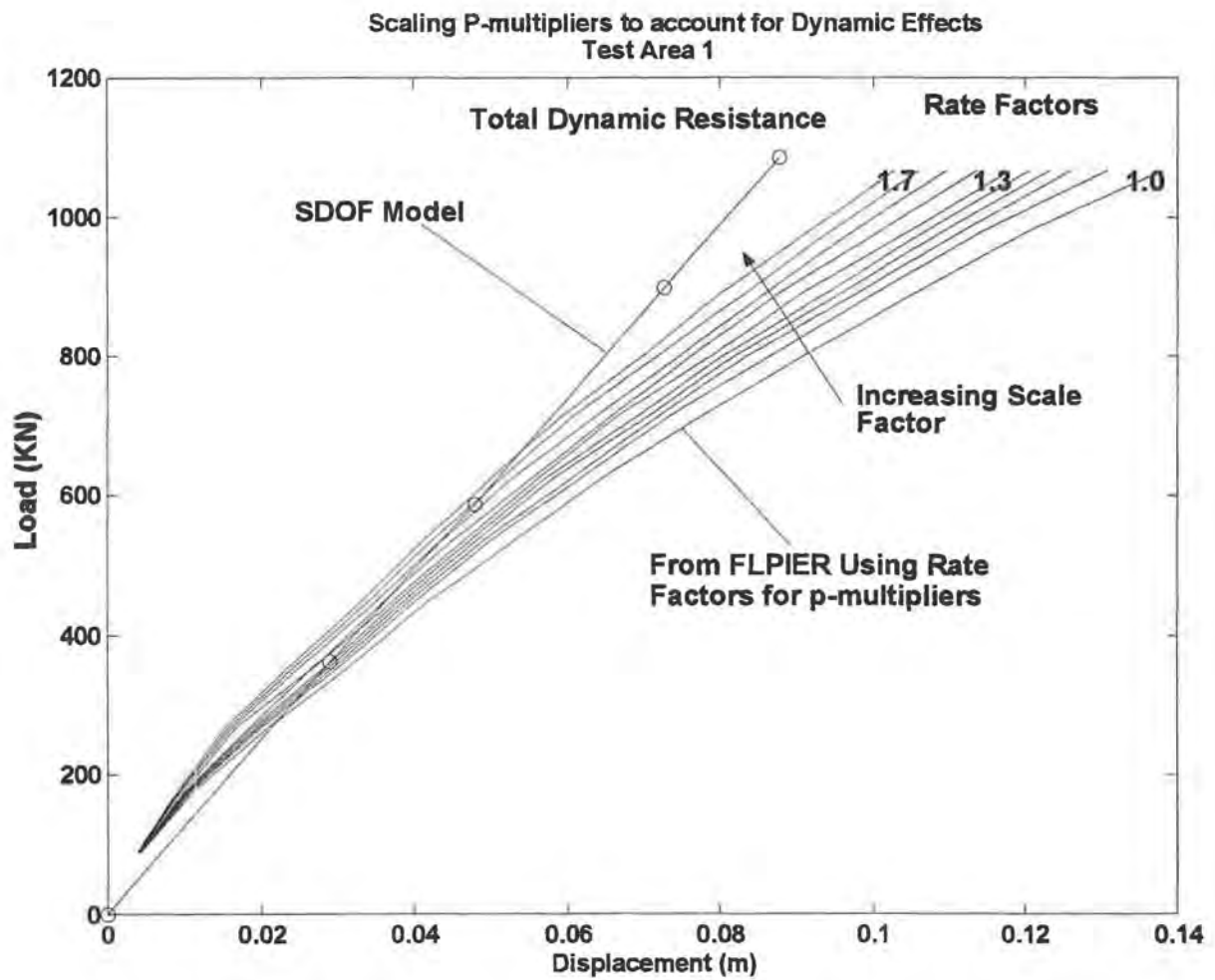
\*\* represents a pile with possibly unreliable axial load information as based on the strain records for the top 2 gauge pairs

Underlined numbers are the original pile numbers

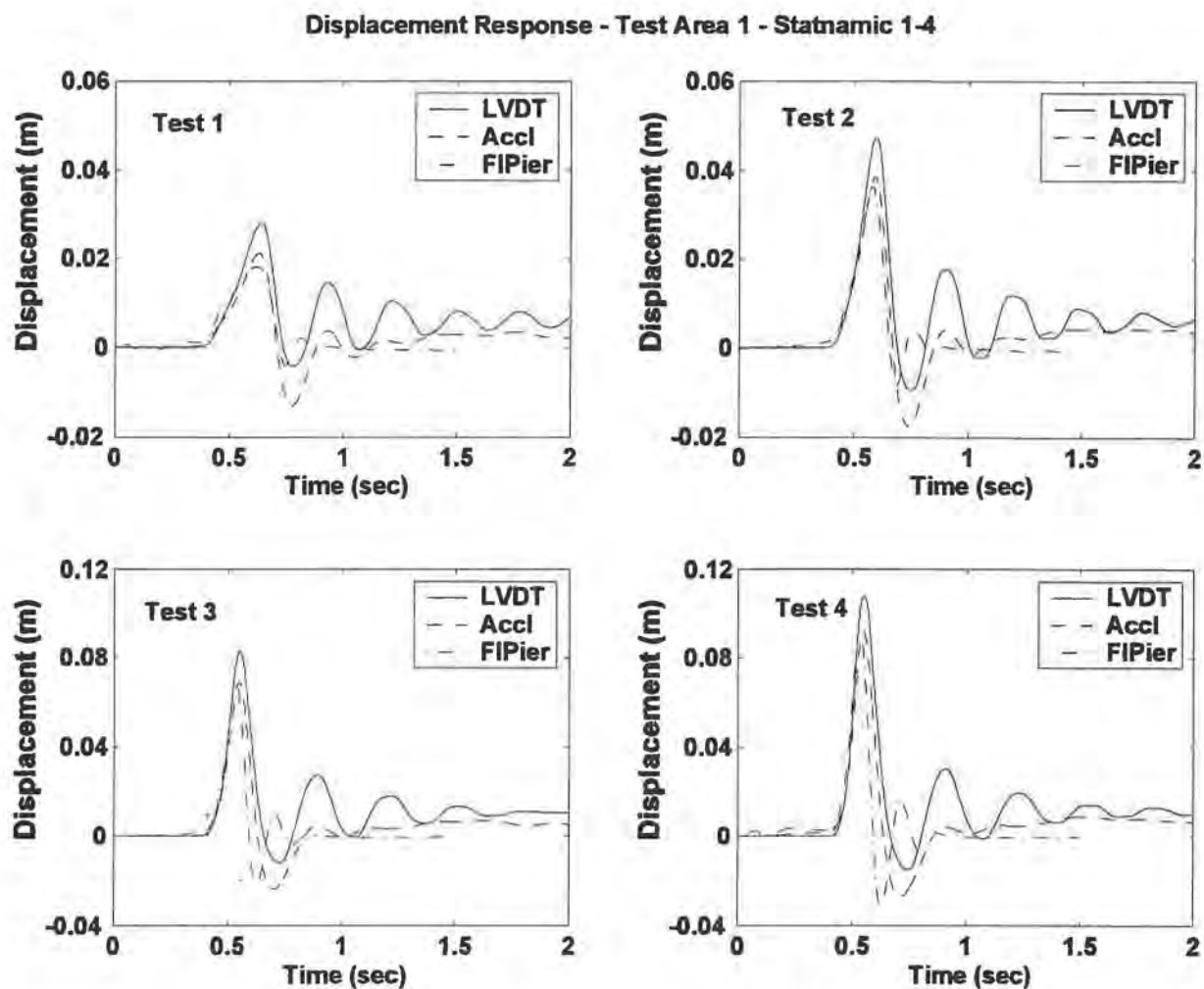
-ve is compression

+ve is tension

**Figure D-62. Axial Load Distribution, Group Static, Test Area 1**



*Figure D-63. Scaling P-multipliers to Account for Dynamic Effects*



*Figure D-64. Displacement Time Histories for Pile Cap from LVDT's, Double-Integrated Accelerometer Readings and as Computed by FLPIER, Test Area 1, Statnamic Tests 1 - 4*

## **APPENDIX E**

### **TESTING AT SPRING VILLA NGES, ALABAMA**

#### **INTRODUCTION**

The foundation load testing at the Spring Villa site consisted of lateral load tests using the NCHRP piles with groups of piles at different pile spacings and using both static and Statnamic loadings. The Spring Villa property is a dedicated geotechnical research site on Auburn University property just south of Opelika, Alabama. This site is a member of the National Geotechnical Experimentation Site (NGES) system, which is administered by the Geo-Council and is composed of six dedicated research sites around the U.S. The site is composed of a residual soil of the Piedmont Plateau and has been subject to extensive previous geotechnical study with a wide variety of in-situ and laboratory techniques [1, 2, 3].

The testing program was concentrated within a small area of the site, as shown on Figure E-1, adjacent to a group of five, 0.45-m-diameter DeWaal piles (displacement-type continuous-flight-auger piles), which were capped with a reinforced concrete pile cap and used as a reaction for static testing. The test pile groups utilized the instrumented NCHRP steel pipe piles (0.27 m in diameter by 12 m long), with a test group of 12 piles at a spacing of 3 diameters center to center and a test group of 9 piles at a spacing of 4 diameters center to center. Static lateral tests on each group were conducted by hydraulic jacking, using the DeWaal group as a reaction in each case. Dynamic loading of each pile group was achieved in the direction opposite to the static loading direction using the Statnamic device. Static lateral tests were also performed on single piles at

locations adjacent to each group.

## SOIL CONDITIONS

The soil is a residual soil typical of the Piedmont Plateau of the southeastern United States between the Atlantic Coastal Plains and the Blue Ridge Mountains and extending from Alabama to Pennsylvania. These soils are derived from weathering of metamorphic rocks, predominantly gneisses and schists of early Paleozoic Age or older [4] and are composed of micaceous sandy silts. Commonly referred to as “saprolite,” these residual soils retain the foliation and structural features of the parent rock but have the texture and appearance of soil. It is common that the clay content of the soil is somewhat higher in the upper few meters due to the more advanced state of weathering.

A number of borings and in-situ tests have been performed in the immediate area of the test foundations. Soil classification data on material from the upper 15 m from both SPT and tube samples are summarized in Table E-1. Groundwater is typically at a depth of 3 m to 4 m below the surface, and varies seasonally.

Strength data include lab tests on undisturbed samples and in-situ tests. Over 20 consolidated undrained and consolidated drained triaxial tests have been performed on samples from generally the 3 m to 12 m depth ranges. These test data suggest that the soil has an effective cohesion,  $c' = 17$  kPa and an effective friction angle,  $\phi' = 31^\circ$ . Much data from unconsolidated, undrained triaxial tests are available for the upper few meters, and a summary of these test results are presented on Figure E-2. The scatter in these data at shallow depths is evident on this figure. This variability is likely due to variations in clay content and the effects of negative pore water pressures at depths above the groundwater table. Figures E-3 and E-4 present in-situ data from

standard penetration tests (SPT) and cone penetration tests (CPT). These figures also reveal the influence of a somewhat stiffer and more cohesive crust in the upper 3 meters. In particular, note the higher friction ratio at shallow depths in the CPT soundings.

Stiffness data are available from a variety of measurements, and perhaps the most meaningful of these are the in-situ measurements of moduli from pressuremeter tests (PMT) and dilatometer tests, presented on Figure E-5. These data similarly show the effects of a surface crust, with significantly higher moduli in the upper 2 to 3 meters than in the 4 to 8 meter depth range.

The many borings and in-situ tests within the site suggest that the soil properties are spatially variable within small (cm) distances. On the whole, the site appears to have reasonably consistent soil properties (as indicated by the CPT and SPT soundings) with the high local variability superimposed on the general pattern. The soils exhibit a trend of higher stiffness and strength in the upper 3 meters, apparently due to higher clay content and pore water pressures above the groundwater level.

## **FOUNDATION INSTRUMENTATION**

The instrumentation scheme was similar to that used in the Wilmington test pile program (Appendix D). This section briefly describes the equipment used to measure response, while specific details regarding instrumentation setup on a test by test basis are described later.

### **Strain Gauges**

Each of the 13 pipe piles was instrumented with full-bridge strain gauges positioned in pairs on opposite faces of the inside of the piles at various depths. Piles marked 1 through 7 were instrumented at 3 levels (6 gauges total), at depths of 2.591, 3.048 and 3.962 meters (8.5, 10 and

13 feet) from the top of the piles. Piles marked 8 through 13 had additional strain gauge pairs at depths of 4.877, 5.791, 6.706 and 7.620 meters (16, 19, 22 and 25 feet) from the pile top, for a total of 14 strain gauges per pile.

### **External Accelerometers**

Piezoelectric ICP<sup>®</sup> type accelerometers manufactured by PCB Piezotronics were mounted on the steel frame or pile cap built around the pile group using magnetic mounting bases on steel plates bonded to the concrete with silicone adhesive. The accelerometers were used primarily to augment LVDT deflection data and to measure rocking and torsion in the cap, and also to provide a means of estimating inertial forces developed in the system during Statnamic testing.

### **Linear Potentiometers**

These have also been referred to loosely as LVDTs. These are resistance-based mechanical displacement measuring devices with 300 mm (12 inches) of travel. The linear potentiometers were used to measure the displacement response of the system during both static and dynamic loading and were mounted with clamps onto a separate reference beam.

### **Load Cells**

Various load cells were used during the testing sequence. The load cells use resistance-based strain gauges to respond to a fast load application. A Geokon 4.5 MN capacity cell was used for all static load testing as well as Statnamic testing on the NCHRP pile group.

### **Hydraulic Jack**



A 3.5-MN-capacity jack was used for all static testing. The maximum stroke was 0.45 meters, and hemispherical bearings were used at both ends to avoid any bending in the jack. The jack was manufactured by Elgood-Mayo Corporation of Lancaster, Pennsylvania.

### **Megadac Data Acquisition System**

The system is manufactured by Optim, Inc. The core consists of the primary data acquisition module (ADC-5616), which can be supplemented by additional expansion modules. Plug-in types of analog to digital data cards (AD-808FB1) were used with this system to monitor various analog devices. The ADC-5616 module allows sampling at the desired rate of 1.0 to 2.0 KHz for Statnamic tests. For static tests, data were typically sampled at 2 to 10 second intervals for the duration of the test. The Megadac system is controlled by a laptop computer using the Test Control Software (TCS) and an IEEE-488 data interface. Test data saved by TCS were exported to various formats such as ASCII and Matlab for further analysis.

### **STATNAMIC LOAD TESTING**

The Statnamic load test provides a method for generating large axial or lateral loads on foundations by "launching" a heavy reaction mass away from the foundation at an acceleration approaching 20 g's. Figure E-6 illustrates the test setup. The energy for the test is generated by burning special fuel pellets in a combustion chamber inside the Statnamic device and allowing the resulting high pressure gas to vent at a controlled rate, which in turn controls the rate at which the foundation is loaded. The reaction mass is initially set up against the side of the foundation and imparts a load that ramps up to its maximum value in a finite amount of time, usually between 0.1 and 0.3 seconds, and then gradually decreases as the mass is propelled away from the foundation

and physical contact between the foundation and the reaction mass ceases. The load is not a sharp impact, but is similar to the case where a moving barge might impact a bridge foundation, even though the ramp time for the latter case may be several times larger, depending on the mass of the barge and the speed at which it was moving. The primary advantages of the Statnamic test are that it is quick, it provides energy in a frequency band close to the fundamental frequency of the foundation, and that it produces significant inertial forces in the system that allows the determination of dynamic system properties. The Statnamic testing system is manufactured by Berminghammer Foundation Equipment of Hamilton, Ontario.

## **INSTALLATION OF THE NCHRP PILES**

The NCHRP pipe piles were driven by the Morris-Shea Bridge Company using a Delmag model D19-32 open-end diesel impact hammer (maximum rated energy of 57 kN-m, or 42 foot-kips). While installing the pile group with the frame the two middle piles (innermost) were driven first, followed by the two middle rows. The middle part of the frame was then tightened around the two middle rows, and this was followed by the driving of the two outer rows and the tightening of the rest of the frame around the entire group. For the 9-pile group, the frame was not used but rather a concrete cap was cast around the piles after installation. The center pile was driven first, followed by the surrounding piles. The actual pile driving sequence and final driving resistance is provided on Table E-2.

## **LOAD TESTING SEQUENCE**

The sequence of installation and testing of the pile foundations at the site was as follows:

- I. Installation of the 12-pile group at 3D c-c spacing with frame; drive the single pile (13);

2. Statnamic testing of 12-pile group, loading toward the east;
3. Static testing of the 12-pile group toward the west by jacking against the DeWaal foundation;
4. Static testing of the single pile (Pile 13) toward the north by jacking against the frame;
5. Extraction of the piles from the 12-pile group setup;
6. Installation of the 9-pile group at 4D c-c spacing (the frame was not used) and driving of the single pile (3);
7. Construction of a cast-in-place concrete cap around the 9-pile group;
8. Static testing of the 9-pile group toward the north by jacking against the DeWaal foundation;
9. Statnamic testing of the 9-pile group toward the south; and
10. Static testing of the single pile (13) toward the east by jacking against the pile cap

Unlike the Wilmington test (Appendix D), it proved to be quite difficult to extract the piles after the first test at the Spring Villa site (Item 5, above). At Wilmington, the contractor had a very large barge-mounted crane with a pulling capacity of several hundred tons. The piles were extracted using a sling choker and simple static pull from this crane. At Spring Villa, the side friction was greater, and the crawler-mounted, 65-ton crane was not able to pull the piles statically. A vibratory hammer was obtained from Pile Equipment Corp. to use for pile extraction. The piles are too small in diameter for the jaws of the vibro hammer to clamp, so that a steel plate had to be welded to the top of each pile for removal. It proved necessary that this welding be fairly substantial in order to survive the vibro extraction process. After several costly, difficult days of rigging, success was finally achieved in extracting the piles. However, the top of each pile was damaged by the cutting and welding required and about 0.5 meter of the top of each pile had to be

cut off. This required care to avoid damaging the wire connections and relocating the hanger within the top of each pile.

In addition to the difficulty in extracting the piles, the frame assembly had become very difficult to use due to the cutting and welding that had been done to ensure that each pile was properly connected after the inevitable small amount of lateral drift that occurs within the guide system during pile driving. The decision was made that the group with a 4D c-c spacing would be constructed using a concrete cap cast around the extensions of the driven piles. This decision was made easier because the contractor had already overextended the budget and time allocated to this project after completion of the testing on the 12-pile group and was intending to leave the job site rather than complete another installation with the frame. The 9-pile group was installed by the contractor without a template but, rather, using conventional ground locations and hammer leads. The concrete cap was formed by personnel from Applied Foundation Testing and by Auburn University graduate students using the forms that had been used for construction of the cap on the DeWaal piles. This cap was 3 m by 3 m in plan, 0.85 m thick, and heavily reinforced with #11 rebars (10 bars in each direction, top and bottom). The piles extended completely through the cap. Every visual indication suggests that this cap behaved as a rigid unit during testing with no visible cracks. The piles were oiled so as to limit bond with the cap and allow removal after demolition of the concrete cap. As of this writing (May, 2000), the cap and piles remain in place.

In order to match the center of the DeWaal cap with the loading point on the frame for static testing of the 12-pile group (and the cap for the 9-pile group), the ground was excavated to lower the surface around the test groups by about 0.5 meters.

The reference frame for support of the displacement transducers consisted of a section of HP14x89 which was about 10 m long and used as a steel beam. This reference beam spanned

between two short H-pile sections that were driven several feet into the ground with the pile hammer.

The first Statnamic testing performed on the 12-pile group achieved fairly large displacements at a load that was somewhat lower than expected. The static test against the DeWaal group went reasonably well, and both of these tests achieved large nonlinear displacements of the group in excess of 50 mm. It appeared that the Statnamic loading had some effect on the initial stiffness of the static loading in the opposite direction, undoubtedly because of permanent set and the oscillations of the group during the dynamic loading. As every other test had been performed with the static first, then the Statnamic test, this test setup was intentionally performed with the dynamic loading first to examine the difference resulting from this loading sequence. These effects will be discussed in more detail during presentation of the results. It is not thought that the loading history made a substantial difference once large lateral displacements were achieved.

The tests on the 9-pile group went well, although some strain gauges failed to respond, as some wires were apparently damaged during cutting / welding / extraction / re-driving. The static test was performed prior to Statnamic testing on this group. In this test the group achieved a lateral displacement of around 17 mm at a load of about 1.6 MN. At this point the load exceeded the capacity of the DeWaal foundation, which was pushed to failure to the south. A plastic hinge was formed at the tops of all 5 of the 0.45-m-diameter reinforced concrete piles in the DeWaal group. Note that the 3 m by 3 m by 0.9 m thick cap of the DeWaal foundation was in contact with the ground, but little or no passive pressure against the face of the cap was mobilized, since the cap extended above ground. The Statnamic loading of the NCHRP 9-pile group thus had no limitation by the reaction foundation, and large lateral displacements of this foundation of around 35 mm were mobilized.



The data will be presented in the following sections, with the static test results presented first, followed by the dynamic test results for each of the groups.

## **STATIC TEST ON 12-PILE GROUP**

The static load test was carried out by pushing the pile group and the DeWaal group apart using a hydraulic jack and a pair of steel H sections welded together to form a box-shaped loading strut. A hemispherical bearing was placed on either side of the loading apparatus so as to avoid bending stresses in the jack or load cell. The load cell, displacement transducers and strain gauges were monitored using the Megadac data acquisition system. The test took approximately 80 minutes to complete. Data were recorded on each channel at a sampling period of 10 seconds. The NCHRP pile group included a total of 12 piles, arrayed in 4 rows of 3 piles each, 7 of which were instrumented with 6 strain gauges, while 5 were instrumented with 14 strain gauges. The piles were spaced 0.819 meters apart, both laterally and along the direction of loading, and were structurally connected together using a steel framework, which served as the cap for the group. The elevations at the topmost gauge level on the piles and the base of the frame were approximately 0.15 meters and 0.6 meters, respectively, above the ground surface. Figure E-7 is a schematic diagram illustrating the layout of individual piles in the group as well as the displacement transducers. Figure E-8 shows the elevation of a single pile on the trailing row, and indicates the levels of attachment of the frame to the pile (load points) and the placement of the LVDTs. The method of attachment of the piles to the frame resulted in pile heads that were essentially fixed to the cap (moment connection).

## **Generalized Displacement Response**

A total of 4 horizontally aligned displacement transducers were used to record the lateral movement of the frame. The transducers were placed at the 4 corners in a grid pattern, which enabled the measurement of the rocking and torsional movements as well. Figure E-9 is a plot of the load vs mean lateral displacement (average of the 4 transducers). The foundation group was loaded to a maximum load of 1.1 MN, which resulted in a total lateral displacement of just under 70 mm. The maximum load was achieved using 7 load steps, with a small hold period of about 5 minutes at each load. The load jack was seen to relax slightly after the initial load was achieved at each step, and the foundation was also seen to creep slightly between successive load steps. The foundation also exhibited a permanent or plastic set of about 25 mm when the load was released fully. In addition to the lateral displacement, the rotational movement of the pile frame was also monitored. Rocking (rotation of the frame in the vertical plane of loading) was computed as the difference in lateral movement between 2 transducers along a vertical line divided by the distance between them. Two measures for rocking rotation were thus obtained, along the north and south edges of the frame. Figure E-10 shows the mean rocking rotation (average of the 2 edges) of the frame as a function of applied load. The maximum recorded mean rocking was seen to be just under 0.02 rad, with the upper edge of the frame being the leading edge. Figure E-10 also includes the plot showing the load vs. torsional movement of the frame. Torsion is defined as the rotation of the frame about a vertical axis. Torsion was computed at the top and bottom edges by taking the difference in the transducer readings and dividing by the horizontal distance between them. The maximum torsion recorded was very small at just under 0.002 rad. Finally, Figure E-11 is a plot of the individual response histories indicated by the 4 displacement transducers. Gauges 86 and 94 located at the top of the frame indicated greater displacements than gauges 87 and 84 located along the bottom, which shows that the upper edge of the frame was the leading edge.

## Strains, Bending Moments, and Load Distribution

A total of 112 strain gauges were used to monitor strains in the 12 piles. Piles 8 through 12 were fully instrumented with 14 gauges each, 7 along each face at the following depths: 2591, 3048, 3962, 4877, 5791, 6706, and 7620 mm from the head of the pile (8.5, 10, 13, 16, 19, 22, and 25 ft), while piles 1 through 7 were instrumented with 6 gauges each, 3 along each face, at depths of 2591, 3048 and 3962 mm (8.5, 10, and 13 ft) from the pile head. The distance from the head of the pile to the base of the frame was 2.14 m. Therefore the top gauge level was above the ground line (by 0.15 m) at a distance of 0.45 m below the bottom of the frame. Bending moments and axial forces in each pile were derived at each time step using the following formulas, after the strain data had been corrected using the calibration factors presented in Appendix F:

$$Ax = AE(s1 + s2)/2 \quad , \text{ and}$$

$$Bm = EI(s1 - s2)/(2y) \quad ,$$

where

$Ax$  = axial load at a particular depth at a particular load/time step,

$Bm$  = bending moment at that depth at that time step

$A$  = pile cross sectional area = 0.0103875 m<sup>2</sup>,

$E$  = modulus of elasticity of pile material = 1.9996E+08 kPa,

$I$  = moment of inertia of pile cross section = 8.8214E+07 mm<sup>4</sup>,

$s1, s2$  = strains indicated by the gauges on opposite faces at the depth of measurement, and

$y$  = distance from centroidal axis of the pile to the centerline of the gauge = 111.125 mm.

The axial load was thus based on the mean axial strain in the pile, while the bending moment was based on the difference of the 2 strain gauge readings. Matlab software was used to process the strain data in a batch mode, and several programs (“m” files) were written using the



Matlab programming language specifically for this task. Matlab was also used to prepare, display and annotate all the graphics for presentation in this report.

All in all, the strain gauges appeared to provide excellent data, although a very few gauges did not function reliably. When gauge readings did not appear reliable, they were estimated from the records of the gauges above and below the malfunctioning gauge. The estimates were checked by deriving axial load and bending moment profiles (as a function of depth at specific times) and studying these to see if they appeared reasonable. The bending moment time history was analyzed for each pile at each gauge location. Figure E-12 is the bending moment response of all gauge levels for all 12 piles presented at a load of 1.1 MN and a pile group displacement of 64 mm.

The maximum values of bending moment for each of the 5 fully instrumented piles are presented in Table E-3. The second column in the table refers to the maximum value of bending moment measured below the ground surface, while column 3 indicates the gauge level from the top of the pile at which this moment was measured. The fourth column indicates the maximum value of moment at the bottom load point (2.14m from pile top) where the frame was connected to the piles. This moment was derived by extrapolating the linear top portion of the moment vs. depth relationship for each pile at the instant of peak load. In most cases the absolute maximum moment in the pile was seen to occur below the soil surface, rather than at the base of the frame (denoted as negative moment), suggesting that either the piles were not rigidly fixed into the frame or that frame rotation during loading caused a significant relaxation of the fixing moments produced by lateral translation. It is also interesting to note that the peak subsurface moments recorded for the lead piles (11 and 12) occurred at a shallower depth than the corresponding peak moments for the trailing piles (8, 9 and 10). Figures E-13 through Figure E-17 are plots of bending moment vs depth for piles 8 through 12, respectively. Each figure presents 3 "time slices," the first at 1140

seconds when the applied load was 576 kN, and the second at 2890 seconds when the applied load was 863 kN, and the third at 3700 seconds when the load was near its peak value of 1106 kN. Each bending moment point on the graph is actually the average of 11 points spaced equally about the time of interest. This averaging was done to negate the effects of spurious variations in the digitized data from point to point that sometimes occur with digital sampling.

The bending moment vs. depth relationships were also used to derive the shear at the pile head at these points in time. The shear at the pile head was computed as the slope of the initial portion of the bending moment curve ( $dM/dZ$ ). This allows a study of the load distribution for all the piles in the group. Table E-4 shows the distribution of pile-head shear interpreted from the bending moment measurements at these times. The values of pile-head shear interpreted in this manner summed to within 3 to 5 % of the load measured by the load cell.

Figure E-18 illustrates the load distribution profile graphically. It plots the distribution on a pile-by-pile basis as well as on a row-by-row basis. The leading row (topmost) carries the maximum shear (about 29 to 30 %); rows 2 and 3 carry progressively less (about 24 % and 20 % respectively), while the trailing row (number 4) increases again to about 26 to 28 %.

An examination of the shear load transfer diagram also reveals that there are significant variations between shear mobilized by piles in a given row with no apparent pattern to the spatial variation other than the broadly general overall trend by row position noted above. The data suggest that spatial variations can be more significant than even row position regarding the shear distribution to a specific individual pile, although the trend of generally decreasing shear to trailing row piles is evident.

Axial forces in the piles interpreted from the strain measurements are presented on Figures E-19 and E-20 for all of the gauges at two load levels. These data appear to show a drop-off in

axial force near the top of the piles. Such behavior is obviously an indication of measurement error. It appears that the axial forces interpreted from the strains are less reliable than the bending moments, undoubtedly due to the large bending stress which must be averaged out of the strains in order to estimate axial force. As with any load cell, accurate measurement of force is compromised by large bending strains. The data show a general trend of tension and compression in the trailing and leading row piles, respectively.

### **STATNAMIC TEST ON 12-PILE GROUP**

A total of 4 Statnamic tests at increasing load levels were conducted on the 12-pile group by loading toward the east. The time lapse between each load level was in the order of one hour. Each test recorded a total of 121 channels of data sampled at a rate of 2000 Hz. The test included the following instrumentation:

- 1 Load Cell,
- 4 Displacement Transducers (LVDTs),
- 112 Strain Gauges, and
- 4 Accelerometers.

The instrumentation layout on the 12-pile group was illustrated on Figure E-7, with an elevation view on Figure E-8. The layout is identical to that of the static test except that the accelerometers were added to the receiver array. The load time histories for all 4 tests are plotted in Figure E-21. The peak values of load achieved for tests 1 through 4 were 374, 717, 1113 and 1378 kN, respectively. The loading impulse ranged between 0.15 and 0.30 seconds, with the larger loads ramping up faster. Note that the load pulse for load 1 was quite long and had an unusual shape. The friction on the base of the sled was so large and the reaction mass used was so high, that

the slide distance was very short and the gas pressure vented somewhat slowly for this test.

### **Generalized Displacement Response**

As for the static loading, the lateral displacement response was monitored at each of the 4 corners of the pile group frame using linear potentiometers. The mean lateral displacement responses for all of the tests have been plotted in Figure E-22, while Figures E-23 and E-24 present the mean rocking and torsional rotation response time histories. A summary of the results is presented in Table E-5.

The peak lateral displacements ranged from 7 to 60 mm, while the mean plastic set was quite small and only amounted to a few mm from the first test to the last. The oscillation was seen to damp out very quickly and showed modest increase with increasing load levels and increasing nonlinearity in the system. The oscillation beyond the exponential decay in the first 0.8 to 1.0 seconds is thought to be due to motion of the reference beams from the shock wave propagating through the earth as a result of the Statnamic event. This small spurious component to the signal should be ignored when trying to back-calculate system properties such as damping ratio.

### **Strains, Bending Moments and Load Distribution**

A total of 112 strain gauges were monitored for the tests, and most of the gauges appeared to work well. After the strain signals had been corrected using the derived calibration factors, the bending moment and axial load time histories were extracted using Matlab routines. The bending moment time history was analyzed for each pile at each gauge location. Figure E-25 shows the peak bending moment response of all gauge levels for all 12 piles for Statnamic test 4 which had a peak load cell value of 1.38 MN.

Comparing the measured moment diagrams for the 12-pile group from Wilmington to those from Auburn (e. g., Statnamic tests in Figure D-25 with those in Figure E-25), it appears that the piles in the Auburn test were not fixed to the frame with a solid moment connection, whereas those in Wilmington were. The way in which the pile heads are fixed to the cap is at least as important to head shear distributions, deformations, and moments than local variations in soil properties from point to point around the footprint of the group. Furthermore, the strain gauge data also indicate that all of pile heads at Auburn were not fixed to the frame in an identical way, which may explain some of the variability of the test results at Auburn. The head fixity conditions also must have been different between the cast-in-place cap and the steel frame cap, which would have affected the comparative responses of the 9- and 12-pile groups. Better fixity evidently existed with the CIP cap.

The maximum values of bending moment for each of the 5 fully instrumented piles are summarized in Table E-6. The second column shows the maximum subsurface bending moment recorded for each pile at the gauge level specified in column 3. Column 4 shows the estimated moment at the base of the frame computed by extrapolation of the initial linear part of the moment vs. depth function at peak load.

Figures E-26 through E-30 provide the bending moment profiles for the fully instrumented piles 8 through 12 for tests 1, 2, 3 and 4 respectively. The times at which the profiles are plotted correspond to times at which the bending moment reached its peak value. It should be noted that peak bending moments do not as a rule occur at the same instant in time for all the piles; there is usually a small phase difference for peak response from pile to pile. As before, every point on each of the graphs representing a bending moment value is actually the average of 11 points spaced equally about the time of interest.



As for the case of static loading, the front row piles (in this case Piles 8 and 10) exhibit maximum bending moments at a shallower depth than do the trailing row piles. This trend is a clear indication of increased load transfer to the soil at shallower depths for the piles in the front row.

Load distribution to individual piles was derived for each Statnamic test at the times specified. Table E-7 shows the actual distribution of pile-head shear at these times. Figure E-31 shows the load distribution profile graphically. Rows are numbered 1 through 4, top to bottom, with row 1 being the leading row in this case. The leading row (row 1) carried the highest proportion of the load (around 27 - 28 %), row 2 carried a significantly lower proportion (around 21 to 23 %), while the load carried by the rows 3 and 4 (22 to 27 %) are only a little less than that carried by row 1. It appears that spatial variability due to apparently random variations, measurement errors, or a combination of the two is more significant than variation due to geometric position. Note that the interpreted shear forces from the static test added to within 3 to 5 % of the measured force in the load cell. Such a simple summation is not possible with the dynamic test because the inertial effects result in peak moments and peak load transfer to the soil that occur at a different time than the peak applied force through the load cell.

### **Pile-Cap Acceleration Response**

The acceleration response of the frame (cap) was monitored using 6 accelerometers, 4 of which were aligned horizontally to record the lateral response of the group, while two were aligned vertically to record the vertical response. The recorded lateral signals were clean and relatively noise free, but the vertically oriented accelerometers had such small signal to noise ratios that the vertical displacements cannot be reliably estimated from these measurements. Table E-8

summarizes the acceleration results.

## INTERPRETATION OF FOUNDATION RESPONSE TO STATNOMIC LOADING USING AN EQUIVALENT SINGLE DEGREE OF FREEDOM MODEL

The dynamic response of each foundation group tested has been modeled using an equivalent single degree of freedom (SDOF) system. The dynamic response of an SDOF system is governed by the following differential equation:

$$Mu'' + Cu' + Ku = F(t) \quad , \quad (E-1)$$

where  $u''$ ,  $u'$ , and  $u$  represent the lateral acceleration, velocity and displacement of the system and define the physical state of the system at any instant of time,  $t$ .  $F(t)$  represents the forcing function.  $M$ ,  $C$  and  $K$  are the generalized mass, damping and stiffness coefficients for the SDOF system and may or may not change with time, velocity or displacement. The mass and the damping coefficients were considered constant during a single loading event. Because soil load-displacement response to lateral loading at large strains is known to be highly nonlinear, the stiffness coefficient  $K$  was modeled as a nonlinear term, which decreases with increasing displacement,  $u$ , within a single loading event. Equation E-1 may also be expressed as follows:

$$F_{\text{inertia}} + F_{\text{damping}} + F_{\text{static}} = F_{\text{statnamic}} \quad , \quad (E-2)$$

where

$F_{\text{inertia}}$  = inertial resistance from effective mass of the foundation,

$F_{\text{damping}}$  = effective viscous damping resistance,

$F_{\text{static}}$  = effective static soil resistance, and

$F_{\text{statnamic}}$  = measured force on the Statnamic load cell.

The Newmark- $\beta$  integration algorithm was used to solve the dynamic equation of motion numerically. Assuming the acceleration varied linearly between consecutive time steps, the response at any time could be computed using a total force balance and the state of the system at the previous step. The solution was implemented using a Matlab program with a graphic user interface whose input consisted of the measured static load vector  $F(t)$ , and the values of the system parameters  $M$ ,  $C$  and  $K$ . The response of the system was obtained by changing the values of  $M$ ,  $C$  and  $K$  interactively until a good match was noted between the measured displacement time history (signals from the displacement transducers), and the simulated response (computed by the SDOF model). The goodness of match between the model response and the measured response was judged by eye by plotting the time histories simultaneously on the same graph. In most cases it was possible to arrive at a good match between the two with a relatively small number of trials. The procedure used for signal matching can be broadly divided into the following steps:

11. Determine the mass coefficient by computing the mass of the foundation above the ground line. The actual participating mass may vary slightly from this number, and  $M$  may be changed slightly ( $\pm 5\%$ , but usually slightly more) during the trials to establish a better match.
12. Estimate the lateral static stiffness of the foundation, and use this value as a starting point for the stiffness parameter  $K$ . Compare the first peak in the computed displacement response with the first peak in the measured response and determine if  $K$  appears reasonable. Increase or decrease  $K$  until a good match is achieved for the amplitude of the first peak. It may also be necessary to vary the mass parameter  $M$  slightly to match the phase of the simulated response to the measured response where the displacement ramps up to its first peak. If  $M$  is chosen to be too large, the computed displacement



response will lag the measured response.

13. Finally, adjust the value of the damping coefficient by changing the damping ratio until the post-loading free vibration parts of the measured and computed displacement responses are in good agreement. The measured response may be affected by significant permanent deformations, cannot be simulated using the simplified SDOF model. The objective, however, is to estimate the amount of damping present in the system, and this can be done by comparing the amplitude decay pattern and the damped frequency of free vibration.

The effective mass  $M$  is comprised of the total mass of the pile cap and portions of individual piles that contribute inertially to the response. The latter is usually restricted to the mass of the piles above the mud line or ground line, but may vary slightly depending on the magnitude of displacement and the degree of nonlinearity of the system. As such, this is the parameter that is easiest to define for SDOF analysis. The mass term affects the amplitude and form of the forced vibration part of the response (duration of Statnamic load), and the frequency of oscillation for the post-loading event where the system undergoes damped free vibration.

The numerical value of the damping coefficient (viscous dashpot constant),  $C$ , has relatively little effect on the response magnitude during the actual loading event, but is significant in determining the amplitude decay and the damped free vibration frequency for post-loading response. In order to relate  $C$  more meaningfully to a system damping parameter, the damping constant may also be expressed as a percent of the critical damping  $C_c$  as follows:

$$\xi = C/C_c = C/[2(KM)^{1/2}] ,$$

where  $\xi$  is termed the damping ratio, and,

$$F_{\text{damping}} = 2 \xi (KM)^{1/2} u' .$$

The magnitude of the first peak in the simulated displacement time history is sensitive to the value of the effective stiffness parameter chosen,  $K$ . The stiffness term also effects the frequency of damped free vibration at the end of the Statnamic loading event.  $K$  is also used to back-calculate a derived static load-displacement response, which may be compared to the load-displacement function obtained from a conventional static test.

### **SDOF Model of 12-Pile Group**

Consistent with the observation that the displacement response of the 12-pile group was strongly nonlinear, the equivalent foundation stiffness was modeled as a nonlinear function of displacement. The effective foundation model stiffness  $K$  was assumed to decrease as an exponential function of displacement, starting from an initial value, and limited by bounds that could be changed within the analysis, using a procedure identical to that described in Appendix D. The analysis itself was designed to simulate each Statnamic test in sequential order, from the lowest to the highest load amplitude. The solution for each test was based upon the previous load and deflection history of the system, and the foundation stiffness  $K$  at the beginning of each test was initialized to the stiffness value at the end of the previous test. The damping ratio was assumed to remain constant for all four tests. Since it is known that the first peak in the simulated displacement response is particularly sensitive to  $K$ , the model parameters were adjusted by trial and error until a good match was observed between the measured and computed first peaks for all four tests. The match is also influenced by the frequency of the computed free vibration response and how closely

it matches the frequency of the measured signal. No attempt was made to model the inelastic deformation observed in the real system (i.e., the permanent set). This was done in an effort to keep the model as simple mathematically as possible and not introduce another set of complex parameters that would influence the simulated behavior.

Figure E-32 shows the match between the measured and computed displacement response for all four Statnamic tests conducted on the 12-pile group at Spring Villa. The terms LC1...LC4 refer to Statnamic load cases 1 through 4, respectively. The abscissa represents the time axis, while the ordinate represents lateral displacement in meters. Figure E-33 is a plot of the nonlinear stiffness time history for all four tests. The system begins with an initial stiffness of 73 MN/m, and degrades to a stiffness of roughly 21 MN/m at the end of the final test. The other system parameters include a mass of 15,000 Kg for the frame and piles and a damping ratio of 0.15.

One objective of this analysis is to derive the equivalent static load deflection curve for the system and compare it to the measured static response of the group recorded at the same location. Figure E-34 compares the measured and derived static responses. The derived static load-displacement relationship was calculated using the parameters defined in Table E-9.  $F_s$  is the peak equivalent static force and is computed as the product of the peak computed displacement  $U_s$  and the value of the equivalent static stiffness  $K$  at that particular time step. Figure E-34 also illustrates the total derived soil resistance  $F_d$  as a function of the displacement  $U_d$  at which it occurs.  $F_d$  is computed as the vector sum of the equivalent static and damping force vectors, where the damping force vector is the product of the scalar damping coefficient and the velocity vector computed by the model.  $F_d$  is thus a function of the time rate at which the foundation is loaded. The peak static force was seen to lag the peak total force for all four load cases, with the phase difference increasing with increasing applied loads and damping forces in the system.

The use of the SDOF model results to examine the Statnamic test results illustrates that the effective static soil response was somewhat stiffer during the Statnamic loading in comparison to the soil stiffness during the static test, which, as stated earlier, was conducted after the Statnamic test for this particular group. It is likely that some portion of the displacement during the static loading was related to degradation from the Statnamic loading, which was done first. The small gap around the piles that resulted from the oscillation of the group undoubtedly contributed to some additional displacements during the static loading. At large displacements, the static test measurements and the derived static response appear to converge. These data also illustrate the rate-dependent contribution of the mobilized soil resistance as indicated by the total static + damping relationship. This effect is seen to be quite small at relatively small displacements but becomes more significant at large loads and displacements.

## **STATIC TEST ON 9-PILE GROUP**

The static load test on the 9-pile group was conducted similarly to that of the 12-pile group by pushing the pile group and the DeWaal group apart using a hydraulic jack. As described previously, the 9 pile group had a spacing of 4D c-c and a cap consisting of cast-in-place reinforced concrete. This likely produced different conditions of pile-to-cap moment fixity for the 9- and the 12-pile groups. Another noteworthy difference is that the distance between the base of the cap and the ground surface was slightly less for the 9-pile group than for the 12-pile group. The same steel box-shaped loading strut was used to apply the load to the group, with a hemispherical bearing placed on either side of the loading apparatus. The load cell, displacement transducers and strain gauges were monitored using the Megadac data acquisition system. The NCHRP pile group included a total of 9 piles, arrayed in 3 rows of 3 piles each, 5 of which were instrumented with 6

strain gauges, while 4 were instrumented with 14 strain gauges. The piles were spaced 1.09 meters apart, both laterally and along the direction of loading, and were structurally connected together using a reinforced concrete cap which was 3 m by 3 m in plan and 0.84 m thick. The elevations at the topmost gauge level on the piles was approximately at the ground surface and the base of the cap was approximately 0.35 meters above the ground surface. Figure E-35 is a schematic diagram illustrating the layout of individual piles in the group as well as the displacement transducers. Figure E-36 shows the elevation of a single pile on the trailing row, and indicates the levels of attachment of the frame to the pile (load points) and the placement of the LVDTs.

The test was conducted in a manner similar to that for the 12-pile group — loading in increments and holding each increment for a period of about 5 minutes. The test took approximately 60 minutes to complete, including recording of data on each channel at a sampling period of 10 seconds. The test was stopped at a load of about 1.6 MN, when the DeWaal group (reaction) of 5 piles yielded and displaced several inches without achieving any increase in load. At this point the 9-pile group had a lateral displacement of around 17 mm and, although the load vs. displacement was nonlinear at this point, appeared to have some additional capacity.

### **Generalized Displacement Response**

A total of 4 horizontally aligned displacement transducers were used to record the lateral movement of the frame. The transducers were placed at the 4 corners of the cap in a grid pattern, which enabled the measurement of the rocking and torsional movement as well as lateral translation.. Figure E-37 is a plot of the load vs. mean lateral displacement (average of the 4 transducers). The foundation group was loaded to a maximum load of 1.6 MN, which resulted in a total lateral displacement of around 17 mm. The maximum load was achieved using 6 load steps,



with a small hold period of about 5 minutes at each load. The load jack was seen to relax slightly after the initial load was achieved at each step, and the foundation was also seen to creep slightly between successive load steps. The foundation also exhibited a permanent or plastic set of less than 3 mm when the load was released fully. Note also that there was some small seating load on the group when the instruments were zeroed to start the test, apparently resulting from seating the load cell and jack and not releasing this pressure completely. This showed up in the load cell as a small negative load measurement when the load cell was disengaged, so the measured load was adjusted by this magnitude for all data analyses. Note that the result is that the load vs displacement plot starts with a small nonzero force at the initial measurement. There is probably an additional few tenths of a mm of displacement associated with this force, but this magnitude is not considered significant.

In addition to the lateral displacement, the rotational movement of the pile cap was also monitored. Rocking (rotation of the frame in the vertical plane of loading) was computed as the difference in lateral movement between 2 transducers along a vertical line divided by the distance between them. Two measures for rocking rotation were thus obtained, along the north and south edges of the cap. Figure E-38 shows the mean rocking rotation (average of the 2 edges) of the frame as a function of applied load. The maximum recorded mean rocking was seen to be approximately 0.005 rad (much smaller than the 12 pile group), with the upper edge of the cap being the leading edge. Figure E-38 also includes the plot showing the load vs. torsional movement of the cap. Torsion is defined as the rotation of the cap about a vertical axis. Torsion was computed at the top and bottom edges by taking the difference in the transducer readings and dividing by the horizontal distance between them. The maximum torsion recorded was very small at around 0.0005 rad. Finally, Figure E-39 is a plot of the individual response histories indicated by the 4 displacement

transducers. Gauges 84 and 82 located at the top of the cap indicated greater displacements than gauges 83 and 88 located along the bottom which shows that the upper edge of the cap was the leading edge (i. e., the rotation motion was a pitching-down motion).

### **Strains, Bending Moments, and Load Distribution**

A total of 86 strain gauges were used to monitor strains in the 9 piles. Piles 10 through 13 were fully instrumented with 14 gauges each, 7 along each face at the following depths below the original top of pile: 2591, 3048, 3962, 4877, 5791, 6706, and 7620 mm (8.5, 10, 13, 16, 19, 22, and 25 ft), while Piles 1 through 7 were instrumented with 6 gauges each, 3 along each face at depths of 2591, 3048 and 3962 mm (8.5, 10, and 13 ft) from the pile top. The piles were marked with a painted stripe on the outside at the level of the top gauge level, and the piles were driven so that this stripe was at approximately the groundline. The base of the cap was approximately 0.35m above the ground. Bending moments and axial forces in each pile were derived at each time step using the following formulas, after the strain data had been corrected using the calibration factors presented in section Appendix F:

$$Ax = AE(s1 + s2)/2 \quad , \quad \text{and}$$

$$Bm = EI(s1 - s2)/(2y) \quad ,$$

where

$Ax$  = axial load at a particular depth at a particular load/time step,

$Bm$  = bending moment at that depth at that time step,

$A$  = pile cross sectional area = 0.0103875 m<sup>2</sup>,

$E$  = modulus of elasticity of pile material = 1.9996E+08 kPa,

$I$  = moment of inertia of pile cross section = 8.8214E+07 mm<sup>4</sup>,

$s1, s2$  = strains indicated by the gauges on opposite faces at the gauge depth, and

$y$  = distance from centroidal axis of the pile to the centerline of the gauge = 111.125 mm.

The axial load was thus based on the mean axial strain in the pile, while the bending moment was based on the difference of the 2 strain gauge readings. The Matlab software was used to process the strain data in a batch mode, and several programs (“m” files) have been written using the Matlab programming language specifically for this task. Matlab was also used to prepare, display and annotate all of the graphics for presentation in this report.

Most of the strain gauges appeared to provide good data, although a some gauges apparently were damaged by the cutting, welding, extraction, and installation of the piles between the tests on the 12- and 9-pile groups and did not function reliably. Readings for each gauge that did not appear to provide a reliable signal were estimated from the records of the gauges above and below it. The estimates were checked by deriving axial load and bending moment profiles (as a function of depth at specific times) and studying these to see if they appeared reasonable. The bending moment time history was analyzed for each pile at each gauge location. Figures E-40 through E-45 provide the bending moment response of all gauge levels for all 9 piles presented at a loads of 0.7, 1.1, and 1.6 MN, respectively.

The maximum values of bending moment for each of the 4 fully instrumented piles is presented in Table E-10. The second column in the table refers to the maximum value of bending moment measured below the ground surface, while column 3 indicates the gauge level from the top of the pile at which this moment was measured. The fourth column indicates the maximum value of moment at the base of the cap. This moment was derived by extrapolating the linear top portion of the moment vs. depth relationship for each pile at the instant of peak load. In general, the absolute maximum moment in the pile occurs at the base of the cap (negative moment). In Table



E-10 the moments at the connection (base of cap) were, in general, slightly larger in absolute value than the maximum subgrade moments ("Maximum B. M.," in the second column of the table). In the static test of the 12-pile group (Table E-3), on the other hand, the maximum moments that were measured at the connections were much smaller in absolute value than the maximum subgrade moments, indicating a structural difference in the two groups that precludes a direct comparison of the results.

Figures E-40 through Figure E-45 also show how the bending moment vs. depth relationship was used to derive the shear at the pile head by computing the slope of the initial portion of the bending moment curve ( $dM/dZ$ ). This allows a study of the load distribution for all the piles in the group. A small error in measured bending moment can lead to a large error in computed shear. The precision in these measurements do not appear sufficient to derive shear by individual piles with accuracy, but the average shear for the group of piles appears to match reasonably well with the overall measured load on the group.

The distribution of pile-head shear interpreted from the bending moment measurements at several values of load are presented on Table E-12 and graphically on Figure E-46. The values of pile-head shear interpreted as described in the above manner summed to within 3 to 5 % of the measured load on the load cell. The leading row (topmost) carried the highest shear (about 44 %), rows 2 and 3 carried progressively less (about 35 % and 21 %, respectively).

Axial forces in the piles interpreted from the strain measurements are presented on Figures E-47 and E-48 for all of the gauges at two load levels. As discussed in the previous section, these data are subject to errors due to the large bending stress that must be averaged out of the strains in order to estimate axial force; accurate measurement of axial force in any load-measuring instrument is compromised by large bending strains. The data show a general trend of tension and

compression in the trailing and leading row piles, respectively.

## **STATNAMIC TEST ON 9-PILE GROUP**

A total of 3 Statnamic tests at increasing load levels were conducted on the 9-pile group by loading toward the south. During each test a total of 101 channels of data were sampled and recorded at a rate of 2000 Hz. The test included the following instrumentation:

- 1 Load Cell,
- 4 Displacement Transducers (LVDTs),
- 86 Strain Gauges, and
- 10 Accelerometers.

The instrumentation layout on the 9-pile group was illustrated on Figure E-35, with an elevation view on Figure E-36. The layout is identical to that of the static test except that the accelerometers were added to the receiver array. The load time histories for all 3 tests are plotted in Figure E-49. The peak values of load achieved for tests 1 through 3 were 470, 1250, and 1950 kN, respectively. The loading impulse ranged between 0.15 and 0.30 seconds, with the higher loads ramping up faster.

### **Generalized Displacement Response**

As for the static loading, the lateral displacement response was monitored at each of the 4 corners of the pile group frame using linear potentiometers. The mean lateral displacement responses for all the tests have been plotted in Figure E-50, while Figures E-51 and E-52 present the mean rocking and torsional rotation response time histories. A summary of the results is tabulated in Table E-12.

The peak lateral displacements ranged from about 5 to 35 mm, while the mean plastic set was quite small and only amounted to a few mm from the first test to the last. The oscillation was seen to damp out very quickly and showed modest increase with increasing load levels and increasing nonlinearity in the system. In general, the measurements of pile cap displacement and acceleration appeared to be very clean and relatively free of spurious noise and oscillations compared to the tests on the 12-pile group, probably due to the use of the concrete cap in lieu of the steel frame.

### **Strains, Bending Moments and Load Distribution**

A total of 86 strain gauges were monitored during the Statnamic tests, and most of the gauges appeared to work well. After the strain signals had been corrected using the derived calibration factors, the bending moment and axial load time histories were extracted using Matlab routines. The bending moment time history was analyzed for each pile at each gauge location. Figures E-53 through E-58 provide the peak bending moment response of all gauge levels for all 9 piles for Statnamic tests 2 and 3, which had a peak load cell values of 1.25 MN and 1.95 MN, respectively.

The maximum values of bending moment for each of the 5 fully instrumented piles are summarized in Table E-13. The second column shows the maximum subsurface bending moment recorded for each pile at the gauge level specified in column 3. Column 4 shows the estimated moment at the base of the frame computed by extrapolation of the initial linear part of the moment vs. depth function at peak load. As with the static test, the relative moments at the cap connections and in the subgrade suggest a solid moment connection (fixed-head conditions), unlike the head fixity for the piles capped by the frame in the 12-pile-group test.

Figures E-53 through E-58 also provide the interpreted shear values for the average pile in

each row. The times at which the profiles are plotted correspond to times at which the bending moment reached its peak value. Table E-14 provides a summary the actual distribution of pile head shear at each Statnamic load incident, and Figure E-59 shows the load distribution profile graphically. Rows are numbered 1 through 3, top to bottom, with row 1 being the leading row in this case. For Statnamic load 3 (a condition essentially unaffected by prior static loading), the row-wise loads are equal, which suggests minimal group action at 4 D spacing.

Figure E-60 provides indicated axial loads in the piles for the time of peak load at Statnamic loading 3.

### **Pile-Head Acceleration Response**

The acceleration response was monitored using 10 accelerometers, all of which were aligned horizontally to record the lateral response of the group. The signals recorded were clean and noise free, and generally of higher quality than the signals obtained with the steel frame. The displacement signals obtained from integration of the acceleration data matched quite well with the measured displacements from the LVDT's. Table E-15 summarizes the acceleration results.

### **SDOF Model of 9-Pile Group**

The Statnamic loading of the 9-pile group was evaluated using the simple single degree of freedom (SDOF) model described previously. Consistent with the observation that the displacement response of the 9-pile group was strongly nonlinear, the equivalent foundation stiffness was modeled as a nonlinear function of displacement. The effective foundation model stiffness  $K$  was assumed to decrease as an exponential function of displacement, starting from an

initial value, and limited by bounds that could be changed within the analysis. The analysis itself was designed to simulate each Statnamic test in sequential order, from the lowest to the highest load amplitude. The solution for each test was based upon the previous load and deflection history of the system, and the foundation stiffness  $K$  at the beginning of each test was initialized to the stiffness value at the end of the previous test. The damping ratio was assumed to remain constant for all four tests. Since it is known that the first peak in the simulated displacement response is particularly sensitive to  $K$ , the model parameters are adjusted by trial and error until a good match was observed between the measured and computed first peaks for all three tests. The match is also influenced by the frequency of the computed free vibration response and how closely it matches the frequency of the measured signal. No attempt was made to model the inelastic deformation observed in the real system (i. e., the permanent set). This was done in an effort to keep the model as mathematically simple as possible and not introduce additional complex parameters that would influence the simulated behavior.

Figure E-61 shows the match between the measured and computed displacement response for all three Statnamic tests conducted on the 9-pile group at Spring Villa. The terms LC1...LC3 refer to Statnamic load cases 1 through 3, respectively. The abscissa represents the time axis, while the ordinate represents lateral displacement in meters. Figure E-62 is a plot of the nonlinear stiffness time history for all four tests. The system starts off with an initial stiffness of 100 MN/m, and degrades to a stiffness of roughly 62 MN/m at the end of the final test. These values are, respectively, much higher than the values for the 12-pile group test (73 MN/m initially and 21 MN/m at the end of the final test), despite the fact that the 9-pile group had fewer piles. This behavior may be due, at least partially, to the differences in head fixity in the two groups and to less pile-soil-pile interaction (higher  $p$ -multipliers) in the 9-pile group. The other system parameters



include a mass of 18,000 Kg for the frame and piles and a damping ratio of 0.15.

One objective of this analysis is to derive the equivalent static load-deflection curve for the system and compare it to the measured static response of the group recorded at the same location. Figure E-63 shows the comparison between the measured and the derived static response. The derived static load-displacement relationship was calculated using the parameters defined in Table E-16.  $F_s$  is the peak equivalent static force and is computed as the product of the peak computed displacement  $U_s$  and the value of the equivalent static stiffness  $K$  at that particular time step. Figure E-63 also illustrates the total derived soil resistance  $F_d$  as a function of the displacement  $U_d$  at which it occurs.  $F_d$  is computed as the vector sum of the equivalent static and damping force vectors, where the damping force vector is the product of the scalar damping coefficient and the velocity vector computed by the model.  $F_d$  is thus a function of the time rate at which the foundation is loaded. The peak static force was seen to lag the peak total force for all four load cases, with the phase difference increasing with increasing applied loads and damping forces in the system.

The results of the SDOF model to examine the Statnamic test illustrate that the effective static soil response was somewhat stiffer during static loading in comparison to the Statnamic test. This trend is the reverse of the trend observed in the 12-pile group; however, the load test sequence was also reversed, with the static test done first in this instance. It is likely that some portion of the displacement during the initial Statnamic loading was related to the permanent displacement left from the static loading, which was done first. At large displacements, the static test measurements and the derived static response would appear to converge. Note also the scale of these plots in relation to the test on the 12-pile group; the stiffer response of this group resulted in smaller total displacements and thus small changes in initial stiffness appear more significant. The

static data also illustrate the rate dependent contribution of the mobilized soil resistance as indicated by the total static + damping relationship. This effect is seen to be quite small throughout the range of mobilized displacements up to 35 mm.

## **STATIC TESTS ON SINGLE PILES**

Two static load tests were conducted at locations illustrated on Figure E-1. The following instruments were used to monitor the response:

- 1 Load Cell,
- 14 Strain Gauges, and
- 2 Displacement Transducers (LVDTs).

The test setup for each pile is illustrated on Figures E-64 and E-65. The displacement response for each test pile was monitored using 2 LVDTs as shown in these figures. The maximum average displacements recorded were 26 and 35 mm for the two piles at a maximum load of around 215 kN. Figure E-66 is a plot of the load-displacement response of the two single test piles.

The bending moments and axial stresses in the Pile 13 were extracted from the corrected strain data and are illustrated for several load values on Figure E-67. The data for Pile 3 were unreliable as a number of the strain gauges appeared to have been damaged. For comparison, the slope of the bending moment line for a cantilever beam (no soil resistance) is also shown for obtaining the values of measured shear at the pile head.

### **Modeling Rate Effects using a Single Degree of Freedom System**

The SDOF model may be used to derive a rate-effect parameter to predict the dynamic resistance of the foundation to loading, which varies with foundation velocity (rate of loading). The

equivalent static and total soil resistance functions computed by the model, along with the average velocity of the foundation during the loading event may be used as follows:

- Compute the effective static stiffness of the foundation,  $K_s$ :

$$K_s = F_s \div U_s ,$$

- Compute the effective total stiffness of the foundation,  $K_t$ :

$$K_t = F_d \div U_d ,$$

- Compute the average rate of displacement of the foundation during the loading event,  $V$ :

$$V = U_s \div t ,$$

where

$t$  = total time for displacement to go from 0 to  $U_s$ .

- Plot the ratio  $K_t/K_s$  as a function of  $V$  for each Statnamic test.

The terms  $F_s$ ,  $U_s$ ,  $F_d$  and  $U_d$  have been defined earlier. The effective static stiffness  $K_s$  is computed at the value of time at which the foundation reaches its maximum displacement,  $U_s$ . The effective total stiffness  $K_t$  is computed as the ratio of the peak total resistance (static + damping) and the displacement at which it occurs. It should be noted that the peak total resistance and the peak static resistance usually do not occur at the same time.

The rate parameter accounts for the influence of damping resistance offered by the foundation during dynamic loading and is a function of both the peak displacement  $U_s$  and the average rate of displacement,  $V$ . It is not meant to be an exact representation of the dynamic foundation resistance, but is meant to serve as a guideline for estimating the resistance that might be mobilized by a forcing function that induces the system to react at a different rate. The rate parameter functions were derived for the Statnamic tests for the two pile groups at Spring Villa. They are illustrated on Figure E-68. Each graph presents the results for the last three Statnamic tests, which have been indicated



by the peak displacement.

## **FEM MODEL OF SPRING VILLA TESTS USING FLPIER**

The computer program FLPIER (Florida Pier) provides a model with which to evaluate the test results in terms of load distribution within groups and reduced efficiencies due to group effects when the group is load statically or with the Statnamic device.

When a group of piles are loaded laterally, the resistance offered by the group is usually not equal to the sum of the resistance of each pile acting alone in isolation. Very importantly, the condition of pile-head fixity within the group plays a major role in the stiffness of a group pile versus the stiffness of an identical isolated pile loaded with a free head. The group resistance is also a function of pile location within the group, and pile spacing. One way to account for group effects is to scale the p-ordinates of the computed p-y curves, and the program FLPIER uses p-multipliers to scale the ordinates of computed p-y curves on a row-by-row basis. For a group with four rows of piles, the default p-multipliers used by the program are as described in Table E-17. These multipliers represent a group efficiency of 70 - 75 % for 3D spacing, and about 95 % for 5D spacing. The p-multipliers may also be defined explicitly for each row by the user.

The results from the tests on the 12 pile group at 3d c-c spacing and the 9 pile group at 4d c-c spacing provide a means of evaluating the design model which is incorporated into FLPIER. This comparison of the conceptual model with field test results provides a means of understanding the test results as well as providing the direct experience with the model which engineers can use to develop judgement and refine or improve such models.

### **Lateral Load Test on Single Pile**

In order to use the FLPIER model to evaluate group effects, it was first necessary to “calibrate” the soil model used for single pile behavior based upon the results of the tests on the two isolated single piles. The two tests were reasonably similar, with small variations attributable to random spacial variations in soil properties on the site. Consistent with the anticipated conditions based on the distribution of undrained shear strength with depth (see Figure E-2), there is a general trend of stiffer cohesive soil in the upper few meters with softer soil below. And, judging from the shear strength data, the effects of dessication and negative pore water pressure in the top few meters make variability of soil strength in the top few meters a significant factor. It is worth noting that the softer of the two single pile tests was in an area which had been excavated about ½ meter below the ground surface in area at the location of the stiffer of the two. Thus, some effect of this crust may have contributed to the slight differences between the two single piles.

An initial estimate of soil strength and stiffness parameters was developed based upon the average anticipated soil properties at the site and using the Reese et al. soil model for p-y curves in clays [4]. Note that there is no widely accepted p-y criterion in use for Piedmont residual silty clay/clayey silt. With minor adjustments in the strength profile, a reasonable match with the single pile static test data was achieved. The final soil properties used in this model utilize an undrained shear strength ( $C_u$ ) that ranges from 207 kPa (0.03 ksi) at the ground surface to 103 kPa (0.015 ksi) at a depth of 2.3 m to 69 kPa (0.010 ksi) at a depth of 10 m. The soil stiffness parameter,  $\epsilon_{50}$ , was taken as 0.07 for the entire length of the pile. The measured and computed lateral load displacement response at the load point are shown in Figure E-69, and the measured and computed bending moment vs depth are shown in Figure E-70. These figures demonstrate that the soil model used captures reasonably well the general behavior of the test pile. It is possible to obtain a fortuitous match of the pile top load vs displacement relationship, but the general agreement of the location of

the maximum bending moment suggests that the distribution of soil resistance in the subsurface is also reasonable.

### **Axial Response of a Single Pile**

No axial static loading tests were performed with which to calibrate the axial response of the pile. However, there have been numerous axial loading tests of other test piles on the project site which suggest that the axial capacity of the piles would not be expected to have been exceeded in the lateral tests on the group. During the process of installation of the 9-pile group, the pile driving analyzer (PDA) was utilized to measure the soil resistance to penetration. A few restrike blows were performed on piles 12 and 9 (pile 9 was driven off to the side) after a period of 3 to 5 hours of setup. CAPWAP analyses of these data suggest an axial capacity of around 1000 KN, with almost all of this in side shear with very small tip resistance. Static axial tests on many drilled shafts and other deep foundations at the site generally suggests that the maximum side shear is mobilized at around 10 mm of displacement, and this general trend is consistent with the data suggested by the CAPWAP analyses of the dynamic test of the steel piles.

### **Lateral Load Tests on Pile Groups**

The static load test on the 12-pile group was modeled using the FLPIER finite element model similar to that used for the Wilmington tests, as was shown in Appendix D. Each pile was modeled using sixteen linear beam elements, each having a length of 0.626 m. The steel frame holding the twelve piles together as a group was designed to transfer applied lateral loads to the individual piles at two levels. For the model, the elevation of the pile cap was set at 0.35 m (the level of the attachment of the frame to the piles at the lower point, which was also the lower load point for each

pile). The pile cap was modeled using shell elements, each 0.276 m in thickness and with an elastic modulus equal to that of steel to account for the total mass of the frame and the pile lengths above 0.35 m. The resulting flexural stiffness of the cap was roughly equal to that of a concrete cap 0.53m (21 inches) thick. The static lateral load was simulated by a combination of equivalent lateral loads and moments applied at the heads of the three piles along the left face (shorter dimension) of the group. The moments were included in the forcing function to account for the offset of the upper load points relative to the elevation of the pile cap used in the model.

Because the pile bending moment data and observations suggest that some internal rotation occurred within the frame, the piles were not modeled as completely fixed to the cap. Some of this internal rotation is thought to be due to the failure of welded connections on cross bracing members and at the pile/frame connections. This “partial fixity” between the piles and the frame introduces some additional degree of uncertainty in the interpretation of the results. However, FLPIER has a provision to model partial fixity, and this provision was exercised with these test results. A partial fixity factor of 0.1 was used at the pile/cap connection to release some of the fixing moment that occurs at this connection.

The 9-pile group was modeled using 9 similar piles, with the elevation of the pile cap set also at 0.35 m (the level of the base of the concrete cap). The pile cap was modeled using shell elements, each 0.85 m in thickness and with an elastic modulus equal to that of concrete ( $3 \times 10^7$  kPa, or 4400 ksi). The static lateral load was simulated by a combination of equivalent lateral loads and moments applied at the heads of the three piles along the left face (shorter dimension) of the group. The moments were included in the forcing function to account for the offset of the upper load points relative to the elevation of the pile cap used in the model. The piles were modeled as fixed to the cap.

The input parameters for the lateral soil model were based upon the values derived from the

analysis of the single-pile test described previously. Both of the pile groups were in areas that had been excavated to about 0.5 m below grade so as to match the loading point elevation with that of the reaction foundation and the Statnamic loading device. Therefore, the uppermost 0.6 m of the soil profile used for the single pile FLPIER model was removed for the analyses of the group tests.

The input parameters for the axial pile-soil interaction model were based on the CAPWAP analyses results of a restrike blow on one of the piles after installation, and also upon the default parameters suggested in FLPIER. Observations of the test results suggest that none of the piles yielded in the axial direction, so the axial pile stiffness is really the only relevant parameter. The soil was defined as a cohesive material with a unit load transfer strength of 70 kPa in the upper 2 m of soil and 140 kPa below. The shear modulus (used for construction of the default t-z curves) was set at 100 times this value for the widely-spaced 9-pile group, 30 times this value for the 12-pile group. The lesser modulus was used for the 12-pile group so as to reduce the axial stiffness somewhat for axial group effects due to the closer pile spacing. The value for the 9-pile group is consistent with the FLPIER help manual recommendations.

#### *Static Response of 12-pile group*

The p-multipliers used for the initial analysis of the 12-pile group were the default values used by FLPIER for a pile group with four rows. These values are 0.3, 0.2, 0.4, and 0.8, starting with the trailing row and ending with the leading row. The computed lateral load displacement response at the base of the cap is shown on Figure E-71, along with the measured static response and the static response derived from the Statnamic test using the SDOF procedure outlined previously. Computed and measured (static) load vs. rotation response is shown on Figure E-72. Note that the Statnamic test was performed prior to the static test, and therefore the measured stiffness in the static test may



be slightly soft due to the permanent set that occurred in the earlier loading in the opposite direction. Observations of the soil near the ground surface suggest that the shallow soils exhibit gapping in the near field around the pile as would occur with cohesive soils. The small permanent set remaining after the previous statnamic loading (around 4 mm) and the resulting near-field gap around the pile adds a small displacement offset prior to mobilization of the full soil resistance to the static test loading. Even though the equivalent static response is derived from the Statnamic measurements, it is possible that this response may be slightly stiffer than a static test performed much more slowly in these cohesive soils due to rate effects on the shearing strength of the soil (rate effects on the overall foundation have been accounted for). So, the research team concludes that the two measured curves represent the expected range of response and that best possible match would be one that is approximately the average of these two curves. Note that the two measured curves appear to converge at large displacement.

The computed lateral displacement at the pile head using the default p-multipliers is seen to be somewhat stiffer than the measured response, although not by a great deal. In order to derive model parameters that more closely match the measurements, the p-multipliers were scaled down by a uniform value until a better match was obtained. The computed displacements and rotations are shown to be very close to the measurements for a model with an additional scaling factor of 0.8 applied (thus, p-multipliers by row were 0.24, 0.16, 0.32, 0.64). There is no magical significance to this factor other than to define the magnitude of the error in the prediction. It appears that the default values are generally within the range of engineering accuracy for most applications. One possible explanation for this overestimation of stiffness may be related to the soil profile at the site. This profile includes a stiffer crust over a somewhat weaker underlying stratum, and this type of profile may tend to amplify the group effects; the group is more greatly influenced by the deeper

soils than is an isolated pile.

In order to evaluate the effects of a more simple model, analyses were performed using a uniform  $p$ -multiplier. Additional plots of lateral displacement and rotation are shown on Figures E-71 and E-72 for a model with the  $p$ -multiplier for all 12 piles set at 0.34 (the average of 0.24, 0.16, 0.32, and 0.64). The overall response with this simple set of  $p$ -multipliers appears to be sufficiently close to the measurements for general engineering and design purposes. A simple, uniform  $p$ -multiplier may have advantages for some seismic analyses in which load reversals occur in multiple directions and the consideration of directional effects makes the analysis much more complex.

Figures E-73 through E-75 provide plots of the computed and measured bending moments as a function of depth for three piles; piles 8 and 10 are in the trailing row, while pile 12 is in the leading row. There is general agreement in the trend of the measured and computed bending profiles, but quite a wide variation exists in the magnitude of the maximum moment values. The computed maximum moments are somewhat less than measured on pile 8 but significantly more than measured on pile 10. These piles are in the same row, so the computed values are identical; the results shown demonstrate the wide variations observed within the group in which measurements were made.

The axial load vs. depth relationships for the piles on the leading and trailing rows have been plotted on Figures E-76 and E-77, along with the axial load profile computed by FLPIER. The measurements of axial load from the strain gauges are quite erratic due to measurement imprecisions, so little insight can be derived from this comparison.

Using the final row-wise  $p$ -multipliers used in FLPIER, the computed pile-head shear distribution at a lateral load of 1111 kN was found to be 21% - 16% - 25% - 38% for trailing to leading rows, respectively. These values compare to the measured distribution of 27% - 21% - 23% -

29% from the static test. The general trend is seen to be similar, but somewhat less extreme variations are observed in the measurements. Of course, the measurements are influenced by apparently random variations within the group attributed to variations in soil response unrelated to spatial position.

In summary, the group effects on the 12-pile group were substantial and slightly greater than those predicted using FLPIER. The stratigraphy of stiff crust over somewhat softer underlying soil is thought to have contributed to the more significant group effects. After calibration using the single pile test data, the FLPIER model for static response of the 12-pile group appears to capture the general observed behavior reasonably well for engineering design purposes. The observed distribution of shear by rows was somewhat less extreme than predicted. The observed distribution by pile was more variable than predicted owing to apparently random variations in soil response, which appear unrelated to spatial position. The use of an averaged  $p$ -multiplier did not reproduce the observed shear distribution pattern, but it appears to have provided results that are suitable for design purposes.

#### *Static Response of 9-pile Group*

The  $p$ -multipliers used for the initial analysis of the 9-pile group were the default values recommended for use in FLPIER for a pile group with three rows. Values used for the spacing of 4 diameters c-c were interpolated between the values given in the help file for 3 d spacing and 5 d spacing; these values are 0.5, 0.625, and 0.9, starting with the trailing row and ending with the leading row. As was the case for the 12-pile group, these default values produce a response that was slightly too stiff, and better agreement was obtained by scaling the  $p$ -multipliers down by a factor of 0.8. The resulting  $p$ -multipliers are 0.4, 0.5, and 0.72 for the trail to lead rows, respectively. The



computed lateral load-displacement response at the base of the cap using these values is shown on Figure E-78, along with the measured static response and the static response derived from the Statnamic test using the SDOF procedure outlined previously. Computed and measured (static) load vs. rotation response is shown on Figure E-79. Note that the static test was performed prior to the Statnamic test in this instance, and therefore the measured initial derived equivalent static test data may be slightly too soft due to the permanent set that occurred in the earlier loading in the opposite direction. In addition, the initial stiffness of the measured static response is a slightly too stiff due to some residual load in the jack that appeared to be present when the instrumentation was zeroed. (This was discovered upon unloading.) So, the research team concludes that the two measured curves represent the expected range of response and that best possible match would be one that is approximately the average of these two curves. Note that the two measured curves appear to converge at large displacement. The rocking rotation measurements were quite small, as lateral translation was the dominant mode of motion.

As was the case for the 12-pile group, the computed lateral displacement at the pile head using the default p-multipliers was too small (system too stiff). The computed response after scaling down the p-multipliers by a uniform factor of 0.8 is seen to match the measurements reasonably well, generally within the range of engineering accuracy for most applications. The stratigraphy (stiff crust over softer soil below) at the location of the 9-pile group is similar to the that at the location of the 12 pile group a few meters away and may be the reason for the slightly smaller p-multipliers.

As with the 12-pile group, analyses were also performed using a uniform p-multiplier. Additional plots of lateral displacement and rotation are shown on Figures E-78 and E-79 for a model with the p-multiplier of all 9 piles set at 0.54 (the average of 0.4, 0.5, and 0.72). The overall response with this simple model appears to be sufficiently close to the observations for general

engineering and design purposes. A simple uniform p-multiplier may have advantages for some seismic analyses in which load reversals occur in multiple directions and the consideration of directional effects makes the analysis much more complex.

Figures E-80 through E-82 provide plots of the computed and measured bending moments as a function of depth for three piles; piles 10 and 11 are in the lead row while pile 13 is in the trailing row. There is general agreement in the trend of the measured and computed bending moment profiles, but the magnitudes of the maximum moment values do not match. Some error in the maximum measured values may be attributed to the strains superimposed from the axial pile forces.

The axial load vs. depth relationship for the piles on the leading and trailing rows have been plotted on Figures E-83 and E-84, along with the axial load profile computed by FLPIER. The measurements of axial load from the strain gauges are quite erratic due to measurement imprecisions, but the outer bounds of the measurements are in rough agreement with the computed axial forces.

Using the final row-wise p-multipliers in FLPIER, the computed pile-head shear distribution at a lateral load of 1333 kN was found to be 19% - 36% - 45% for trailing to leading rows, respectively. These values are virtually identical to the measured distribution from the static test (average by rows). However, this excellent agreement may be fortuitous, as the Statnamic loading in the opposite direction indicated load distributions that were more nearly uniform. As for all of the previous pile group tests in this study, the measurements are influenced by apparently random variations within the group attributed to variations in soil response unrelated to spatial position.

In summary, the group effects on the 9-pile group were substantial and slightly greater than that predicted using FLPIER. The stratigraphy of stiff crust over somewhat softer underlying soil is thought to contribute to the more significant group effects. After calibration using the single pile test data, the FLPIER model for static response of the 9 pile group appears to capture the general

observed behavior reasonably well for engineering design purposes. The observed distribution by pile was more variable than predicted, owing apparently to random variations in soil response (p-y behavior), which appears unrelated to spatial position. The use of an averaged p-multiplier does not reproduce the shear distribution pattern but appears to provide results which are suitable for design purposes.

#### *Dynamic Response Using FLPIERD*

In order to evaluate the dynamic version of FLPIER that was developed for this project, FLPIERD, the site-calibrated static p-y curves, pile geometries, cap properties, p-multipliers adjusted to average uniform static values (as described above) and the Statnamic force measurements from the load cell were sent to the computational research team at the University of Florida. In each case the pile group model arrangement that was used was identical to the arrangement for the static tests, except for the load time history provided as input. For the Spring Villa 12-pile group, the partial fixity at the pile/cap connection was used exactly as it was with the static analyses. The model used includes both velocity-dependent damping and hysteretic damping in the p-y curves, as described in Appendix C. Some minor structural damping was included, in the form of proportional damping equal to  $(0.015 \times \text{cap mass}) + (0.01 \times \text{cap stiffness}) + N[0.01 \times \text{pile mass}) + 0.01 \times \text{pile stiffness}]$ , where N is the number of piles in the group. Some other parameters were varied for one test case as will be discussed. The results of these computations were returned in the form of the FLPIERD output files. The plots provided in this section of the report were generated from those files by the experimental research team at Auburn University.

For the 12-pile group at Spring Villa, the inputs to FLPIERD were similar to those for the Wilmington test for Test Area 1, except for the differences in site-calibrated p-y curves due to the

soil differences and the partial fixity parameter. Presented on Figure E-85 are the computed and measured displacement time histories for the 12-pile group at the Auburn Spring Villa Test Site. For this test case, FLPIERD is seen to match reasonably well with the measured displacement data in terms of both amplitude and frequency. Note that the LVDT and accelerometer data are very similar for this test, indicating little movement of the reference beam. It is not immediately apparent why the model appears to provide such good agreement at this site and fares so poorly for the Wilmington data. Analyses were performed for these two test cases with the radiation damping set to zero; this made virtually no difference in the computed response as the damping component appears to be dominated by hysteretic damping.

The FLPIERD model for the 9-pile group are thought to provide the most realistic computed response due to the excellent measurements obtained on the concrete cap and the confidence that this cap provides a rigid and well-defined end condition. Presented on Figure E-86 are the computed and measured displacement time histories for the second Statnamic loading of the 9-pile group. The computed initial peak displacement is relatively near the measured value (although somewhat low), and the frequency response is fairly similar. Presented on Figure E-87 are the FLPIERD results for the third Statnamic loading of the 9-pile group, computed using dynamic soil parameters similar to the previous runs. These computed data are also reasonably close to the measured response.

The third Statnamic loading of the 9-pile group was used to evaluate the effects of various input soil parameters within FLPIERD so as to develop some sense of the relative importance of these. Also shown on Figure E-87 is a computed response for which a dynamic rate effect has been added to the soil p-y curves. This effect has been included as outlined in Appendix C, with a soil factor F2 of 0.07 and a baseline (static) loading rate of  $7\text{E-}6$  m/s (1 inch/hour). The effect of loading rate using these parameters is seen to be negligible, as the two computed curves are virtually identical.

FLPIERD was performed with mass added to the p-y curves so as to represent some contribution of participating soil mass within the pile group. Data are presented on Figure E-88 which illustrate the effect of adding mass equal to  $\frac{1}{2}$  of the soil mass within the group, distributed evenly to the p-y curves on the group piles. The effect is seen to be most significant in extending the period of oscillation. The effect on the amplitude of motion is fairly small for this group.

Data are presented on Figure E-89 to illustrate the effect of radiation damping on the overall computed response. The influence of this parameter is seen to be very minor; the computed damping in this foundation is clearly dominated by hysteresis.

The conclusion resulting from these parametric runs using FLPIERD is that the dynamic response of the model of the test foundation is dominated by the static stiffness, the overall mass of the system, and the hysteresis in the p-y curves.

## SUMMARY

The results of the testing program at the Auburn Spring Villa Test Site and the analyses of the data can be summarized as follows:

1. With only a few small exceptions, the instrumentation and measurements appear to provide reliable indications of the behavior. The strain gauge pairs within the pile provided generally reliable bending moment measurements, although the superposed axial forces appear to contribute to some measurement errors in converting the measured strains to bending moment. The superposed bending strains made the measured axial forces in the piles subject to large measurement errors. In essence, these steel pipe piles do not make very good load cells when large bending stresses are imposed and measurements are obtained using only an averaged pair of strain sensors. Historically, field loading tests using a pinned connection



have avoided some of these measurement problems since axial and bending forces are not superposed on the piles; however, such tests are less realistic foundation models than the fully coupled foundation tests performed as part of this research.

2. The group effects were substantial, and slightly larger than expected using the default p-multipliers for both the 3 d and 4 d center-to-center spacing. Close agreement was obtained between measured and computed results when p-multipliers were scaled down by a factor of 0.8. The differences between the 3 d and 4 d center-to-center spacing predicted by using the interpolated default p-multipliers in the FLPIER code appear to be approximately correct.
3. The pile axial stiffness for the 4d spacing appeared to be somewhat higher than was the case for the 3d spacing. It might be suggested that designers may apply judgement and use somewhat softer t-z curves for closely spaced groups of piles (accomplished by using a somewhat smaller shear modulus within FLPIER), but the measurements of group rotation for these two test cases are insufficient to develop specific design guidelines. No piles were observed to yield in the axial direction during these tests.
4. The load distribution to the piles in the group by average row position was somewhat less extreme than computed using the row-by-row p-multipliers in FLPIER.
5. The actual measured load distribution to the individual piles in the group was somewhat more extreme than computed using the row-by-row p-multipliers in FLPIER. There appeared to be significant and substantial variation in individual pile stiffness that was unrelated to geometric position alone. Random spatial variability in soil response due to stratigraphic variations, installation effects, or other uncontrolled variables were at least as important as geometric position in determining the actual shear distribution to an individual pile within the group. The general pattern of greater load to the leading row and less to

trailing rows could only be discerned by looking at average response for piles in a given row. These factors were observed not only for the piles driven within the frame template, but also for piles driven in the free field for the 9-pile group, which had a cast-in-place concrete cap constructed after pile driving was completed.

6. The use of the frame for pile group testing proved to be difficult, time consuming, and lead to uncertainties relating to small connection details. While the difficulties with the use of this frame could be resolved, the use of a cast-in-place concrete cap proved to be much more reliable, cost effective, and provided better measurements. The use of the frame on future projects is not recommended.
7. The static FLPIER computer model using a single average P-multiplier (equal to the weighted average of all the P-multipliers by row position) provided a good prediction of overall behavior. Given the many other uncertainties in the actual distribution of shear and moment, this simple approach may be sufficient for many engineering design applications.
8. The interpretation of the Statnamic loading using the simple single degree of freedom (SDOF) model appears to provide a relatively good correlation with static test results. The rate of loading effects with the Statnamic loading device appear to be relatively modest, although increasing with large displacements. The Statnamic device provided the capability to push the 9-pile group to large lateral displacements after the reaction foundation failed during the static testing and was therefore a very valuable part of the test program.
9. In general, the static version of FLPIER was very successful in modeling the test results. The partial fixity at the pile/frame connection appears to be modeled appropriately using this feature of FLPIER. The dynamic version did a reasonable job of modeling the Statnamic loadings of the 12 and 9 pile groups at Spring Villa, capturing the peak displacements and

frequency of motion reasonably well. This agreement was achieved by (1) using as inputs to the model static p-y curves for the soil, such as the Reese et al. p-y curve formulation for stiff clay with small changes to calibrate the p-y curves to the behavior of reference, or "control," piles at the test site, (2) defining (internally) unloading branches to the p-y curves in which hysteretic damping was included in the system by allowing the p-y curves to "loop," as described in Appendix C, (3) by including modest material damping (as proportional damping), as defined in this chapter, for the piles and cap, and (4) using a uniform average of the default static p-multipliers.

10. Sensitivity studies conducted using the FLPIERD model for the 9 pile group suggests that the most important parameters controlling the computed dynamic response to inertial lateral loading are the static soil stiffness (including axial stiffness of individual piles), the overall mass of the foundation, and the hysteresis damping provided by the p-y curves. Radiation damping, structural damping, rate effects in soil stiffness (as defined using the default parameters outlined in Appendix C), the use of uniform average p-multipliers in lieu of row-by-row values, and the addition of a modest amount of soil mass had relatively small effects on the computed response.

## REFERENCES

1. Brown, D. A. and Vinson, J., "Comparison of strength and stiffness parameters for a Piedmont residual soil." Proceedings of the First International Conference on Site Characterization - ISC'98, Atlanta, GA, USA (April, 1998), pp.1229-1234.
2. Vinson, J. and Brown, D., "Site characterization of the Spring Villa geotechnical test site and a comparison of strength and stiffness parameters for a Piedmont residual soil." *Report*



- No. IR-97-04, Highway Research Center, Harbert Engineering Center, Auburn University, AL, (1997), 385 p.
3. Mayne, P.W., Brown, D., Vinson, J., Schneider, J., and Finke, K., "Site Characterization of Piedmont Residual Soils at the NGES, Opelika, Alabama." *National Geotechnical Experimentation Sites*, GSP No. 93, ASCE, Reston, VA, (2000), pp. 160-185.
  4. Sowers, G.F., and Richardson, T.L., "Residual Soils of the Piedmont and Blue Ridge." *Transportation Research Record No. 919*, National Academy Press, Washington, D.C., (1985), pp. 10-16.
  5. Reese, L.C. and Welch, R.C., "Lateral Loading of Deep Foundations in Stiff Clay." *Journal of the Geotechnical Engineering Division*, ASCE, Vol. 101, No. GT7 (1975), pp. 633-649.

Table E-1. Soil Classification Data

Test	No. Tests	Avg	Std Dev
water content	64	34%	7.5%

Test	No. Tests	Avg	Std Dev
% sand	48	47%	17%
% silt	22	33%	8%
% clay	22	10%	6%
LL*	22	46	10
PI	22	8	6
unit wt. (kN/m <sup>3</sup> )	35	18.2	0.5

\* Liquid Limit (LL) and Plasticity Index (PI) data do not include 20 tests which were reported as “nonplastic”.

Manually insert Table E-2 here



<i>Table E-3. Maximum Bending Moments - 3 by 4 Pile Group Static Test</i>			
Pile Number	Maximum B.M. (N.m)	Gauge Level from Top	B.M. at Connection (N.m)
12	-1.11e+05	3	-2.00e+03
11	-7.65e+04	3	2.40e+04
10	-5.68e+04	4	2.20e+04
9	-7.89e+04	4	-4.00e+04
8	-1.22e+05	4	6.50e+04

Sign convention is reversed from standard convention for positive and negative moment in piles

<i>Table E-4. Pile-Head Shear Distribution - 3 by 4 Pile Group Static Load Test</i>			
Pile Number	Shear @ Load = 576 kN (kN)	Shear @ Load = 863 kN (kN)	Shear @ Load = 1106 kN (kN)
1	-44	-68	-79
2	-51	-75	-92
3	-50	-74	-80
4	-55	-80	-108
5	-41	-73	-99
6	-72	-109	-142
7	-48	-68	-75
8	-67	-98	-136
9	-10	-16	-18
10	-27	-38	-52
11	-47	-75	-96
12	-44	-61	-78

<i>Table E-5. Displacement Response - 3 by 4 Pile Group Statnamic Tests</i>				
Test Number	1	2	3	4
Maximum Displacement (mm)	7.1	20.3	41.5	60.1
Maximum Rocking Rotation (rad)	0.0029	0.0085	0.0177	0.0295
Maximum Torsional Rotation (rad)	0.00032	0.0010	0.0012	0.0024
Mean Set (mm)	0.3	1.6	1.0	1.6

Table E-6. Maximum Bending Moments - 3 by 4 Pile Group Statnamic Tests			
Pile Number	Maximum B.M. (N.m)	Gauge Level from Top	B.M. at Connection (N.m)
Test 1			
8	2.581E+04	3	-5.00E+03
9	1.602E+04	3	-5.30E+02
10	1.185E+04	3	-5.15E+02
11	1.852E+04	3	-3.90E+03
12	2.506E+04	3	-7.78E+03
Test 2			
8	6.539E+04	3	-1.50E+04
9	3.636E+04	3	-1.60E+03
10	2.890E+04	3	-1.47E+03
11	3.916E+04	3	-1.02E+04
12	5.250E+04	3	-2.21E+04
Test 3			
8	1.150E+05	3	-3.40E+03
9	6.259E+04	3	1.59E+04
10	5.239E+04	3	2.30E+04
11	6.401E+04	4	-6.94E+03
12	8.531E+04	4	-1.25E+04
Test 4			
8	1.688E+05	3	3.10E+04
9	9.247E+04	4	4.40E+04
10	7.257E+04	3	2.00E+04
11	9.734E+04	5	-5.95E+03
12	1.281E+05	4	-2.11E+04

<i>Table E-7. Pile-Head Shear Distribution - 3 by 4 Pile Group Statnamic Tests</i>				
Pile Number	Shear - Test 1 (kN)	Shear - Test 2 (kN)	Shear - Test 3 (kN)	Shear - Test 4 (kN)
1	32	58	75	77
2	34	61	92	104
3	32	63	73	74
4	37	66	94	94
5	34	66	88	102
6	30	50	80	105
7	29	51	67	71
8	32	77	107	122
9	16	31	31	24
10	13	27	38	42
11	19	33	44	52
12	27	52	61	81



*Table E-8. Acceleration Results - 3 by 4 Pile Group Statnamic Tests*

Test Number	Peak Average Acceleration (g's)	Time (sec)
1	0.871	0.821
2	1.995	0.562
3	6.196	0.551
4	10.094	0.527

<i>Table E-9. SDOF Model Results for 3 by 4 Pile Group</i>				
Computed Response				
Load Case	$U_s$ (mm)	$F_s$ (kN)	$U_d$ (mm)	$F_d$ (kN)
Test 1	7.67E+00	3.99E+02	7.64E+00	4.01E+02
Test 2	1.96E+01	7.78E+02	1.90E+01	7.97E+02
Test 3	3.83E+01	1.11E+03	3.57E+01	1.18E+03
Test 4	5.75E+02	1.21E+03	4.80E+01	1.43E+03

<i>Table E-10. Maximum Bending Moments - 3 by 3 Pile Group Static Test</i>			
Pile Number	Maximum B.M. (N.m)	Gauge Level from Top	B.M. at Connection (N.m)
13	2.20e+04	4	-3.07e+04
12	3.10e+04	3	-1.05e+04
11	3.84e+04	3	-2.11e+04
10	4.41e+04	4	-1.18e+05

<i>Table E-11. Pile-Head Load Distribution - 3 by 3 Pile Group Static Test</i>			
Row Number	Pile Number	Shear @ Load = 1143 kN (kN)	Shear @ Load = 1579 kN (kN)
1	4, 10, 11	330	510
2	1, 7, 12	264	399
3	5, 6, 13	162	213

<i>Table E-12. Displacement Response -3 by 3 Pile Group Statnamic Tests</i>			
Test Number	1	2	3
Maximum Displacement (mm)	5.1	17.0	34.0
Maximum Rocking Rotation (rad)	0.0014	0.0029	0.0065
Maximum Torsional Rotation (rad)	0.00034	0.00070	0.0014
Mean Set (mm)	1.1	1.8	2.1

<i>Table E-13. Maximum Bending Moments - 3 by 3 Pile Group Static Tests</i>			
Pile Number	Maximum B.M. (N.m)	Gauge Level from Top	B.M. at Connection (N.m)
Test 1			
10	-1.451E+04	4	4.188E+04
11	-1.501E+04	3	3.744E+04
12	-1.314E+04	3	1.164E+04
13	-1.383E+04	3	1.560E+04
Test 2			
10	-5.184E+04	4	1.152E+05
11	-3.823E+04	4	1.148E+05
12	-3.783E+04	3	4.531E+04
13	-4.196E+04	4	5.072E+04
Test 3			
10	-8.421E+04	4	1.742E+05
11	-7.285E+04	5	1.976E+05
12	-5.891E+04	3	8.729E+04
13	-8.218E+04	4	9.501E+04

<i>Table E-14. Pile-Head Load Distribution - 3 by 3 Pile Group Statnamic Tests</i>			
Row Number	Pile Number	Shear - Test 2 (kN)	Shear - Test 3 (kN)
1	4, 10, 11	-351	-495
2	1, 7, 12	-384	-522
3	5, 6, 13	-270	-459

<i>Table E-15. Acceleration Results - 3 by 3 Pile Group Statnamic Tests</i>		
Test Number	Peak Average Acceleration (g's)	Time (sec)
1	0.824	0.576
2	3.170	0.517
3	7.418	0.493



<i>Table E-16. SDOF Model Results for 3 by 3 Pile Group</i>				
Computed Response				
Load Case	$U_s$ (mm)	$F_s$ (kN)	$U_d$ (mm)	$F_d$ (kN)
Test 1	5.30E+00	5.24E+02	5.30E+00	5.26E+02
Test 2	1.78E+01	1.34E+02	1.74E+01	1.38E+03
Test 3	3.46E+01	2.13E+03	3.22E+01	2.25E+03

<i>Table E-17. Default p-multipliers - FLPIER</i>		
Row	p-multiplier	p-multiplier
	Spacing = 3 diameters	Spacing = 5 diameters
Leading	0.80	1.00
2nd	0.40	0.85
3rd	0.20	0.70
Trailing	0.30	0.70

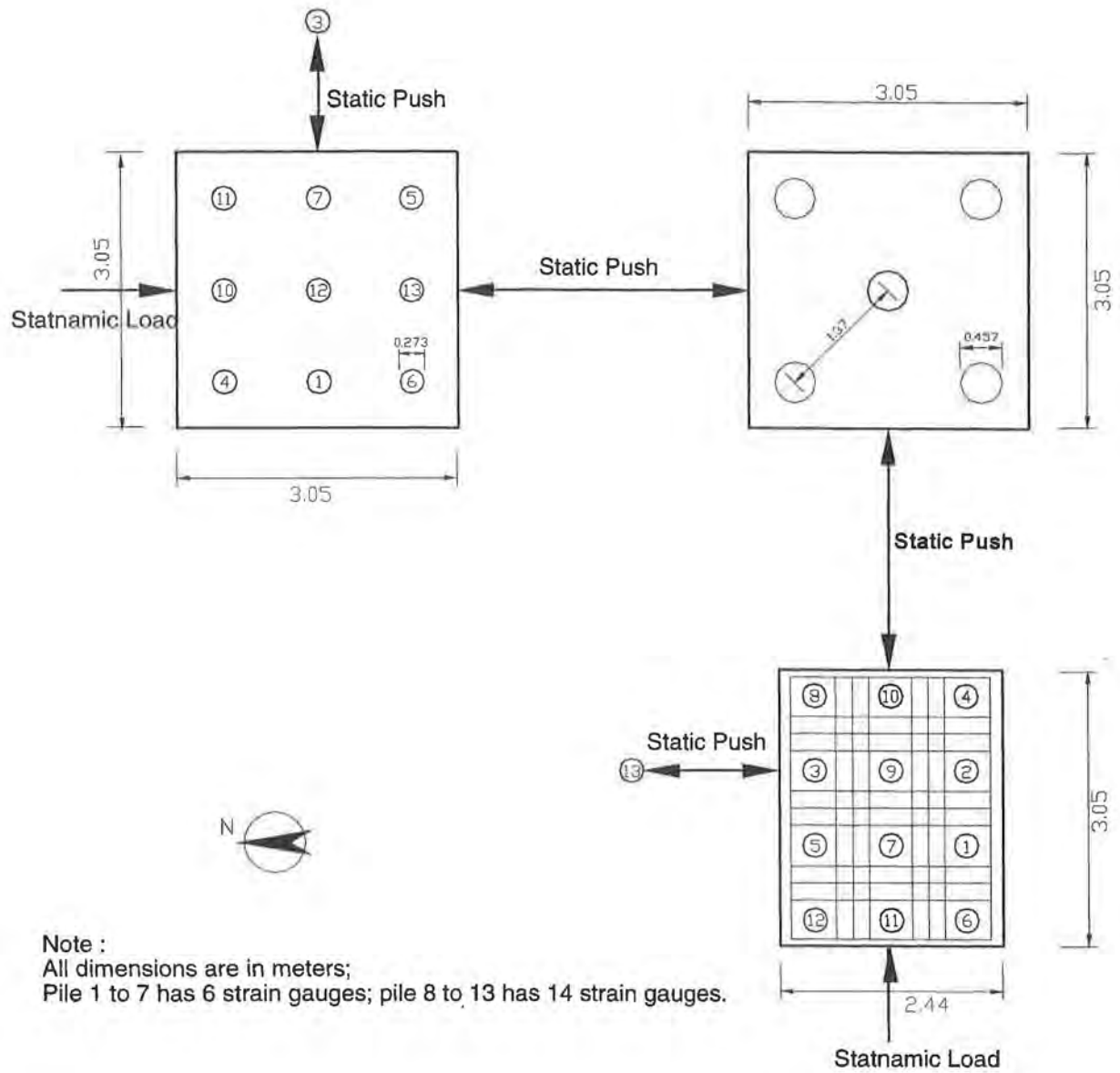


Figure E-1. Site Plan for Spring Villa Testing Program

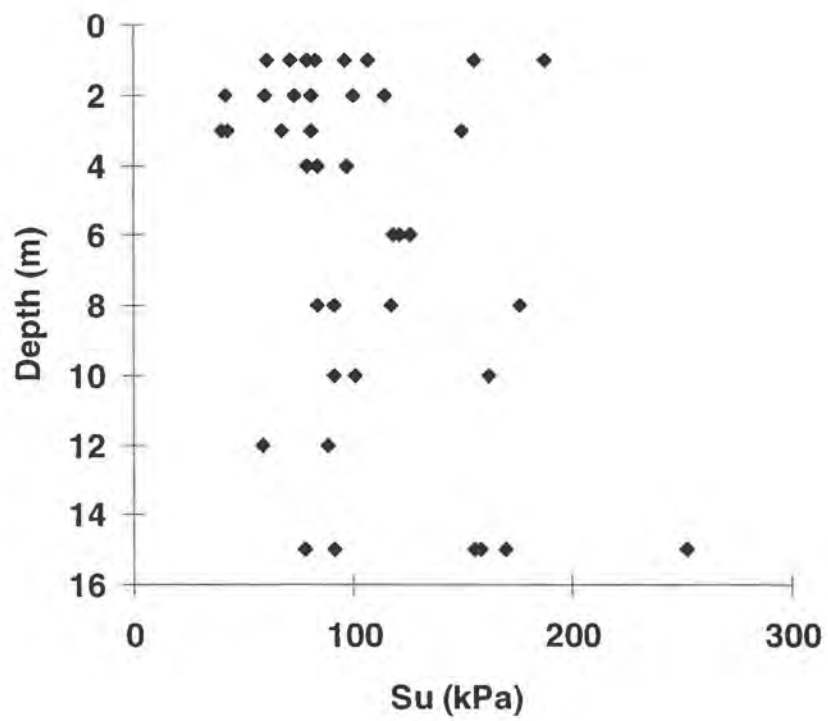


Figure E-2. Undrained Shear Strength ( $s_u$ ) vs. Depth

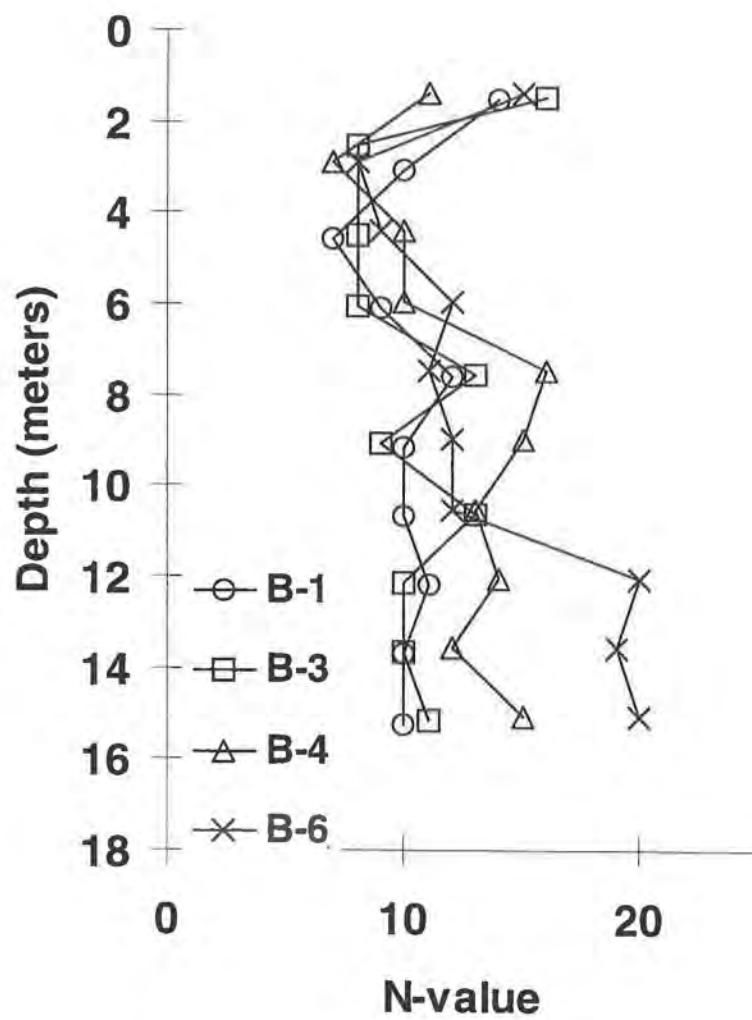


Figure E-3. SPT N Value vs. Depth

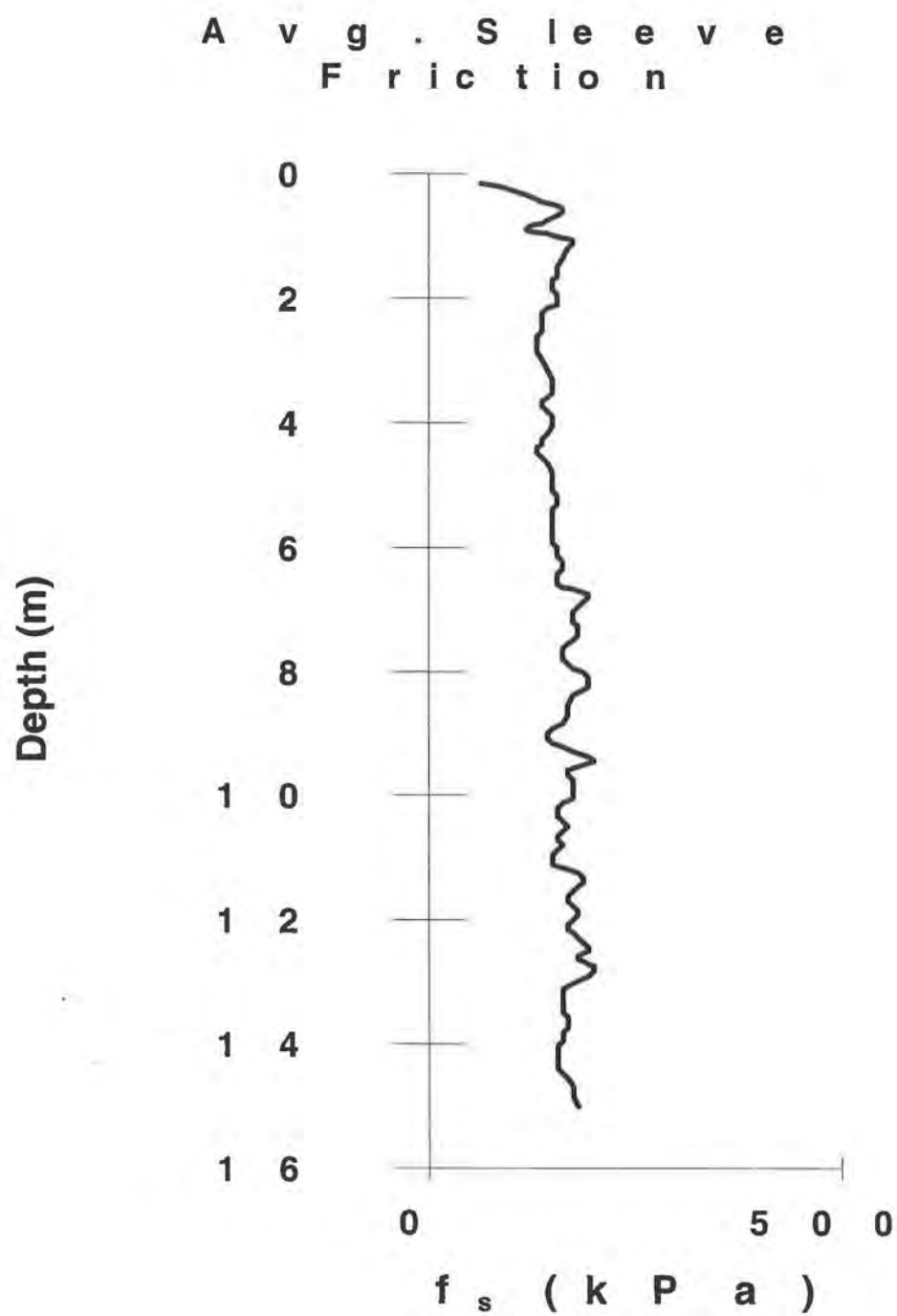


Figure E-4. CPT Data

# Y o u n g ' s M o d u l u s D e r i v e d F r o m D M T

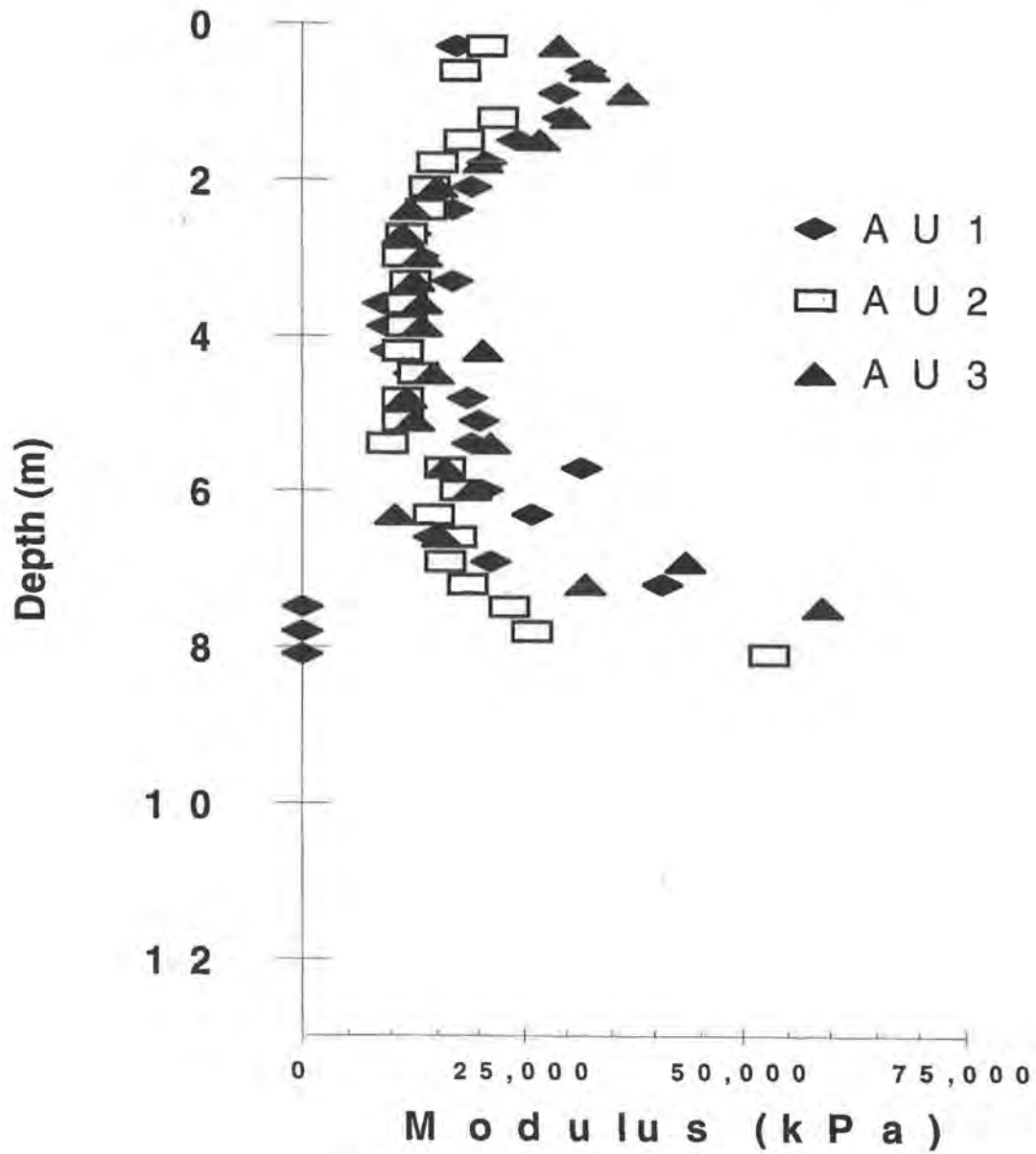
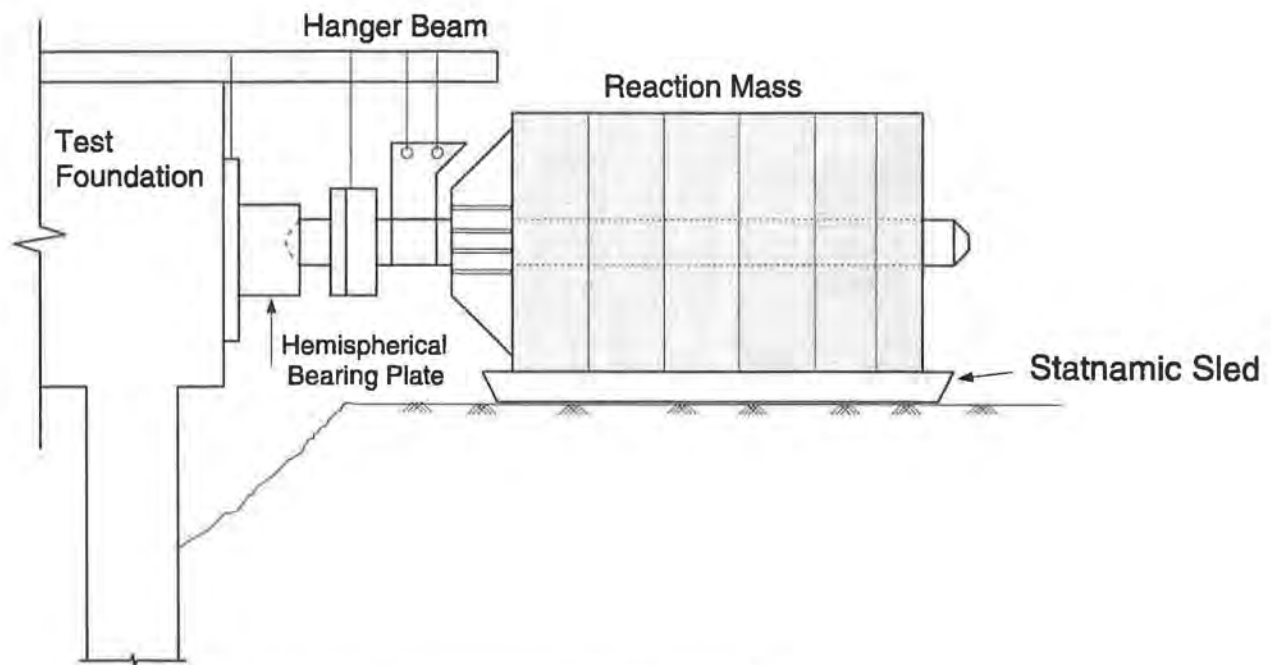


Figure E-5. Moduli Derived from DMT and CPT



1. Statnamic device is placed against test foundation
2. Pelletized fuel inside piston is ignited
3. Expanding gasses push reaction mass away from foundation imparting an equal and opposite thrust on the foundation

*Figure E-6. Test Arrangement for Statnamic Loading*





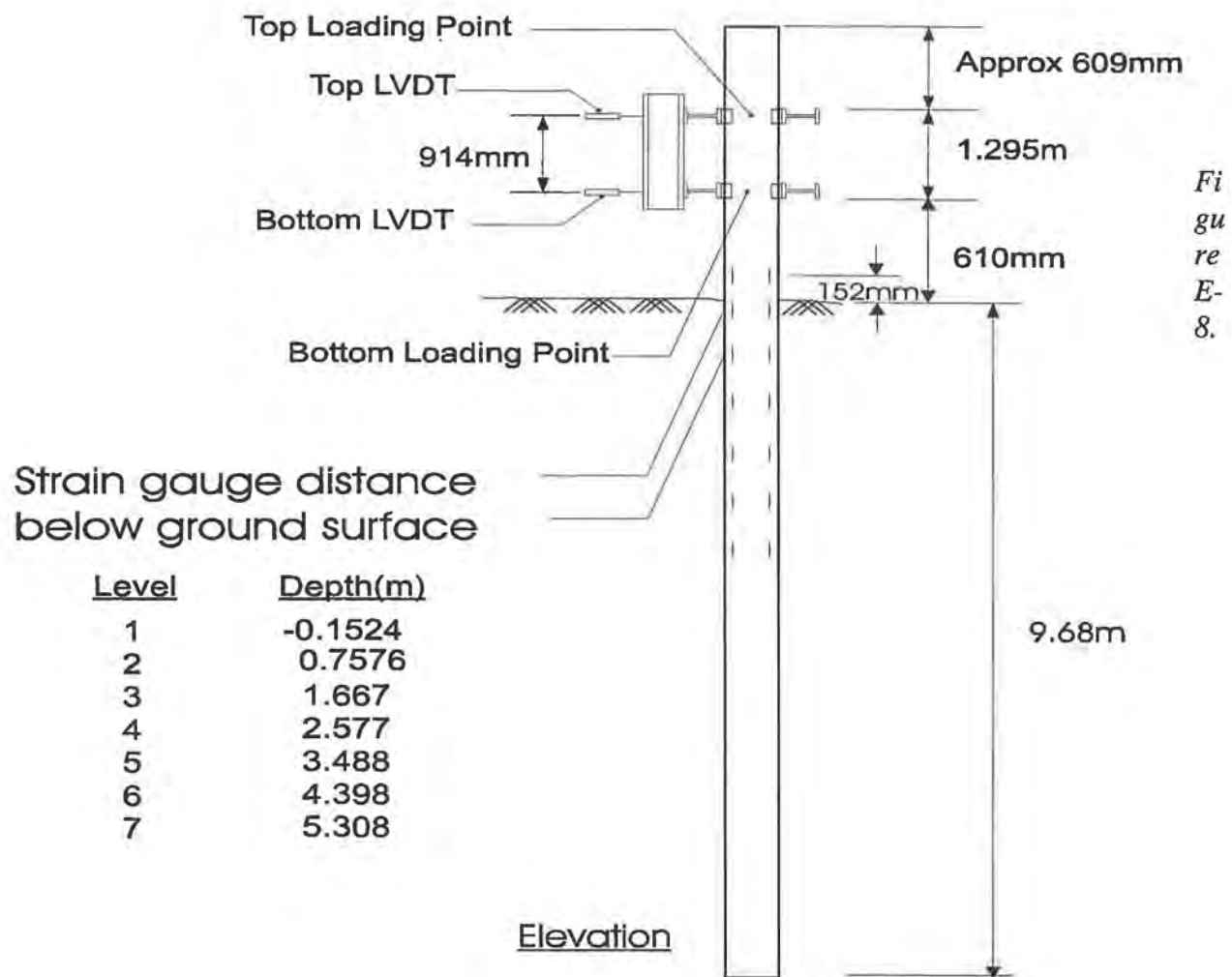
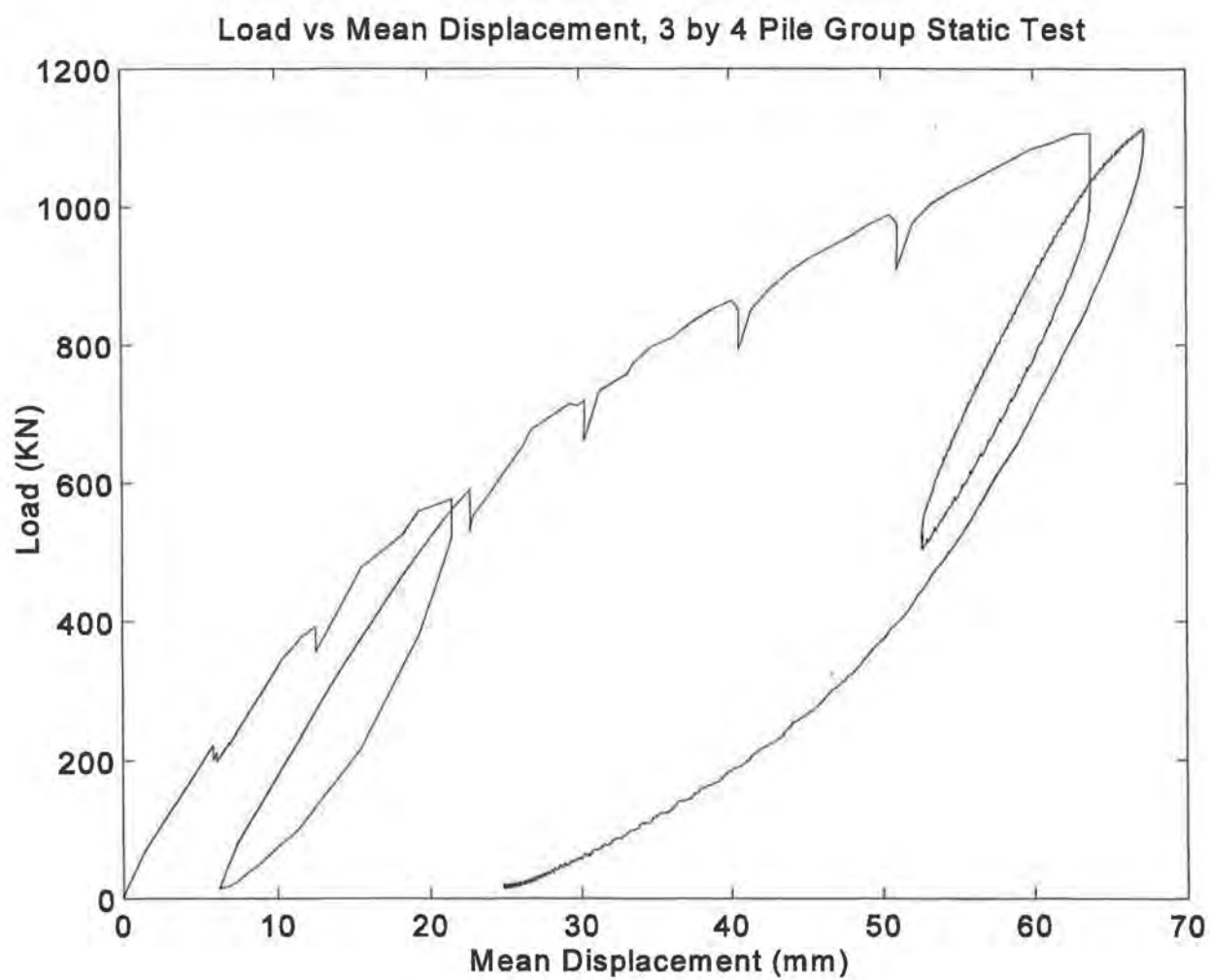
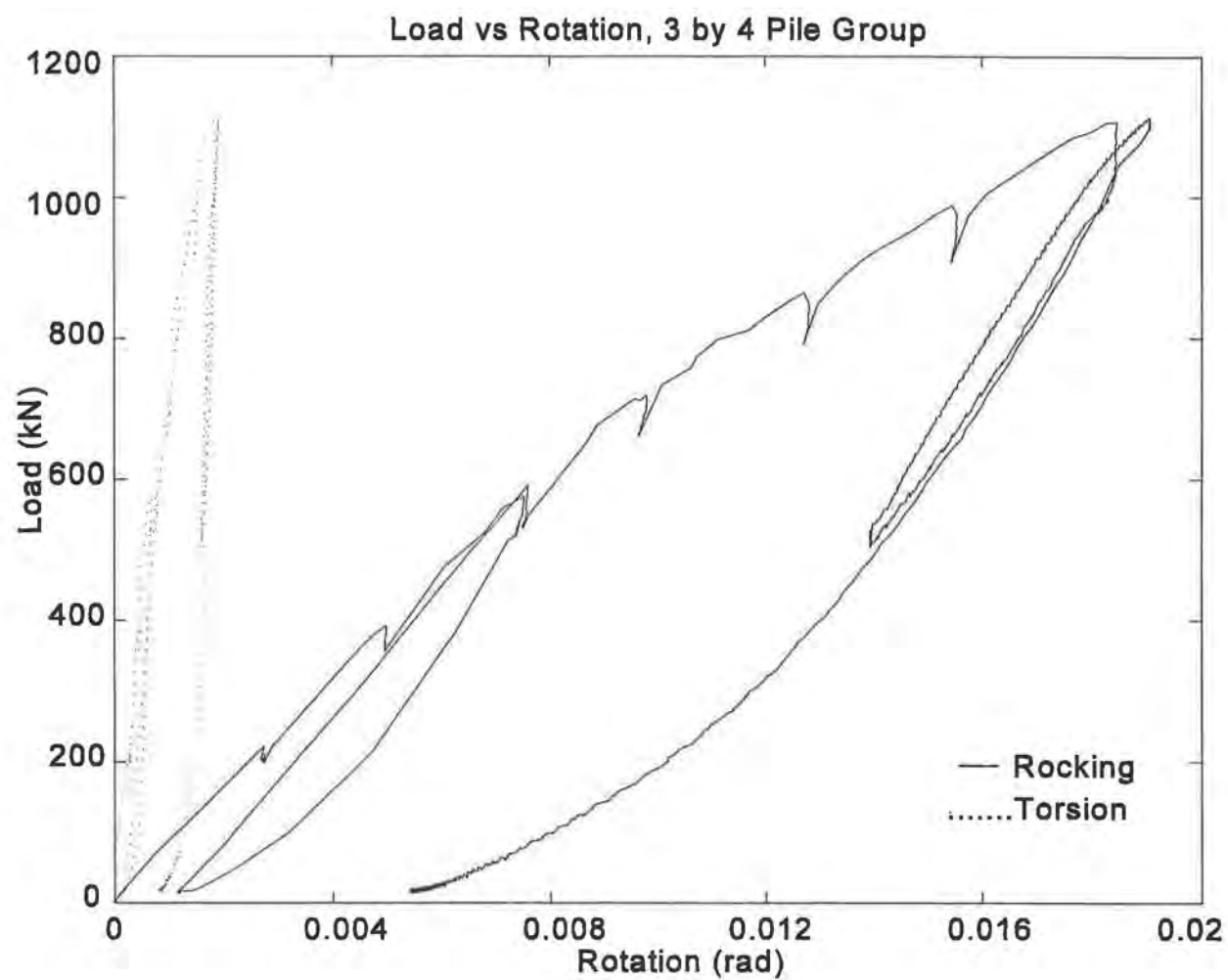


Figure E-8.

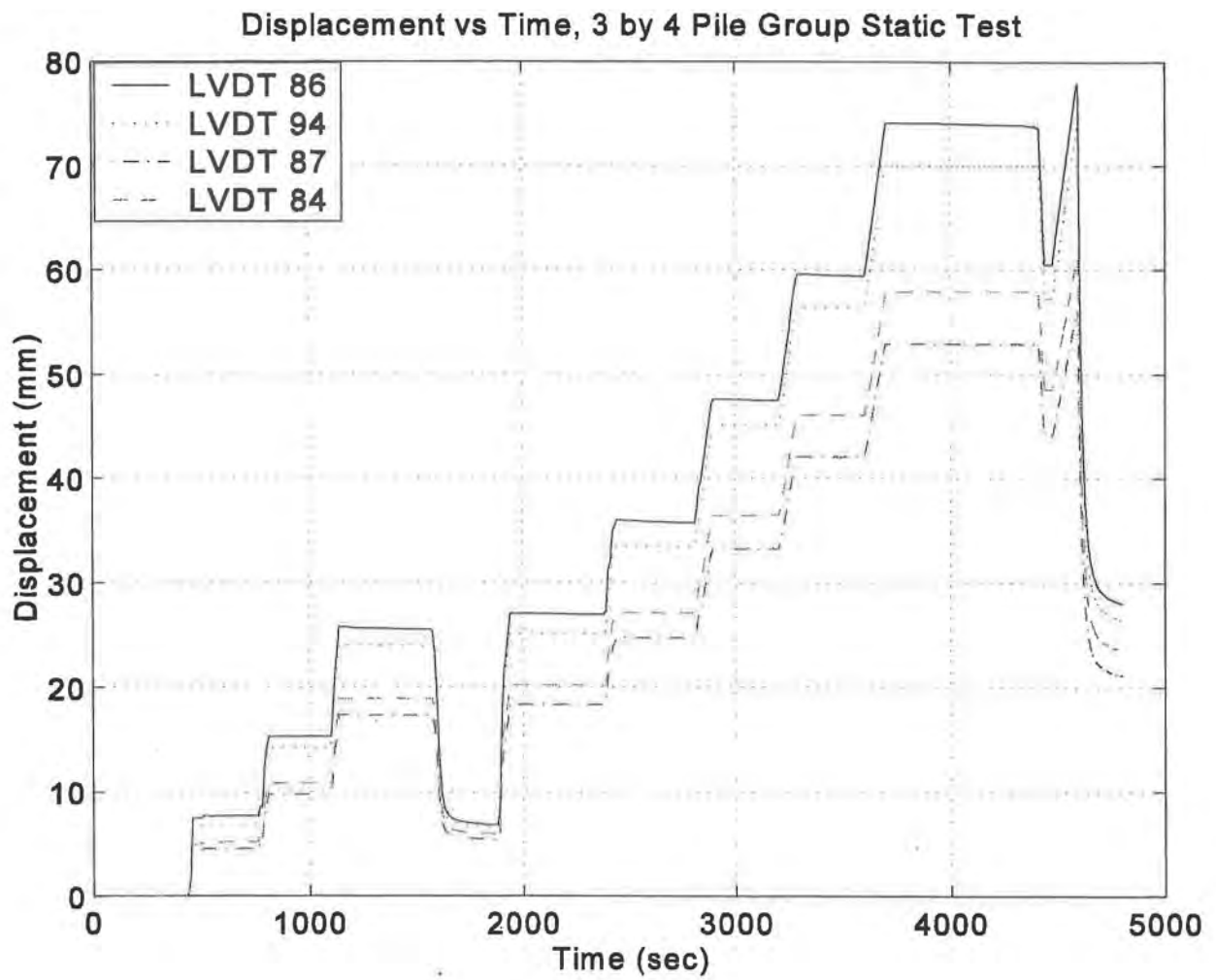
Figure E-8. Load and Instrumentation Setup for 12-Pile Group



*Figure E-9. Load vs Mean Displacement, 3 by 4 Pile Group Static Test*



*Figure E-10. Load vs. Mean Rocking and Torsional Rotation, 3 by 4 Pile Group Static Test*



*Figure E-11. Displacement Time History, 3 by 4 Pile Group Static Test*

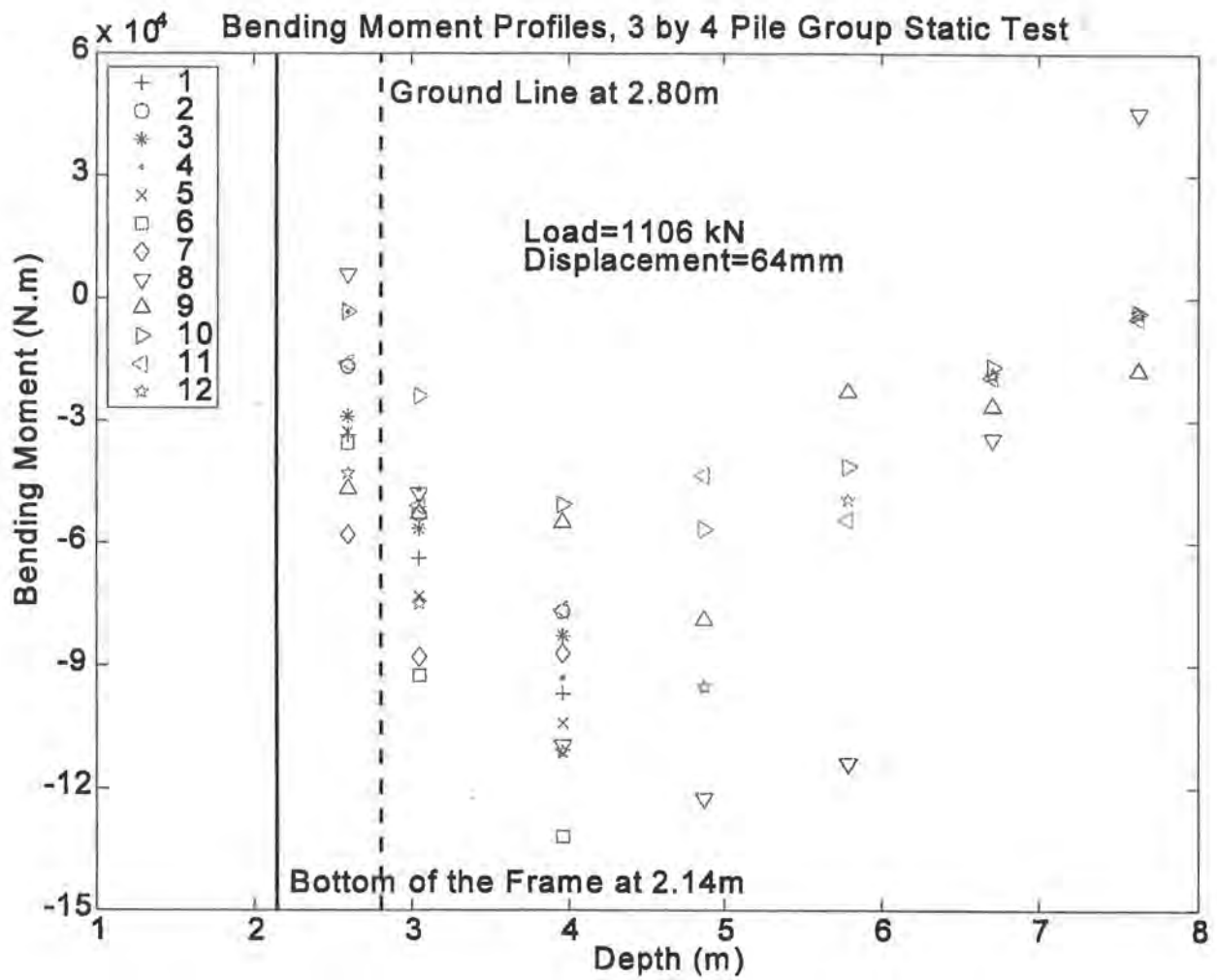


Figure E-12. Bending Moment Profiles at Load = 1106 kN, 3 by 4 Pile Group Static Test

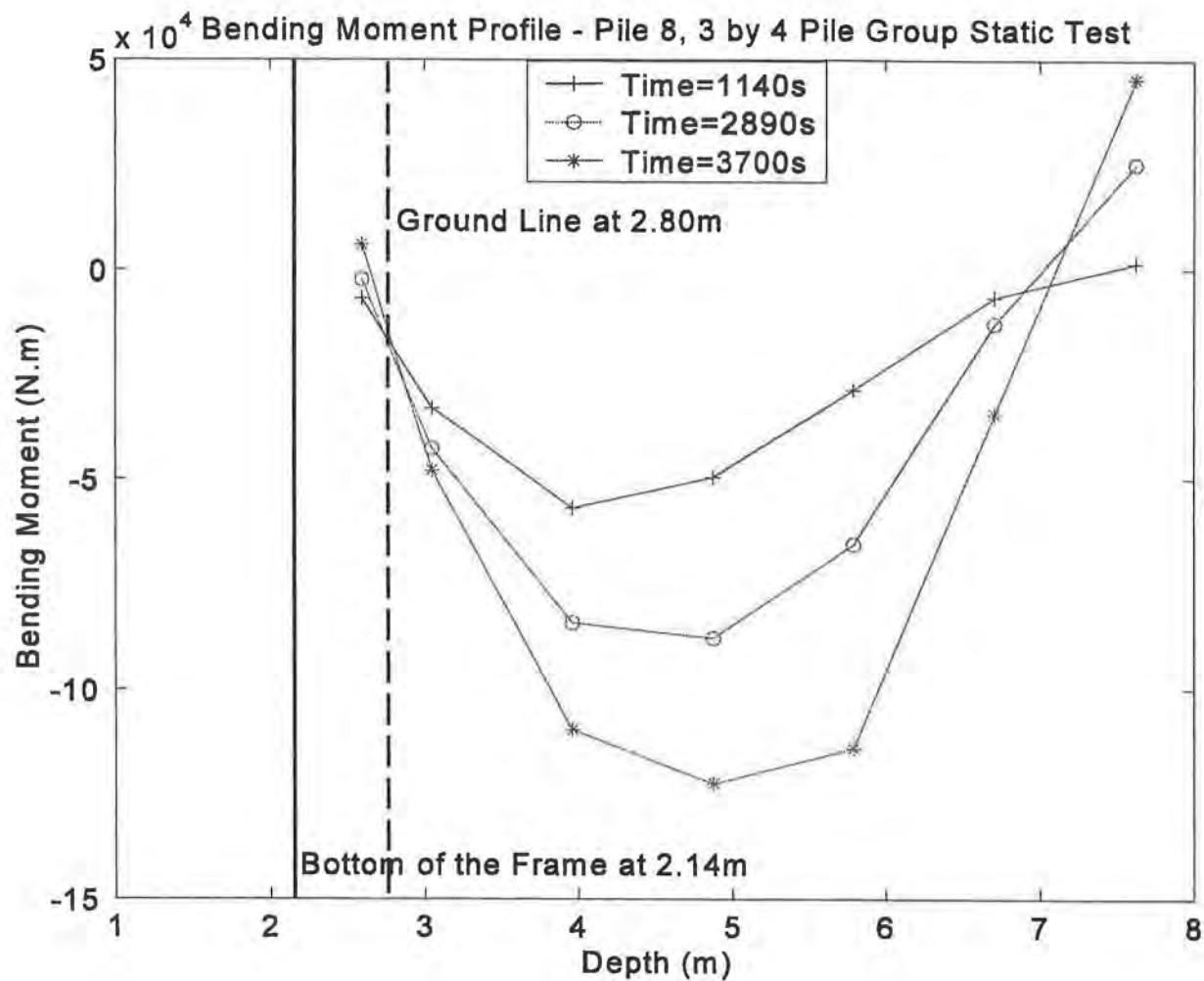


Figure E-13. Bending Moment Profiles - Pile 8, 3 by 4 Pile Group Static Test

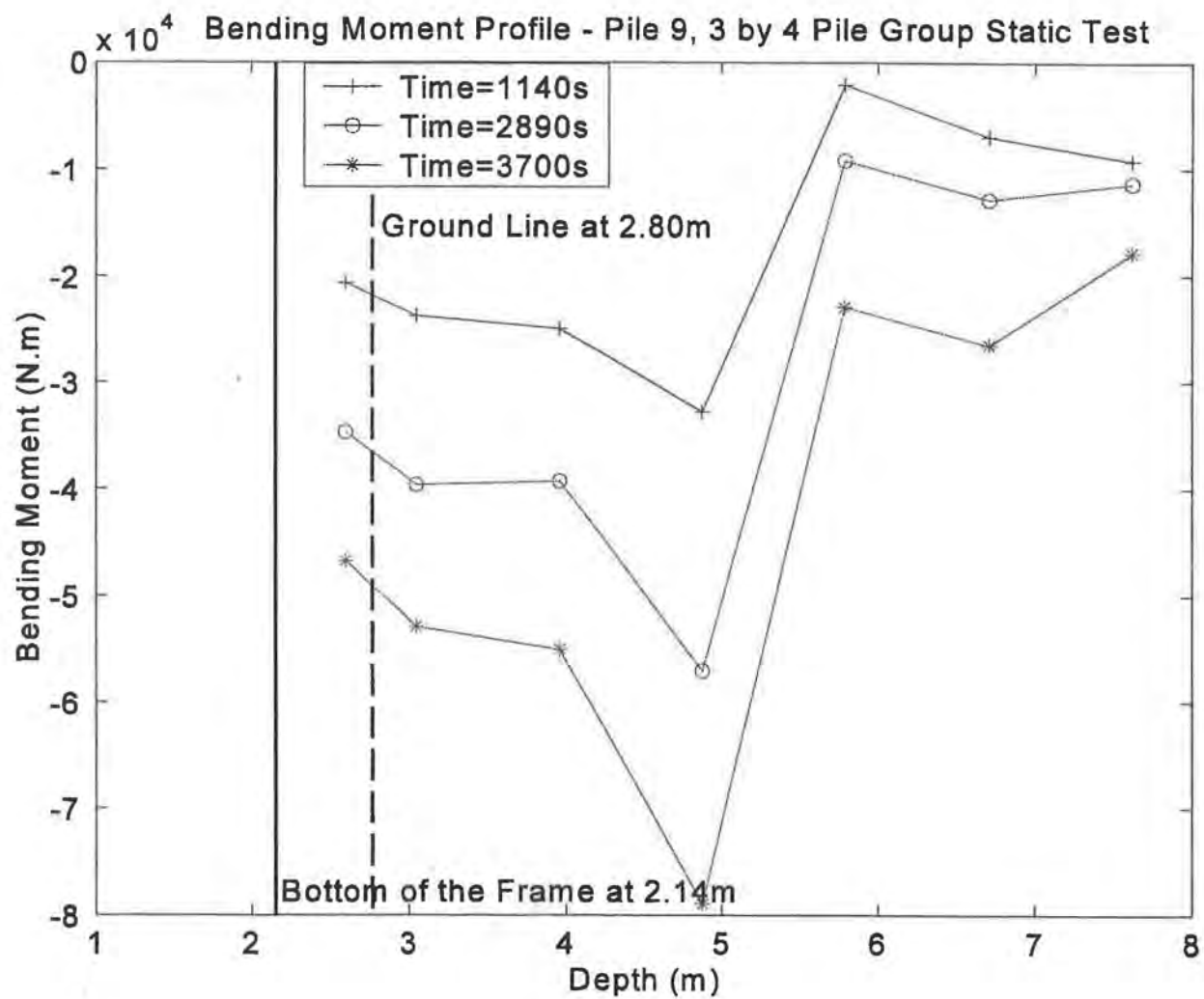


Figure E-14. Bending Moment Profiles - Pile 9, 3 by 4 Pile Group Static Test



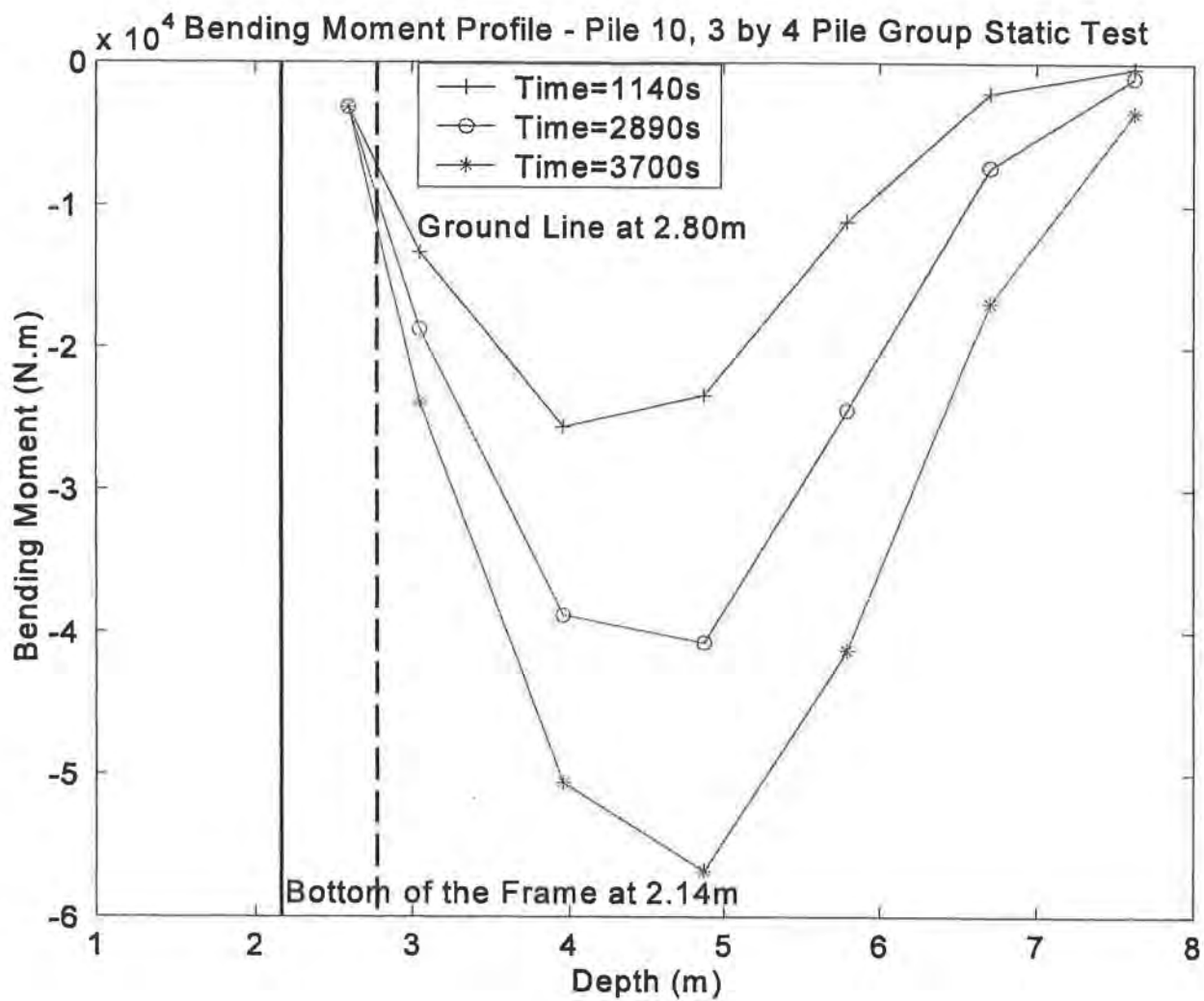


Figure E-15. Bending Moment Profiles - Pile 10, 3 by 4 Pile Group Static Test

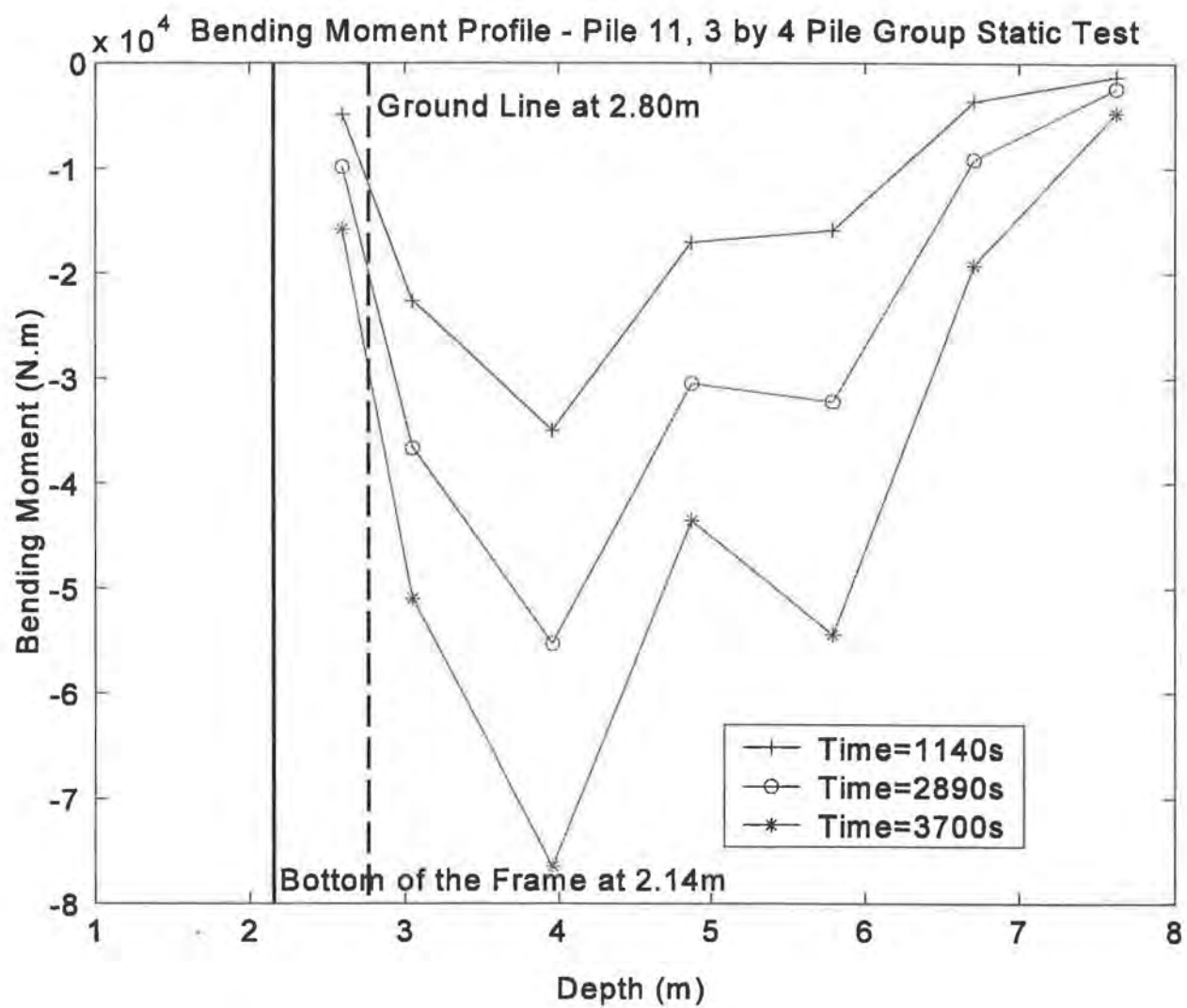


Figure E-16. Bending Moment Profiles - Pile 11, 3 by 4 Pile Group Static Test

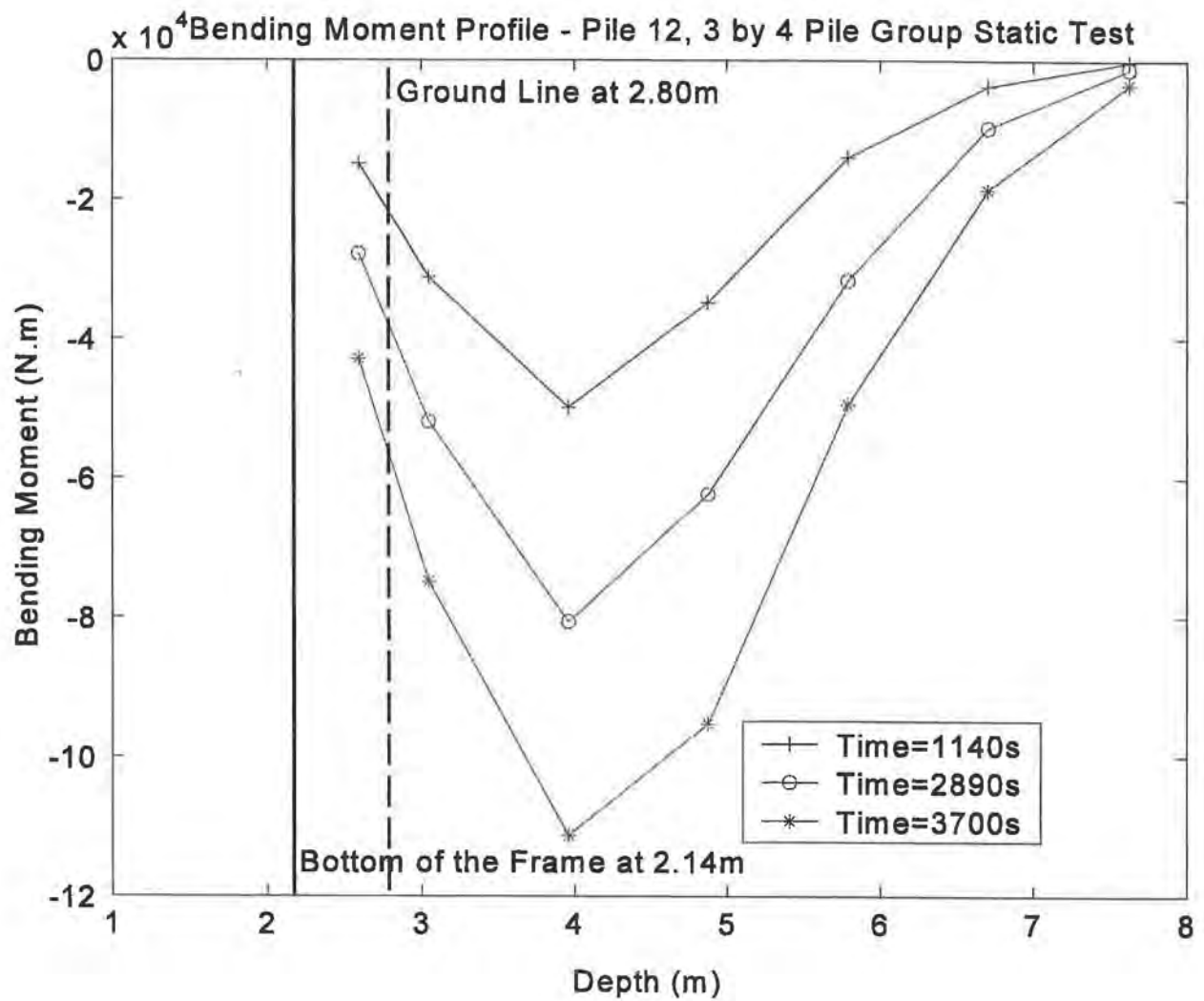



Figure E-17. Bending Moment Profiles - Pile 12, 3 by 4 Pile Group Static Test

Load Transferred to Individual Piles (kN)			Load Transferred To Row (kN)	% Load Transferred
[71.6,109.1,141.8] ⑥	[46.9,74.8,95.6] ⑪	[44.4,60.7,78.0] ⑫	[162.9,244.6,315.4]	[29/29/30]
[44.1,67.9,78.7] ①	[48.2,67.7,74.6] ⑦	[41.4,73.0,98.5] ⑤	[133.7,208.6,251.8]	[24/25/24]
[51.0,75.0,91.9] ②	[10.1,15.8,17.5] ⑨	[50.1,73.6,80.0] ③	[111.2,164.4,189.4]	[20/20/18]
[55.4,80.0,107.7] ④	[26.7,37.7,51.8] ⑩	[67.0,97.7,136.3] ⑧	[149.1,215.4,295.8]	[27/26/28]


 Direction of Static Load

- Every circle represents one pile in the group
- The number within the circle represents the pile number
- The 3 numbers above a pile represent the pile head shear at loads of 576 kN, 863 kN and 1106 kN respectively
- The rightmost column of numbers indicates the total lateral load transferred to that particular row for that particular load

*Figure E-18. Static Pile-Head Shear Distribution, 3 by 4 Pile Group*

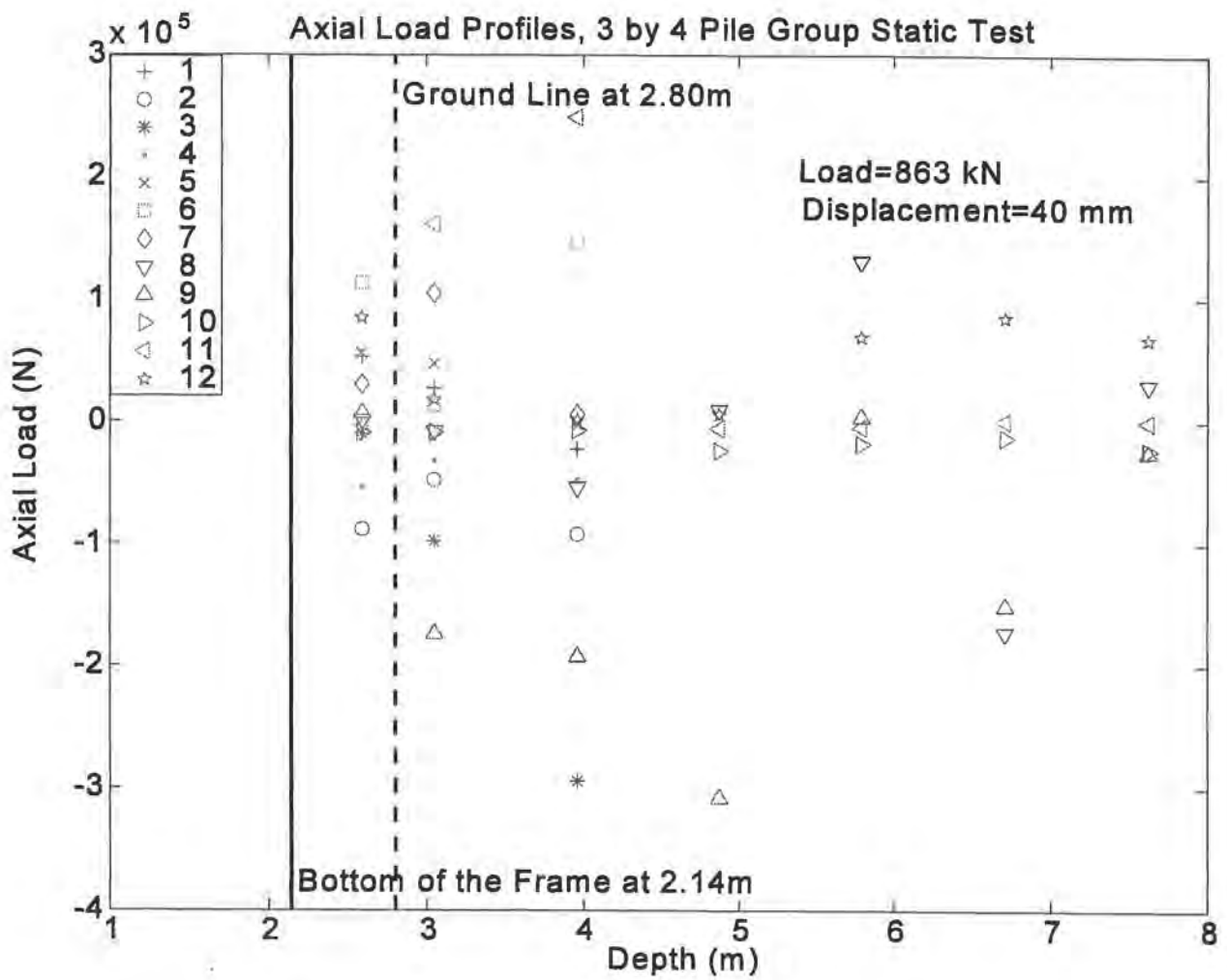


Figure E-19. Axial Load Profiles at Load = 863 kN, 3 by 4 Pile Group Static Test

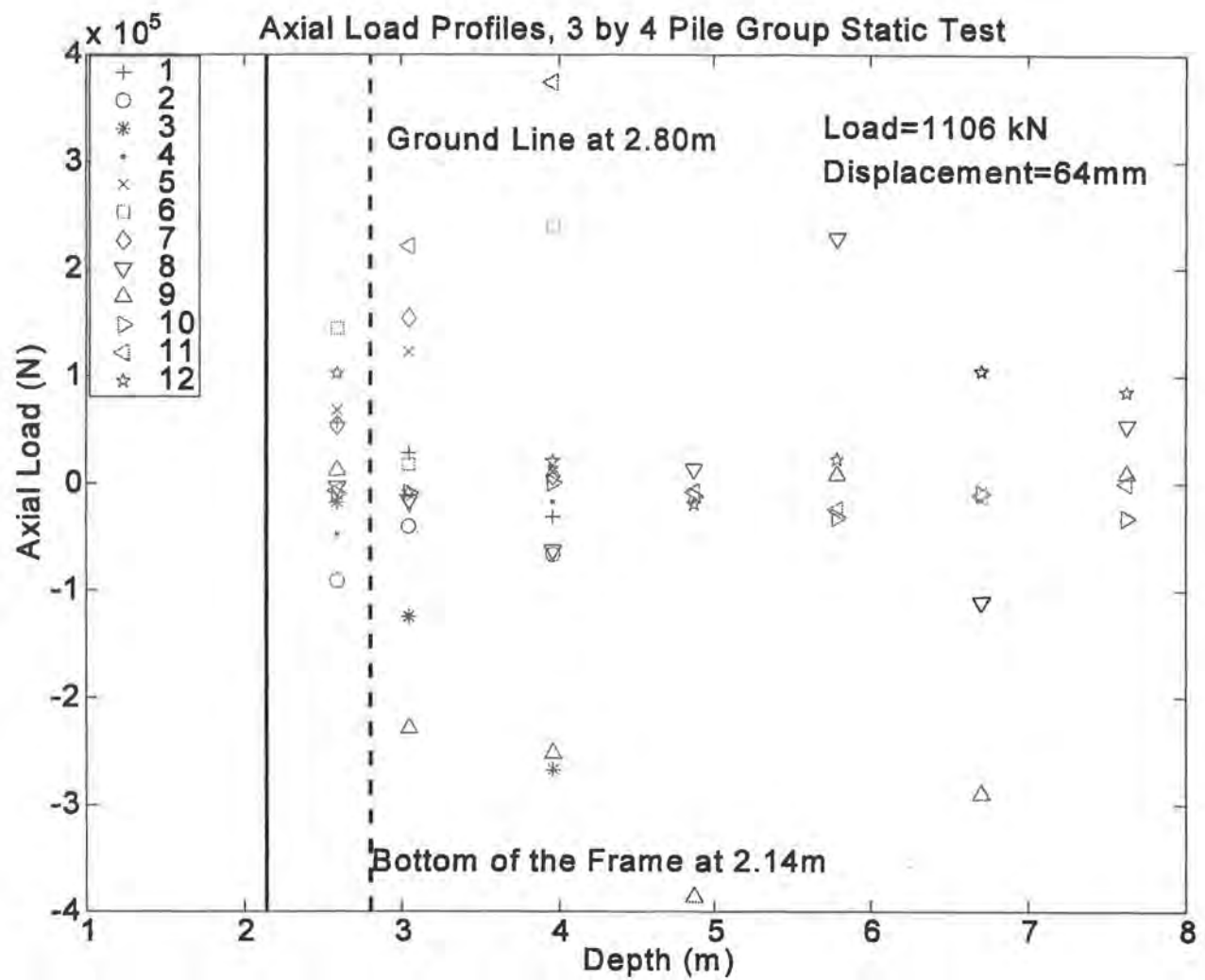
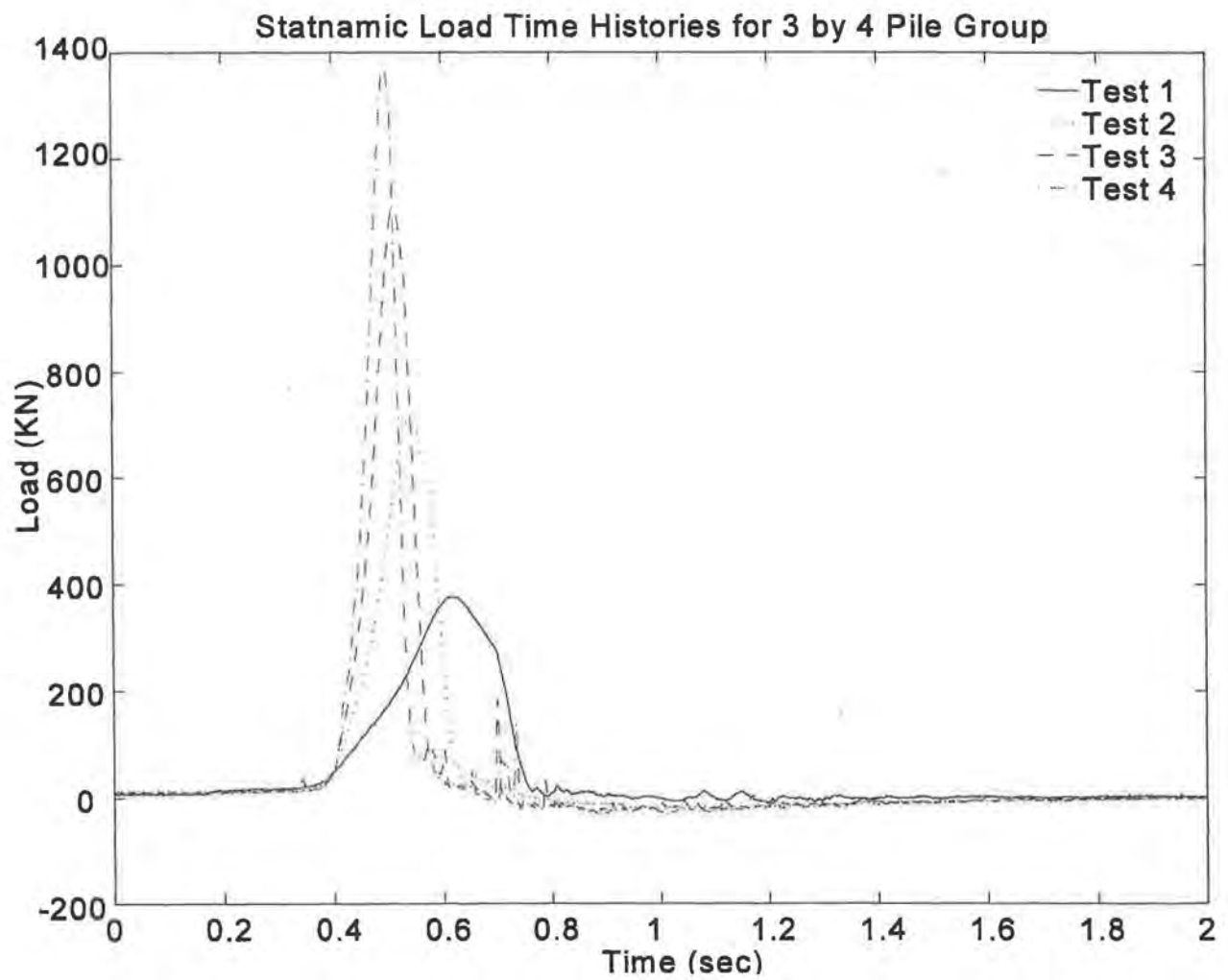


Figure E-20. Axial Load Profiles at Load = 1106 kN, 3 by 4 Pile Group Static Test



*Figure E-21. Load Time Histories, 3 by 4 Pile Group Statnamic Tests*

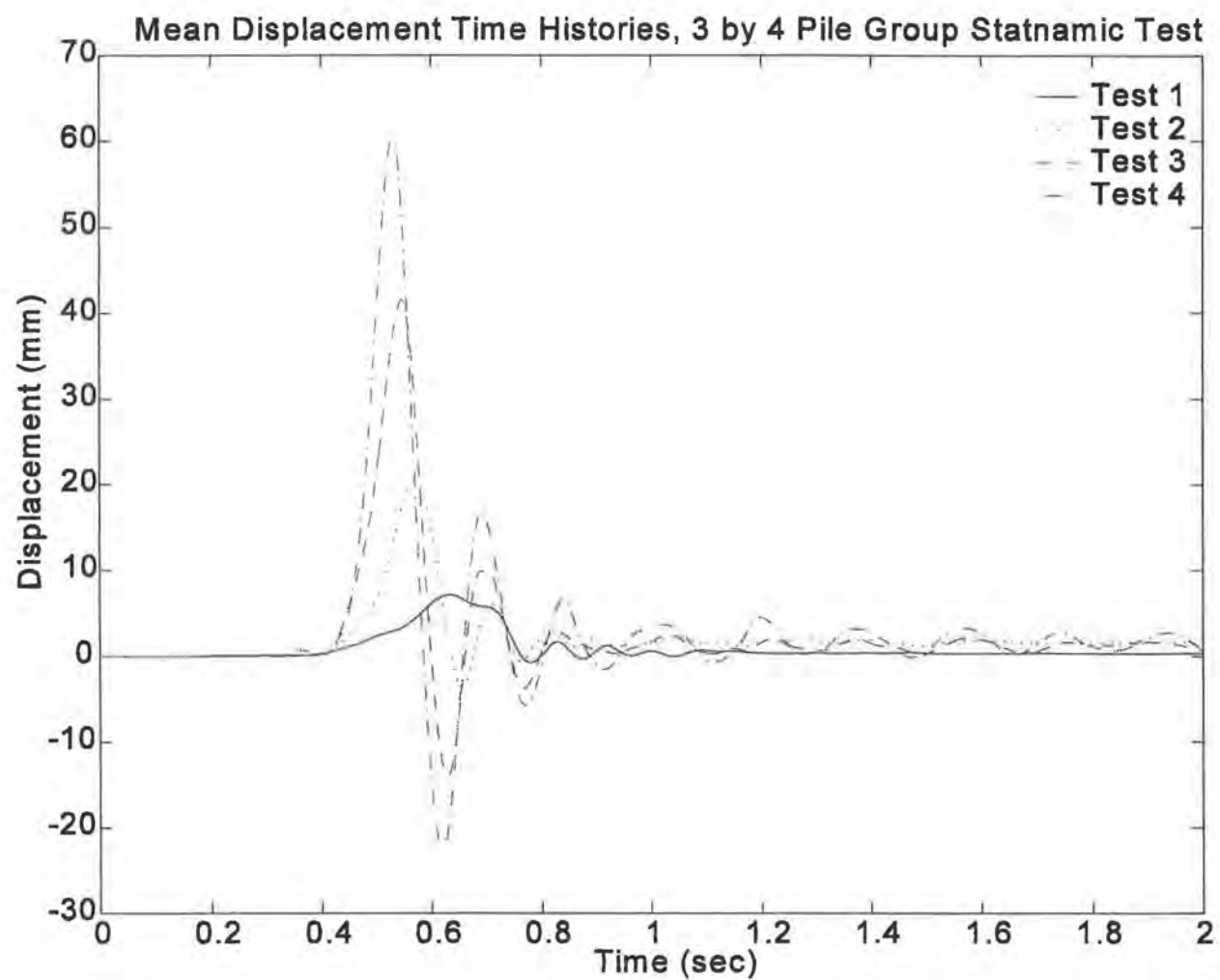


Figure E-22. Displacement Time Histories, 3 by 4 Pile Group Statnamic Tests



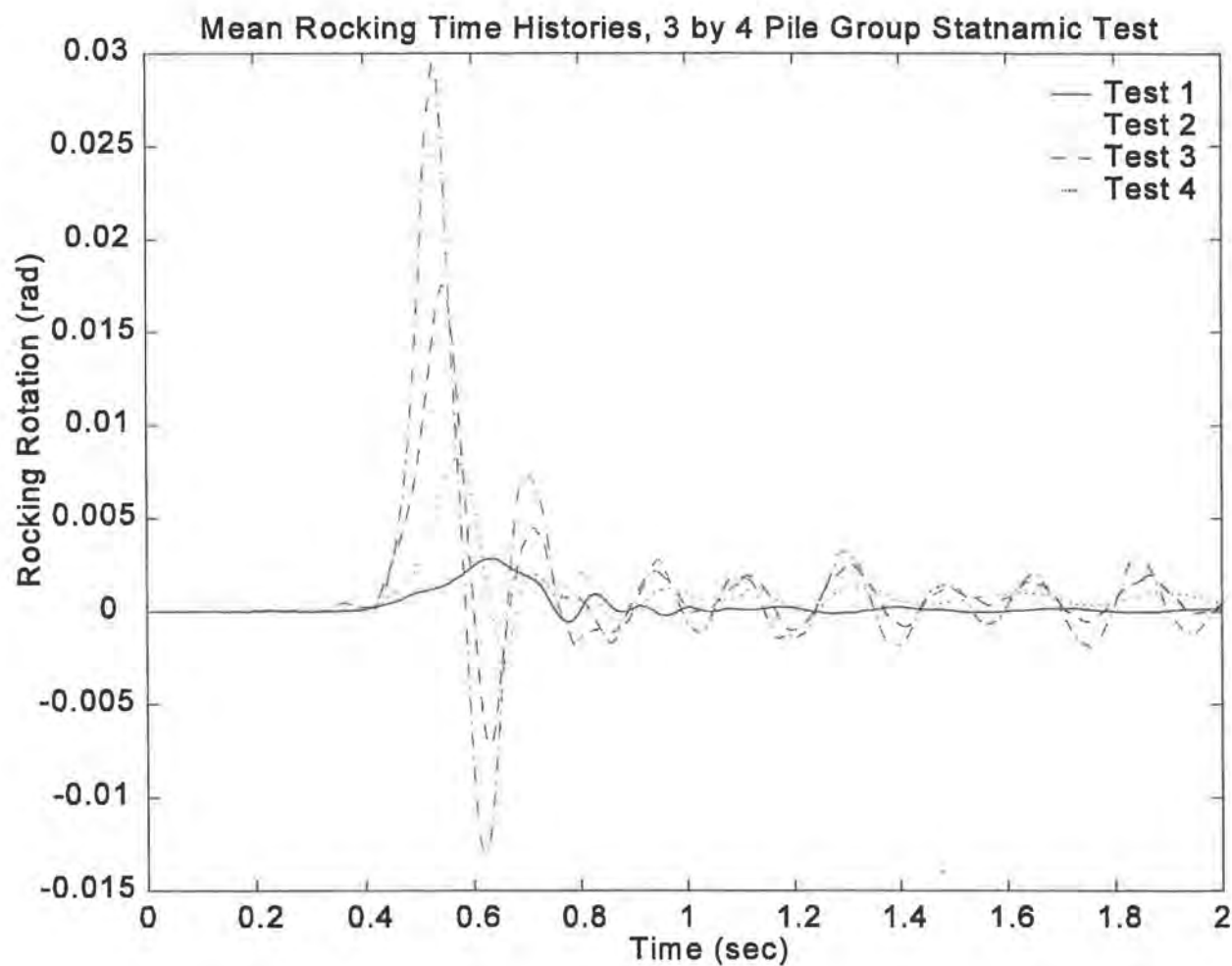


Figure E-23. Rocking Rotation Time Histories, 3 by 4 Pile Group Statnamic Tests

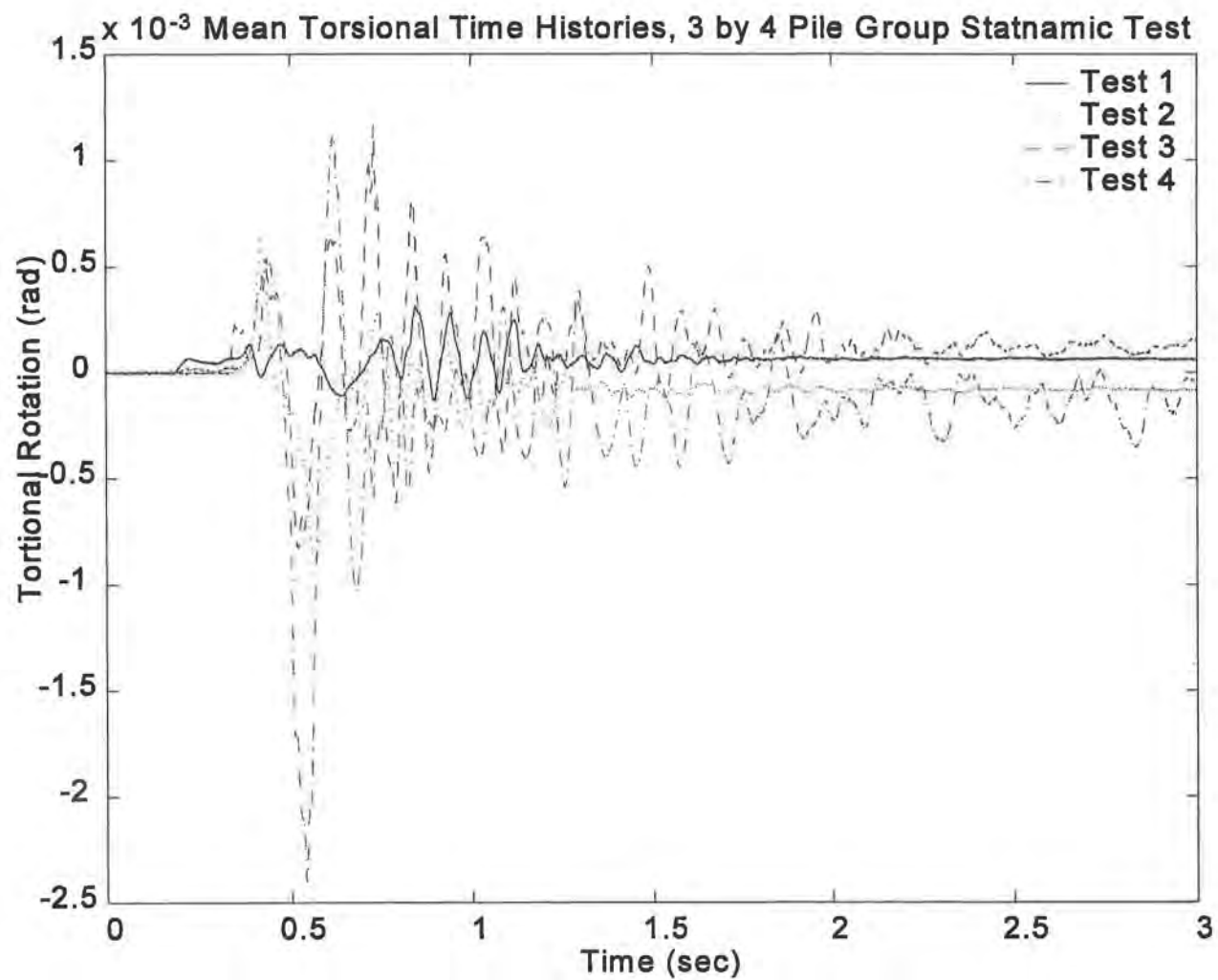


Figure E-24. Torsional Rotation Time Histories, 3 by 4 Pile Group Statnamic Tests

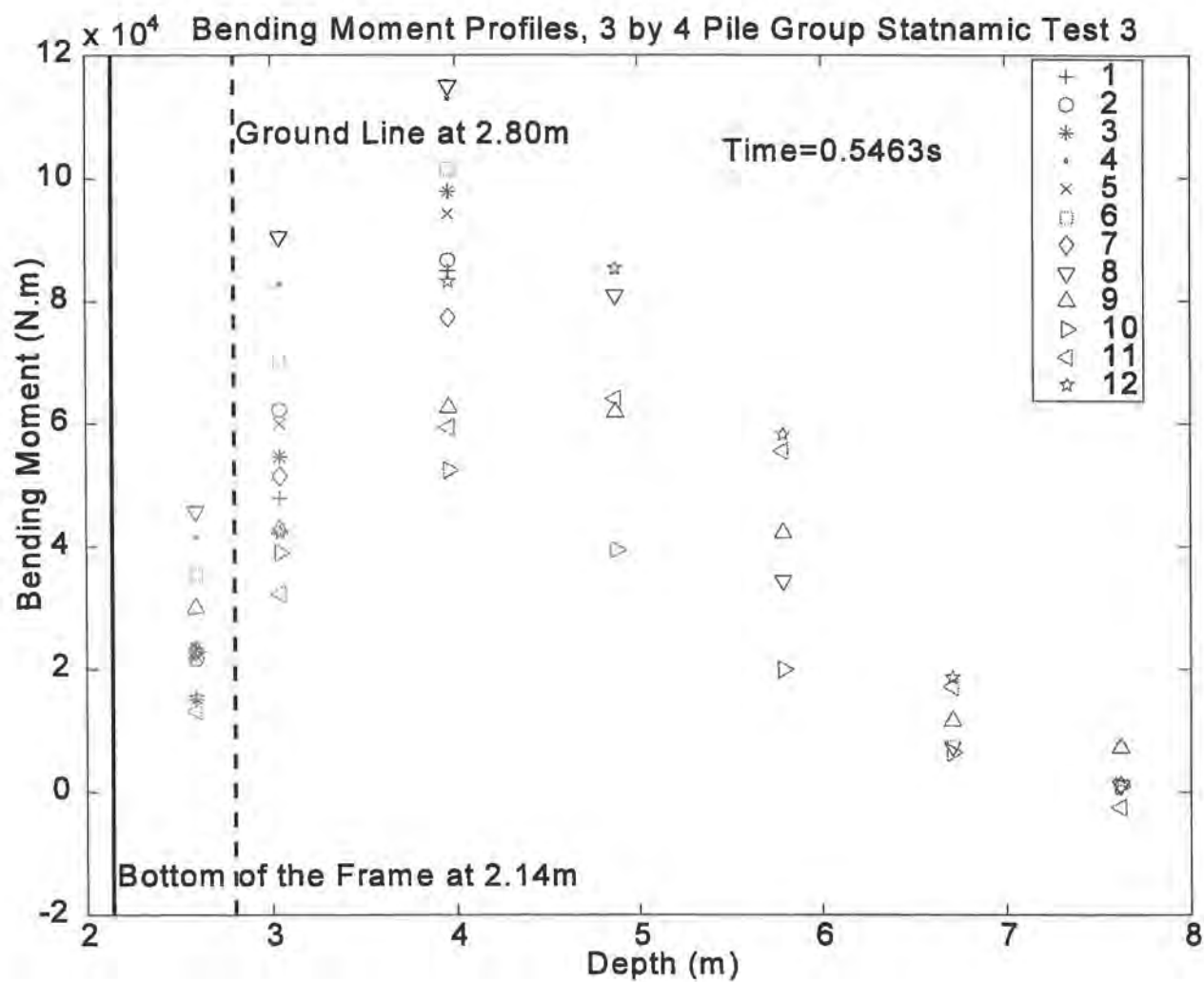


Figure E-25. Bending Moment Profiles, 3 by 4 Pile Group Statnamic Test 3

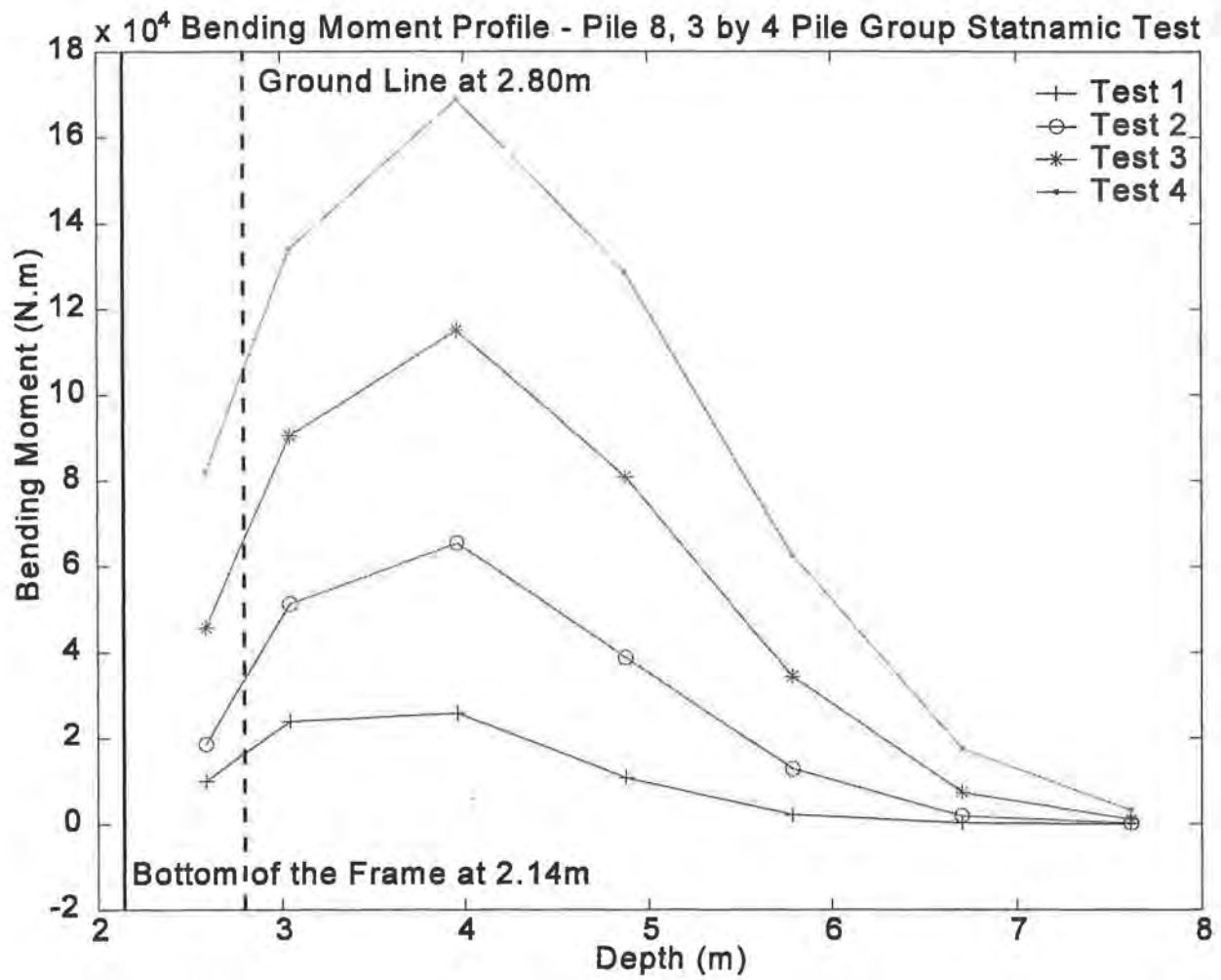


Figure E-26. Bending Moment Profiles - Pile 8, 3 by 4 Pile Group Statnamic Test

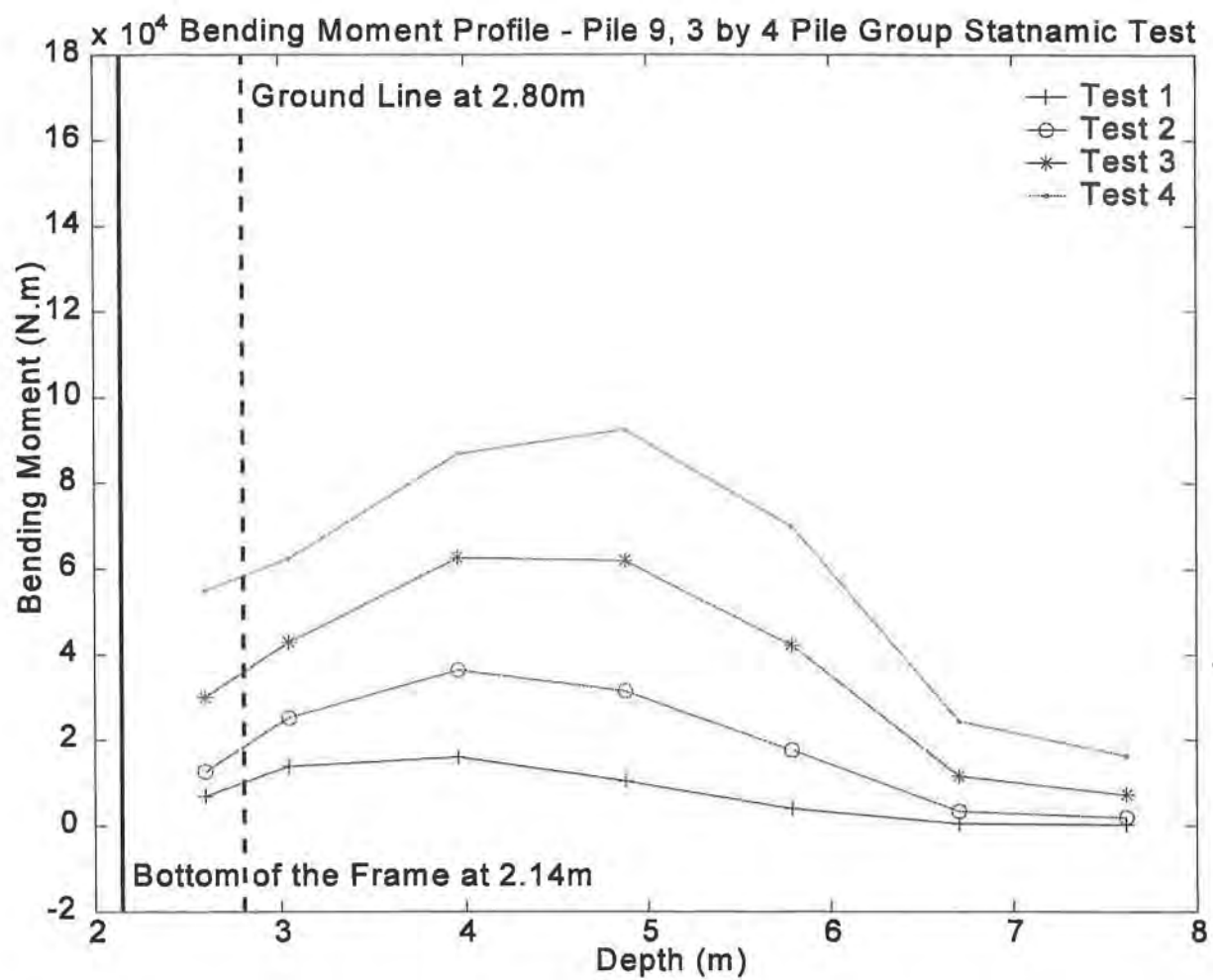


Figure E-27. Bending Moment Profiles - Pile 9, 3 by 4 Pile Group Statnamic Test

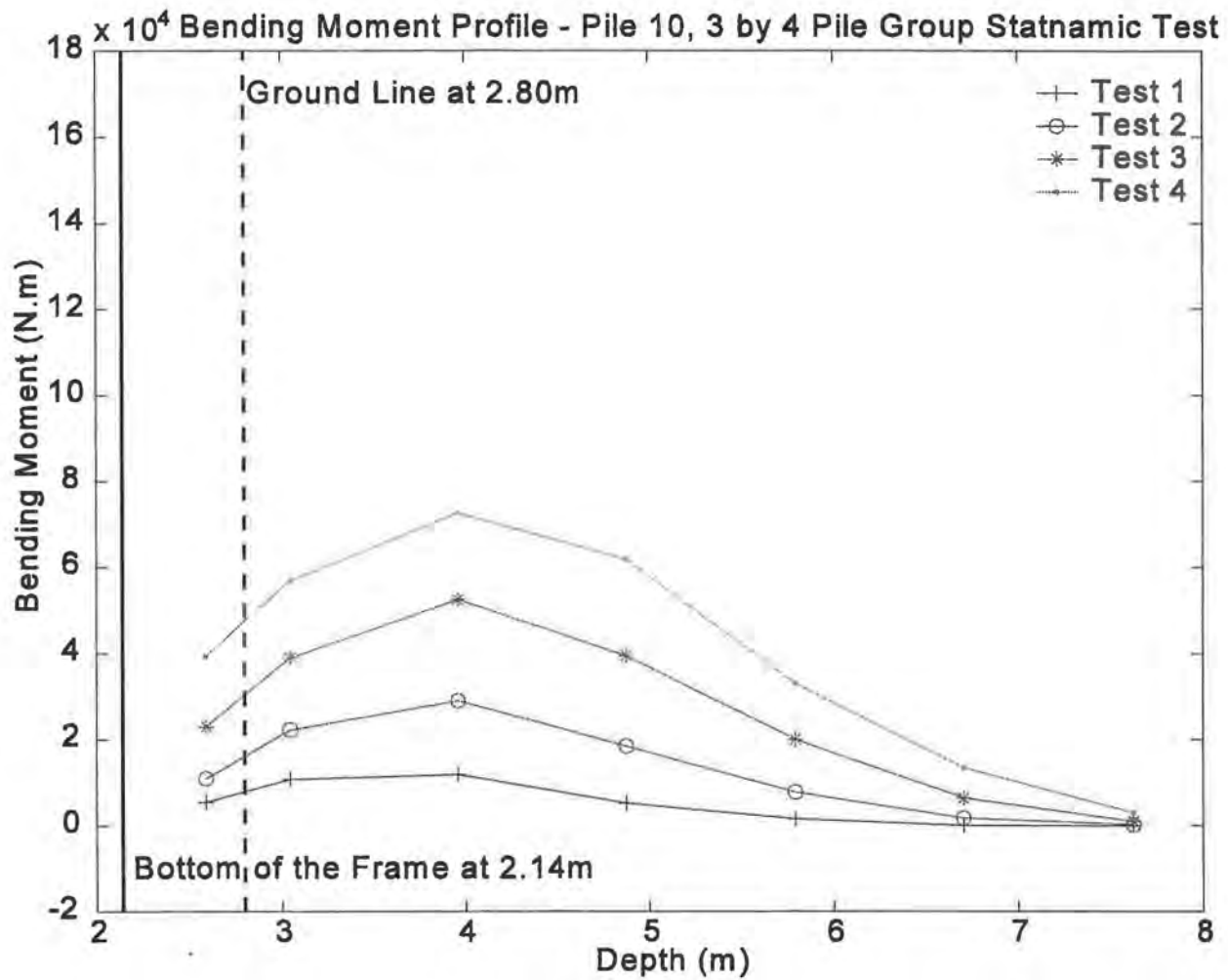


Figure E-28. Bending Moment Profiles - Pile 10, 3 by 4 Pile Group Statnamic Test

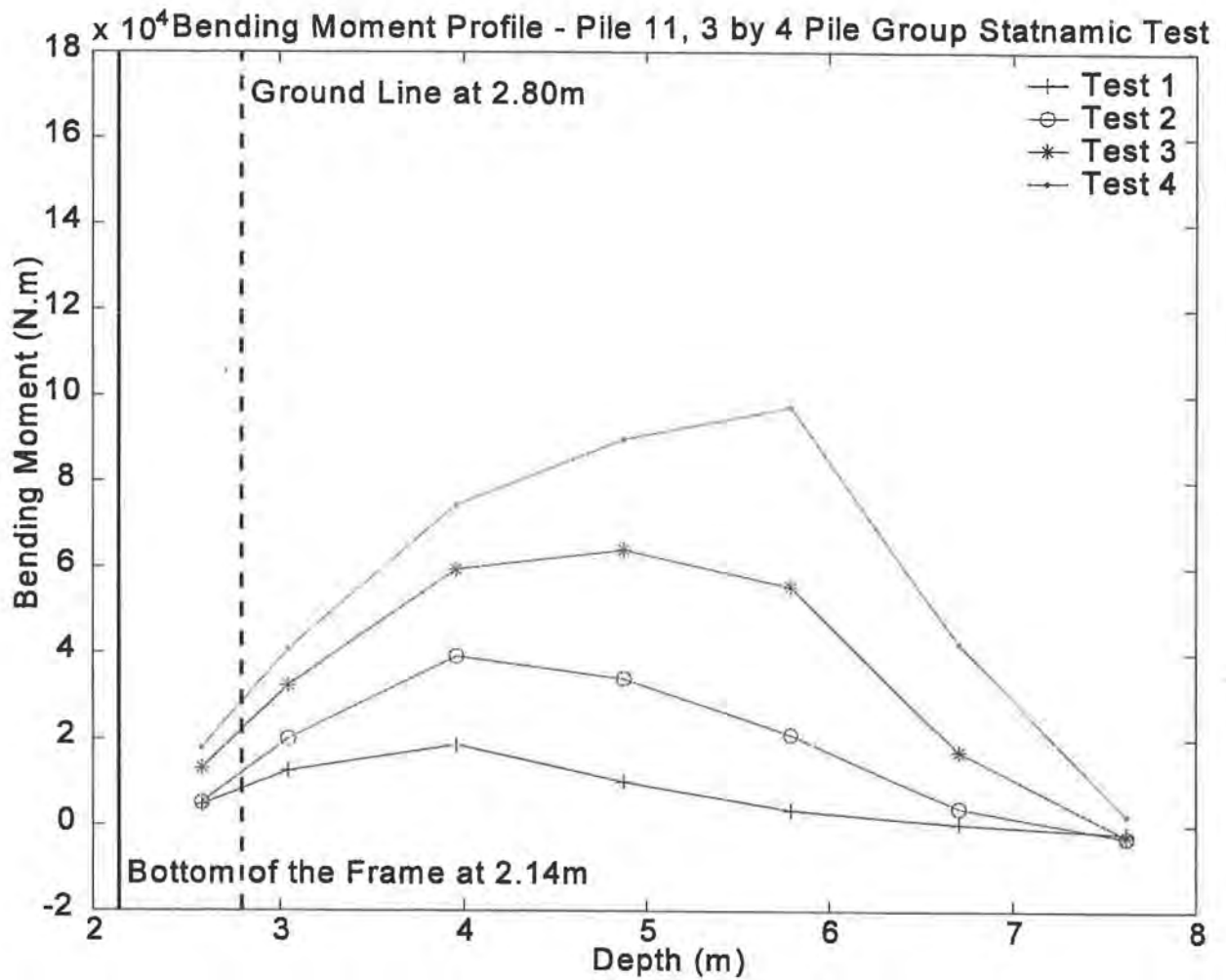


Figure E-29. Bending Moment Profiles - Pile 11, 3 by 4 Pile Group Statnamic Test

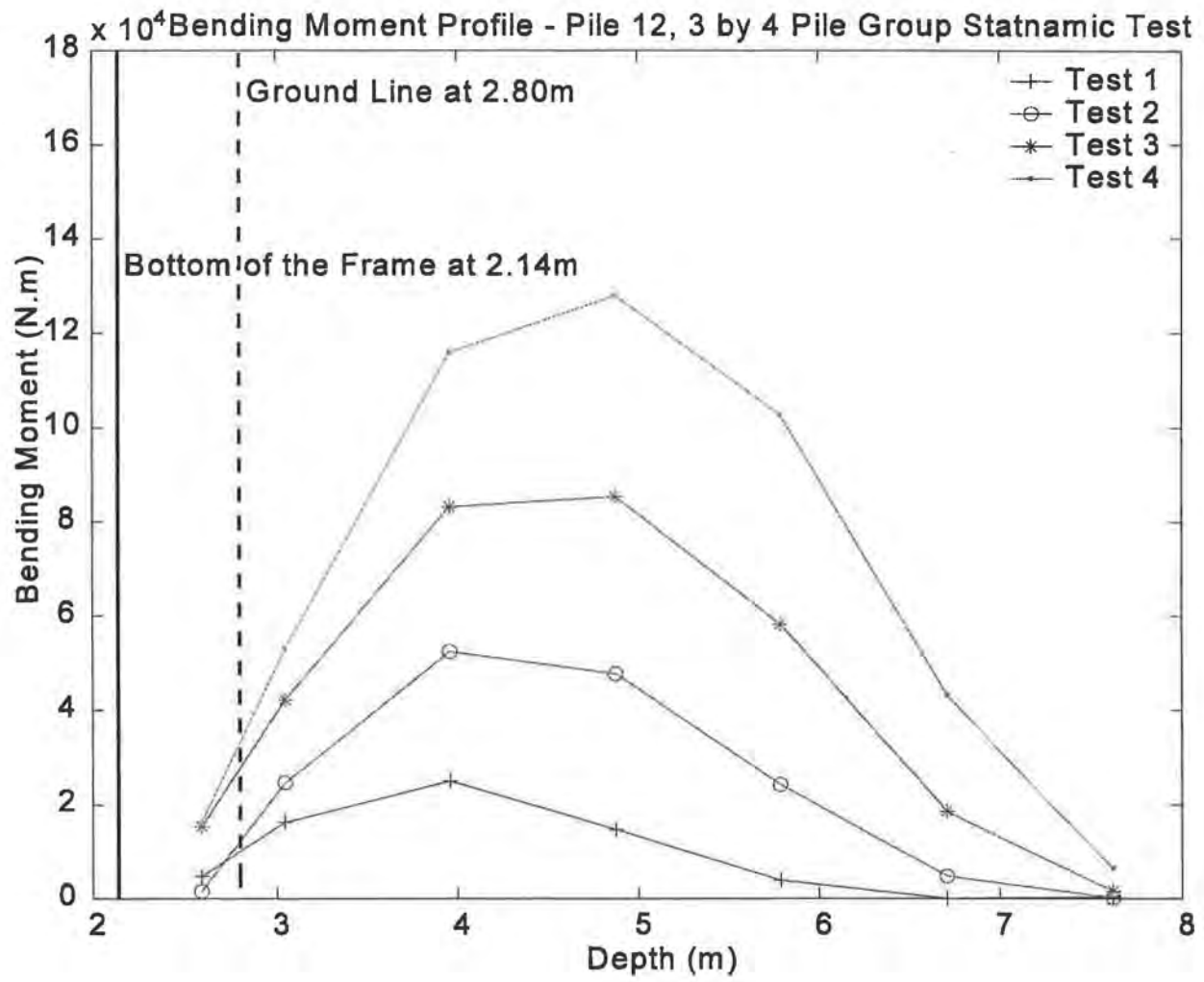



Figure E-30. Bending Moment Profiles - Pile 12, 3 by 4 Pile Group Statnamic Test

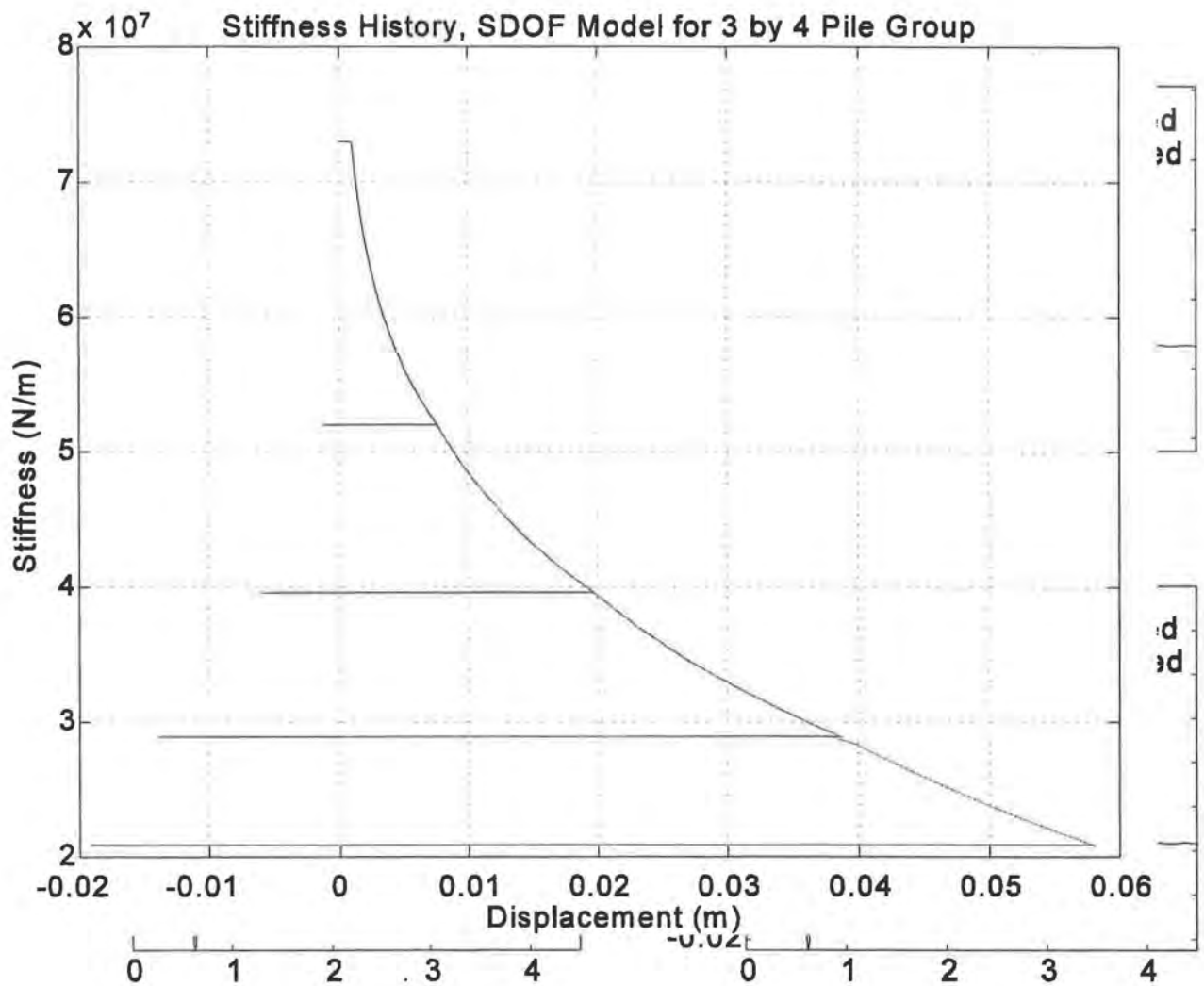


Loads Transferred to Individual Piles (kN)			Load Transferred to Row (kN)	% Load Transferred
<div> <div>8</div> <div>[107.3,122.4]</div> </div> <div> <div>10</div> <div>[38.1,42.0]</div> </div> <div> <div>4</div> <div>[93.7,94.0]</div> </div>			[239.1,258.4]	[28 / 27]
<div> <div>3</div> <div>[72.8,74.0]</div> </div> <div> <div>9</div> <div>[30.7,23.8]</div> </div> <div> <div>2</div> <div>[92.4,103.7]</div> </div>			[195.9,201.5]	[23 / 22]
<div> <div>5</div> <div>[87.5,101.5]</div> </div> <div> <div>7</div> <div>[66.9,70.8]</div> </div> <div> <div>1</div> <div>[75.1,77.2]</div> </div>			[229.5,249.5]	[27 / 26]
<div> <div>12</div> <div>[60.7,81.3]</div> </div> <div> <div>11</div> <div>[43.8,51.8]</div> </div> <div> <div>6</div> <div>[79.6,105.1]</div> </div>			[184.1,238.2]	[22 / 25]

 Direction of Statnamic Load

- Every circle represents one pile in the group
- The number within the circle represents the pile number
- The 2 numbers immediately to the right of a pile represent the pile head shear at peak displacement for tests 3 and 4, respectively
- The rightmost columns of numbers indicate the total lateral load transferred to that particular row for that particular load

Figure E-31. Pile Head Shear Distribution, 3 by 4 Pile Group Statnamic Test 3 - 4

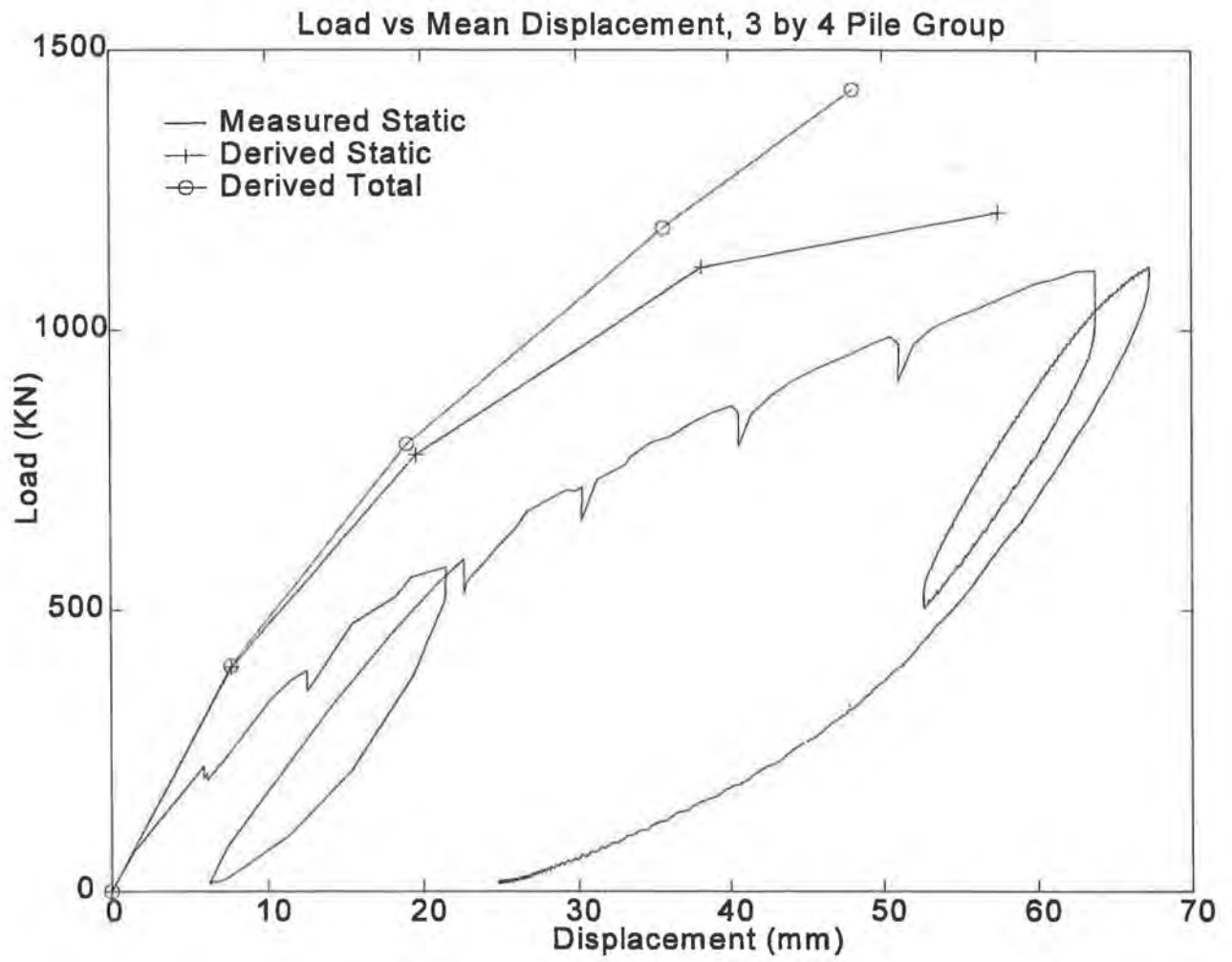


Fi  
gu  
re  
E-  
32

For all the four figures,  
X axis : Time (sec)  
Y axis : Displacement (m)

*Computed vs. Measured Lateral Response, 3 by 4 Pile Group*

Figure E-33. Stiffness History, SDOF Model for 3 by 4 Pile Group



*Figure E-34. Derived Static Load Deflection Response, 3 by 4 Pile Group*

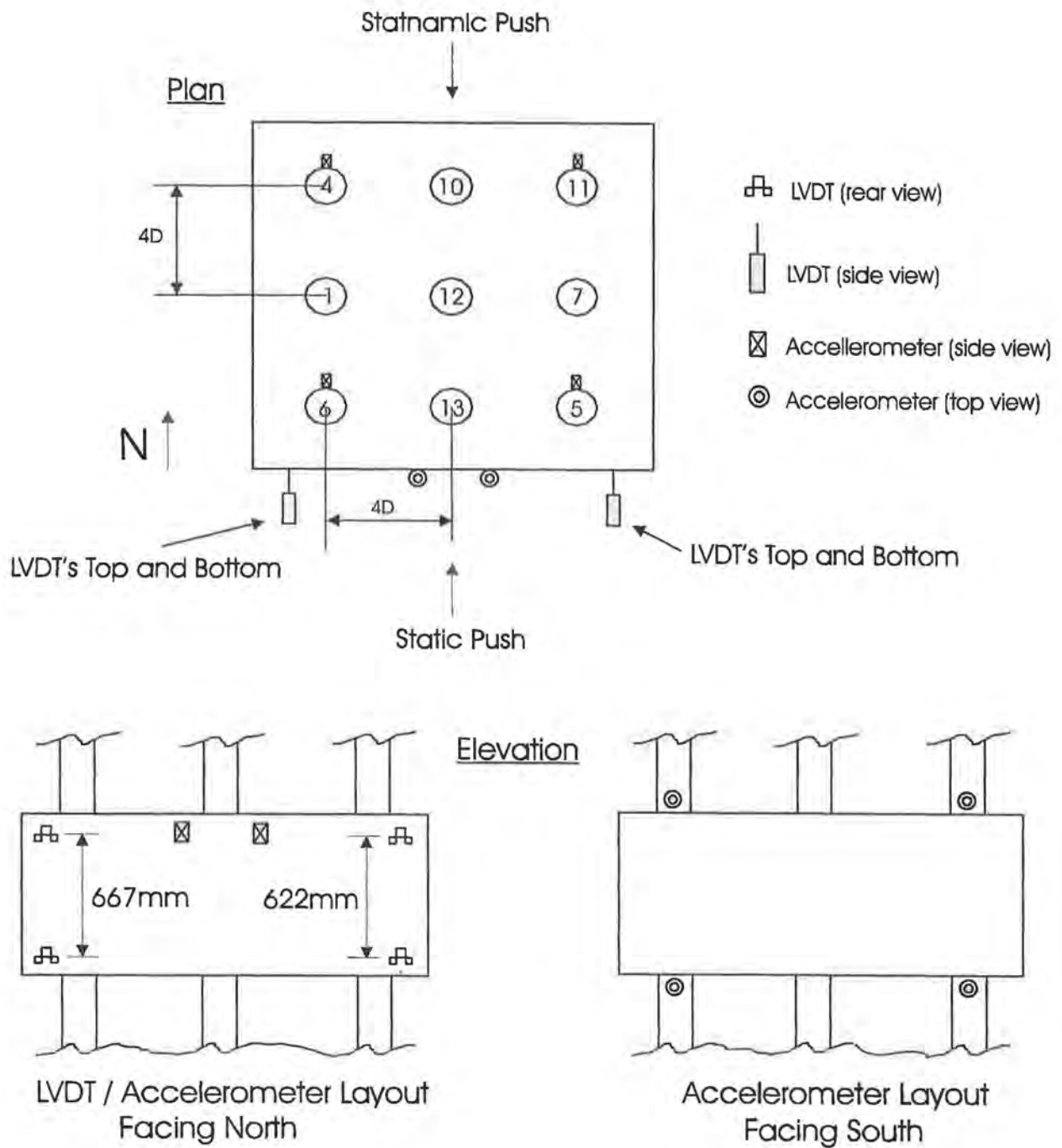


Figure E-35. Pile Layout for 9-Pile Group

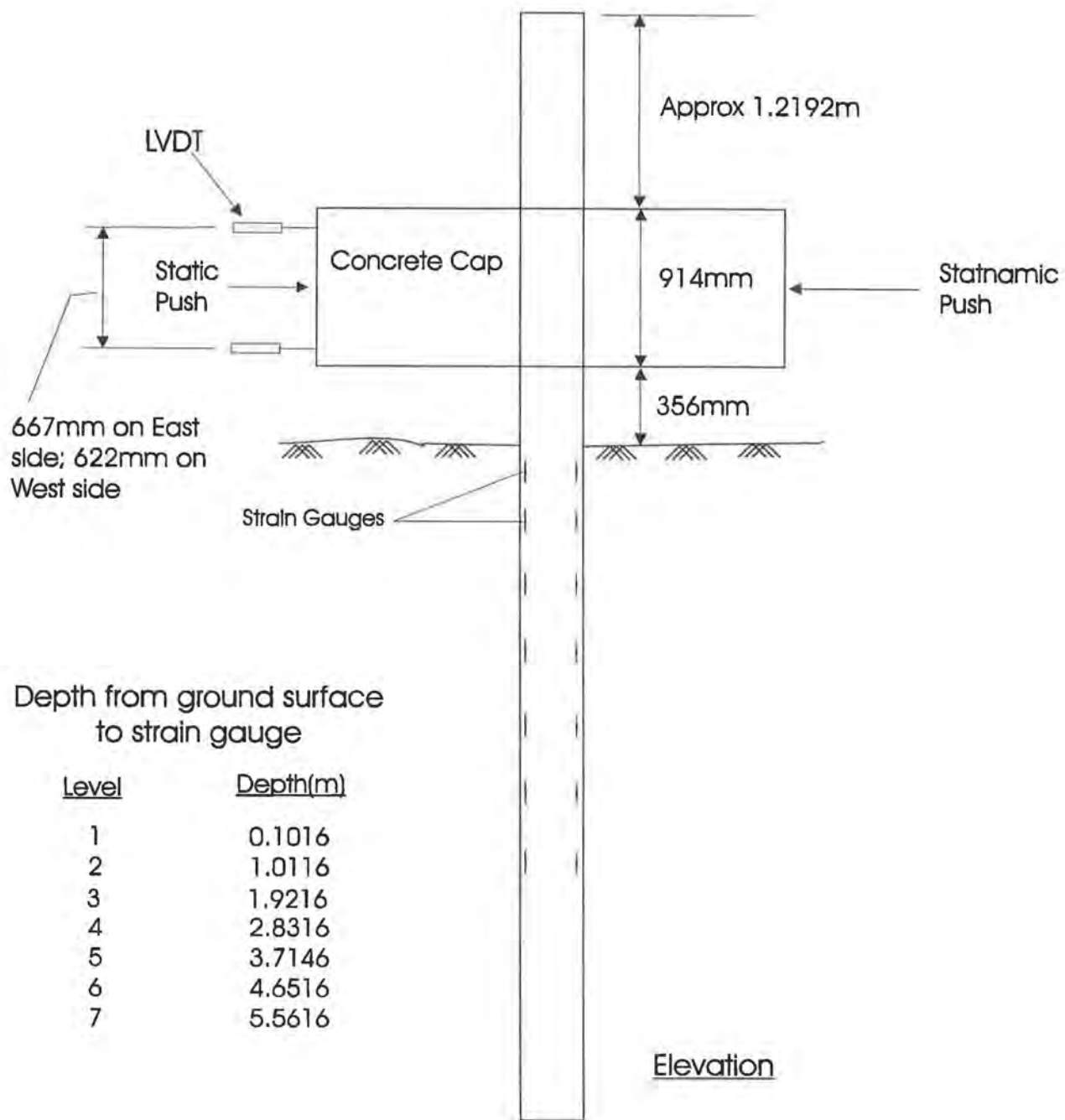


Figure E-36. Load and Instrumentation Setup for 9-Pile Group

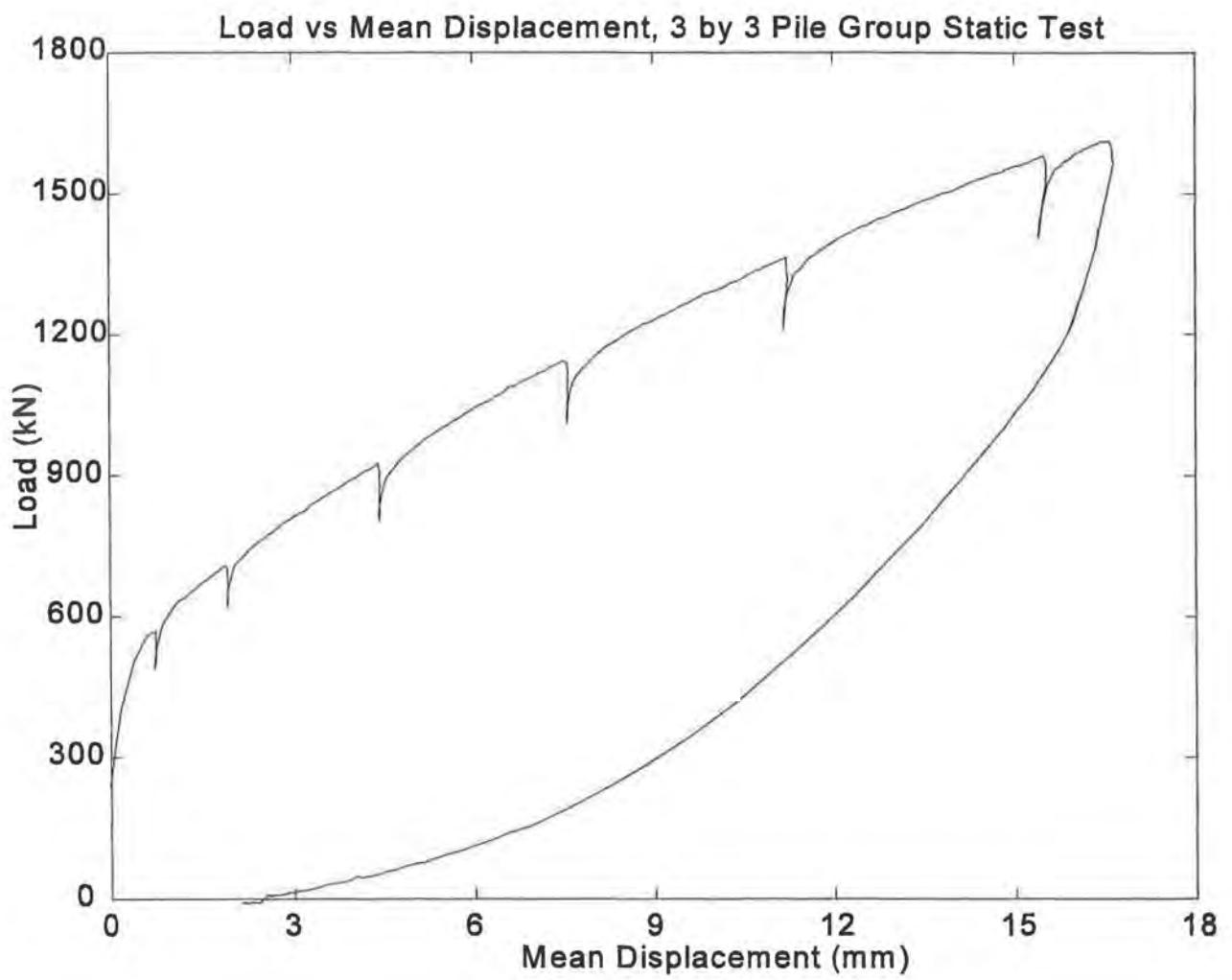


Figure E-37. Load vs Mean Displacement, 3 by 3 Pile Group Static Test

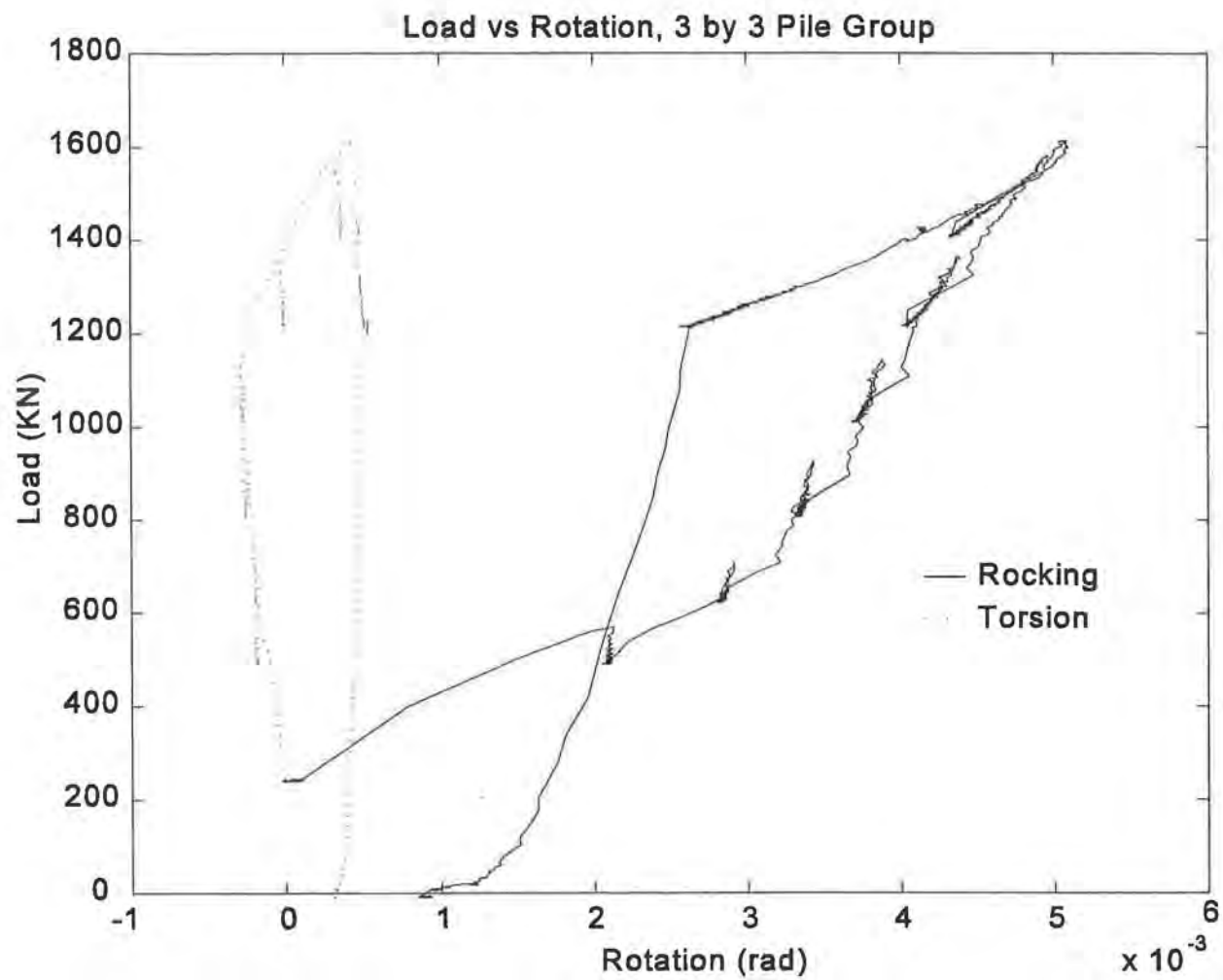
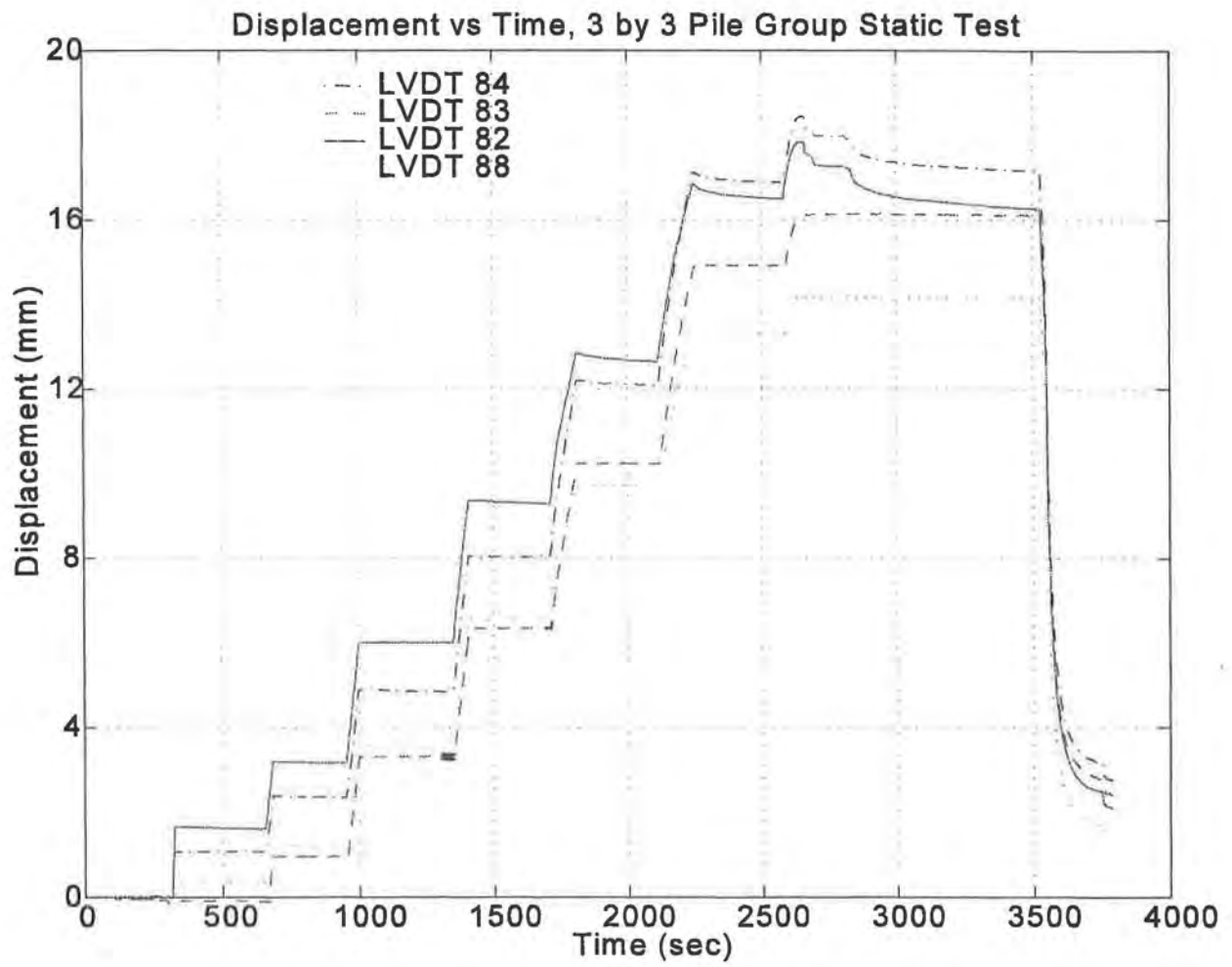


Figure E-38. Load vs Mean Rocking and Torsional Rotation, 3 by 3 Pile Group Static Test





*Figure E-39. Displacement Time History, 3 by 3 Pile Group Static Test*

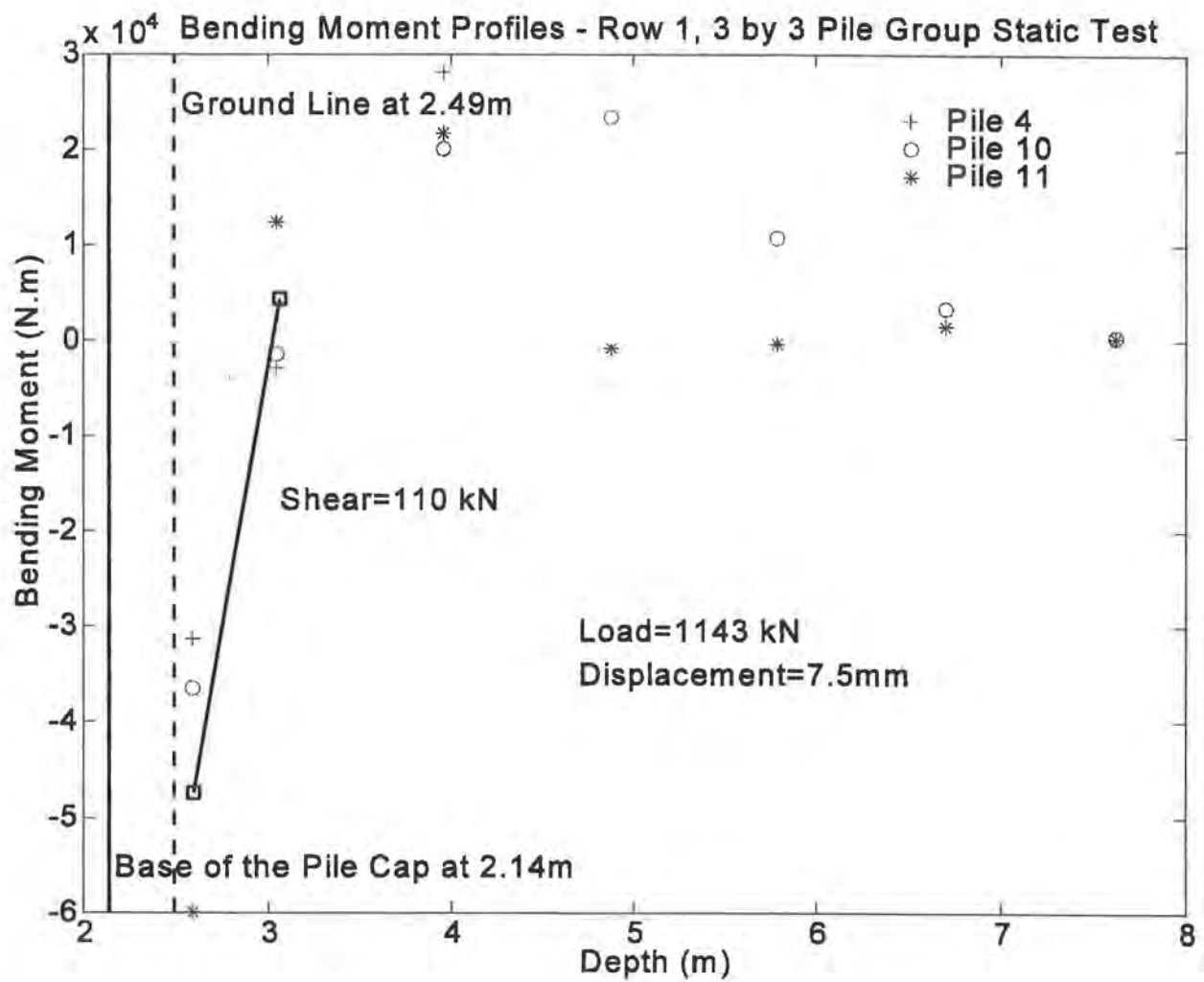


Figure E-40. Bending Moment Profiles at Load = 1143 kN - Row 1, 3 by 3 Pile Group Static Test

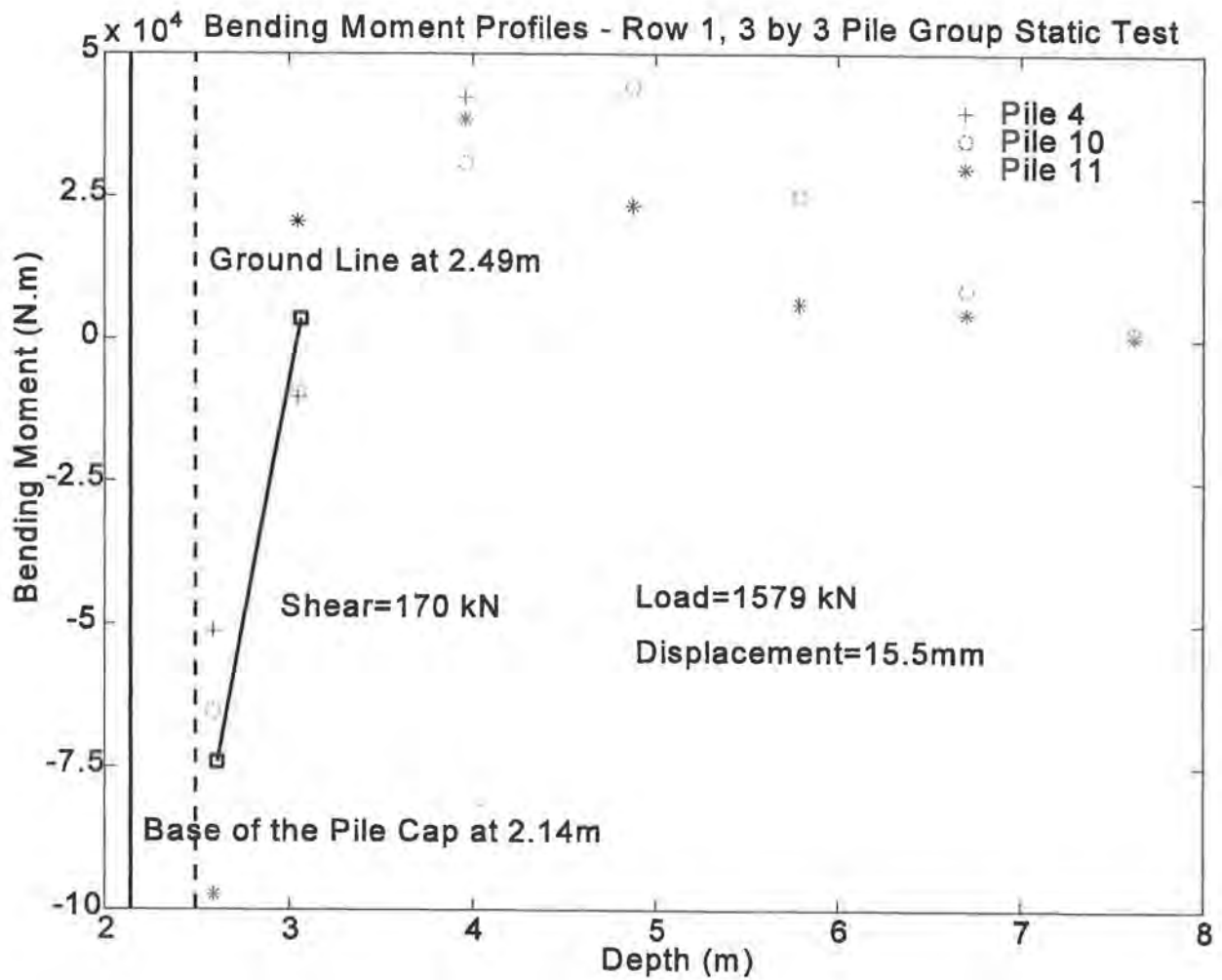


Figure E-41. Bending Moment Profiles at Load = 1579 kN - Row 1, 3 by 3 Pile Group Static Test

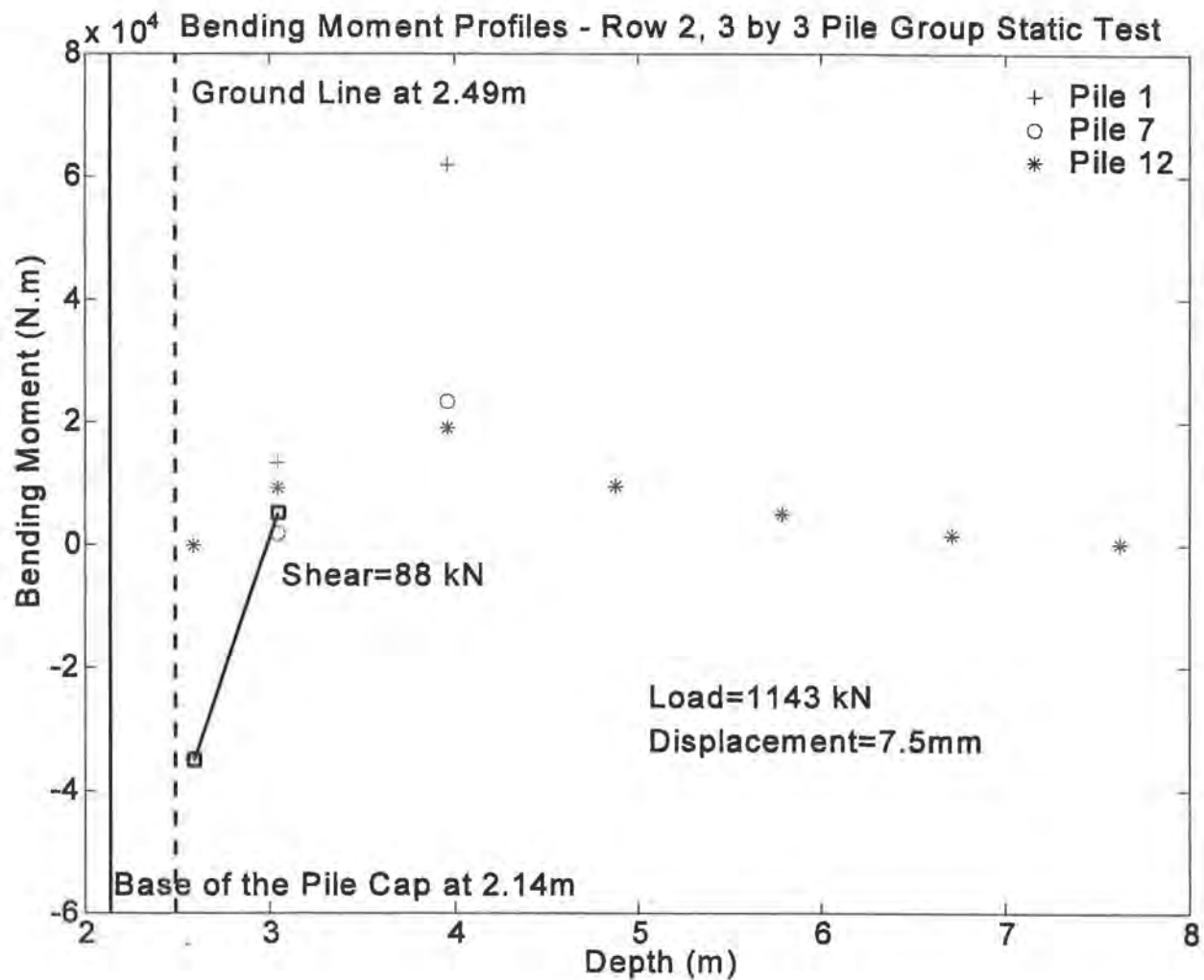


Figure E-42. Bending Moment Profiles at Load = 1143 kN - Row 2, 3 by 3 Pile Group Static Test

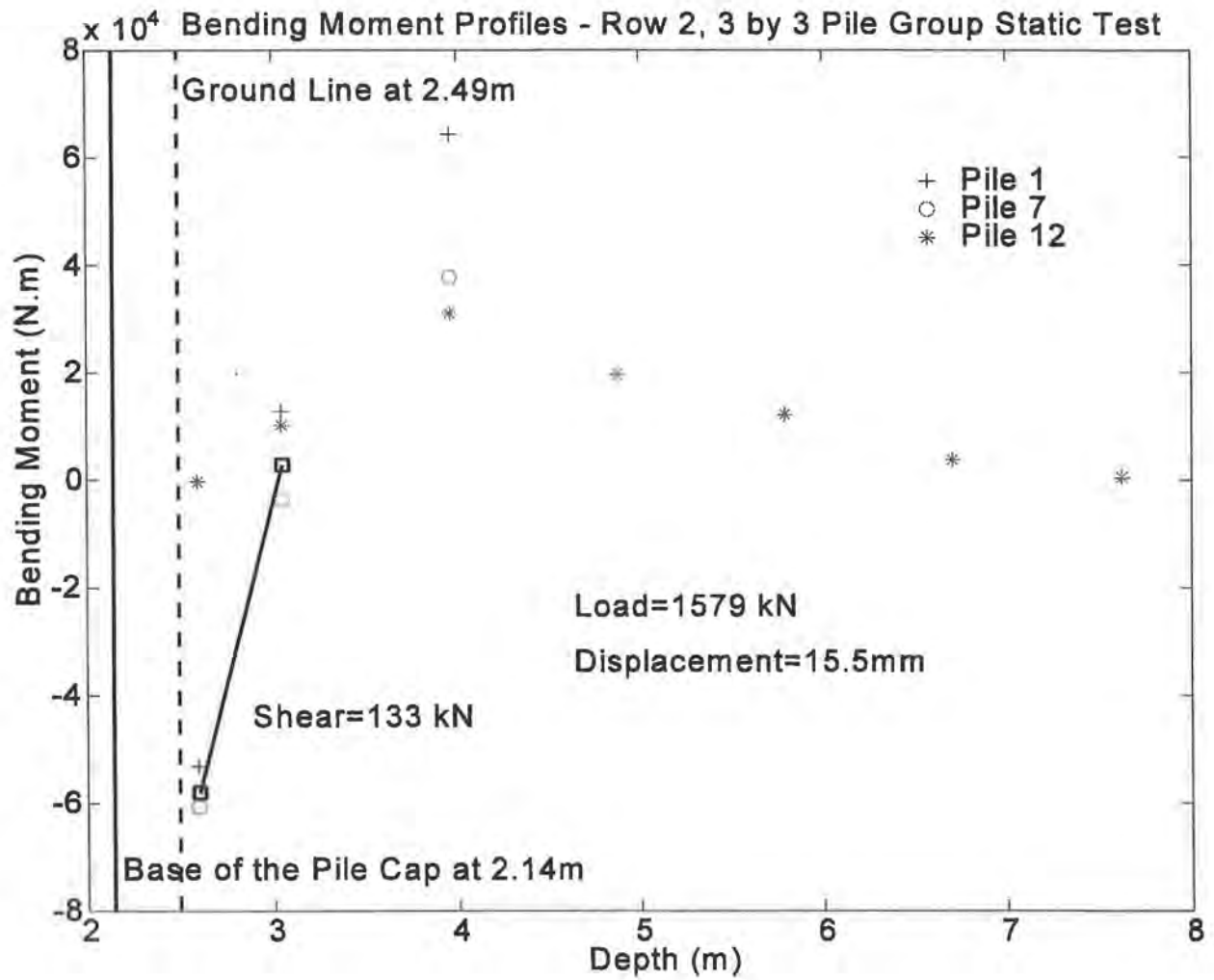


Figure E-43. Bending Moment Profiles at Load = 1579 kN - Row 2, 3 by 3 Pile Group Static Test

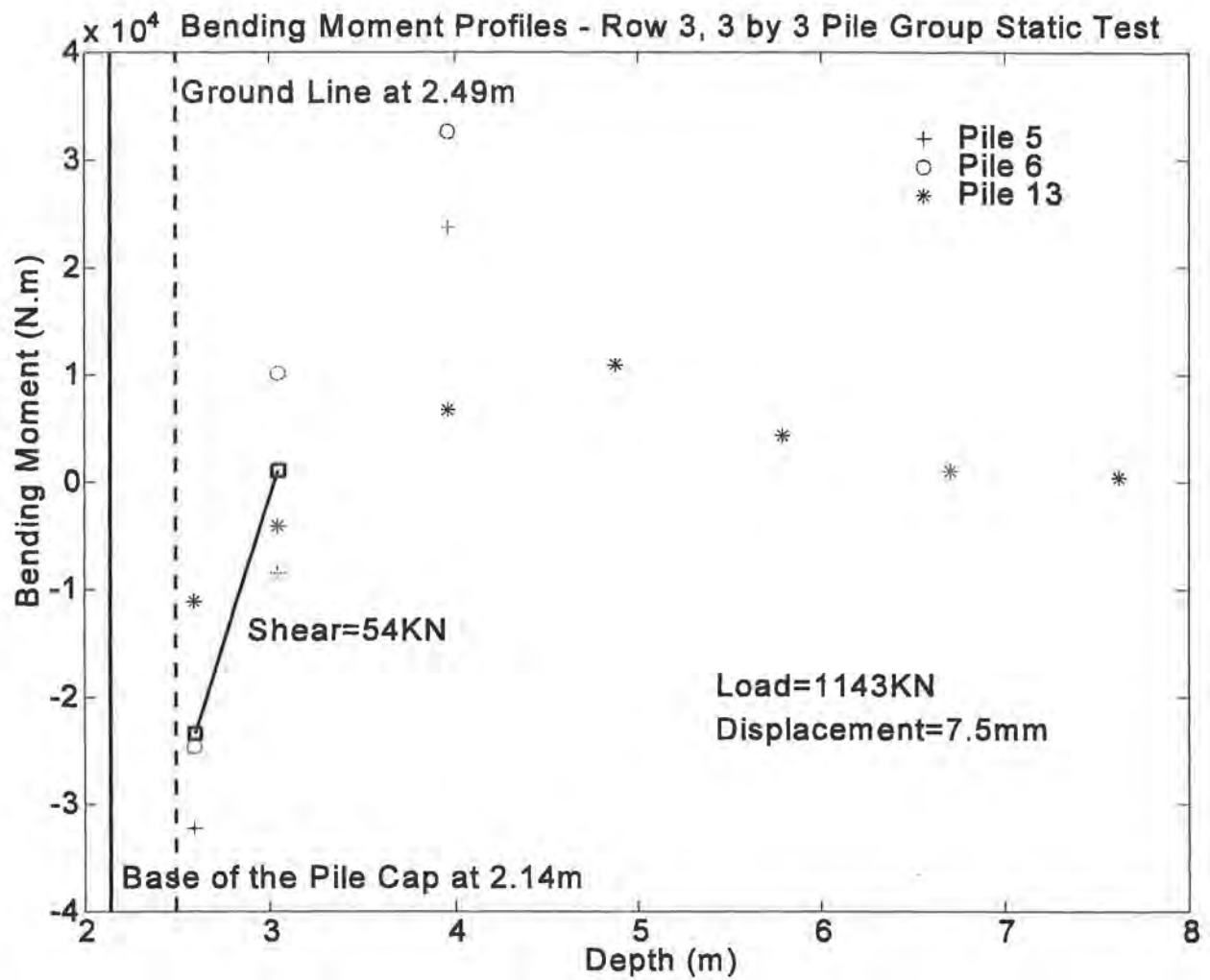


Figure E-44. Bending Moment Profiles at Load = 1143 kN - Row 3, 3 by 3 Pile Group Static Test

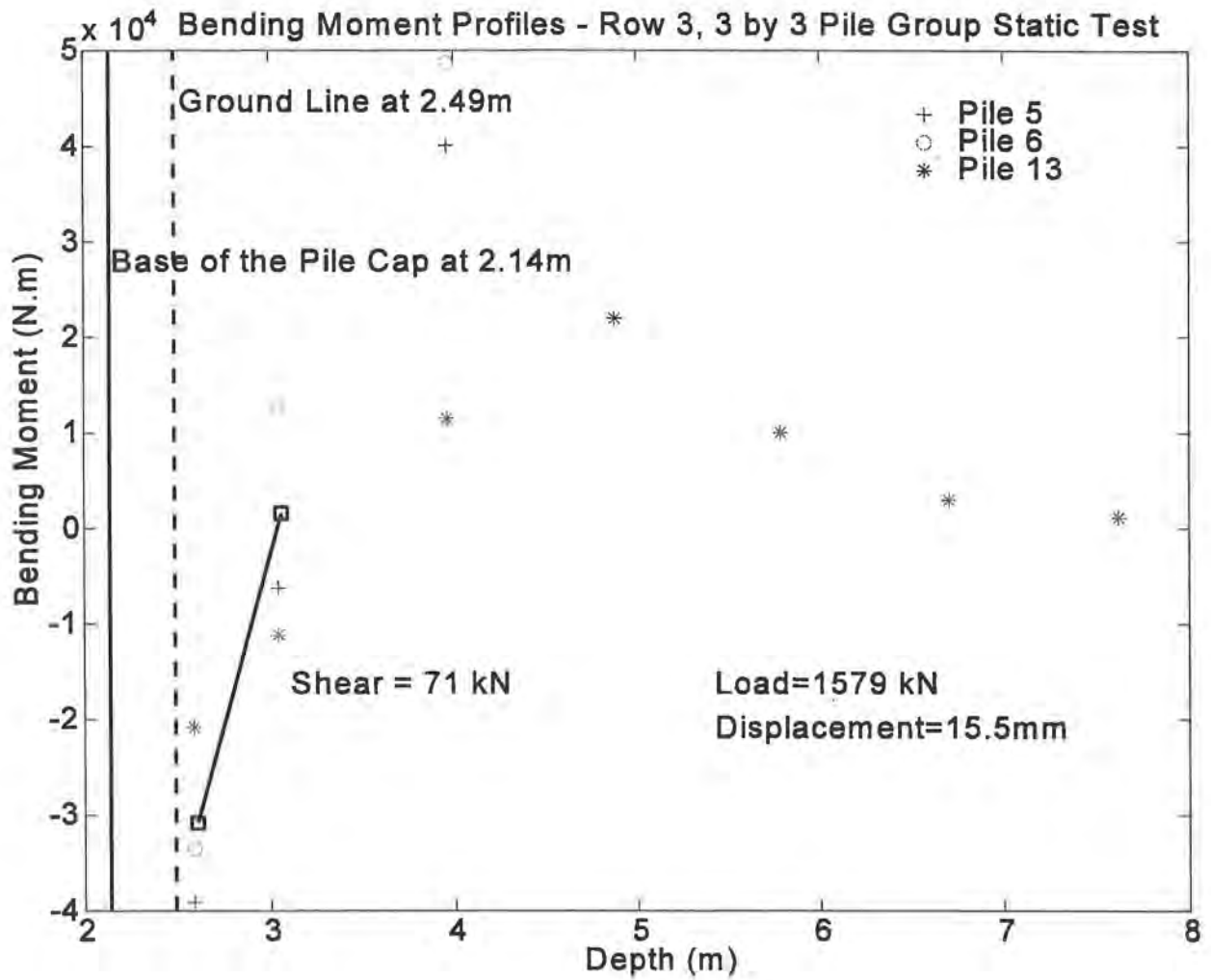



Figure E-45. Bending Moment Profiles at Load = 1579 kN - Row 3, 3 by 3 Pile Group Static Test

Pile Group Layout	Load Transferred To Row (kN)	% Load Transferred
<div> <div>4</div> <div>10</div> <div>11</div> </div>	[330, 510]	[44/45]
<div> <div>1</div> <div>12</div> <div>7</div> </div>	[264, 399]	[35/36]
<div> <div>6</div> <div>13</div> <div>5</div> </div>	[162, 213]	[21/19]


 Direction of Static Load

- Every circle represents one pile in the group
  - The number within the circle represents the pile number
  - The second column of numbers indicates the total lateral load transferred to the indicated row at loads of 1143 kN and 1579 kN ,respectively
- The final column represents the percentage of this measured summed load that was transferred to each indicated row

*Figure E-46. Static Pile-Head Shear Distribution, 3 by 3 Pile Group*



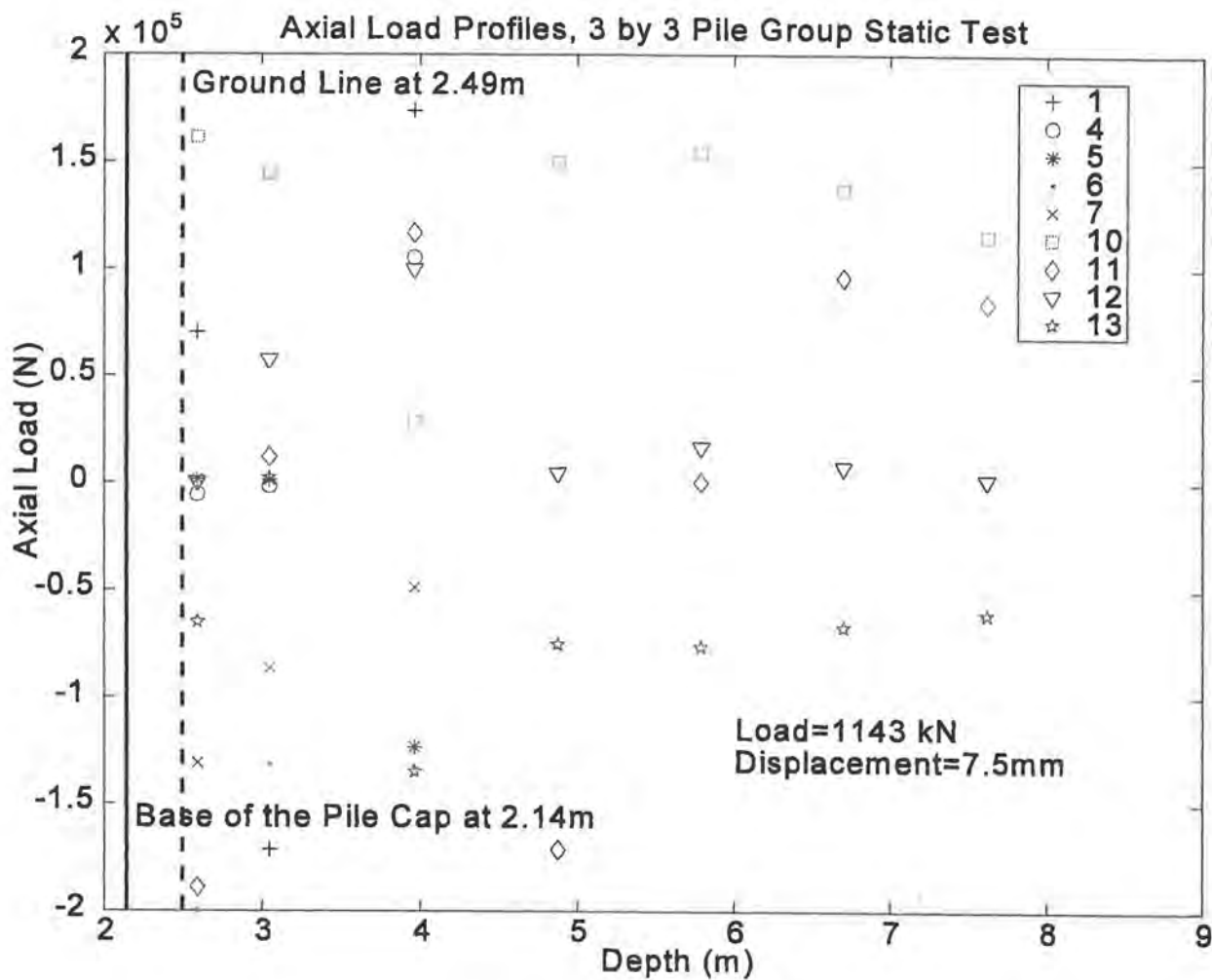


Figure E-47. Axial Load Profiles at Load = 1143 kN, 3 by 3 Pile Group Static Test

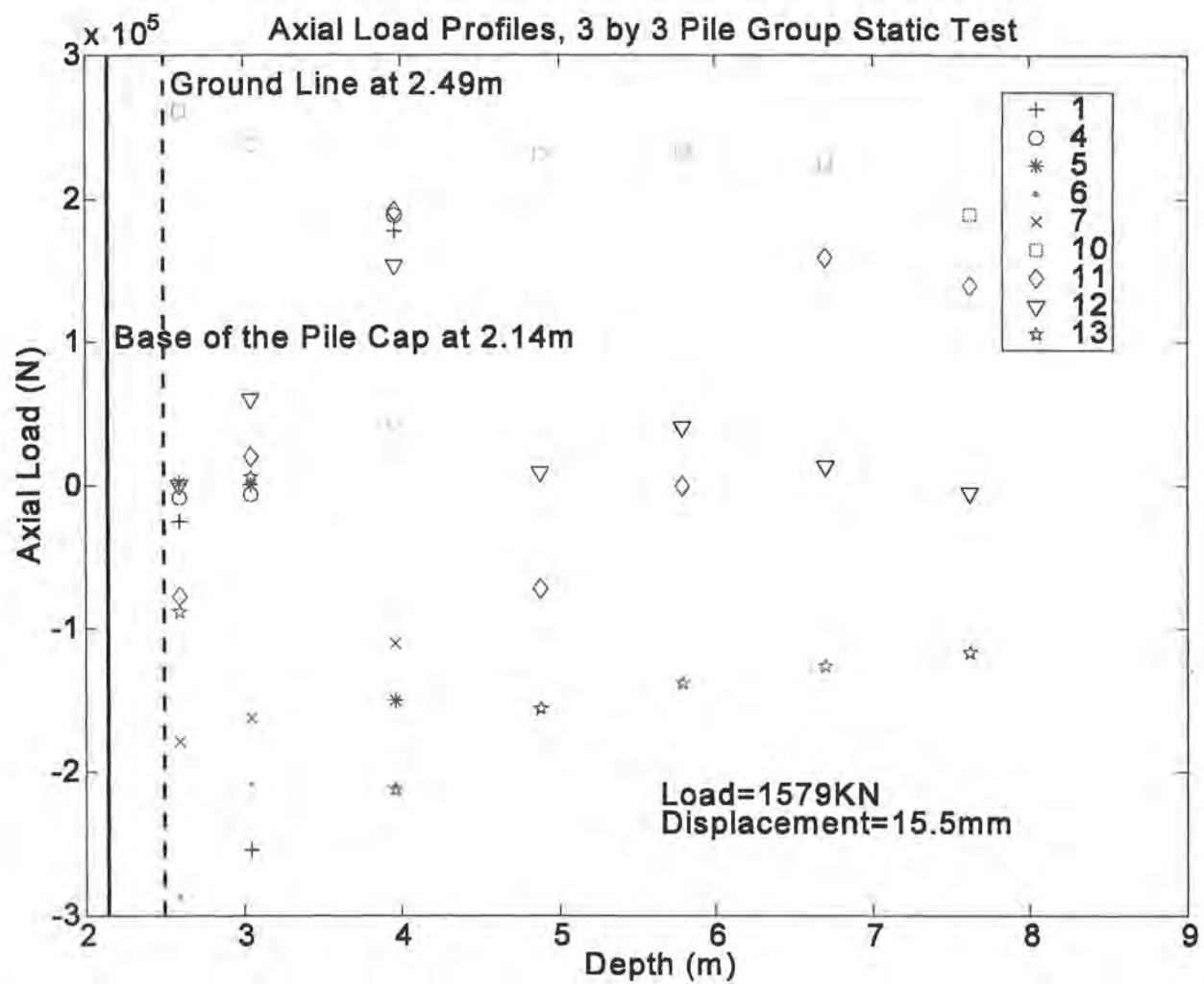
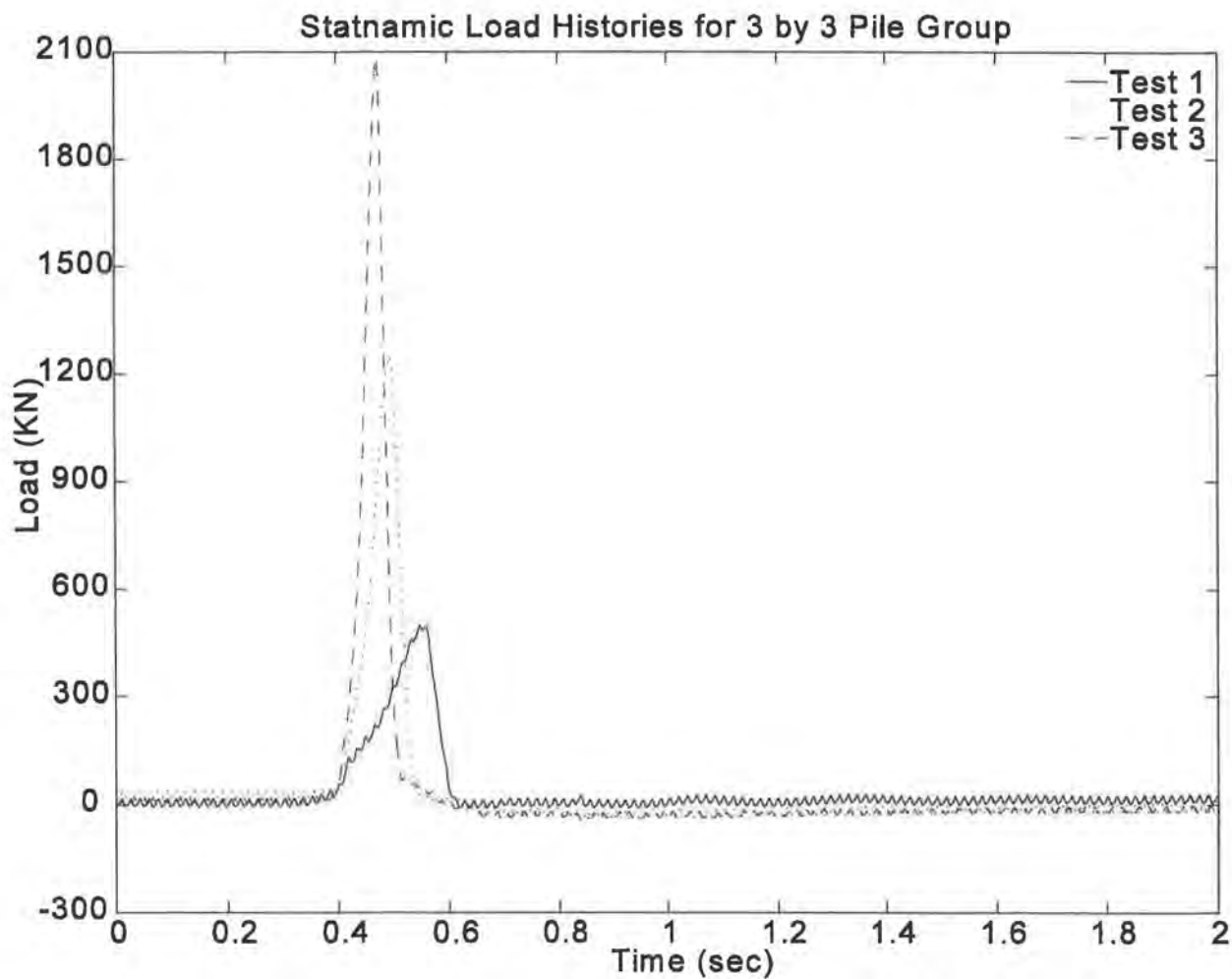
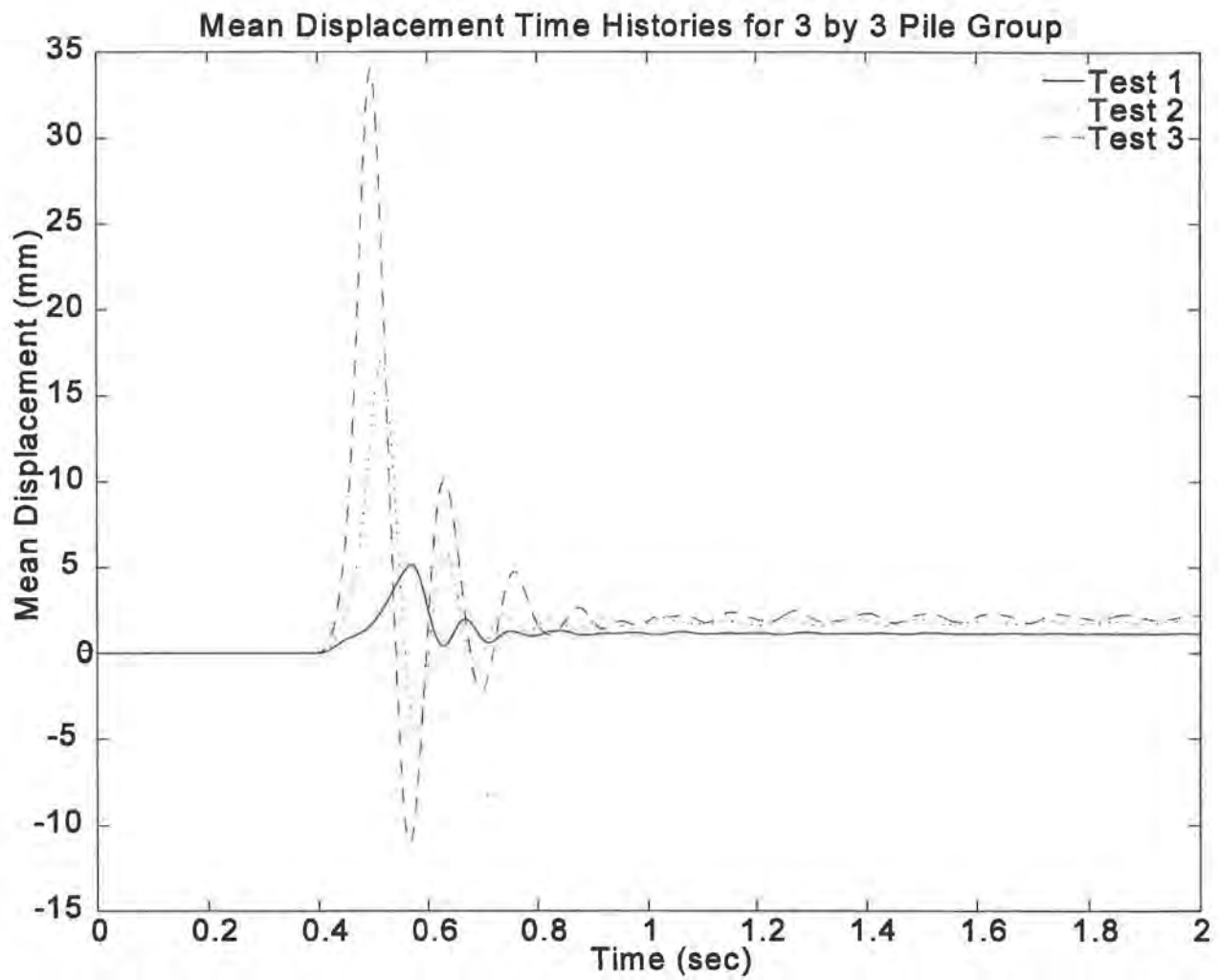


Figure E-48. Axial Load Profiles at Load = 1579 kN, 3 by 3 Pile Group Static Test



*Figure E-49. Load Time Histories, 3 by 3 Pile Group Statnamic Tests*



*Figure E-50. Displacement Time Histories, 3 by 3 Pile Group Static Tests*

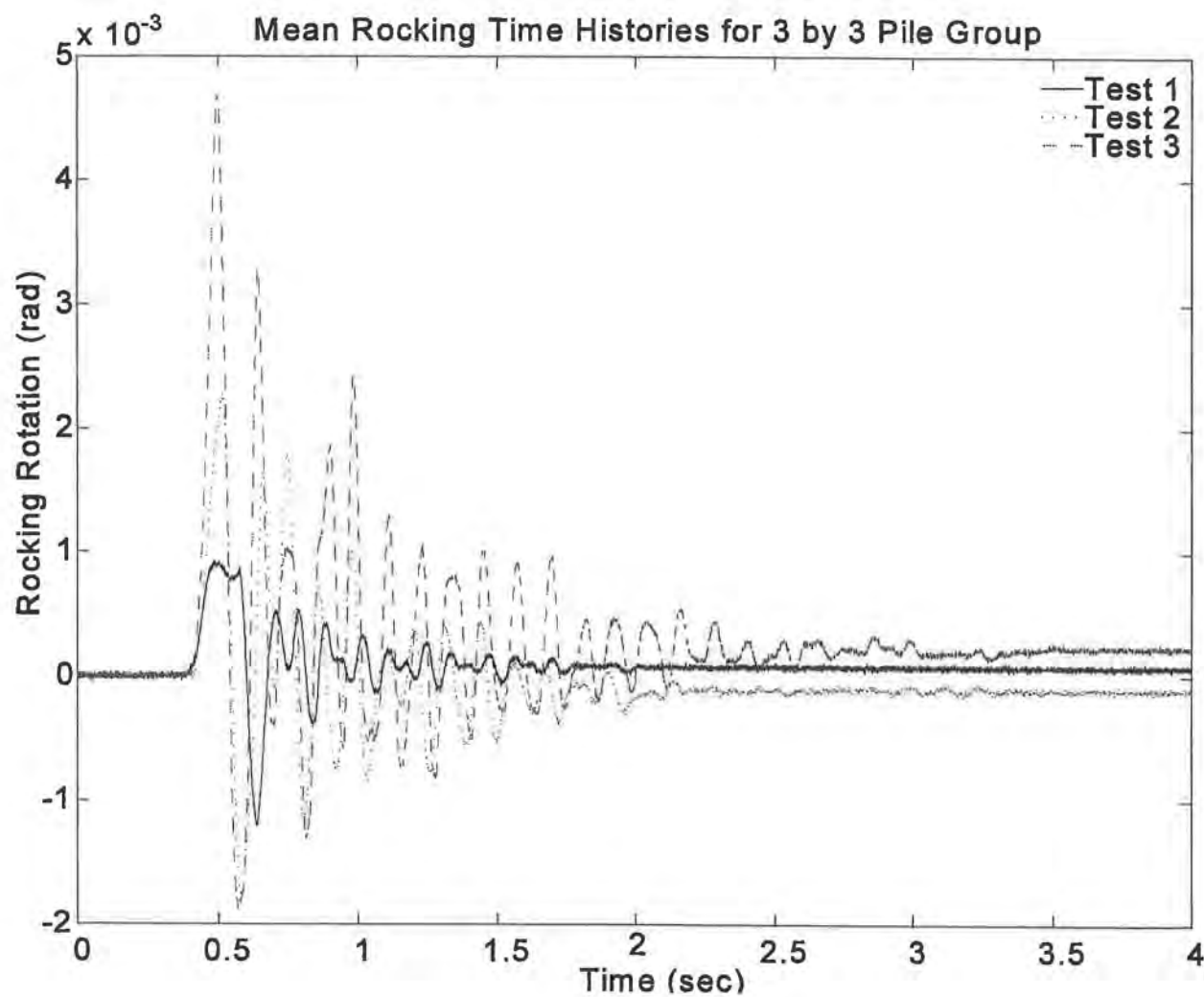


Figure E-51. Rocking Rotation Time Histories, 3 by 3 Pile Group Static Tests

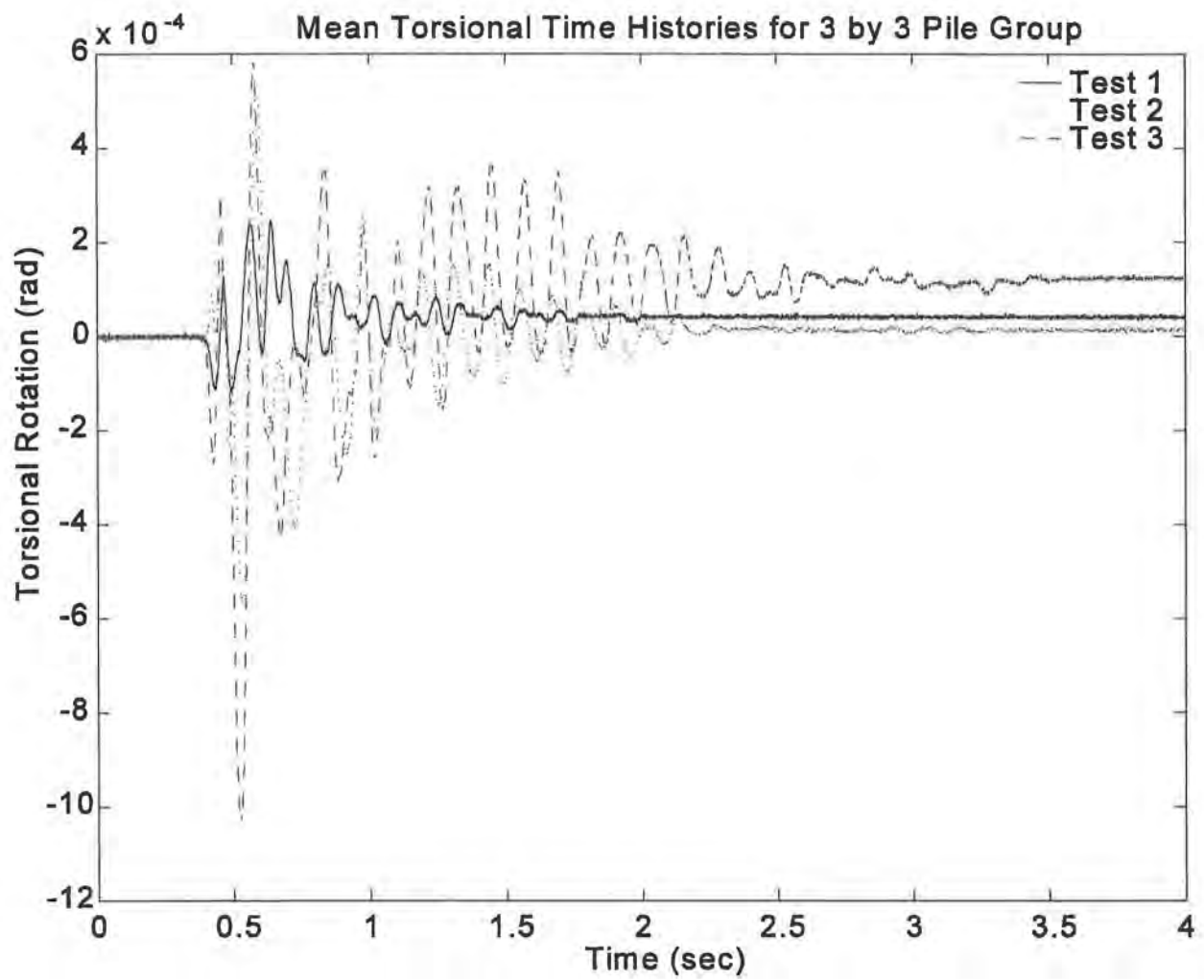


Figure E-52. Torsional Rotation Time Histories, 3 by 3 Pile Group Statnamic Tests

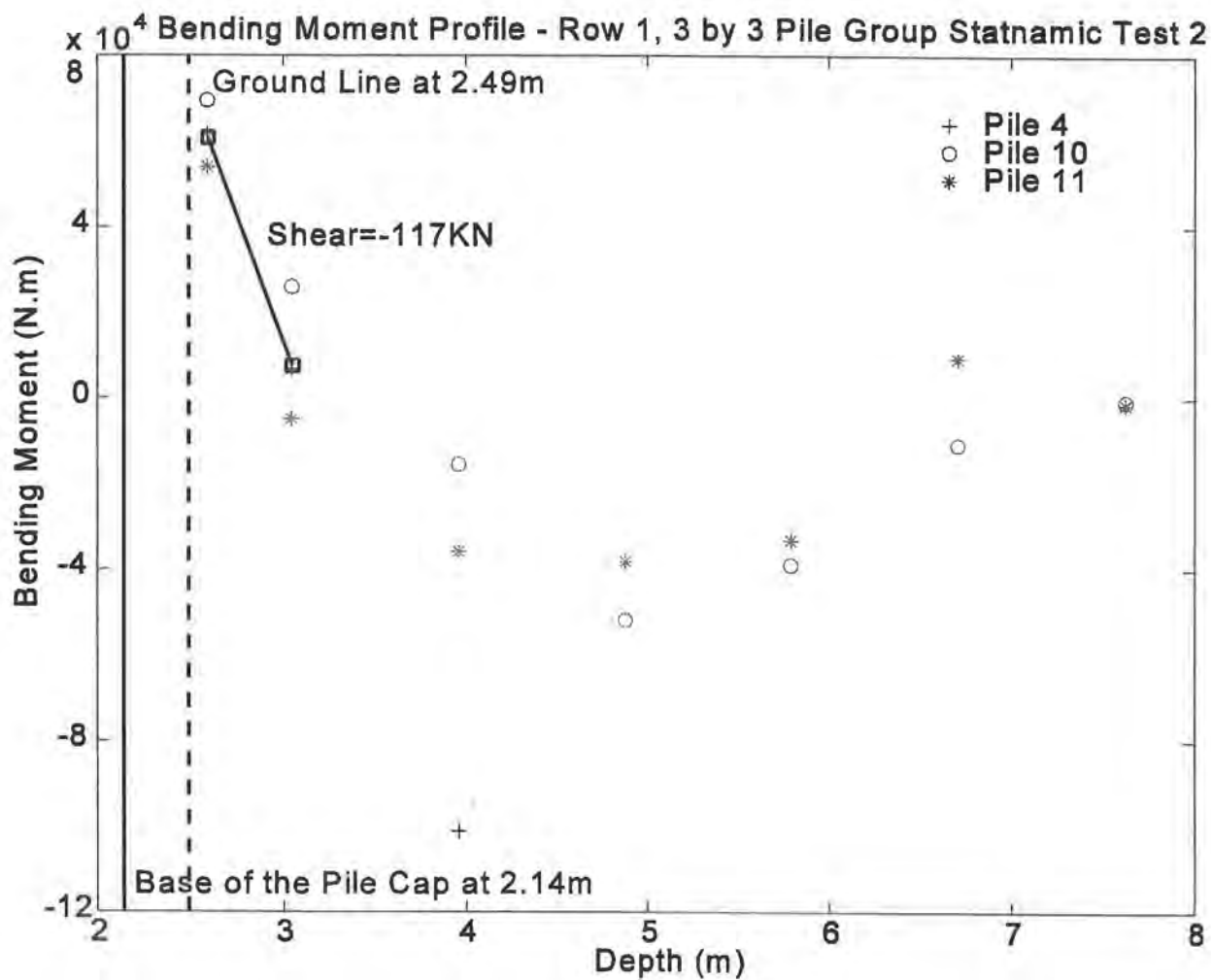


Figure E-53. Bending Moment Profiles - Row 1, 3 by 3 Pile Group Statnamic Test 2

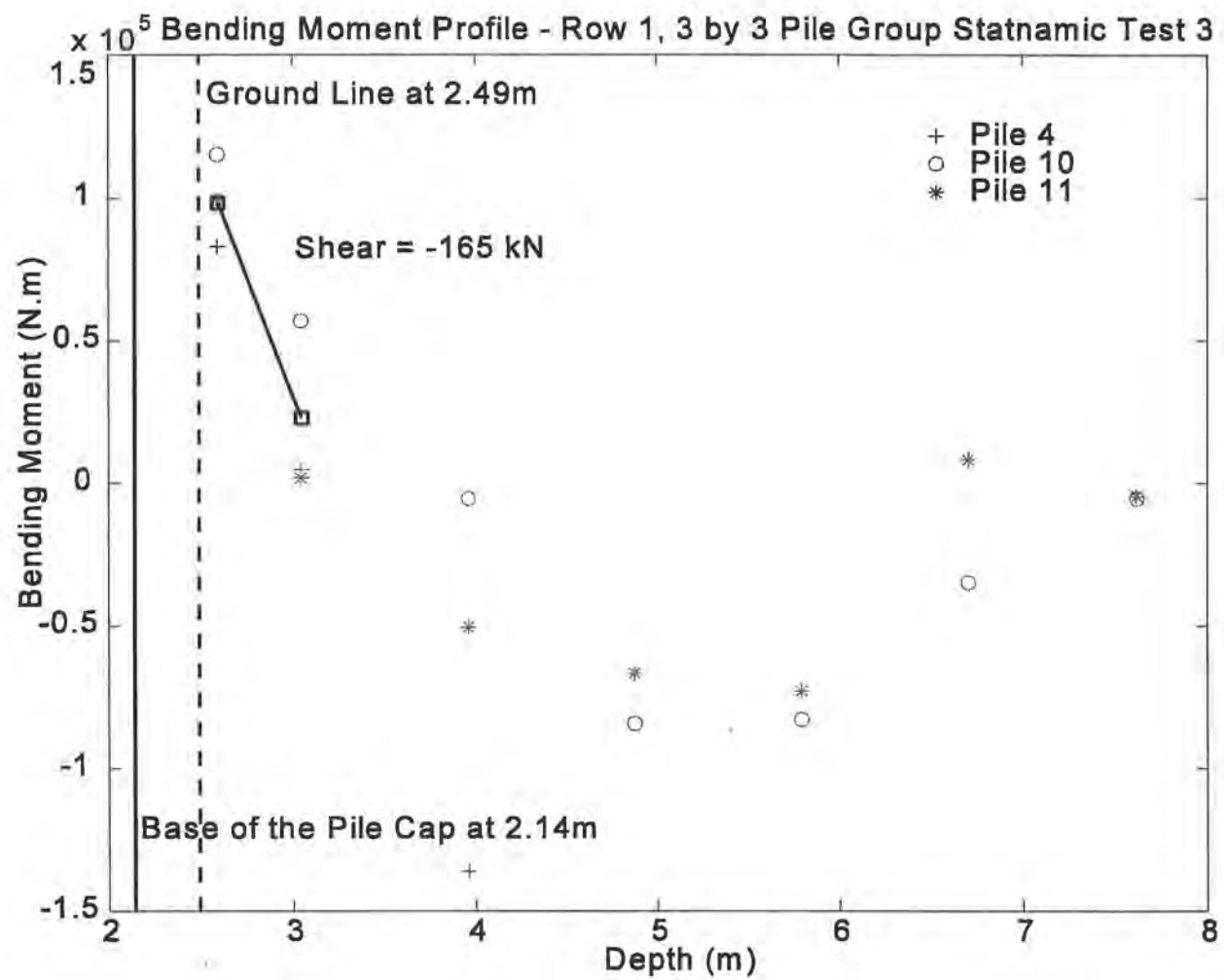


Figure E-54. Bending Moment Profiles - Row 1, 3 by 3 Pile Group Statnamic Test 3



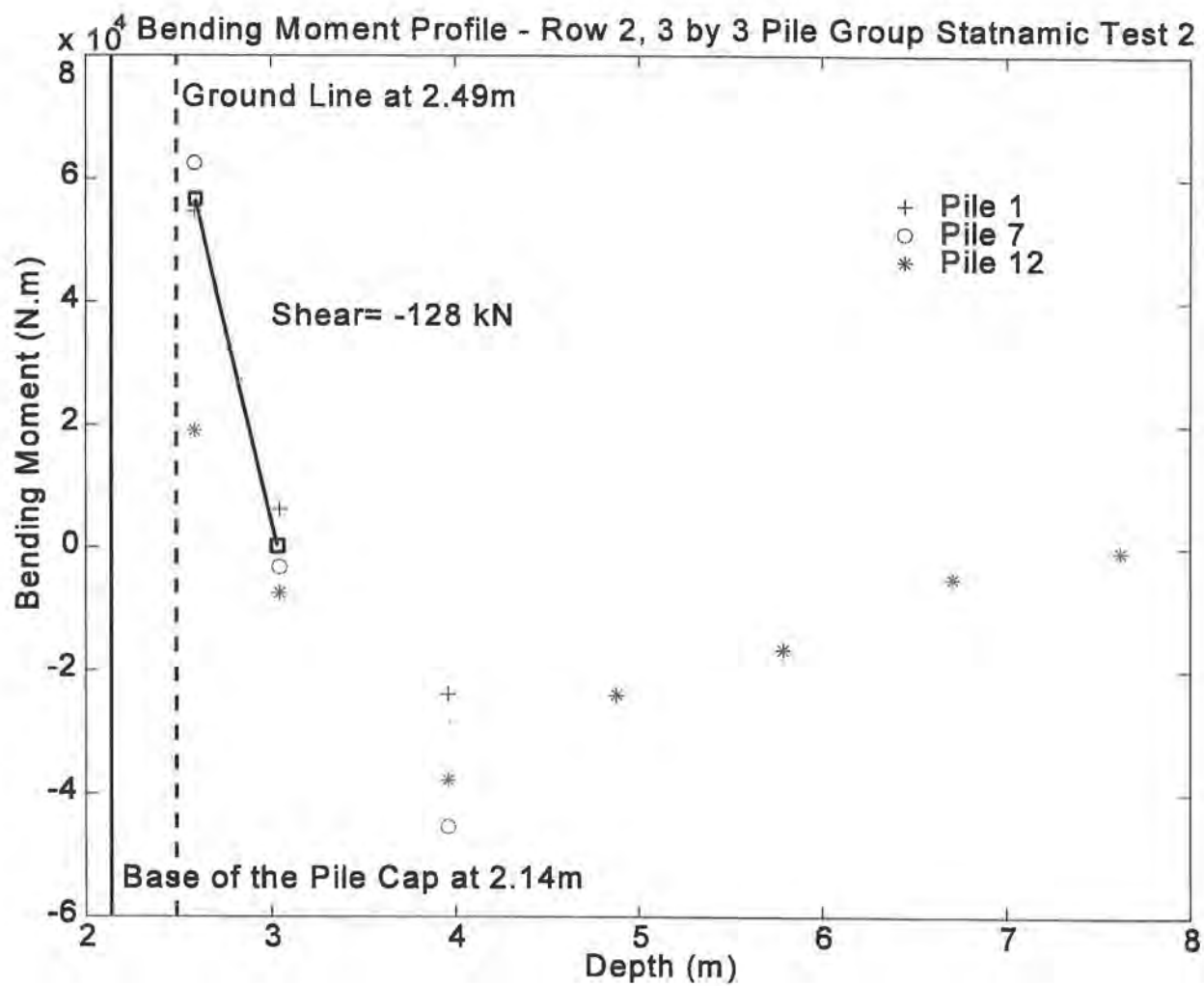


Figure E-55. Bending Moment Profiles - Row 2, 3 by 3 Pile Group Statnamic Test 2

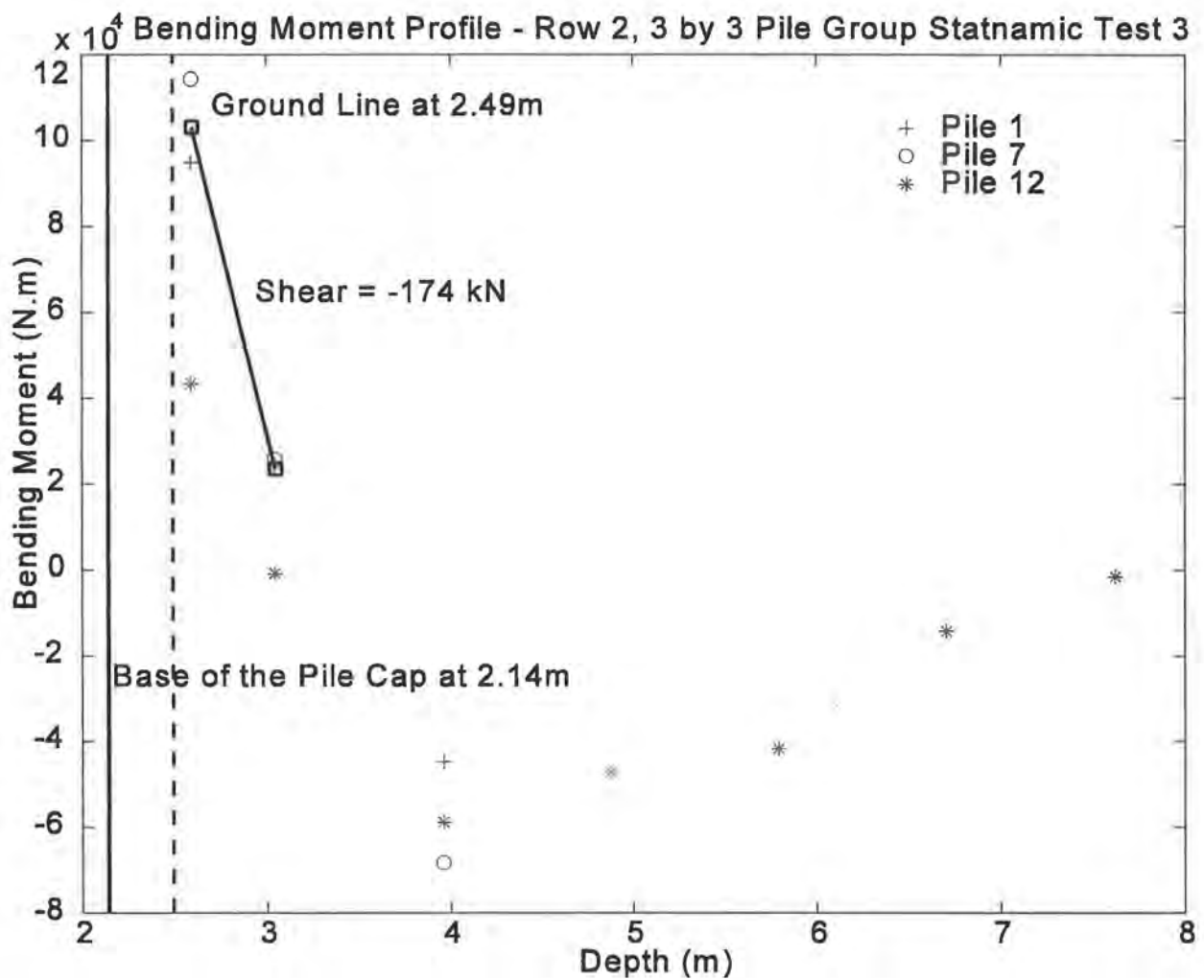


Figure E-56. Bending Moment Profiles - Row 2, 3 by 3 Pile Group Statnamic Test 3

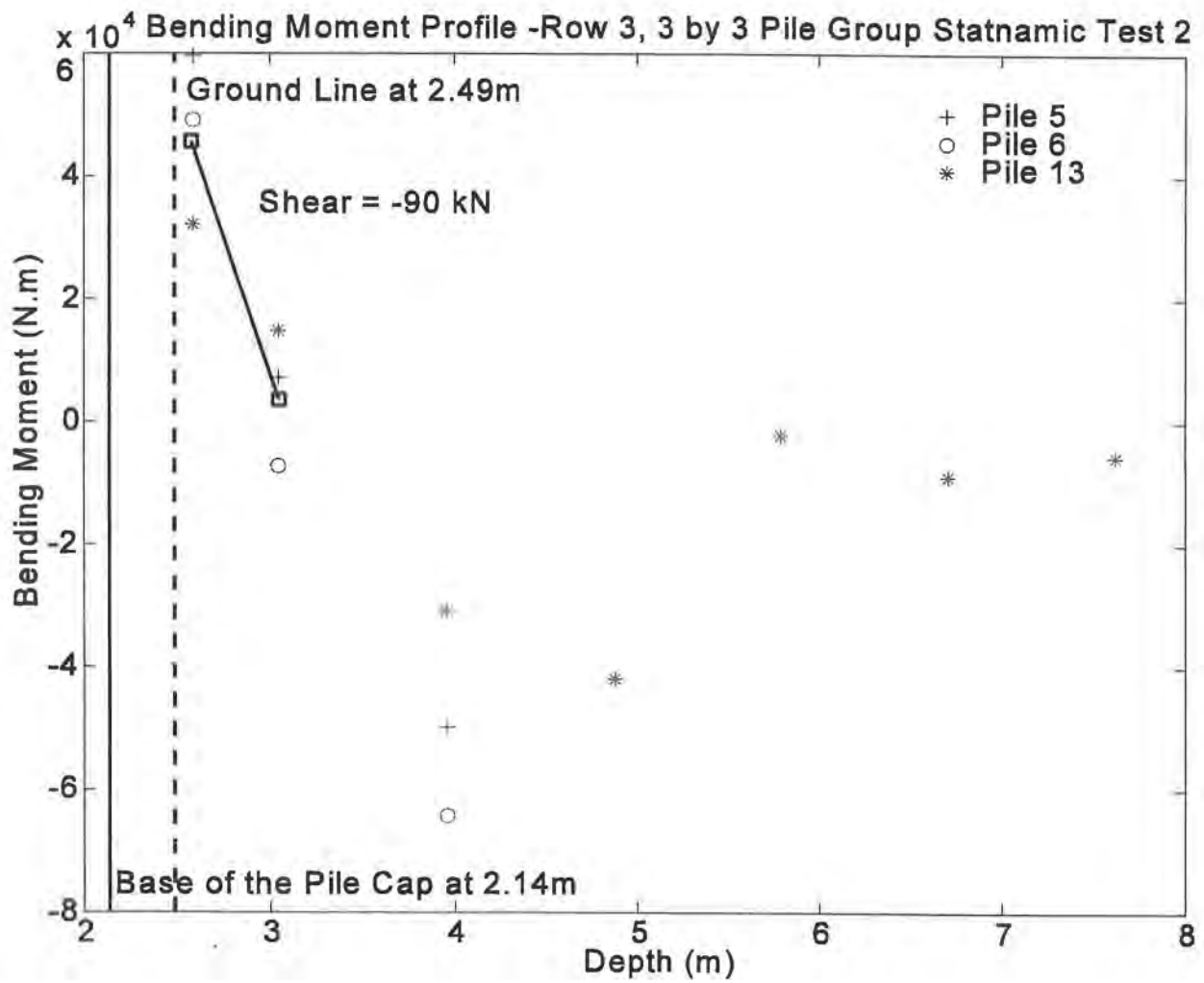


Figure E-57. Bending Moment Profiles - Row 3, 3 by 3 Pile Group Statnamic Test 2

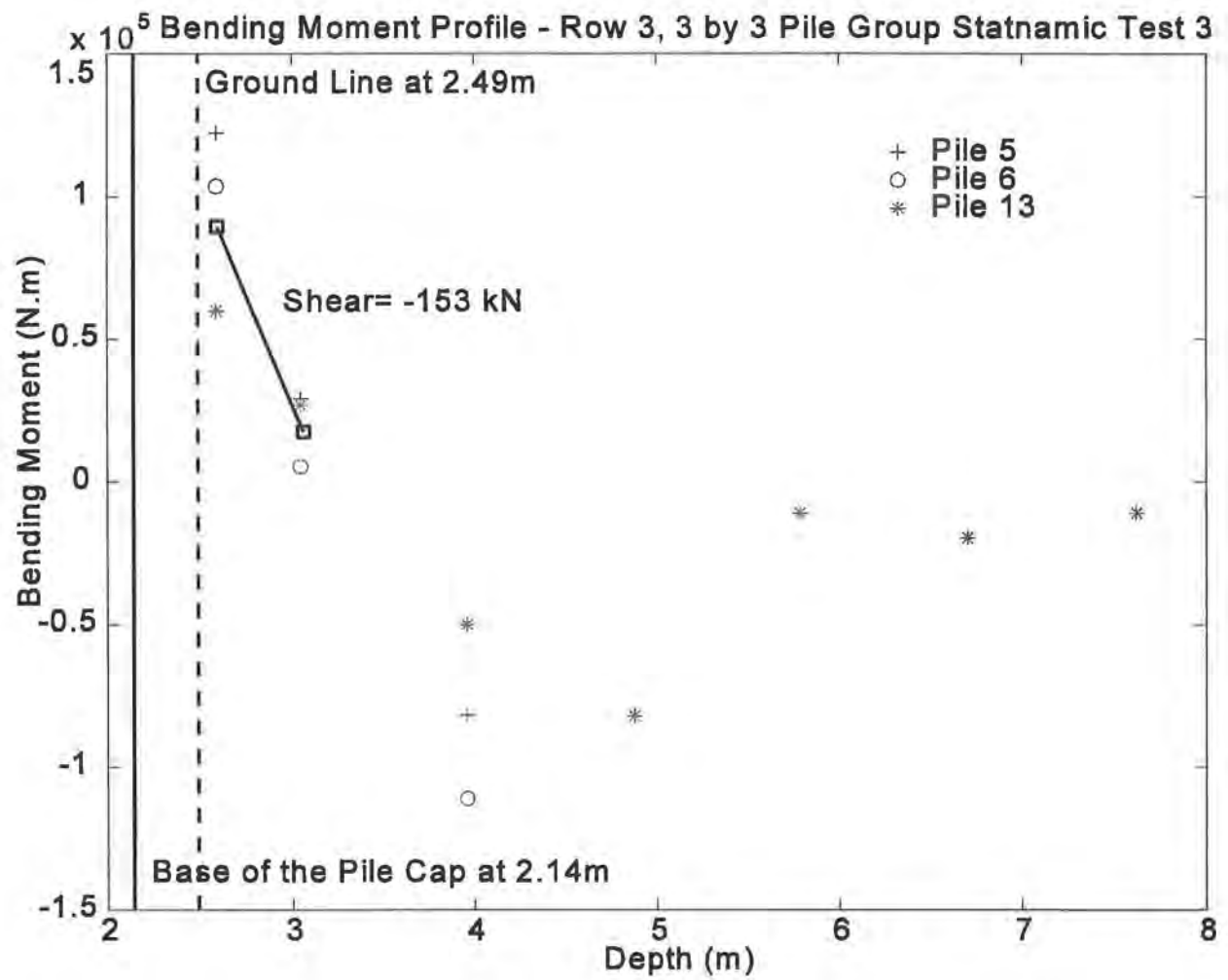



Figure E-58. Bending Moment Profiles - Row 3, 3 by 3 Pile Group Statnamic Test 3

Pile Group Layout	Load Transferred To Row (kN)	% Load Transferred
<div> <div>5</div> <div>13</div> <div>6</div> </div>	[270, 459]	[27 / 31]
<div> <div>7</div> <div>12</div> <div>1</div> </div>	[384, 522]	[38 / 35]
<div> <div>11</div> <div>10</div> <div>4</div> </div>	[351, 495]	[35 / 34]


 Direction of Static Load

- Every circle represents one pile in the group
- The number within the circle represents the pile number
- The second column of numbers indicates the total lateral load transferred to a particular row at peak displacement for Static tests 2 and 3

*Figure E-59. Pile Head Shear Distribution, 3 by 3 Pile Group Static Tests 2 and 3*

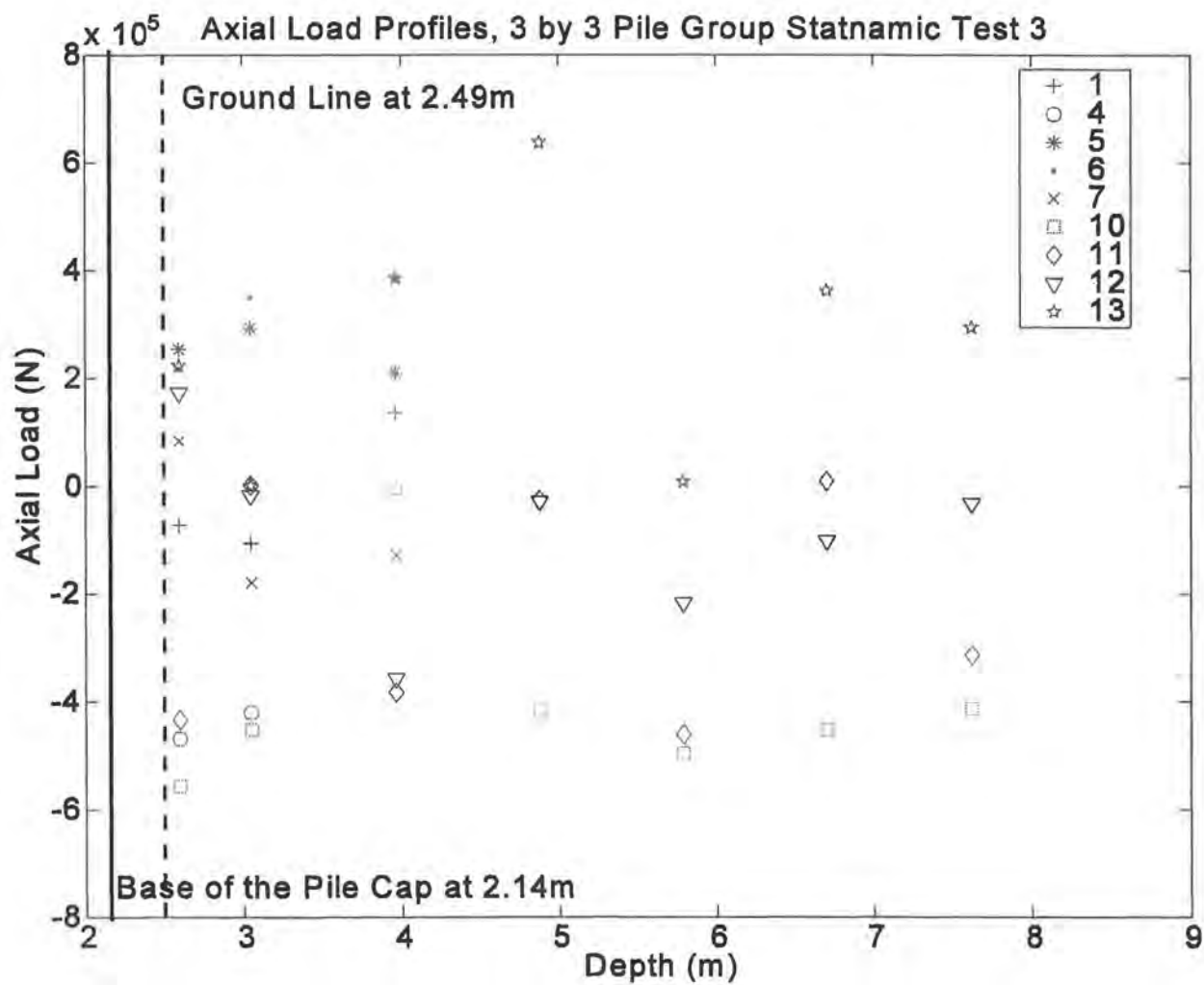


Figure E-60. Axial Load Profiles, 3 by 3 Pile Group Statnamic Test 3

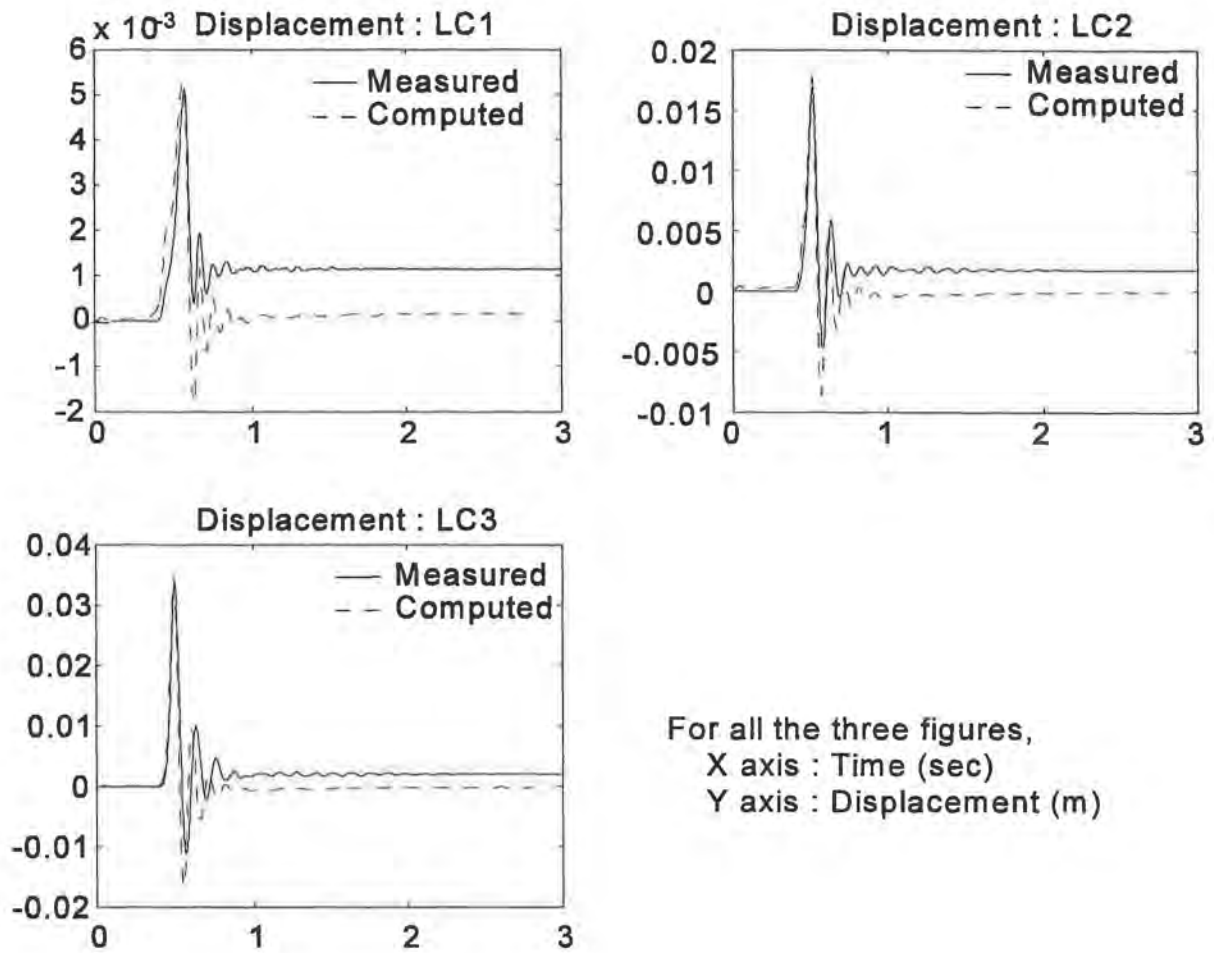


Figure E-61. Computed vs. Measured Lateral Response, 3 by 3 Pile Group

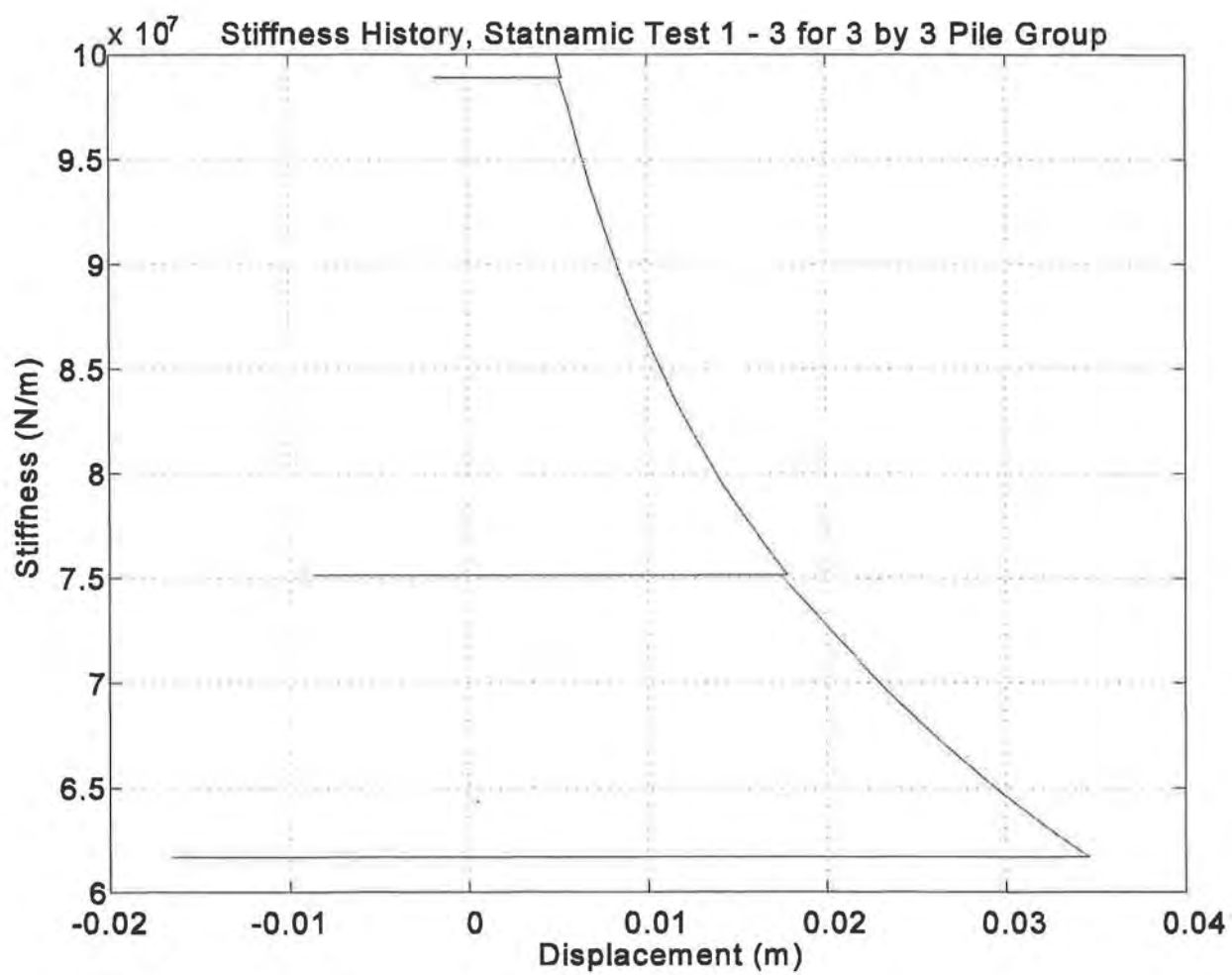
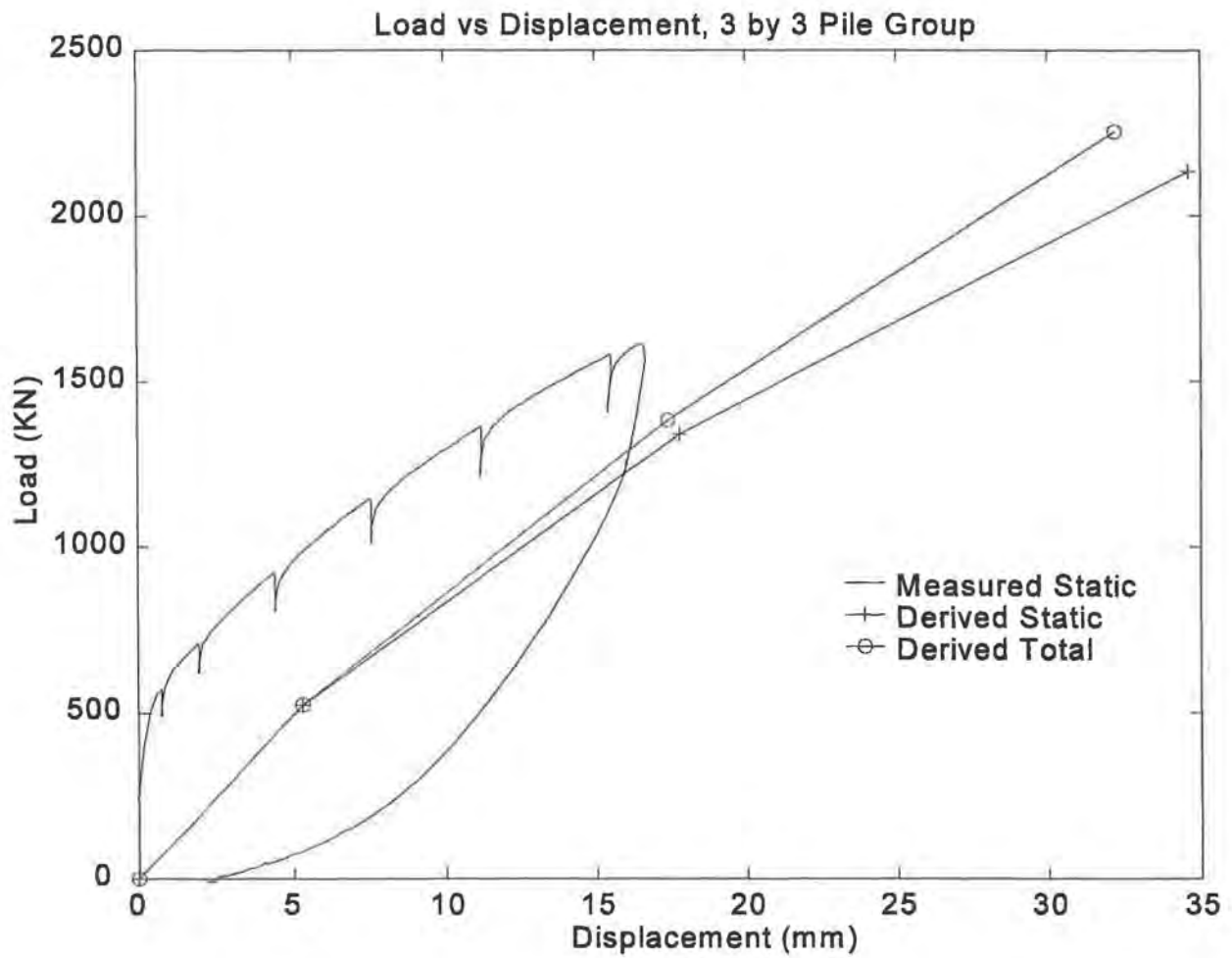


Figure E-62. Stiffness History, SDOF Model for 3 by 3 Pile Group





*Figure E-63. Derived Static Load-Deflection Response, 3 by 3 Pile Group*

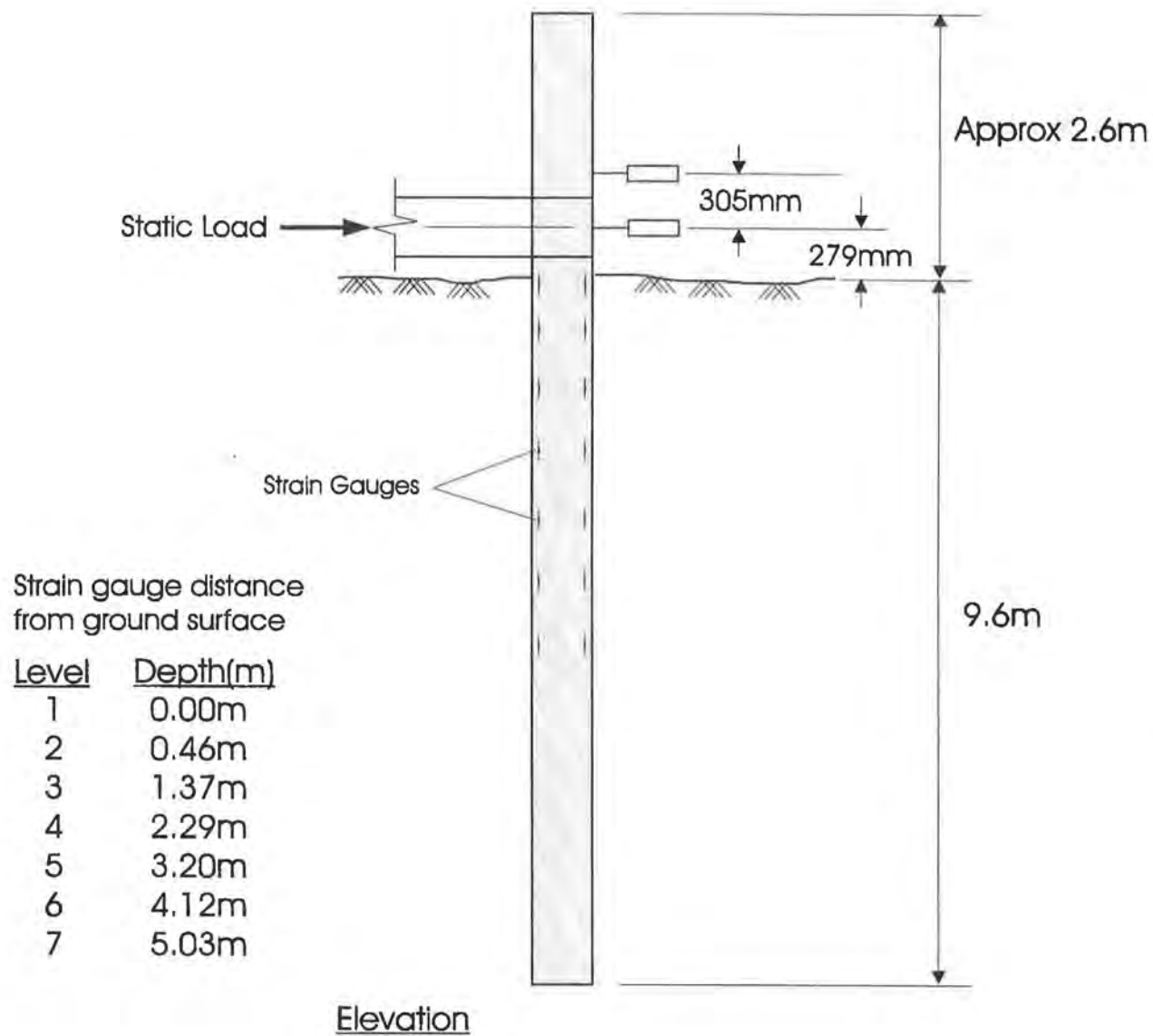


Figure E-64. Single Pile Setup Against 12-Pile Group (Pile 13)

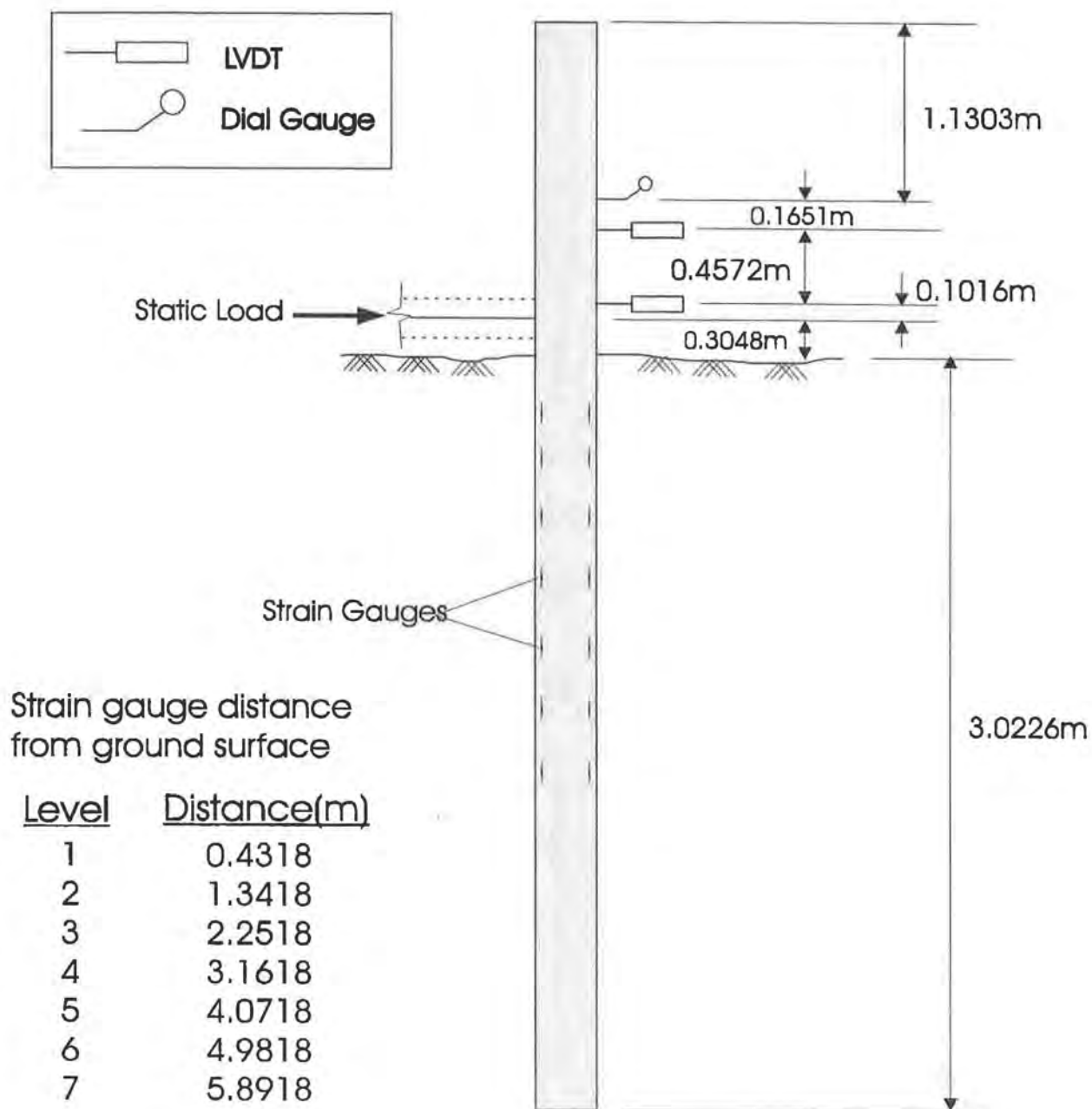
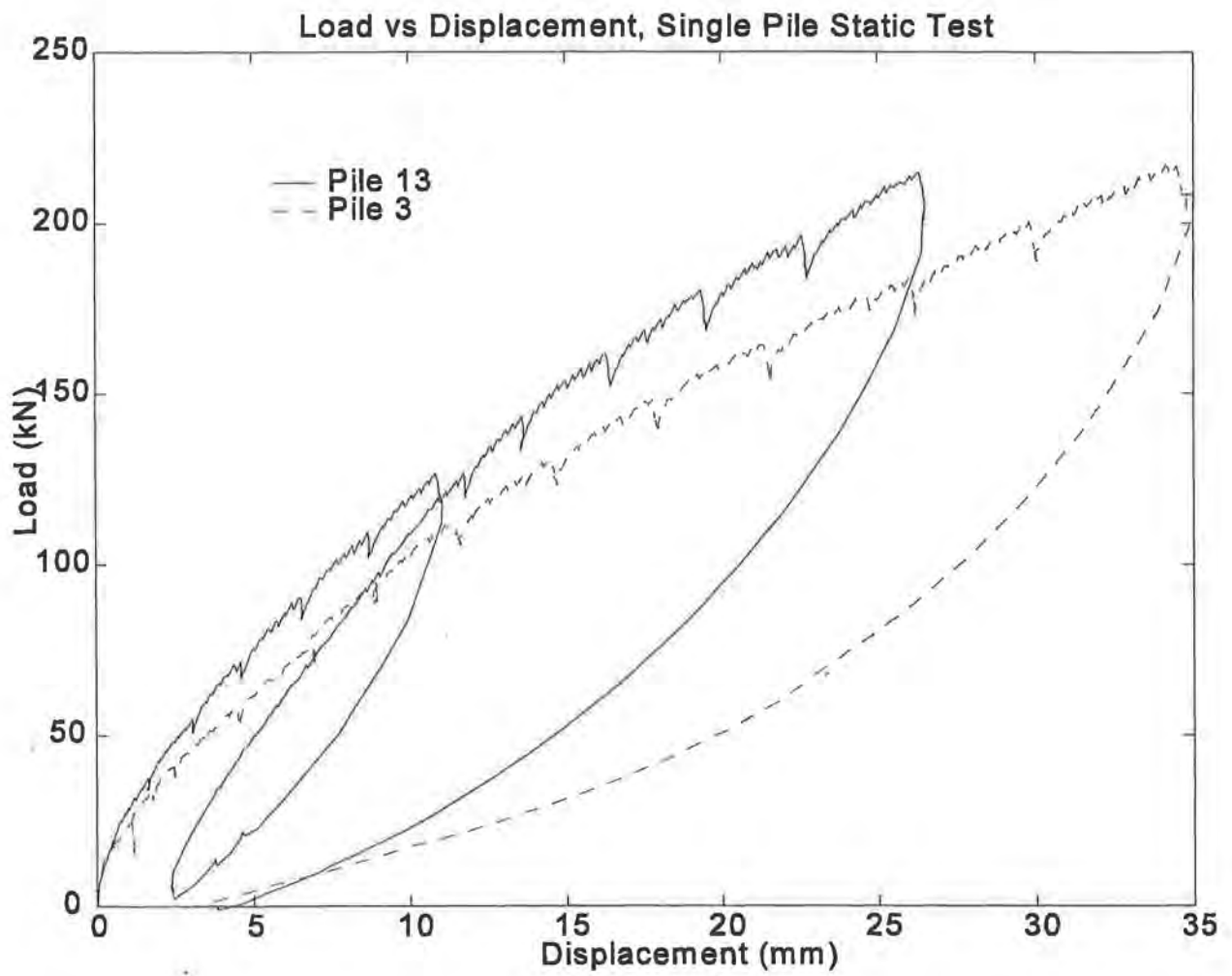


Figure E-65. Single Pile Setup Against 9-Pile Group (Pile 3)



*Figure E-66. Load vs. Displacement for Single Pile Static Tests*

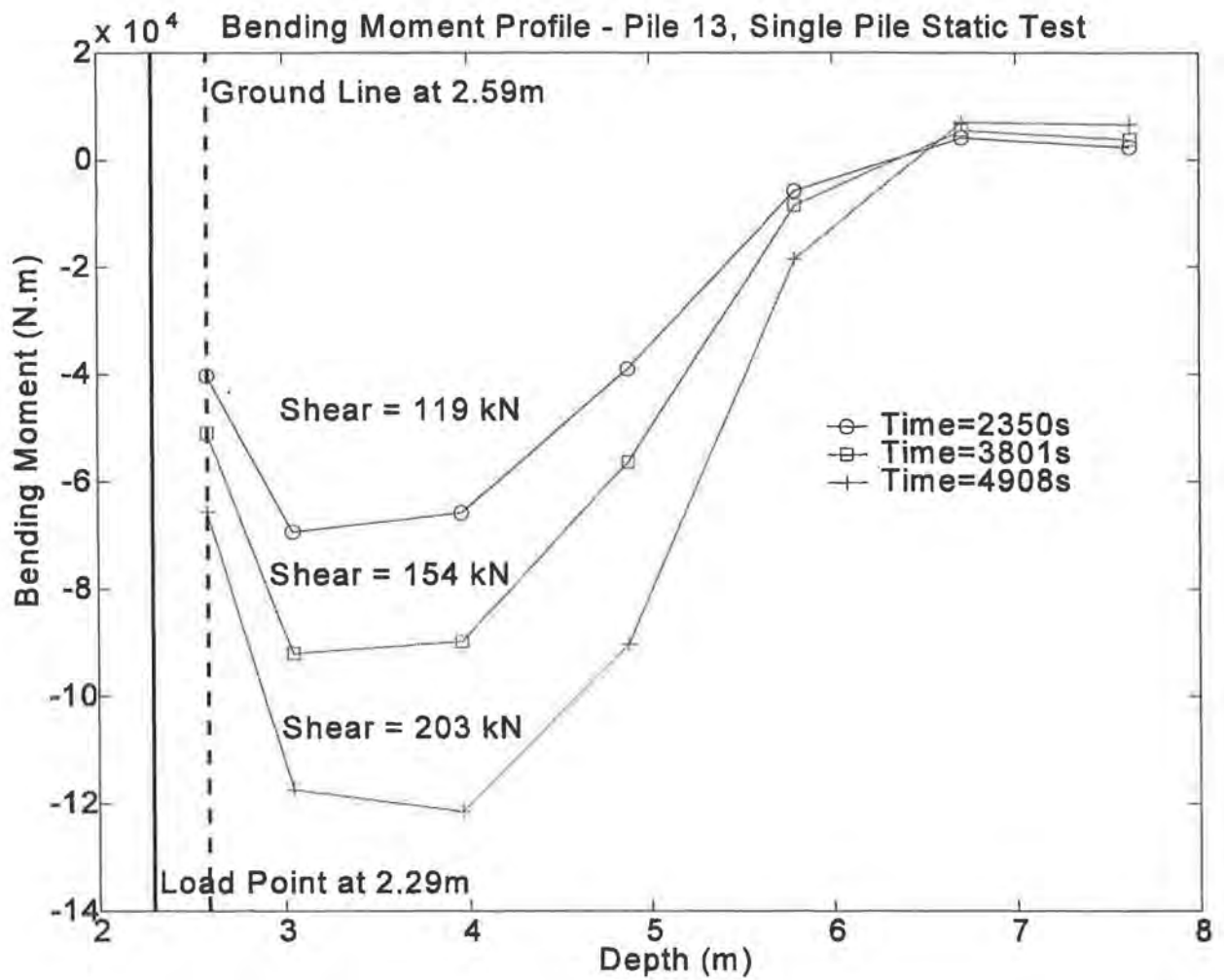
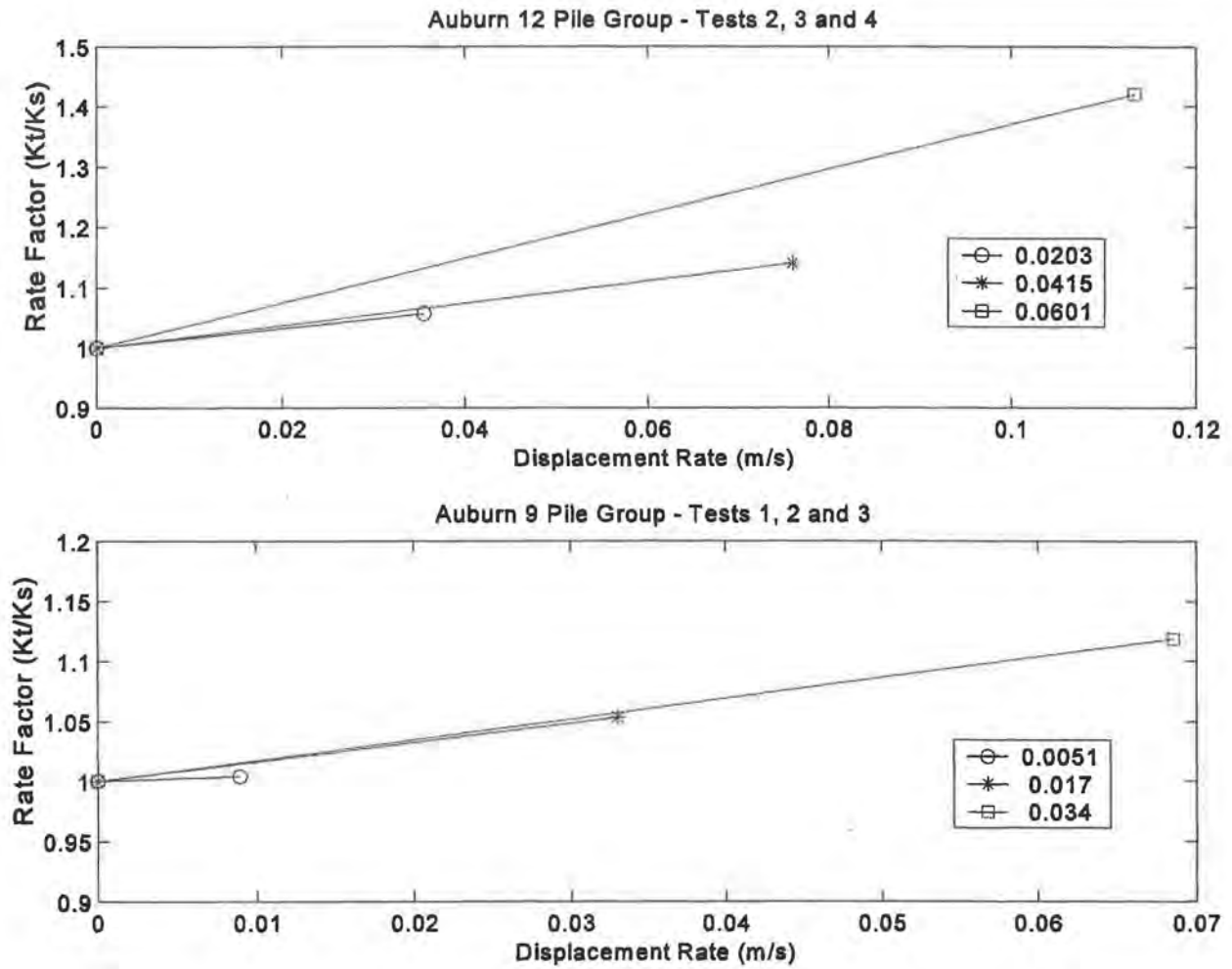
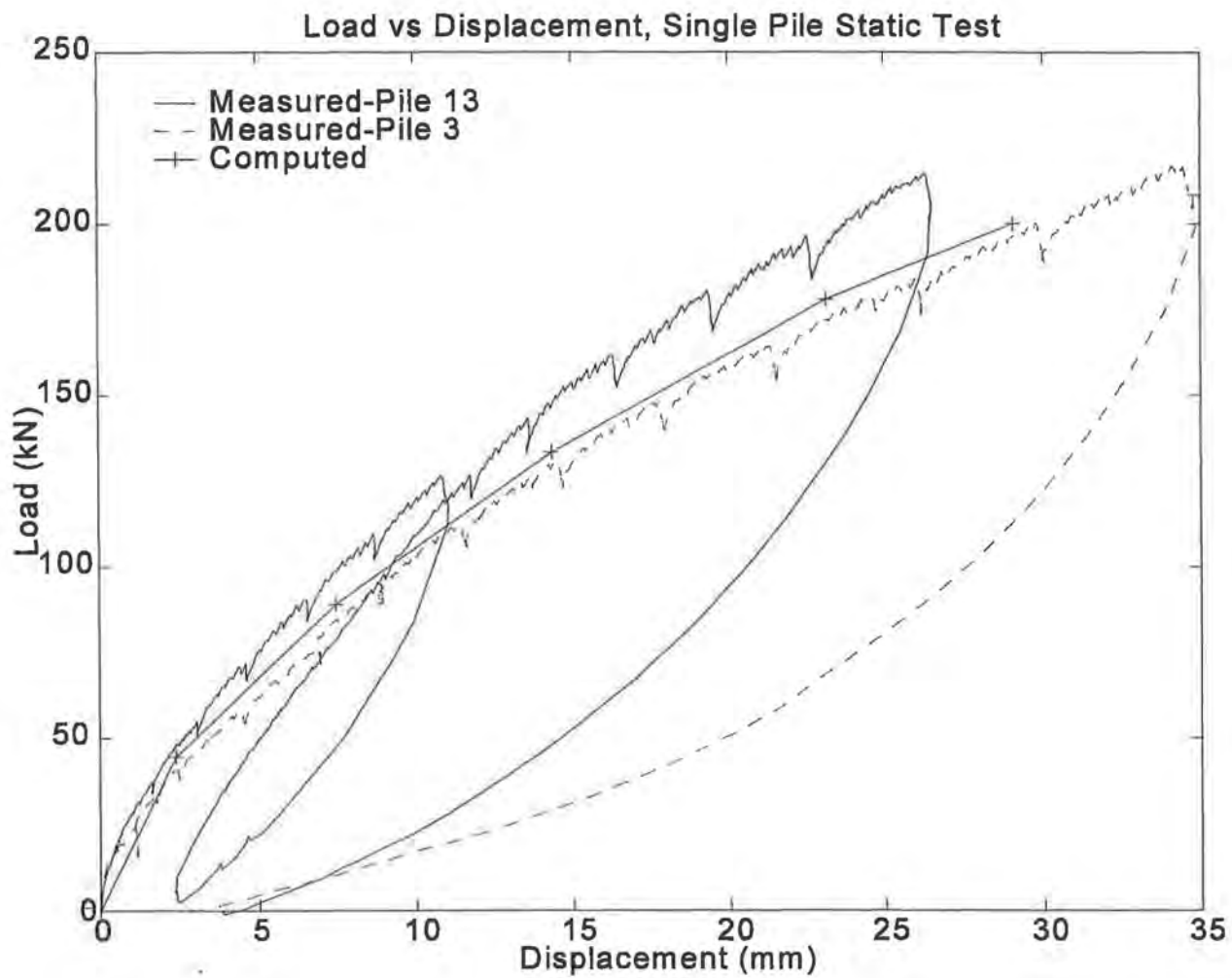


Figure E-67. Bending Moment Profile - Pile 13, Single Pile Static Test



*Figure E-68. Rate Effect Parameters, Spring Villa, Statnamic Tests*



*Figure E-69. Measured and Computed Static Head Load vs. Displacement, Single Piles*

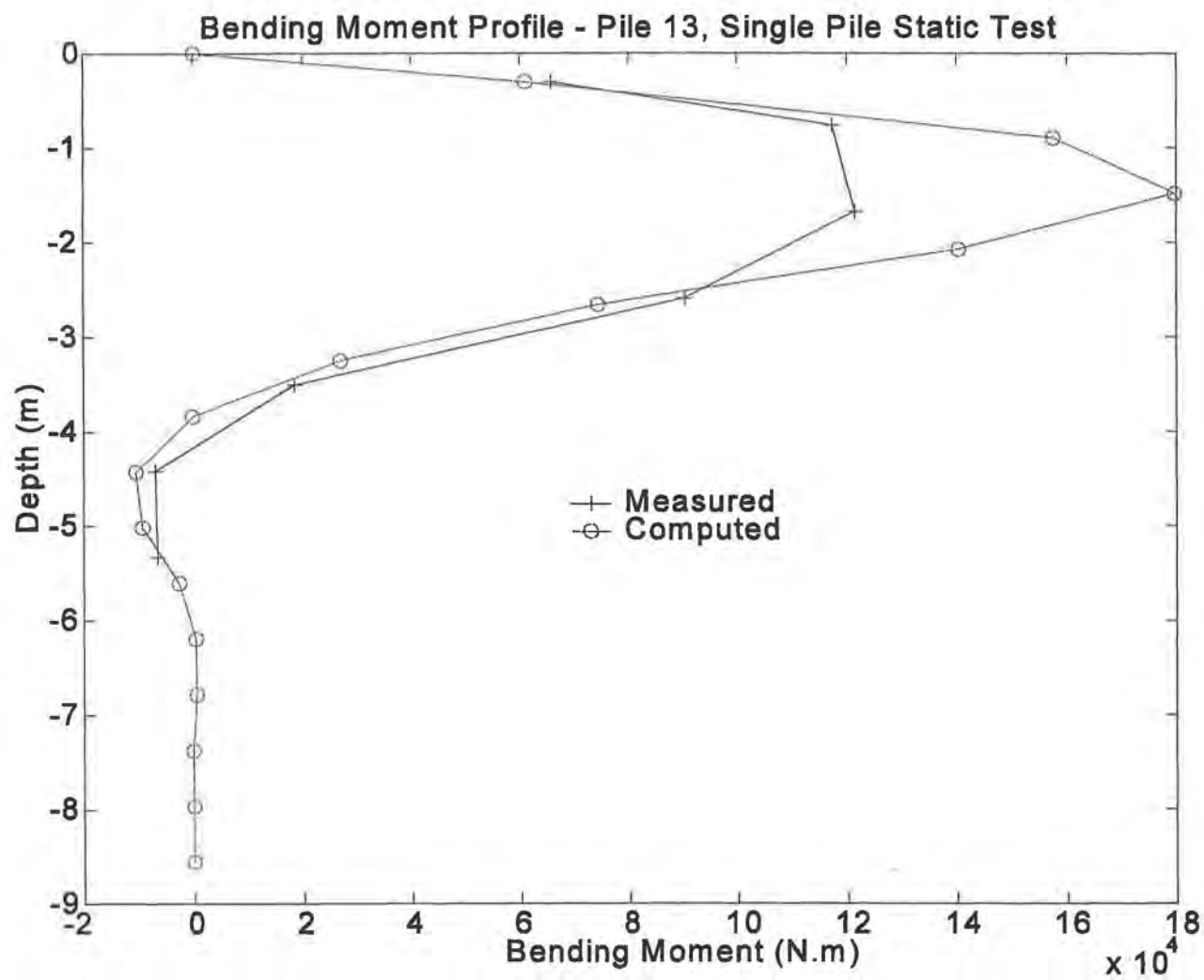
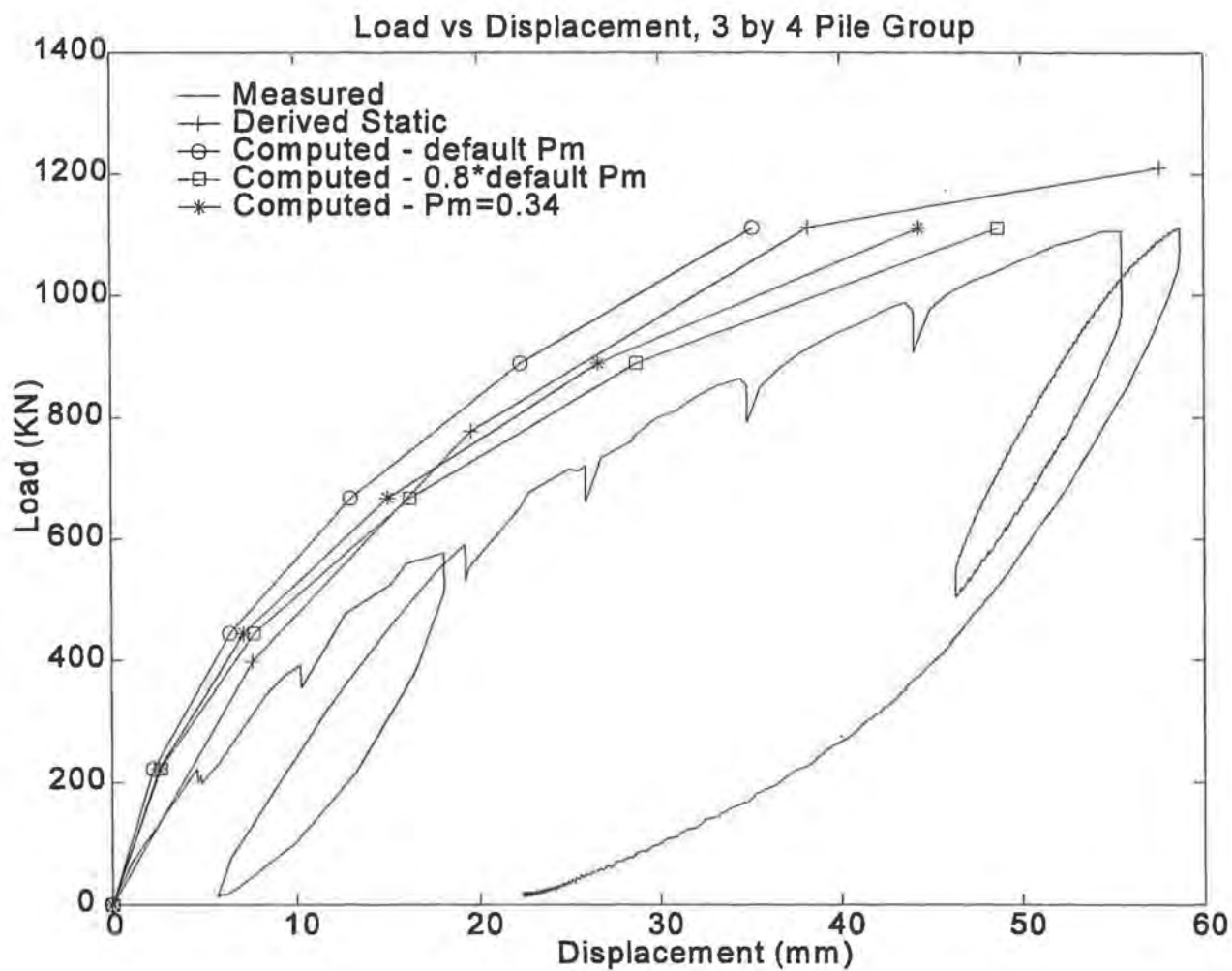


Figure E-70. Measured and Computed Bending Moment Profiles for Single Pile P13





*Figure E-71. Measured and Computed Static Pile-Head Response of 3 by 4 Group*

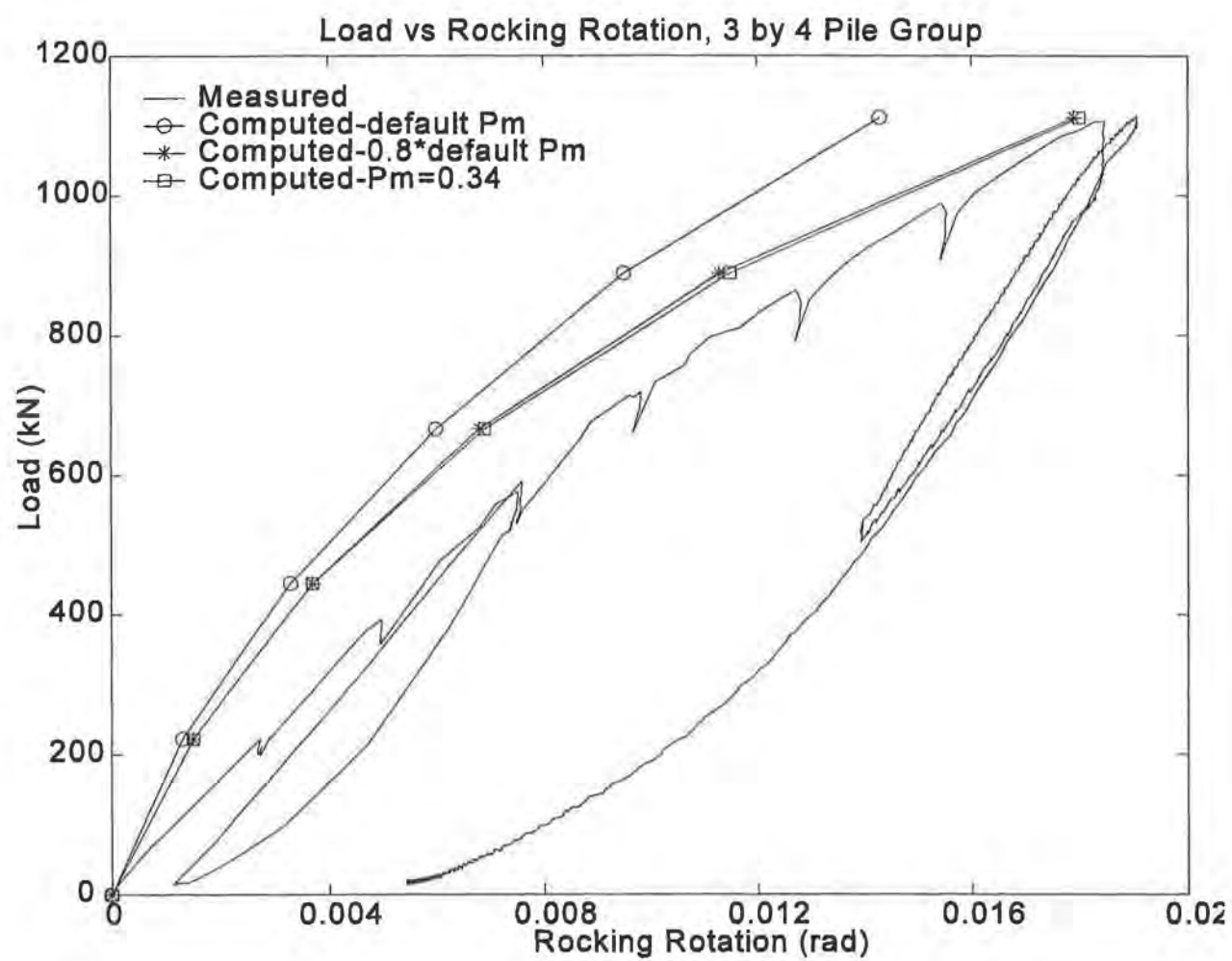


Figure E-72. Rocking Rotation vs. Horizontal Cap Load, Static Test, 3 by 4 Pile Group

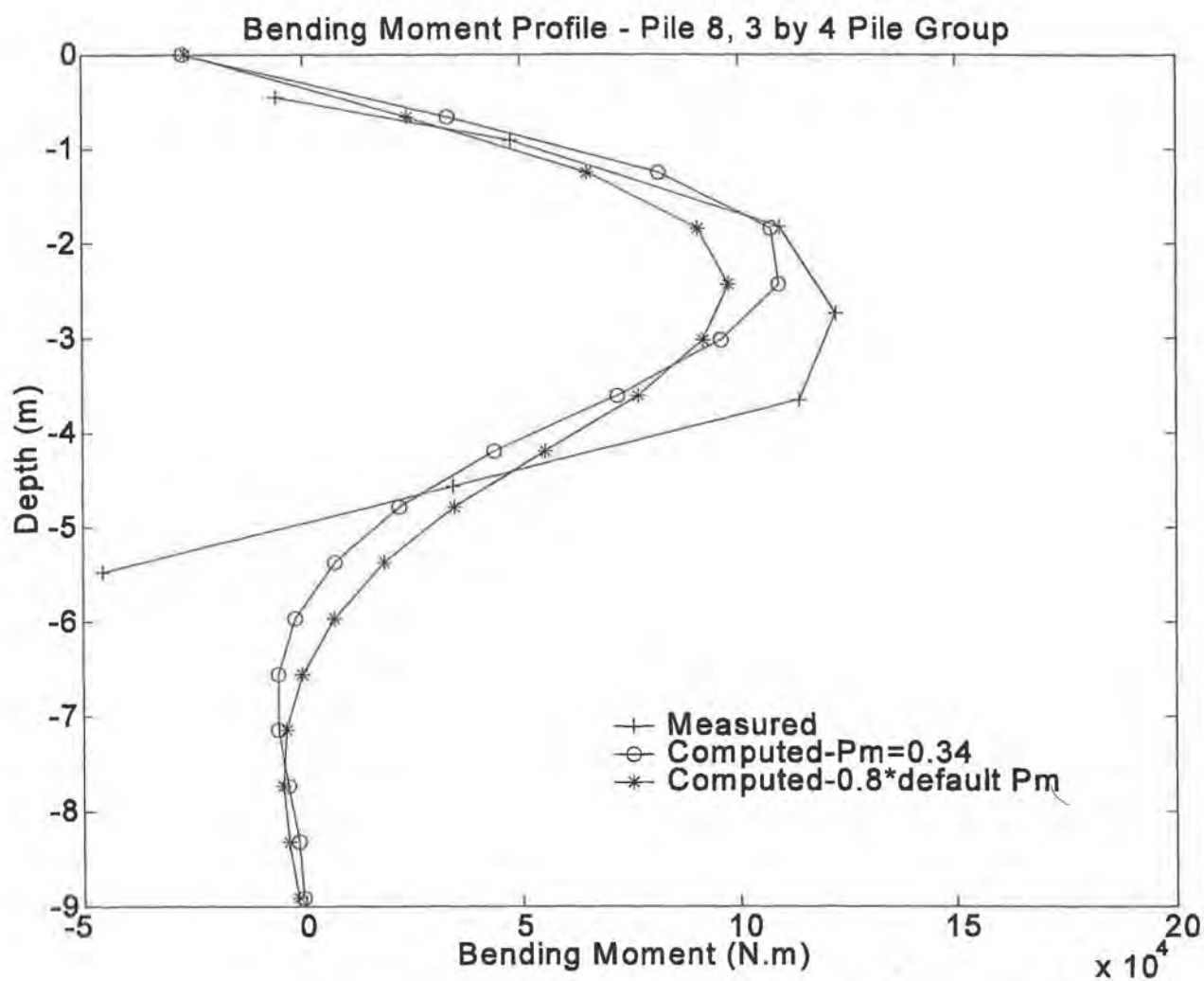


Figure E-73. Bending Moment Profile in Pile 8, Static Test on 3 by 4 Pile Group, Load = 1111 kN

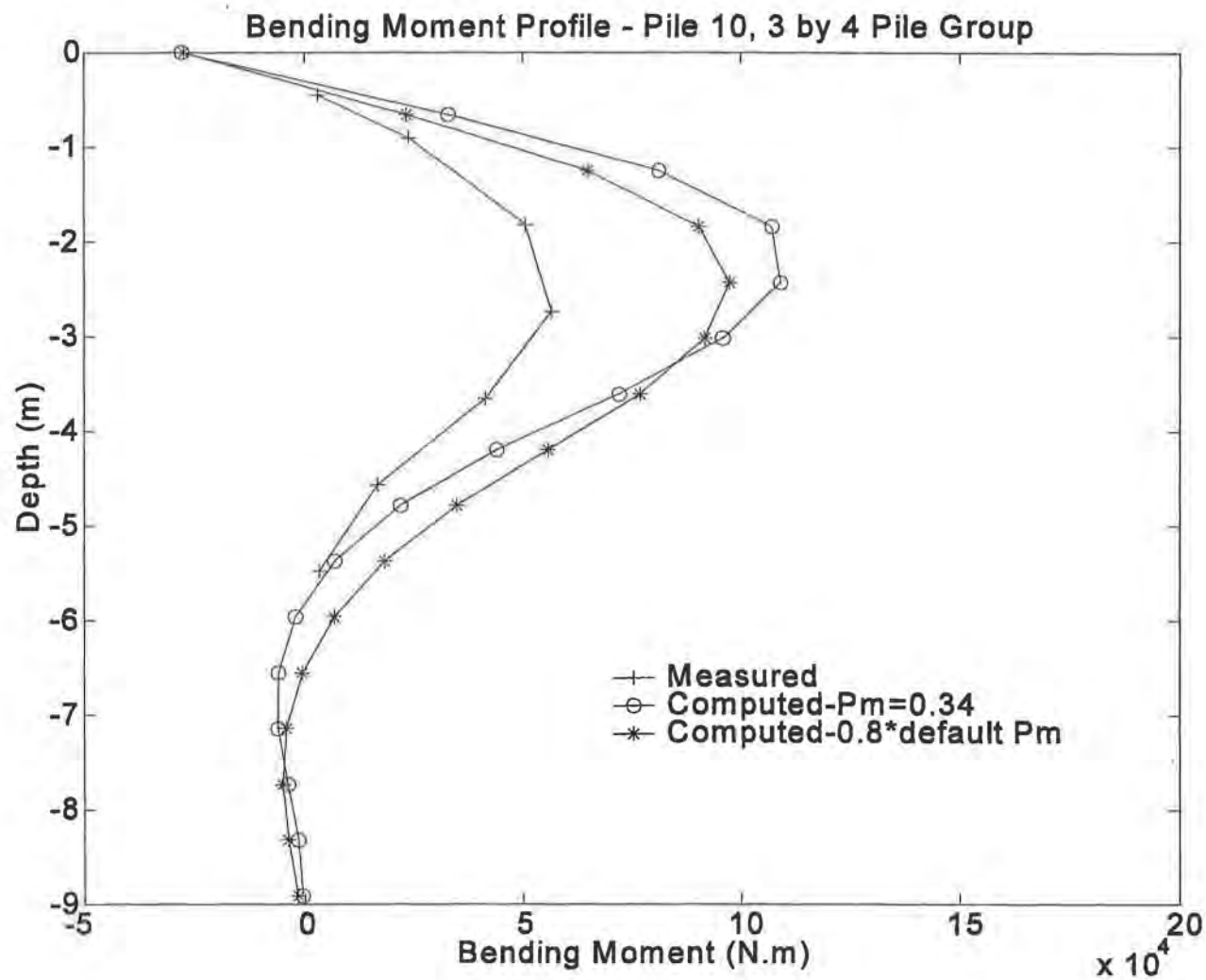
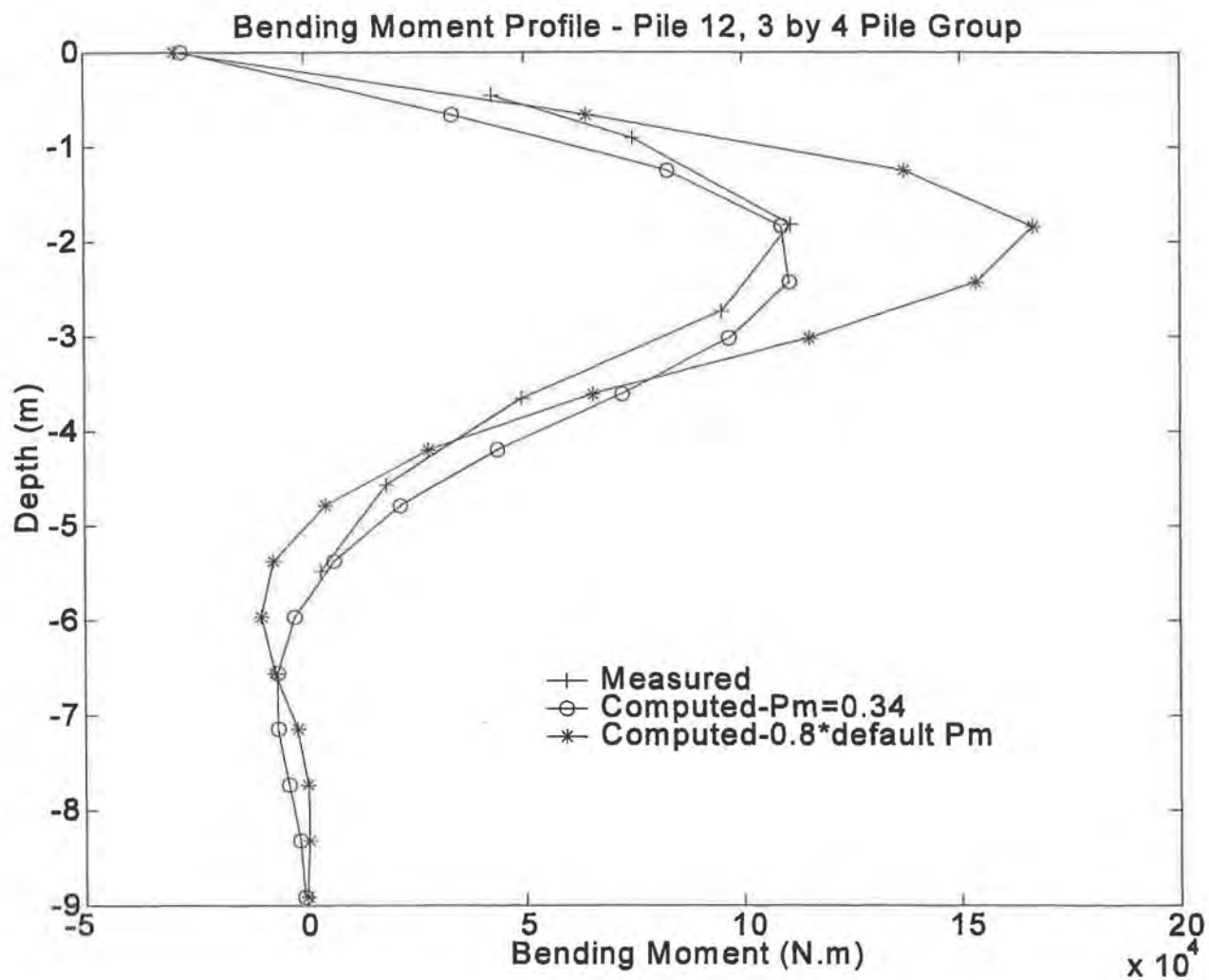


Figure E-74. Bending Moment Profile in Pile 10, Static Test on 3 by 4 Pile Group,  
Load = 1111 kN



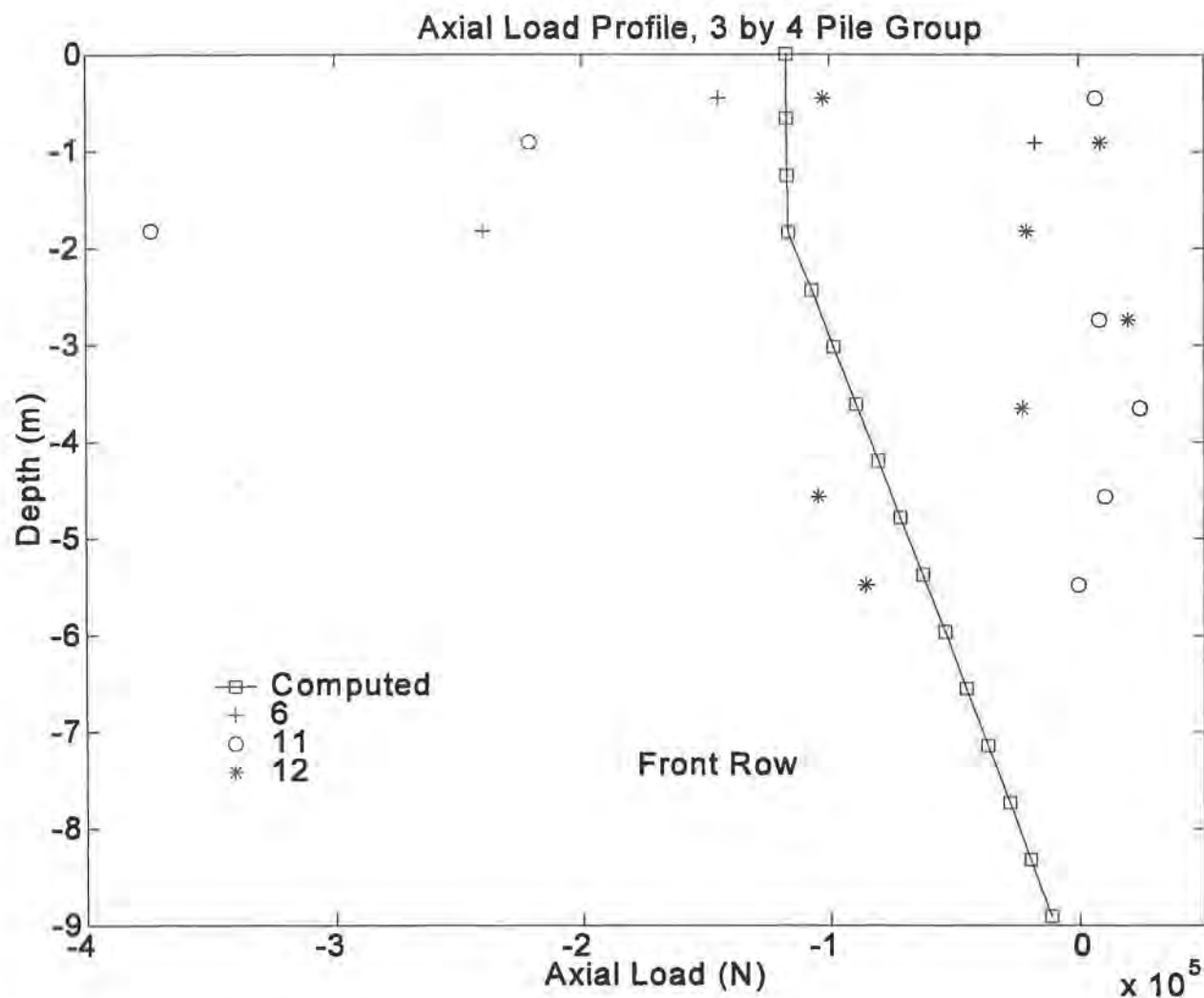
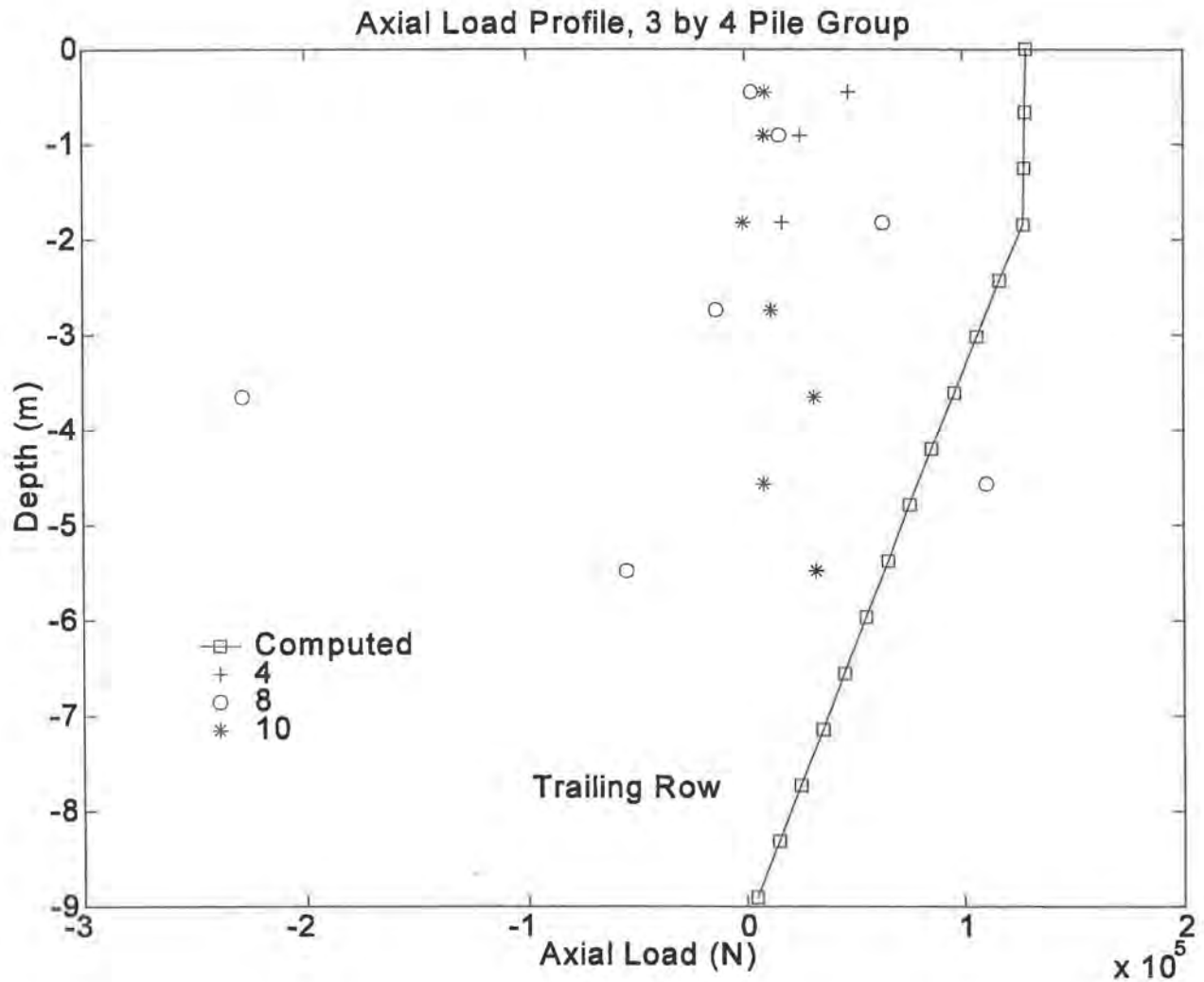


Figure E-75. Bending Moment Profile in Pile 12, Static Test on 3 by 4 Pile Group, Load = 1111 kN

Note: Negative loads are compressive.

Figure E-76. Axial Load vs. Depth in Leading-Row Piles in Static Test on 3 by 4 Pile Group, Horizontal Group Load = 1111 kN



*Note: Positive loads are tensile.*

*Figure E-77. Axial Load vs. Depth in Trailing-Row Piles in Static Test on 3 by 4 Pile Group, Horizontal Group Load = 1111 kN*

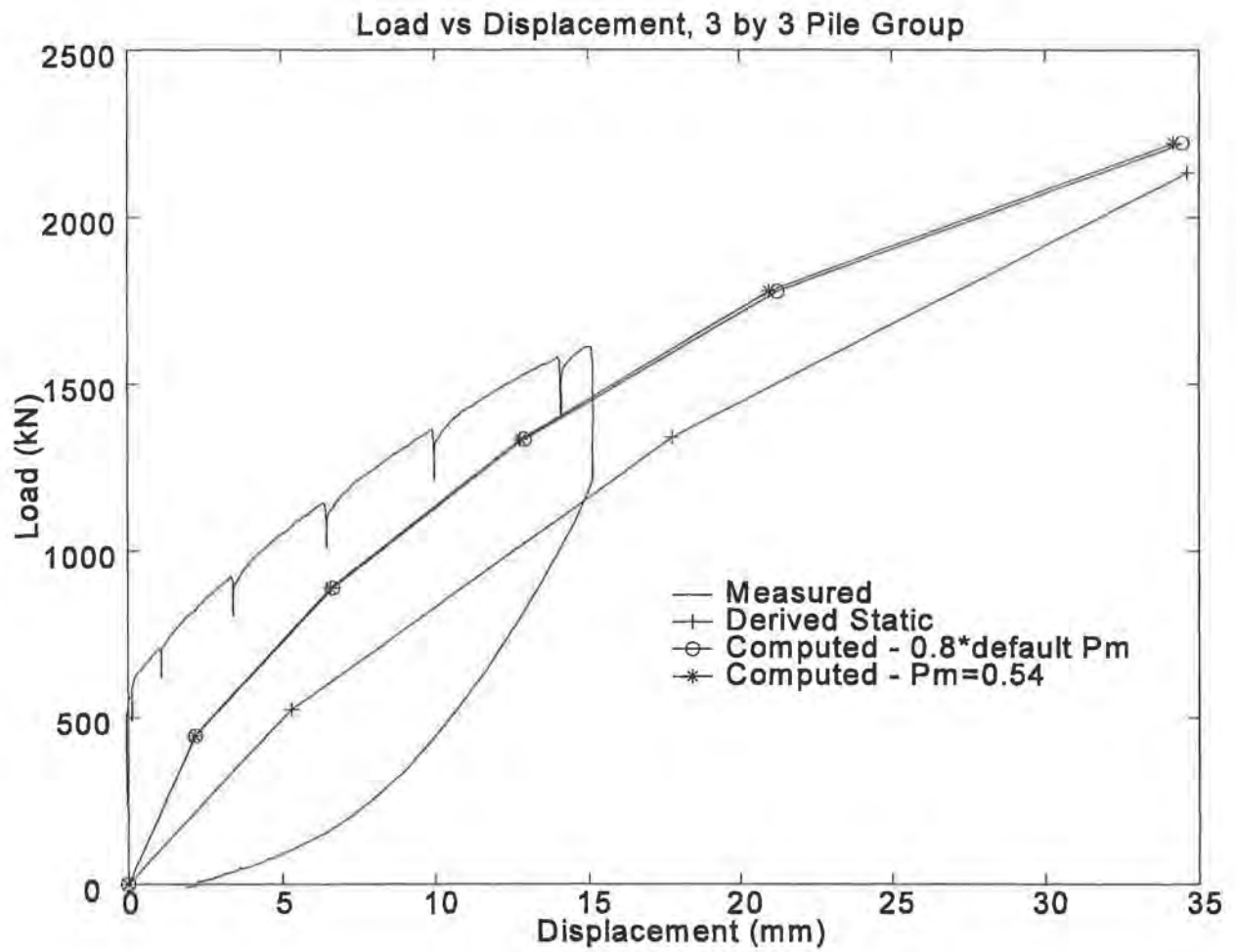
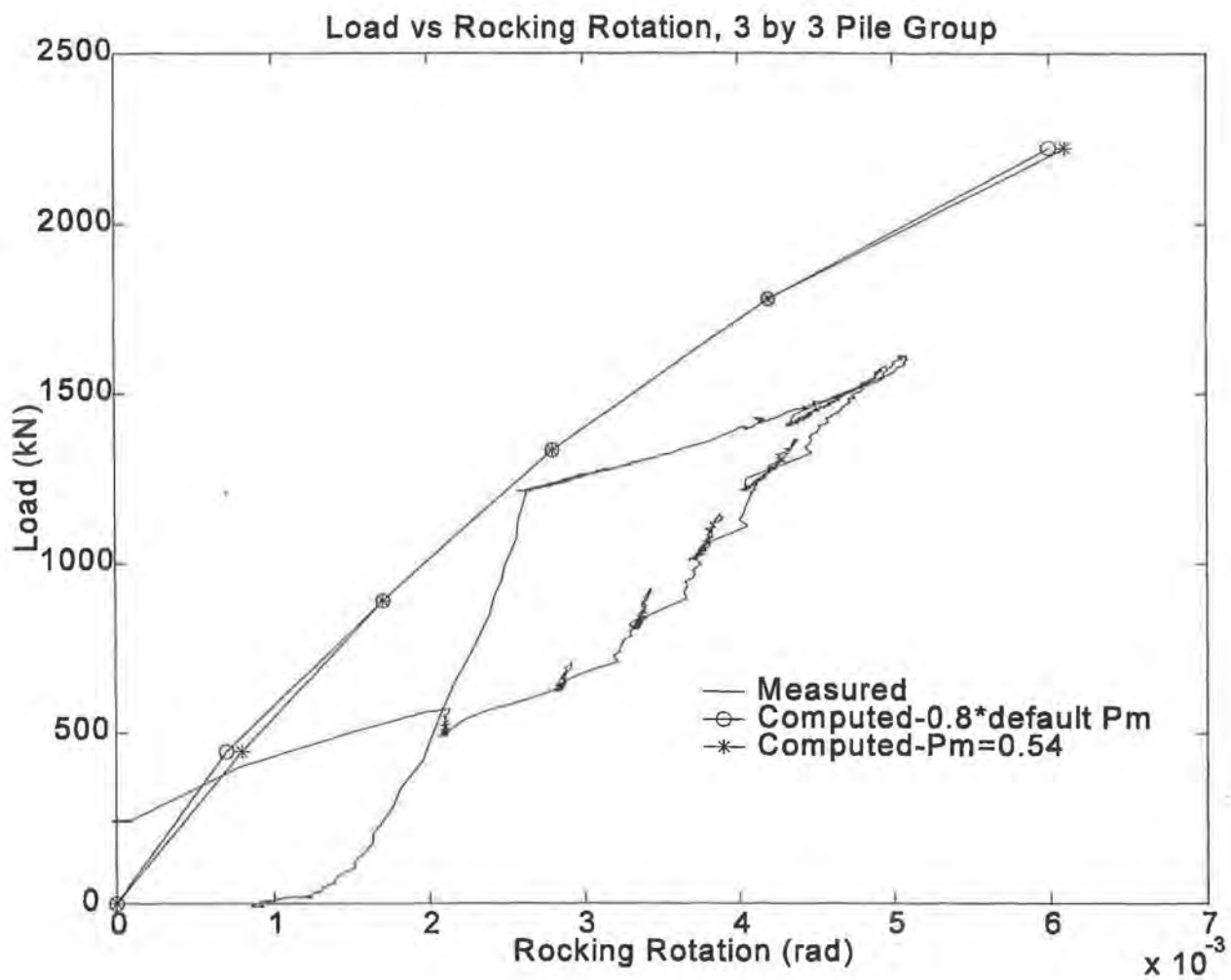


Figure E-78. Load vs. Displacement for Static Test on 3 by 3 Pile Group





*Figure E-79. Load vs. Rocking Rotation for Static Test on 3 by 3 Pile Group*

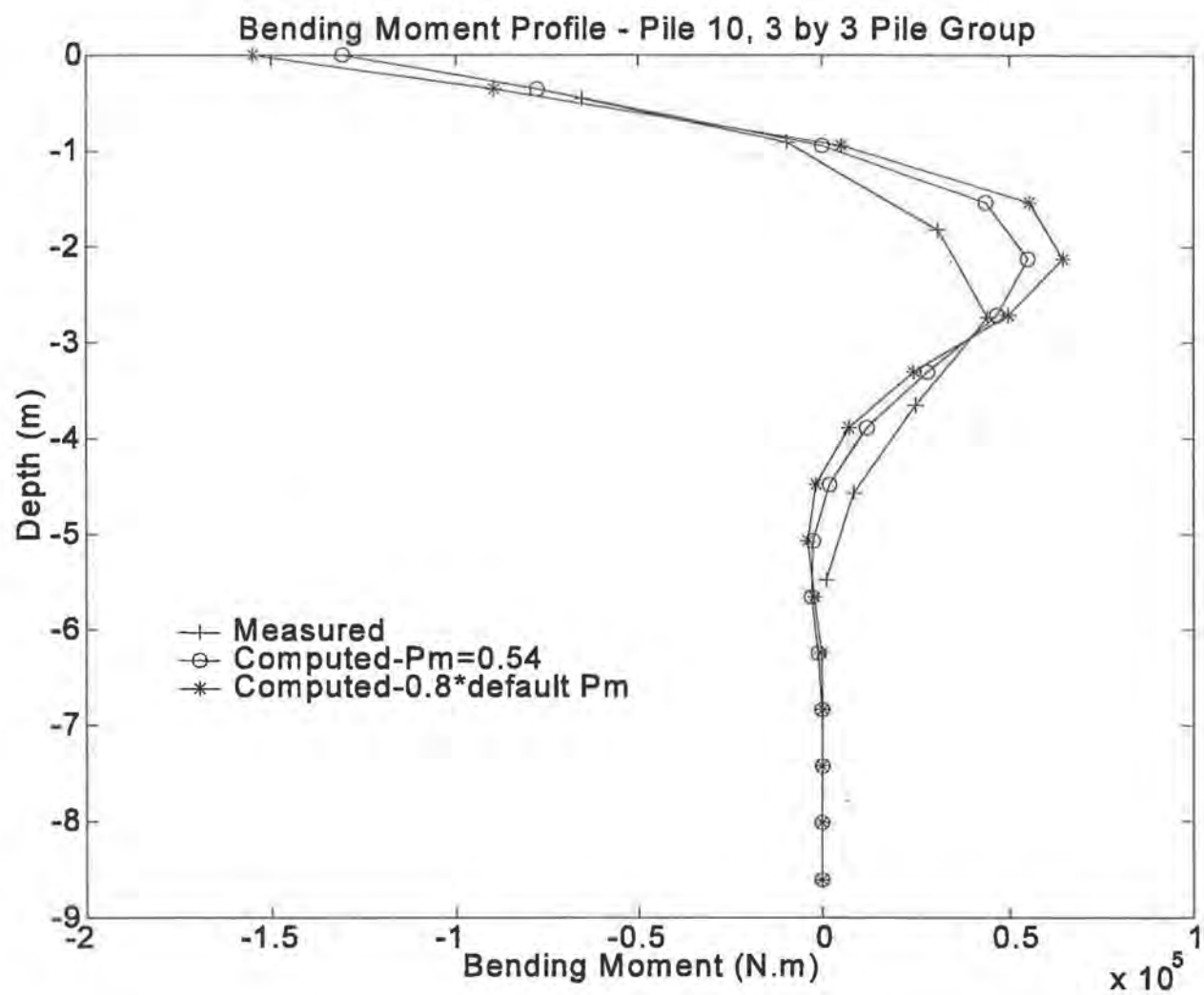
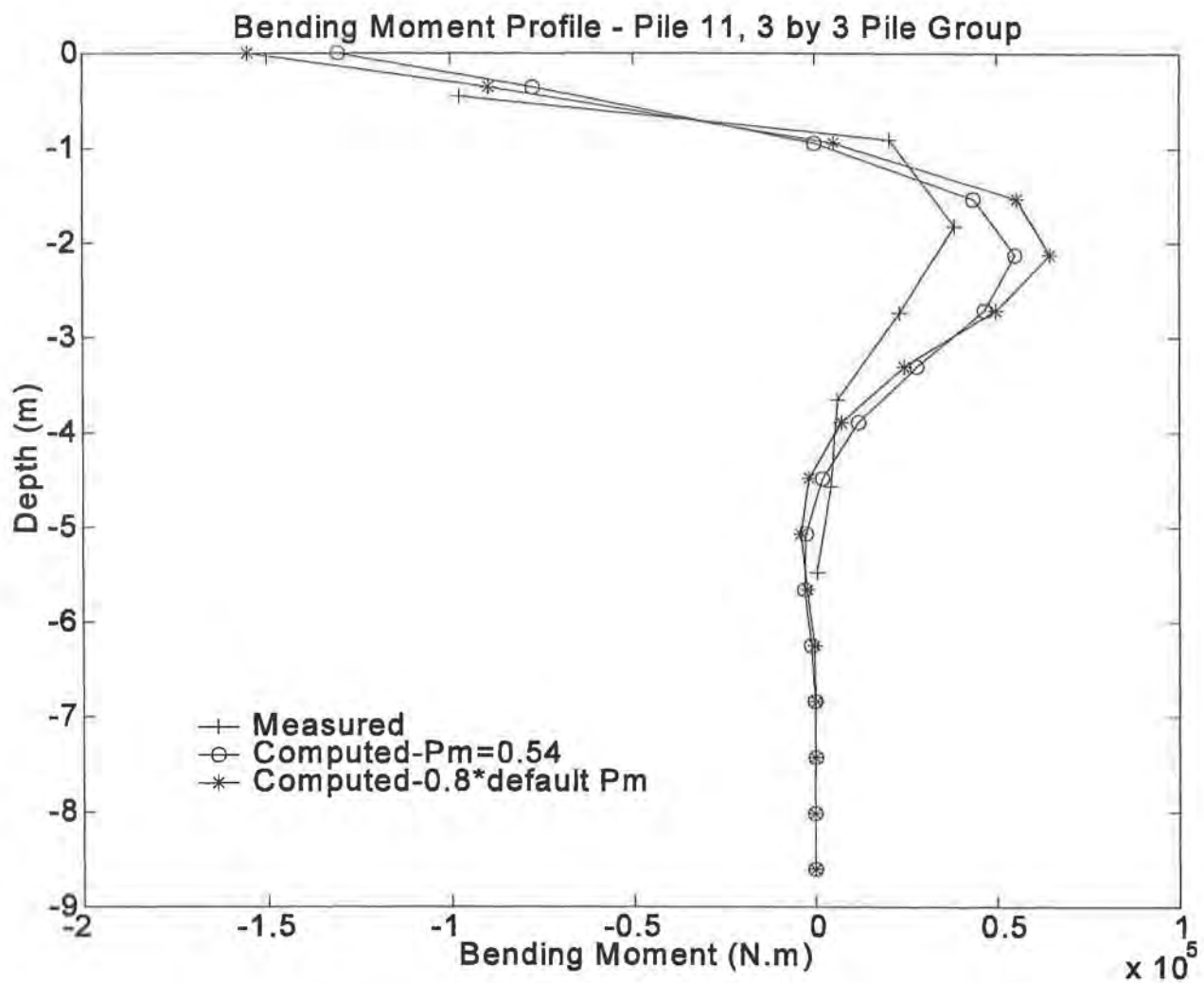


Figure E-80. Bending Moment Profile for Pile 10, Static Test, 3 by 3 Pile Group,  
Load = 1333 kN



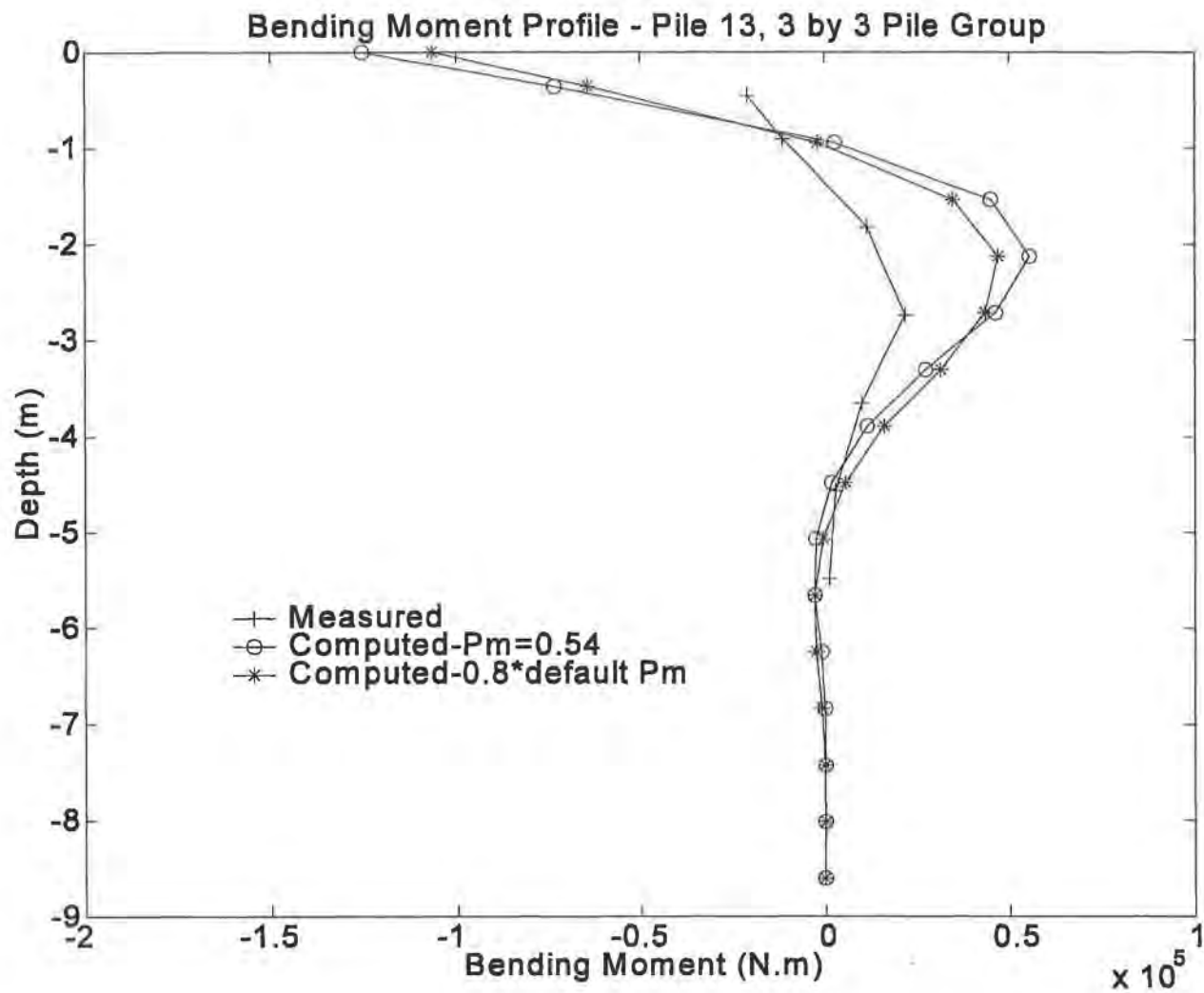


Figure E-81. Bending Moment Profile for Pile 11, Static Test, 3 by 3 Pile Group,  
Load = 1333 kN

Figure E-82. Bending Moment Profile for Pile 13, Static Test, 3 by 3 Pile Group,  
Load = 1333 kN

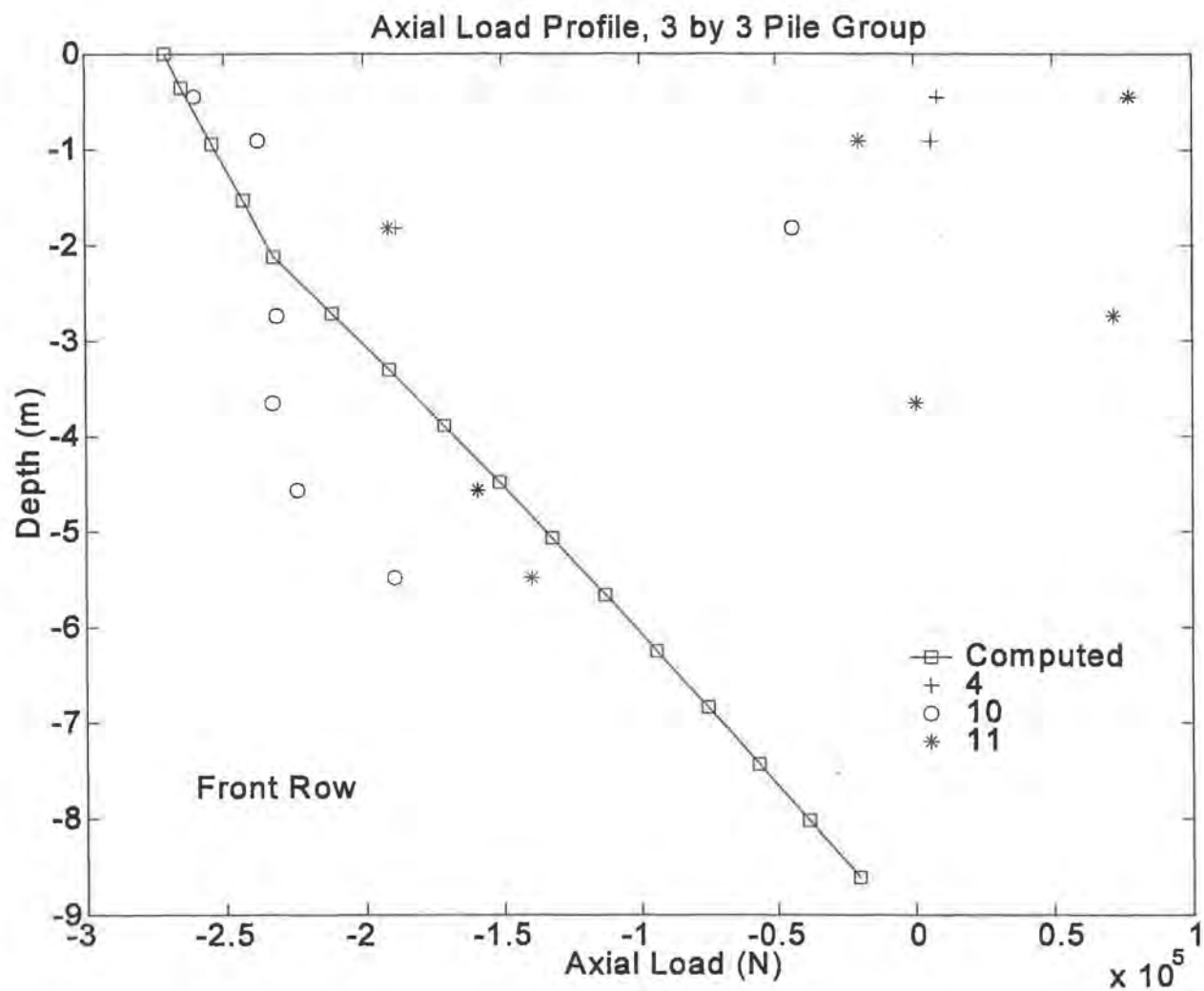


Figure E-83. Axial Load Profiles for Piles on Leading Row, Static Test on 3 by 3 Pile Group

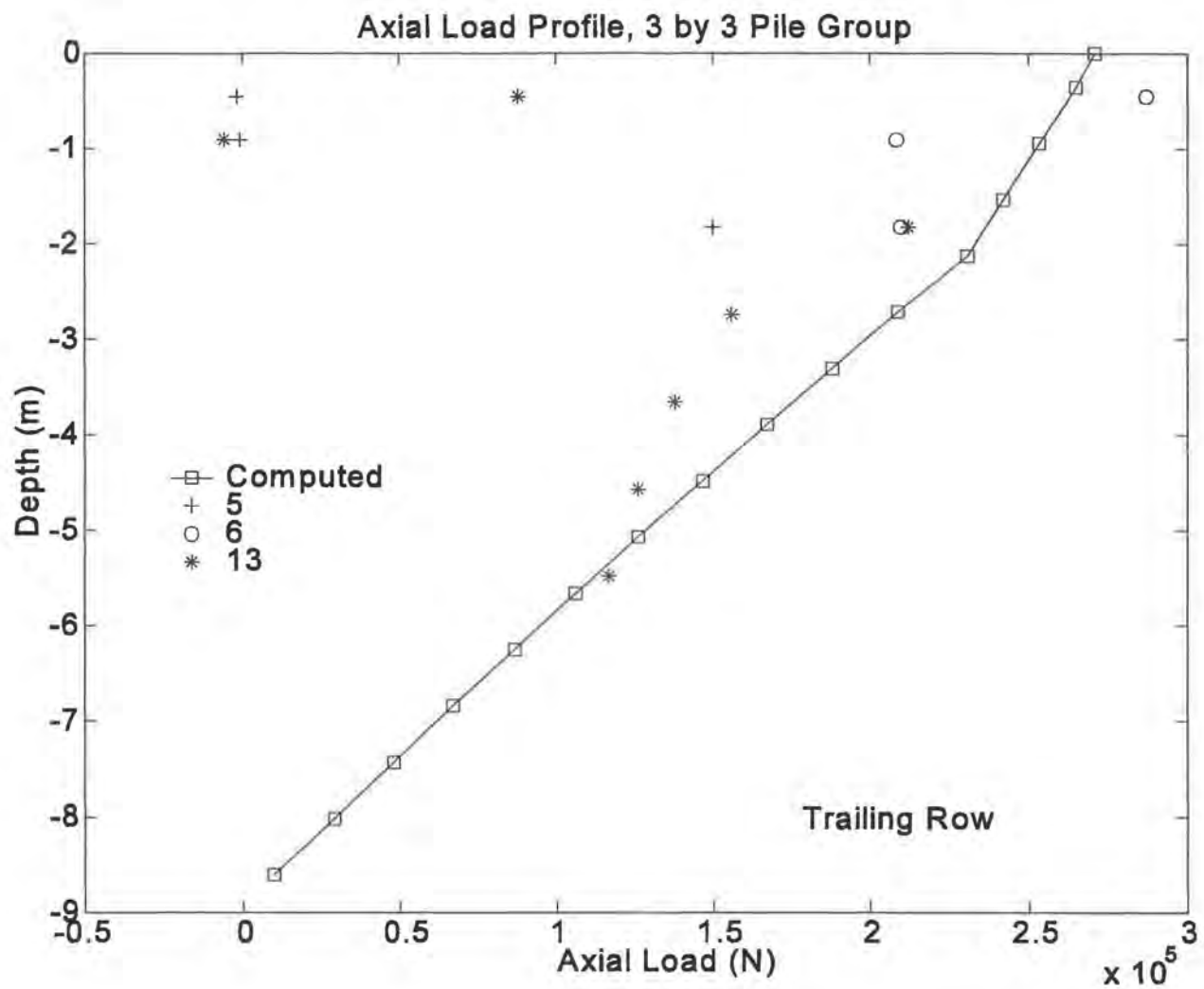


Figure E-84. Axial Load Profiles for Piles on Trailing Row, Static Test on 3 by 3 Pile Group

Displacement Response, 3 by 3 Pile Group Statnamic Test 1-4

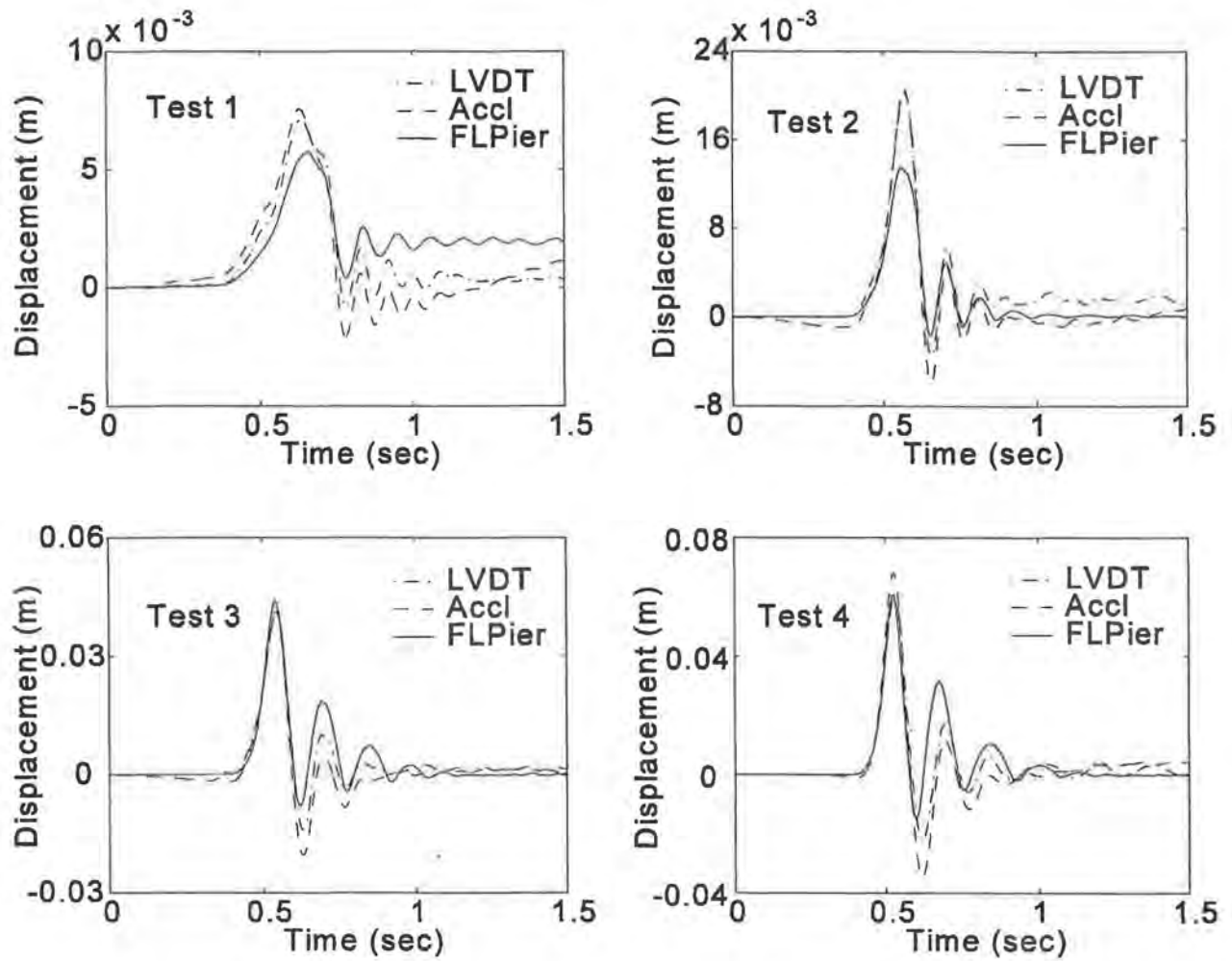


Figure E-85. Horizontal Response Time Histories for Statnamic Tests on 3 by 4 Pile Group

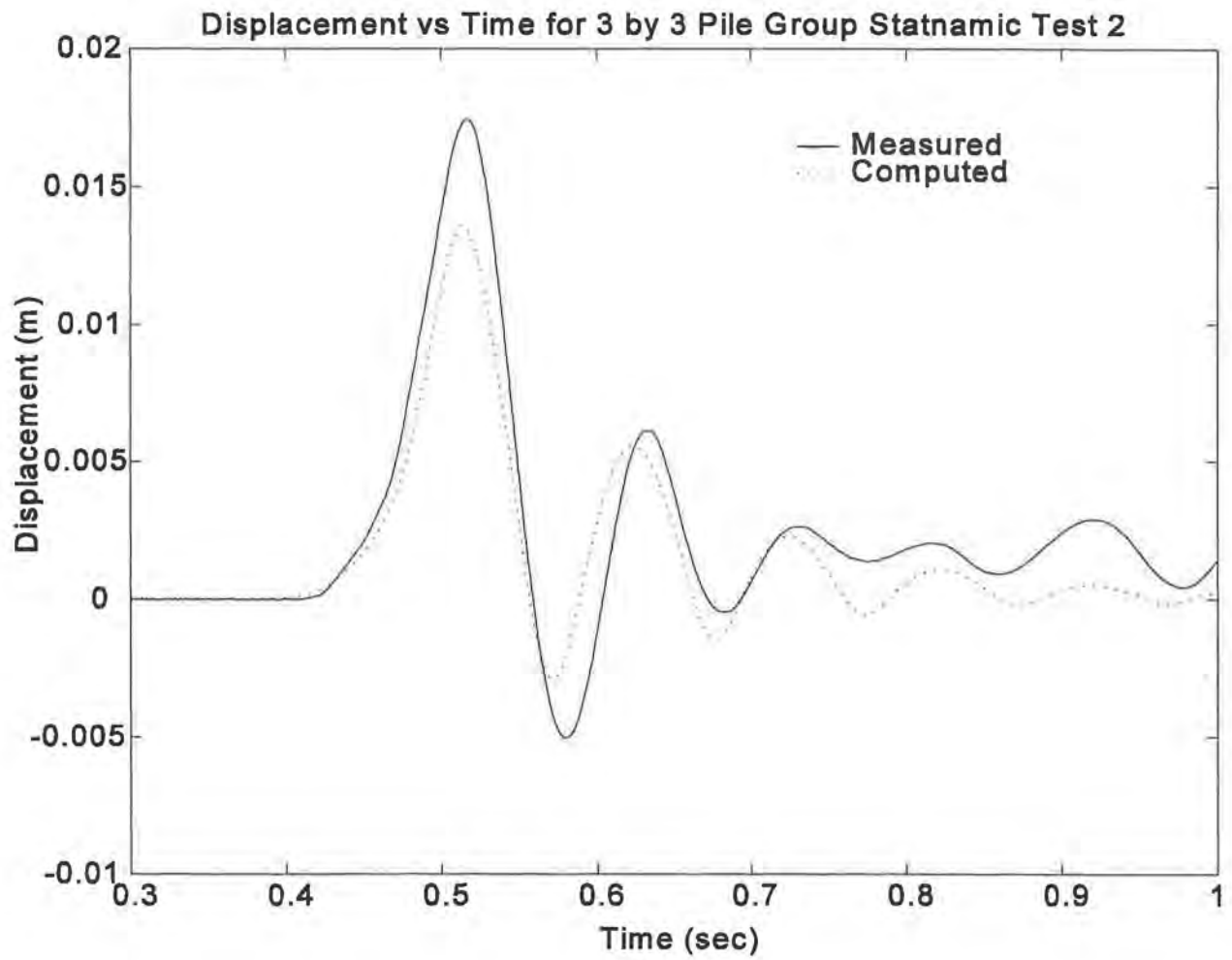
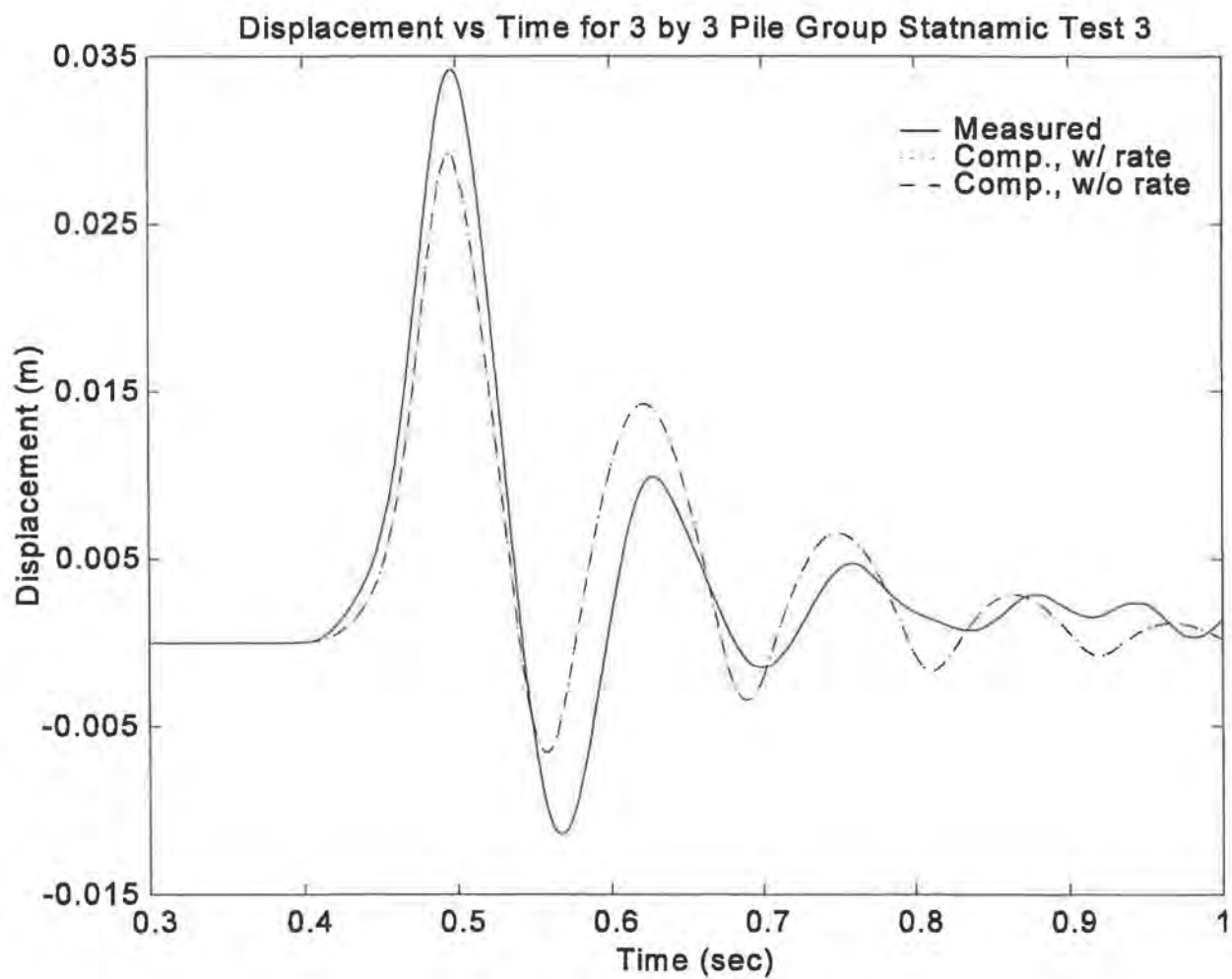


Figure E-86. Lateral Cap Displacement Time History for Statnamic Test 2 on 3 by 3 Pile Group





*Figure E-87. Lateral Cap Displacement Time History for Statnamic Test 3 on 3 by 3 Pile Group*

**APPENDIX F**  
**CALIBRATION OF STRAIN GAUGES AND CORRECTION**  
**OF RAW STRAIN DATA**

A detailed analysis of the strain data obtained at the Wilmington, North Carolina, test site required that the calibration factors for the strain gauges mounted on the NCHRP test piles be determined by direct measurement. It was thus necessary to calibrate the gauges before the piles were used at another test location and also to correct the strain data already recorded. The piles were shipped to the structural testing laboratory at Auburn University, where each pile was tested individually following the procedure described in the following section.

**TEST PROCEDURE**

The objective was to measure the strains indicated by the gauges under a set of known loading conditions, then compare the measured strains to the theoretical strains, and hence compute the calibration factor for each gauge individually. It was decided to load each pile under simply supported conditions with a concentrated load at its center as shown in Figure F-1. Each support reaction is known (half of the total applied load **P**) and thus the bending moments can be computed exactly at each gauge location. In addition, the data acquisition system can balance out the gauges prior to the application of the load **P**, which effectively removes the effects of bending due to self-weight (this can be done because the stresses and strains in the pile remain linear for the range

of loads applied). Strain readings can be obtained at changing values of  $P$ , and the results plotted in the form of measured strains vs. theoretical strains on a gauge-by-gauge basis. The step by step procedure adopted was as follows:

- Supports were erected at points A and B exactly 10.973 meters (36 feet) apart. Each support consisted of a pair of steel tension rods tied down to the floor and placed 0.61 meters (2 feet) apart, plus a pair of wooden 4x4 sections placed on the ground between the 2 rods. The pile was moved into place using the overhead crane and placed on the wooden blocks such that the overlap at each end (between the support point and the corresponding pile edge) was the same. The pile was then turned around so that the strain gauges were aligned along two lines exactly along the bottom and the top of the pile (maximum distance from the plane of bending). The strain gauges were then hooked up to the Megadac data acquisition system and balanced (zeroed out), which removed the effects of strain caused by bending due to self weight.
- Hollow steel box sections approximately 3 (in.) x 3 (in.) in cross section and a little over 0.61 meters (2 feet) in length with holes drilled through opposite faces at each end were then slipped down through the tension rods and clamped down in contact with the piles so as to provide support against uplift. The overhead crane was positioned directly over the center of the span 5.486 meters (18 feet) from each support, and the end of the cable from the crane was attached to a reinforced band of fabric 101.6 mm (4 inches) wide wound around the pile. A load cell was placed between the end of the crane cable and the ends of the cloth band to measure the tensile force exerted by the crane.

- A series of vertical loads was then applied to the pile by pulling upward the crane in increments of 4.448 kN (1000 lbs) up to a maximum of 35.584 kN (8000 lbs). The load-unload cycle was carried out twice in this manner; the piles were then rotated 180° and the gauges balanced again, then tested with two more cycles of load. This ensured that the response of each gauge was measured under both tensile and compressive conditions. Sixty data sets were recorded for each pile and the data were exported to Matlab format for analysis.

## DATA REDUCTION AND ANALYSIS

A program using the Matlab code was then used to reduce the data. Input to the program consisted of the values recorded by the load cell (load vector **P**) and the 60 raw strain data files exported from the Megadac. The program was used to compute the theoretical strain for each strain gauge and plot it as a function of the measured strain at each load point, positive and negative, of the load vector **P**. This produced a graph for every gauge in every pile, for a total of 126 gauges. The data were further analyzed using a least squares based fitting technique. Three possible linear fits to the data were computed and plotted on the same graph (measured vs. theoretical strain):

- a fit based on the points when the gauge was subjected to compressive loading
- a fit based on the points when the gauge was subjected to tensile loading, and
- a fit based on all the points on the graph, both tensile and compressive. The calibration graph for each gauge is available upon request.

The key to reading the graphs is as follows:

- *Actual*  
refers to experimentally observed data points (60 total)
- *All Data*  
refers to a fit based on all data points
- *Side 1* - fit based on  
Gauges (1-3) or (1-7): Positive/compressive data points  
Gauges (4-6) or (8-14): Negative/tensile data points
- *Side 2* - fit based on  
Gauges (1-3) or (1-7): Negative/tensile data points  
Gauges (4-6) or (8-14): Positive/compressive data points

The linear regression analysis provided 2 constants for each best fit line of the form:

$$E_a = E_m \times m + c ,$$

where

$E_a$  = actual/theoretical strain,

$E_m$  = measured strain,

$m$  = slope of the best fit line, and

$c$  = intercept of the best fit line.

The intercept  $c$  for the most part is very small, is probably a result of measurement error, and can thus be neglected for practical purposes. In this case, the slope of the line  $m$  becomes the correction factor by which the measured strain must be multiplied to arrive at the true strain. The values of correction factor  $m$  for each gauge are tabulated on the following pages.

PILE 1			
Gauge Number	Positive	Negative	All
1	1.6407	1.5046	1.5676
2	1.4628	1.5157	1.4826
3	1.7781	1.5868	1.6653
4	1.9082	1.9292	1.9058
5	1.7656	1.4397	1.5578
6	1.5116	1.3894	1.4309

PILE 2			
Gauge Number	Positive	Negative	All
1	1.8521	1.8968	1.8574
2	1.7642	1.6942	1.7199
3	1.6238	1.6102	1.6332
4	1.9909	2.1374	2.0719
5	1.2047	1.1834	1.1927
6	1.2287	1.2036	1.2347

PILE 3			
Gauge Number	Positive	Negative	All
1	1.8489	1.8302	1.8358
2		Does Not Work	
3	1.6146	1.5602	1.5631
4	2.0271	2.0283	2.0222
5	1.4381	1.3980	1.4119
6	2.2358	2.3388	2.3716

PILE 4			
Gauge Number	Positive	Negative	All
1	2.2103	2.3003	2.2415
2	1.8812	1.8776	1.8672
3	2.1048	1.9935	2.0492
4	2.2551	2.2709	2.2692
5	1.7139	1.7141	1.7179
6	2.1476	2.1576	2.1891

PILE 5			
Gauge Number	Positive	Negative	All
1	1.8654	1.8844	1.8469
2	1.8336	1.8157	1.8049
3	1.9749	1.9970	1.9827
4	1.8644	1.8526	1.8499
5	1.8769	1.7941	1.8312
6	1.7593	1.7273	1.7418

PILE 6			
Gauge Number	Positive	Negative	All
1	1.9959	2.0834	1.9942
2	1.8302	1.8635	1.8122
3	1.5683	1.6217	1.5679
4	1.7950	1.7280	1.7498
5	1.9170	1.8009	1.8510
6	1.8801	1.7611	1.8176

PILE 7			
Gauge Number	Positive	Negative	All
1	1.8390	1.5864	1.6804
2	1.5035	1.4549	1.4546
3	1.8493	1.8464	1.9330
4	1.8253	1.8215	1.8089
5	1.8963	1.9381	1.9081
6	1.8696	1.9206	1.8940

PILE 8			
Gauge Number	Positive	Negative	All
1	1.7310	1.7600	1.7470
2	1.2950	1.2872	1.2871
3	1.4448	1.3923	1.4220
4	1.8527	1.8394	1.8481
5	1.2538	1.2286	1.2461
6	1.6954	1.5881	1.6434
7	1.7059	1.6897	1.7024
8	1.8617	1.8736	1.8689
9	1.7265	1.7048	1.7173
10	1.7718	1.7710	1.7752
11	1.8690	1.8392	1.8661
12	1.6649	1.5948	1.6395
13	1.7572	1.7368	1.7594
14	1.5413	1.4237	1.4739

PILE 9			
Gauge Number	Positive	Negative	All
1	1.8656	1.9137	1.8766
2	1.8542	1.9055	1.8703
3	1.5524	1.4304	1.4692
4	1.8075	1.8294	1.8147
5	1.8414	1.8888	1.8661
6	1.7429	1.6741	1.7201
7	1.7799	1.7624	1.7693
8	1.8945	1.8794	1.9238
9	1.6244	1.4248	1.5468
10	-1.5272	-1.6693	-1.6305
11	1.7135	1.6882	1.7186
12	1.8295	1.7478	1.8109
13	1.8401	1.8132	1.8550
14	1.7348	1.7493	1.7648

PILE 10			
Gauge Number	Positive	Negative	All
1	1.9325	1.8925	1.9042
2	1.8029	1.8291	1.8067
3	1.5215	1.4939	1.5092
4	1.8609	1.8096	1.8266
5	1.9908	2.0925	2.0292
6	1.8544	1.7112	1.7858
7	1.3033	1.3408	1.3145
8	1.4507	1.4703	1.4652
9	-1.7978	-1.8908	-1.8488
10	1.8531	1.7644	1.8141
11	2.0406	2.0630	2.0577
12	1.4441	1.3871	1.4065
13	1.6490	1.4717	1.5690
14	1.6430	1.6171	1.6364



Gauge Number	PILE 11		
	Positive	Negative	All
1	1.9403	1.9123	1.9488
2	1.1853	1.1188	1.1773
3	1.2454	1.1858	1.2278
4	1.6685	1.7179	1.7160
5	1.4683	1.3261	1.4169
6	1.4033	1.3151	1.3657
7	1.6599	1.6241	1.6745
8	1.7958	1.8228	1.8410
9	1.2960	1.2581	1.2962
10	1.5750	1.6202	1.6362
11	1.6702	1.7696	1.7528
12	1.3090	1.2652	1.3027
13	1.5622	1.5418	1.5812
14	1.6301	1.5039	1.5892

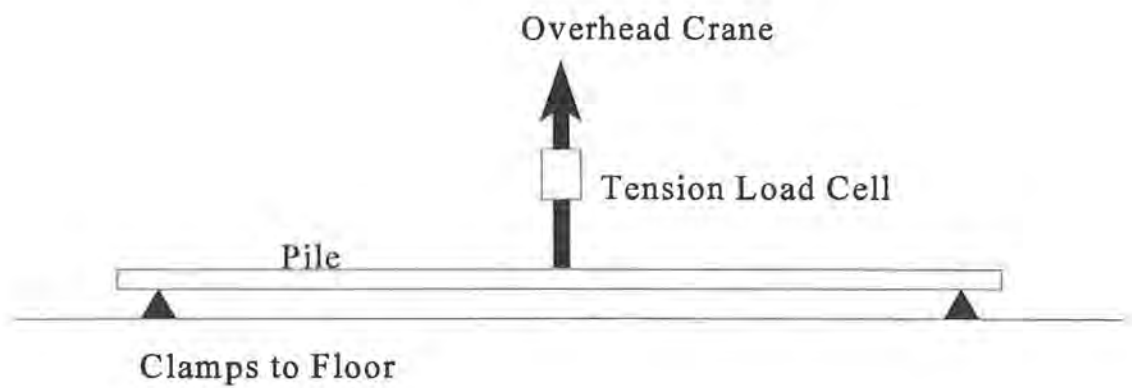
Gauge Number	PILE 12		
	Positive	Negative	All
1	1.8771	1.9669	1.9090
2	1.4423	1.5008	1.4725
3	1.4299	1.3570	1.3750
4	1.7487	1.7876	1.7681
5	1.6673	1.5608	1.6186
6	1.8771	1.7659	1.8495
7	1.7224	1.7736	1.7510
8	1.8112	1.6761	1.7344
9	1.6869	1.5017	1.5836
10	1.8044	1.8089	1.8000
11	1.9182	1.9228	1.9223
12	1.5614	1.2958	1.4282
13	1.6887	1.4856	1.5905
14	1.7475	1.7733	1.7584

Gauge Number	PILE 13		
	Positive	Negative	All
1	1.8009	1.8060	1.8127
2	1.1628	1.1575	1.1603
3	1.1636	1.1297	1.1571
4	1.6652	1.6920	1.7330
5	1.2452	1.2269	1.2781
6	1.3397	1.2628	1.3230
7	1.6566	1.5386	1.6069
8	1.9285	1.9425	1.9433
9	1.2527	1.1526	1.1891
10	1.0420	1.0685	1.0506
11	1.6266	1.7047	1.6658
12	1.3735	1.2873	1.3124
13	1.7180	1.7149	1.7243
14	1.3067	1.1909	1.2281

## CORRECTION OF RAW STRAIN DATA

The calibration factors obtained by the testing described above were used to correct the raw strain data measured at the Wilmington test site by the strain gauges mounted on the NCHRP group piles. The correction is in effect a software fix to the problem using a Matlab program written specifically for this purpose. The program *strn\_corr.m* has been included in Appendix C of this report. Every raw strain data point in the time history of each gauge was corrected using the appropriate positive or negative factor which it read from a database in Matlab file format (filename: *strn\_corr.mat*). The database contains the correction factors for each gauge in sequential order, from either 1 through 6 (piles 1 - 7) or from 1 through 14 (piles 8 - 13). The 2 lines of gauges on each pile are marked as *side 1* or *side 2* in order to identify each gauge uniquely for later analysis. Since the side numbers were not recorded during testing at Wilmington, a trial and error procedure had to be adopted in order to identify each gauge individually and apply the appropriate

correction factors. Identifying the strain gauge order (or sides) correctly resulted in a bending moment profile which appeared reasonable, while incorrect identification of the sides resulted in a bending moment profile that was obviously incorrect.



*Figure F-1 Schematic of Pile Calibration Setup*

## APPENDIX G

### DATA FILES FOR FLPIER(D) FOR EXAMPLE PROBLEM

**File *design\_stdyn.in* :**

```

PROBLEM
NCHRP - Cooper River Bridge. Static Analysis using Dynamic p-y curve
kips, inches
:
PRINT
L=0 M=0 D=0 O=0 S=0 P=0 T=0 F=0 C=0 B=0 I=0
:
CONTROL
1 U= 0 S= 0 V= 0. : NUMLC
S= 0 T= 0 0.0 P= 2
I= 50 T= 1.
:
FILE
NSEG= 1 S= 0.E+00 M= 0.E+00 P= 1.
L= 1080. M= 1 C= 0. , 0. , S= 0. , 0. , 0. , 60. , 0. , 0. , 0. ,
29000. , K= \
1
NL= 0 D= 60. V= 0. TH= 1.5 HPI= 0 T= 1 C= 0 : (round)
E= 0. H= 1 S= 5 A= 1.
5 4 : NPX, NPY
48. 180. 180. 48.
48. 180. 48.
0.3 0.2 0.3 0.4 0.8
0.3 0.3 0.4 0.8
:
MISSING
14 : number of missing pile
1 1
2 1
3 1
4 1
5 1
1 2
5 2
1 3
5 3
1 4
2 4
3 4
4 4
5 4
:
SOIL
L= 2 C= 0 W= 17: Nlayers,kcyc,wfreq
0. 0. 0.66E-04 0.3E-02 0.2E-01 0. 1.5 0.3E-01 0.15 360. 4. 1. 1. 0. 0.
0. \
0. 0. 0. B= 0. E= -360. -720. V=2000
0. 0. 0.66E-04 0.3E-02 0.2E-01 0. 1.5 0.3E-01 0.15

```

```

0. 0.5 0.71E-04 0.3E-01 0.5E-02 0.3E-01 1.5 0.3 0.15 480. 5. 1. 1. 0.
0. \
0. 0. 0. 0. B= 0. E= -720. -1200. V=2000
0. 5. 0.71E-04 0.3E-01 0.5E-02 0.3E-01 1.5 0.3 0.15
1.5 0.3 0.27 1. : Soil tip stiffness information
:
STRUCTURE
N= 2 S= 180. H= 240. O= 138. C= 5 B= 4, 4 W= 120. A= 0, 0 P= 0,
0.00000, 0. \
J= 1 T= 0, 0
I= 0.44E+06 0.44E+06 J= 0.23E+06 A= 2304. E= 29000. G= 11154. S =8.7e-5
I= 0.44E+06 0.44E+06 J= 0.23E+06 A= 2304. E= 29000. G= 11154. S =8.7e-5
I= 0.44E+06 0.44E+06 J= 0.23E+06 A= 2304. E= 29000. G= 11154. S =8.7e-5
:
CAP
E= 4400. U= 0.2 T= 48. S =8.7e-5
:
LOAD
1 L=1 F= 2000./6 0. 0. 0. 0. 0.
2 L=1 F= 2000./6 0. 0. 0. 0. 0.
3 L=1 F= 2000./6 0. 0. 0. 0. 0.
4 L=1 F= 2000./6 0. 0. 0. 0. 0.
5 L=1 F= 2000./6 0. 0. 0. 0. 0.
6 L=1 F= 2000./6 0. 0. 0. 0. 0.
:

```

### ***File design\_dyn\_gap.in :***

```

PROBLEM
NCHRP - Cooper River Bridge. Dynamic Analysis
kips, inches
:
PRINT
L=0 M=0 D=0 O=0 S=0 P=0 T=0 F=0 C=0 B=0 I=0 Z=1
:
CONTROL
1 U= 0 S= 0 V= 0. ; NUMLC
S= 0 T= 0 0. P= 2
I= 50 T= 15.
:
PILE
NSEG= 1 S= 0.E+00 M= 0.E+00 P= 1.
L= 1080. M= 1 C= 0. , 0. , S= 0. , 0. , 0. , 60. , 0. , 0. , 0. ,
29000. , K= \
1
NL= 0 D= 60. V= 0. TH= 1.5 HPI= 0 T= 1 C= 0 : (round)
E= 0. H= 1 S= 5 A= 1.
5 4 : NPX, NPY
48. 180. 180. 48.
48. 180. 48.
0.3 0.4 0.8
1.0 1.0
:
MISSING
14 : number of missing pile

```

```

1 1
2 1
3 1
4 1
5 1
1 2
5 2
1 3
5 3
1 4
2 4
3 4
4 4
5 4
:
SOIL
L= 2 C= 0 : Nlayers,kcyc
0. 0. 0.66E-04 0.3E-02 0.2E-01 0. 1.5 0.3E-01 0.15 360. 4. 1. 1. 0. 0.
0. \
0. 0. 0. B= 0. E= -360. -720. M=1
0. 0. 0.66E-04 0.3E-02 0.2E-01 0. 1.5 0.3E-01 0.15
0. 0.5 0.71E-04 0.3E-01 0.5E-02 0.3E-01 1.5 0.3 0.15 480. 5. 1. 1. 0.
0. \
0. 0. 0. B= 0. E= -720. -1200. M=1
0. 5. 0.71E-04 0.3E-01 0.5E-02 0.3E-01 1.5 0.3 0.15
1.5 0.3 0.27 1. : Soil tip stiffness information
:
STRUCTURE
N= 2 S= 180. H= 240. O= 138. C= 5 B= 4, 4 W= 120. A= 0, 0 P= 0,
0.00000, 0. \
J= 1 T= 0, 0
I= 0.44E+06 0.44E+06 J= 0.23E+06 A= 2304. E= 29000. G= 11154. S=8.7e-5
I= 0.44E+06 0.44E+06 J= 0.23E+06 A= 2304. E= 29000. G= 11154. S=8.7e-5
I= 0.44E+06 0.44E+06 J= 0.23E+06 A= 2304. E= 29000. G= 11154. S=8.7e-5
:
CAP
E= 4400. U= 0.2 T= 48. M= 2.25e-07 S=8.7e-5
:
DYN
Y=0 S= 750 C= 1 F= 0.04, 0.01, 0.001, 0.001, 0.015 0.015 J= 6.76e-07 \
K=2.25e-07 O=2 P=2,1,4 W=1,1,1
:
STIF
S= 1
:
SCND
B= 1
:
TRANSIENT
T= 0.02 L= 1 P= 1576 Q= 1 G= 386.4
N= 1,211,1 F= L, N, N, N, N, N
0.00 0.00630 0.02 0.00364 0.04 0.00099 0.06 0.00428
0.08 0.00758 0.10 0.01087 0.12 0.00682 0.14 0.00277
0.16 -0.00128 0.18 0.00368 0.20 0.00864 0.22 0.01360
0.24 0.00727 0.26 0.00094 0.28 0.00420 0.30 0.00221
0.32 0.00021 0.34 0.00444 0.36 0.00867 0.38 0.01290
0.40 0.01713 0.42 -0.00343 0.44 -0.02400 0.46 -0.00992

```

0.48	0.00416	0.50	0.00528	0.52	0.01653	0.54	0.02779
0.56	0.03904	0.58	0.02449	0.60	0.00995	0.62	0.00961
0.64	0.00926	0.66	0.00892	0.68	-0.00486	0.70	-0.01864
0.72	-0.03242	0.74	-0.03365	0.76	-0.05723	0.78	-0.04534
0.80	-0.03346	0.82	-0.03201	0.84	-0.03056	0.86	-0.02911
0.88	-0.02766	0.90	-0.04116	0.92	-0.05466	0.94	-0.06816
0.96	-0.08166	0.98	-0.06846	1.00	-0.05527	1.02	-0.04208
1.04	-0.04259	1.06	-0.04311	1.08	-0.02428	1.10	-0.00545
1.12	0.01338	1.14	0.03221	1.16	0.05104	1.18	0.06987
1.20	0.08870	1.22	0.04524	1.24	0.00179	1.26	-0.04167
1.28	-0.08513	1.30	-0.12858	1.32	-0.17204	1.34	-0.12908
1.36	-0.08613	1.38	-0.08902	1.40	-0.09192	1.42	-0.09482
1.44	-0.09324	1.46	-0.09166	1.48	-0.09478	1.50	-0.09789
1.52	-0.12902	1.54	-0.07652	1.56	-0.02401	1.58	0.02849
1.60	0.08099	1.62	0.13350	1.64	0.18600	1.66	0.23850
1.68	0.21993	1.70	0.20135	1.72	0.18277	1.74	0.16420
1.76	0.14562	1.78	0.16143	1.80	0.17725	1.82	0.13215
1.84	0.08705	1.86	0.04196	1.88	-0.00314	1.90	-0.04824
1.92	-0.09334	1.94	-0.13843	1.96	-0.18353	1.98	-0.22863
2.00	-0.27372	2.02	-0.31882	2.04	-0.25024	2.06	-0.18166
2.08	-0.11309	2.10	-0.04451	2.12	0.02407	2.14	0.09265
2.16	0.16123	2.18	0.22981	2.20	0.29839	2.22	0.23197
2.24	0.16554	2.26	0.09912	2.28	0.03270	2.30	-0.03372
2.32	-0.10014	2.34	-0.16656	2.36	-0.23299	2.38	-0.29941
2.40	-0.00421	2.42	0.29099	2.44	0.22380	2.46	0.15662
2.48	0.08943	2.50	0.02224	2.52	-0.04495	2.54	0.01834
2.56	0.08163	2.58	0.14491	2.60	0.20820	2.62	0.18973
2.64	0.17125	2.66	0.13759	2.68	0.10393	2.70	0.07027
2.72	0.03661	2.74	0.00295	2.76	-0.03071	2.78	-0.00561
2.80	0.01948	2.82	0.04458	2.84	0.06468	2.86	0.08478
2.88	0.10487	2.90	0.05895	2.92	0.01303	2.94	-0.03289
2.96	-0.07882	2.98	-0.03556	3.00	0.00771	3.02	0.05097
3.04	0.01013	3.06	-0.03071	3.08	-0.07156	3.10	-0.11240
3.12	-0.15324	3.14	-0.11314	3.16	-0.07304	3.18	-0.03294
3.20	0.00715	3.22	-0.06350	3.24	-0.13415	3.26	-0.20480
3.28	-0.12482	3.30	-0.04485	3.32	0.03513	3.34	0.11510
3.36	0.19508	3.38	0.12301	3.40	0.05094	3.42	-0.02113
3.44	-0.09320	3.46	-0.02663	3.48	0.03995	3.50	0.10653
3.52	0.17311	3.54	0.11283	3.56	0.05255	3.58	-0.00772
3.60	0.01064	3.62	0.02900	3.64	0.04737	3.66	0.06573
3.68	0.02021	3.70	-0.02530	3.72	-0.07081	3.74	-0.04107
3.76	-0.01133	3.78	0.00288	3.80	0.01709	3.82	0.03131
3.84	-0.02278	3.86	-0.07686	3.88	-0.13095	3.90	-0.18504
3.92	-0.14347	3.94	-0.10190	3.96	-0.06034	3.98	-0.01877
4.00	0.02280	4.02	-0.00996	4.04	-0.04272	4.06	-0.02147
4.08	-0.00021	4.10	0.02104	4.12	-0.01459	4.14	-0.05022
4.16	-0.08585	4.18	-0.12148	4.20	-0.15711	4.22	-0.19274
4.24	-0.22837	4.26	-0.18145	4.28	-0.13453	4.30	-0.08761
4.32	-0.04069	4.34	0.00623	4.36	0.05316	4.38	0.10008
4.40	0.14700	4.42	0.09754	4.44	0.04808	4.46	-0.00138
4.48	0.05141	4.50	0.10420	4.52	0.15699	4.54	0.20979
4.56	0.26258	4.58	0.16996	4.60	0.07734	4.62	-0.01527
4.64	-0.10789	4.66	-0.20051	4.68	-0.06786	4.70	0.06479
4.72	0.01671	4.74	-0.03137	4.76	-0.07945	4.78	-0.12753
4.80	-0.17561	4.82	-0.22369	4.84	-0.27177	4.86	-0.15851
4.88	-0.04525	4.90	0.06802	4.92	0.18128	4.94	0.14464
4.96	0.10800	4.98	0.07137	5.00	0.03473	5.02	0.09666
5.04	0.15860	5.06	0.22053	5.08	0.18296	5.10	0.14538
5.12	0.10780	5.14	0.07023	5.16	0.03265	5.18	0.06649
5.20	0.10033	5.22	0.13417	5.24	0.10337	5.26	0.07257
5.28	0.04177	5.30	0.01097	5.32	-0.01983	5.34	0.04438
5.36	0.10860	5.38	0.17281	5.40	0.10416	5.42	0.03551
5.44	-0.03315	5.46	-0.10180	5.48	-0.07262	5.50	-0.04344

5.52	-0.01426	5.54	0.01492	5.56	-0.02025	5.58	-0.05543
5.60	-0.09060	5.62	-0.12578	5.64	-0.16095	5.66	-0.19613
5.68	-0.14784	5.70	-0.09955	5.72	-0.05127	5.74	-0.00298
5.76	-0.01952	5.78	-0.03605	5.80	-0.05259	5.82	-0.04182
5.84	-0.03106	5.86	-0.02903	5.88	-0.02699	5.90	0.02515
5.92	0.01770	5.94	0.02213	5.96	0.02656	5.98	0.00419
6.00	-0.01819	6.02	-0.04057	6.04	-0.06294	6.06	-0.02417
6.08	0.01460	6.10	0.05337	6.12	0.02428	6.14	-0.00480
6.16	-0.03389	6.18	-0.00557	6.20	0.02274	6.22	0.00679
6.24	-0.00915	6.26	-0.02509	6.28	-0.04103	6.30	-0.05698
6.32	-0.01826	6.34	0.02046	6.36	0.00454	6.38	-0.01138
6.40	-0.00215	6.42	0.00708	6.44	0.00496	6.46	0.00285
6.48	0.00074	6.50	-0.00534	6.52	-0.01141	6.54	0.00361
6.56	0.01863	6.58	0.03365	6.60	0.04867	6.62	0.03040
6.64	0.01213	6.66	-0.00614	6.68	-0.02441	6.70	0.01375
6.72	0.01099	6.74	0.00823	6.76	0.00547	6.78	0.00812
6.80	0.01077	6.82	-0.00692	6.84	-0.02461	6.86	-0.04230
6.88	-0.05999	6.90	-0.07768	6.92	-0.09538	6.94	-0.06209
6.96	-0.02880	6.98	0.00448	7.00	0.03777	7.02	0.01773
7.04	-0.00231	7.06	-0.02235	7.08	0.01791	7.10	0.05816
7.12	0.03738	7.14	0.01660	7.16	-0.00418	7.18	-0.02496
7.20	-0.04574	7.22	-0.02071	7.24	0.00432	7.26	0.02935
7.28	0.01526	7.30	0.01806	7.32	0.02086	7.34	0.00793
7.36	-0.00501	7.38	-0.01795	7.40	-0.03089	7.42	-0.01841
7.44	-0.00593	7.46	0.00655	7.48	-0.02519	7.50	-0.05693
7.52	-0.04045	7.54	-0.02398	7.56	-0.00750	7.58	0.00897
7.60	0.00384	7.62	-0.00129	7.64	-0.00642	7.66	-0.01156
7.68	-0.02619	7.70	-0.04082	7.72	-0.05545	7.74	-0.04366
7.76	-0.03188	7.78	-0.06964	7.80	-0.05634	7.82	-0.04303
7.84	-0.02972	7.86	-0.01642	7.88	-0.00311	7.90	0.01020
7.92	0.02350	7.94	0.03681	7.96	0.05011	7.98	0.02436
8.00	-0.00139	8.02	-0.02714	8.04	-0.00309	8.06	0.02096
8.08	0.04501	8.10	0.06906	8.12	0.05773	8.14	0.04640
8.16	0.03507	8.18	0.03357	8.20	0.03207	8.22	0.03057
8.24	0.03250	8.26	0.03444	8.28	0.03637	8.30	0.01348
8.32	-0.00942	8.34	-0.03231	8.36	-0.02997	8.38	-0.03095
8.40	-0.03192	8.42	-0.02588	8.44	-0.01984	8.46	-0.01379
8.48	-0.00775	8.50	-0.01449	8.52	-0.02123	8.54	0.01523
8.56	0.05170	8.58	0.08816	8.60	0.12463	8.62	0.16109
8.64	0.12987	8.66	0.09864	8.68	0.06741	8.70	0.03618
8.72	0.00495	8.74	0.00420	8.76	0.00345	8.78	0.00269
8.80	-0.05922	8.82	-0.12112	8.84	-0.18303	8.86	-0.12043
8.88	-0.05782	8.90	0.00479	8.92	0.06740	8.94	0.13001
8.96	0.08373	8.98	0.03745	9.00	0.06979	9.02	0.10213
9.04	-0.03517	9.06	-0.17247	9.08	-0.13763	9.10	-0.10278
9.12	-0.06794	9.14	-0.03310	9.16	-0.03647	9.18	-0.03984
9.20	-0.00517	9.22	0.02950	9.24	0.06417	9.26	0.09883
9.28	0.13350	9.30	0.05924	9.32	-0.01503	9.34	-0.08929
9.36	-0.16355	9.38	-0.06096	9.40	0.04164	9.42	0.01551
9.44	-0.01061	9.46	-0.03674	9.48	-0.06287	9.50	-0.08899
9.52	-0.05430	9.54	-0.01961	9.56	0.01508	9.58	0.04977
9.60	0.08446	9.62	0.05023	9.64	0.01600	9.66	-0.01823
9.68	-0.05246	9.70	-0.08669	9.72	-0.06769	9.74	-0.04870
9.76	-0.02970	9.78	-0.01071	9.80	0.00829	9.82	-0.00314
9.84	0.02966	9.86	0.06246	9.88	-0.00234	9.90	-0.06714
9.92	-0.04051	9.94	-0.01388	9.96	0.01274	9.98	0.00805
10.00	0.03024	10.02	0.05243	10.04	0.02351	10.06	-0.00541
10.08	-0.03432	10.10	-0.06324	10.12	-0.09215	10.14	-0.12107
10.16	-0.08450	10.18	-0.04794	10.20	-0.01137	10.22	0.02520
10.24	0.06177	10.26	0.04028	10.28	0.01880	10.30	0.04456
10.32	0.07032	10.34	0.09608	10.36	0.12184	10.38	0.06350
10.40	0.00517	10.42	-0.05317	10.44	-0.03124	10.46	-0.00930
10.48	0.01263	10.50	0.03457	10.52	0.03283	10.54	0.03109



10.56	0.02935	10.58	0.04511	10.60	0.06087	10.62	0.07663
10.64	0.09239	10.66	0.05742	10.68	0.02245	10.70	-0.01252
10.72	0.00680	10.74	0.02611	10.76	0.04543	10.78	0.01571
10.80	-0.01402	10.82	-0.04374	10.84	-0.07347	10.86	-0.03990
10.88	-0.00633	10.90	0.02724	10.92	0.06080	10.94	0.03669
10.96	0.01258	10.98	-0.01153	11.00	-0.03564	11.02	-0.00677
11.04	0.02210	11.06	0.05098	11.08	0.07985	11.10	0.06915
11.12	0.05845	11.14	0.04775	11.16	0.03706	11.18	0.02636
11.20	0.05822	11.22	0.09009	11.24	0.12196	11.26	0.10069
11.28	0.07943	11.30	0.05816	11.32	0.03689	11.34	0.01563
11.36	-0.00564	11.38	-0.02690	11.40	-0.04817	11.42	-0.06944
11.44	-0.09070	11.46	-0.11197	11.48	-0.11521	11.50	-0.11846
11.52	-0.12170	11.54	-0.12494	11.56	-0.16500	11.58	-0.20505
11.60	-0.15713	11.62	-0.10921	11.64	-0.06129	11.66	-0.01337
11.68	0.03455	11.70	0.08247	11.72	0.07576	11.74	0.06906
11.76	0.06236	11.78	0.08735	11.80	0.11235	11.82	0.13734
11.84	0.12175	11.86	0.10616	11.88	0.09057	11.90	0.07498
11.92	0.08011	11.94	0.08524	11.96	0.09037	11.98	0.06208
12.00	0.03378	12.02	0.00549	12.04	-0.02281	12.06	-0.05444
12.08	-0.04030	12.10	-0.02615	12.12	-0.01201	12.14	-0.02028
12.16	-0.02855	12.18	-0.06243	12.20	-0.03524	12.22	-0.00805
12.24	-0.04948	12.26	-0.03643	12.28	-0.02337	12.30	-0.03368
12.32	-0.01879	12.34	-0.00389	12.36	0.01100	12.38	0.02589
12.40	0.01446	12.42	0.00303	12.44	-0.00840	12.46	0.00463
12.48	0.01766	12.50	0.03069	12.52	0.04372	12.54	0.02165
12.56	-0.00042	12.58	-0.02249	12.60	-0.04456	12.62	-0.03638
12.64	-0.02819	12.66	-0.02001	12.68	-0.01182	12.70	-0.02445
12.72	-0.03707	12.74	-0.04969	12.76	-0.05882	12.78	-0.06795
12.80	-0.07707	12.82	-0.08620	12.84	-0.09533	12.86	-0.06276
12.88	-0.03018	12.90	0.00239	12.92	0.03496	12.94	0.04399
12.96	0.05301	12.98	0.03176	13.00	0.01051	13.02	-0.01073
13.04	-0.03198	13.06	-0.05323	13.08	0.00186	13.10	0.05696
13.12	0.01985	13.14	-0.01726	13.16	-0.05438	13.18	-0.01204
13.20	0.03031	13.22	0.07265	13.24	0.11499	13.26	0.07237
13.28	0.02975	13.30	-0.01288	13.32	0.01212	13.34	0.03711
13.36	0.03517	13.38	0.03323	13.40	0.01853	13.42	0.00383
13.44	0.00342	13.46	-0.02181	13.48	-0.04704	13.50	-0.07227
13.52	-0.09750	13.54	-0.12273	13.56	-0.08317	13.58	-0.04362
13.60	-0.00407	13.62	0.03549	13.64	0.07504	13.66	0.11460
13.68	0.07769	13.70	0.04078	13.72	0.00387	13.74	0.00284
13.76	0.00182	13.78	-0.05513	13.80	0.04732	13.82	0.05223
13.84	0.05715	13.86	0.06206	13.88	0.06698	13.90	0.07189
13.92	0.02705	13.94	-0.01779	13.96	-0.06263	13.98	-0.10747
14.00	-0.15232	14.02	-0.12591	14.04	-0.09950	14.06	-0.07309
14.08	-0.04668	14.10	-0.02027	14.12	0.00614	14.14	0.03255
14.16	0.00859	14.18	-0.01537	14.20	-0.03932	14.22	-0.06328
14.24	-0.03322	14.26	-0.00315	14.28	0.02691	14.30	0.01196
14.32	-0.00300	14.34	0.00335	14.36	0.00970	14.38	0.01605
14.40	0.02239	14.42	0.04215	14.44	0.06191	14.46	0.08167
14.48	0.03477	14.50	-0.01212	14.52	-0.01309	14.54	-0.01407
14.56	-0.05274	14.58	-0.02544	14.60	0.00186	14.62	0.02916
14.64	0.05646	14.66	0.08376	14.68	0.01754	14.70	-0.04869
14.72	-0.02074	14.74	0.00722	14.76	0.03517	14.78	-0.00528
14.80	-0.04572	14.82	-0.08617	14.84	-0.06960	14.86	-0.05303
14.88	-0.03646	14.90	-0.01989	14.92	-0.00332	14.94	0.01325
14.96	0.02982	14.98	0.01101	15.00	-0.00781	15.02	-0.02662
15.04	-0.00563	15.06	0.01536	15.08	0.03635	15.10	0.05734
15.12	0.03159	15.14	0.00584	15.16	-0.01992	15.18	-0.00201
15.20	0.01589	15.22	-0.01024	15.24	-0.03636	15.26	-0.06249
15.28	-0.04780	15.30	-0.03311	15.32	-0.04941	15.34	-0.06570
15.36	-0.08200	15.38	-0.04980	15.40	-0.01760	15.42	0.01460
15.44	0.04680	15.46	0.07900	15.48	0.04750	15.50	0.01600
15.52	-0.01550	15.54	-0.00102	15.56	0.01347	15.58	0.02795

15.60	0.04244	15.62	0.05692	15.64	0.03781	15.66	0.01870
15.68	-0.00041	15.70	-0.01952	15.72	-0.00427	15.74	0.01098
15.76	0.02623	15.78	0.04148	15.80	0.01821	15.82	-0.00506
15.84	-0.00874	15.86	-0.03726	15.88	-0.06579	15.90	-0.02600
15.92	0.01380	15.94	0.05359	15.96	0.09338	15.98	0.05883
16.00	0.02429	16.02	-0.01026	16.04	-0.04480	16.06	-0.01083
16.08	-0.01869	16.10	-0.02655	16.12	-0.03441	16.14	-0.02503
16.16	-0.01564	16.18	-0.00626	16.20	-0.01009	16.22	-0.01392
16.24	0.01490	16.26	0.04372	16.28	0.03463	16.30	0.02098
16.32	0.00733	16.34	-0.00632	16.36	-0.01997	16.38	0.00767
16.40	0.03532	16.42	0.03409	16.44	0.03287	16.46	0.03164
16.48	0.02403	16.50	0.01642	16.52	0.00982	16.54	0.00322
16.56	-0.00339	16.58	0.02202	16.60	-0.01941	16.62	-0.06085
16.64	-0.10228	16.66	-0.07847	16.68	-0.05466	16.70	-0.03084
16.72	-0.00703	16.74	0.01678	16.76	0.01946	16.78	0.02214
16.80	0.02483	16.82	0.01809	16.84	-0.00202	16.86	-0.02213
16.88	-0.00278	16.90	0.01656	16.92	0.03590	16.94	0.05525
16.96	0.07459	16.98	0.06203	17.00	0.04948	17.02	0.03692
17.04	-0.00145	17.06	0.04599	17.08	0.04079	17.10	0.03558
17.12	0.03037	17.14	0.03626	17.16	0.04215	17.18	0.04803
17.20	0.05392	17.22	0.04947	17.24	0.04502	17.26	0.04056
17.28	0.03611	17.30	0.03166	17.32	0.00614	17.34	-0.01937
17.36	-0.04489	17.38	-0.07040	17.40	-0.09592	17.42	-0.07745
17.44	-0.05899	17.46	-0.04052	17.48	-0.02206	17.50	-0.00359
17.52	0.01487	17.54	0.01005	17.56	0.00523	17.58	0.00041
17.60	-0.00441	17.62	-0.00923	17.64	-0.01189	17.66	-0.01523
17.68	-0.01856	17.70	-0.02190	17.72	-0.00983	17.74	0.00224
17.76	0.01431	17.78	0.00335	17.80	-0.00760	17.82	-0.01856
17.84	-0.00737	17.86	0.00383	17.88	0.01502	17.90	0.02622
17.92	0.01016	17.94	-0.00590	17.96	-0.02196	17.98	-0.00121
18.00	0.01953	18.02	0.04027	18.04	0.02826	18.06	0.01625
18.08	0.00424	18.10	0.00196	18.12	-0.00031	18.14	-0.00258
18.16	-0.00486	18.18	-0.00713	18.20	-0.00941	18.22	-0.01168
18.24	-0.01396	18.26	-0.01750	18.28	-0.02104	18.30	-0.02458
18.32	-0.02813	18.34	-0.03167	18.36	-0.03521	18.38	-0.04205
18.40	-0.04889	18.42	-0.03559	18.44	-0.02229	18.46	-0.00899
18.48	0.00431	18.50	0.01762	18.52	0.00714	18.54	-0.00334
18.56	-0.01383	18.58	0.01314	18.60	0.04011	18.62	0.06708
18.64	0.04820	18.66	0.02932	18.68	0.01043	18.70	-0.00845
18.72	-0.02733	18.74	-0.04621	18.76	-0.03155	18.78	-0.01688
18.80	-0.00222	18.82	0.01244	18.84	0.02683	18.86	0.04121
18.88	0.05559	18.90	0.03253	18.92	0.00946	18.94	-0.01360
18.96	-0.01432	18.98	-0.01504	19.00	-0.01576	19.02	-0.04209
19.04	-0.02685	19.06	-0.01161	19.08	0.00363	19.10	0.01887
19.12	0.03411	19.14	0.03115	19.16	0.02819	19.18	0.02917
19.20	0.03015	19.22	0.03113	19.24	0.00388	19.26	-0.02337
19.28	-0.05062	19.30	-0.03820	19.32	-0.02579	19.34	-0.01337
19.36	-0.00095	19.38	0.01146	19.40	0.02388	19.42	0.03629
19.44	0.01047	19.46	-0.01535	19.48	-0.04117	19.50	-0.06699
19.52	-0.05207	19.54	-0.03715	19.56	-0.02222	19.58	-0.00730
19.60	0.00762	19.62	0.02254	19.64	0.03747	19.66	0.04001
19.68	0.04256	19.70	0.04507	19.72	0.04759	19.74	0.05010
19.76	0.04545	19.78	0.04080	19.80	0.02876	19.82	0.01671
19.84	0.00467	19.86	-0.00738	19.88	-0.00116	19.90	0.00506
19.92	0.01128	19.94	0.01750	19.96	-0.00211	19.98	-0.02173
20.00	-0.04135	20.02	-0.06096	20.04	-0.08058	20.06	-0.06995
20.08	-0.05931	20.10	-0.04868	20.12	-0.03805	20.14	-0.02557
20.16	-0.01310	20.18	-0.00063	20.20	0.01185	20.22	0.02432
20.24	0.03680	20.26	0.04927	20.28	0.02974	20.30	0.01021
20.32	-0.00932	20.34	-0.02884	20.36	-0.04837	20.38	-0.06790
20.40	-0.04862	20.42	-0.02934	20.44	-0.01006	20.46	0.00922
20.48	0.02851	20.50	0.04779	20.52	0.02456	20.54	0.00133
20.56	-0.02190	20.58	-0.04513	20.60	-0.06836	20.62	-0.04978

20.64	-0.03120	20.66	-0.01262	20.68	0.00596	20.70	0.02453
20.72	0.04311	20.74	0.06169	20.76	0.08027	20.78	0.09885
20.80	0.06452	20.82	0.03019	20.84	-0.00414	20.86	-0.03848
20.88	-0.07281	20.90	-0.05999	20.92	-0.04717	20.94	-0.03435
20.96	-0.03231	20.98	-0.03028	21.00	-0.02824	21.02	-0.00396
21.04	0.02032	21.06	0.00313	21.08	-0.01406	21.10	-0.03124
21.12	-0.04843	21.14	-0.06562	21.16	-0.05132	21.18	-0.03702
21.20	-0.02272	21.22	-0.00843	21.24	0.00587	21.26	0.02017
21.28	0.02698	21.30	0.03379	21.32	0.04061	21.34	0.04742
21.36	0.05423	21.38	0.03535	21.40	0.01647	21.42	0.01622
21.44	0.01598	21.46	0.01574	21.48	0.00747	21.50	-0.00080
21.52	-0.00907	21.54	0.00072	21.56	0.01051	21.58	0.02030
21.60	0.03009	21.62	0.03989	21.64	0.03478	21.66	0.02967
21.68	0.02457	21.70	0.03075	21.72	0.03694	21.74	0.04313
21.76	0.04931	21.78	0.05550	21.80	0.06168	21.82	-0.00526
21.84	-0.07220	21.86	-0.06336	21.88	-0.05451	21.90	-0.04566
21.92	-0.03681	21.94	-0.03678	21.96	-0.03675	21.98	-0.03672
22.00	-0.01765	22.02	0.00143	22.04	0.02051	22.06	0.03958
22.08	0.05866	22.10	0.03556	22.12	0.01245	22.14	-0.01066
22.16	-0.03376	22.18	-0.05687	22.20	-0.04502	22.22	-0.03317
22.24	-0.02131	22.26	-0.00946	22.28	0.00239	22.30	-0.00208
22.32	-0.00654	22.34	-0.01101	22.36	-0.01548	22.38	-0.01200
22.40	-0.00851	22.42	-0.00503	22.44	-0.00154	22.46	0.00195
22.48	0.00051	22.50	-0.00092	22.52	0.01135	22.54	0.02363
22.56	0.03590	22.58	0.04818	22.60	0.06045	22.62	0.07273
22.64	0.02847	22.66	-0.01579	22.68	-0.06004	22.70	-0.05069
22.72	-0.04134	22.74	-0.03199	22.76	-0.03135	22.78	-0.03071
22.80	-0.03007	22.82	-0.01863	22.84	-0.00719	22.86	0.00425
22.88	0.01570	22.90	0.02714	22.92	0.03858	22.94	0.02975
22.96	0.02092	22.98	0.02334	23.00	0.02576	23.02	0.02819
23.04	0.03061	23.06	0.03304	23.08	0.01371	23.10	-0.00561
23.12	-0.02494	23.14	-0.02208	23.16	-0.01923	23.18	-0.01638
23.20	-0.01353	23.22	-0.01261	23.24	-0.01170	23.26	-0.00169
23.28	0.00833	23.30	0.01834	23.32	0.02835	23.34	0.03836
23.36	0.04838	23.38	0.03749	23.40	0.02660	23.42	0.01571
23.44	0.00482	23.46	-0.00607	23.48	-0.01696	23.50	-0.00780
23.52	0.00136	23.54	0.01052	23.56	0.01968	23.58	0.02884
23.60	-0.00504	23.62	-0.03893	23.64	-0.02342	23.66	-0.00791
23.68	0.00759	23.70	0.02310	23.72	0.00707	23.74	-0.00895
23.76	-0.02498	23.78	-0.04100	23.80	-0.05703	23.82	-0.02920
23.84	-0.00137	23.86	0.02645	23.88	0.05428	23.90	0.03587
23.92	0.01746	23.94	-0.00096	23.96	-0.01937	23.98	-0.03778
24.00	-0.02281	24.02	-0.00784	24.04	0.00713	24.06	0.02210
24.08	0.03707	24.10	0.05204	24.12	0.06701	24.14	0.08198
24.16	0.03085	24.18	-0.02027	24.20	-0.07140	24.22	-0.12253
24.24	-0.08644	24.26	-0.05035	24.28	-0.01426	24.30	0.02183
24.32	0.05792	24.34	0.09400	24.36	0.13009	24.38	0.03611
24.40	-0.05787	24.42	-0.04802	24.44	-0.03817	24.46	-0.02832
24.48	-0.01846	24.50	-0.00861	24.52	-0.03652	24.54	-0.06444
24.56	-0.06169	24.58	-0.05894	24.60	-0.05618	24.62	-0.06073
24.64	-0.06528	24.66	-0.04628	24.68	-0.02728	24.70	-0.00829
24.72	0.01071	24.74	0.02970	24.76	0.03138	24.78	0.03306
24.80	0.03474	24.82	0.03642	24.84	0.04574	24.86	0.05506
24.88	0.06439	24.90	0.07371	24.92	0.08303	24.94	0.03605
24.96	-0.01092	24.98	-0.05790	25.00	-0.04696	25.02	-0.03602
25.04	-0.02508	25.06	-0.01414	25.08	-0.03561	25.10	-0.05708
25.12	-0.07855	25.14	-0.06304	25.16	-0.04753	25.18	-0.03203
25.20	-0.01652	25.22	-0.00102	25.24	0.00922	25.26	0.01946
25.28	0.02970	25.30	0.03993	25.32	0.05017	25.34	0.06041
25.36	0.07065	25.38	0.08089	25.40	-0.00192	25.42	-0.08473
25.44	-0.07032	25.46	-0.05590	25.48	-0.04148	25.50	-0.05296
25.52	-0.06443	25.54	-0.07590	25.56	-0.08738	25.58	-0.09885
25.60	-0.06798	25.62	-0.03710	25.64	-0.00623	25.66	0.02465

25.68	0.05553	25.70	0.08640	25.72	0.11728	25.74	0.14815
25.76	0.08715	25.78	0.02615	25.80	-0.03485	25.82	-0.09584
25.84	-0.07100	25.86	-0.04616	25.88	-0.02132	25.90	0.00353
25.92	0.02837	25.94	0.05321	25.96	-0.00469	25.98	-0.06258
26.00	-0.12048	26.02	-0.09960	26.04	-0.07872	26.06	-0.05784
26.08	-0.03696	26.10	-0.01608	26.12	0.00480	26.14	0.02568
26.16	0.04656	26.18	0.06744	26.20	0.08832	26.22	0.10920
26.24	0.13008	26.26	0.10995	26.28	0.08982	26.30	0.06969
26.32	0.04955	26.34	0.04006	26.36	0.03056	26.38	0.02107
26.40	0.01158	26.42	0.00780	26.44	0.00402	26.46	0.00024
26.48	-0.00354	26.50	-0.00732	26.52	-0.01110	26.54	-0.00780
26.56	-0.00450	26.58	-0.00120	26.60	0.00210	26.62	0.00540
26.64	-0.00831	26.66	-0.02203	26.68	-0.03575	26.70	-0.04947
26.72	-0.06319	26.74	-0.05046	26.76	-0.03773	26.78	-0.02500
26.80	-0.01227	26.82	0.00046	26.84	0.00482	26.86	0.00919
26.88	0.01355	26.90	0.01791	26.92	0.02228	26.94	0.00883
26.96	-0.00462	26.98	-0.01807	27.00	-0.03152	27.02	-0.02276
27.04	-0.01401	27.06	-0.00526	27.08	0.00350	27.10	0.01225
27.12	0.02101	27.14	0.01437	27.16	0.00773	27.18	0.00110
27.20	0.00823	27.22	0.01537	27.24	0.02251	27.26	0.01713
27.28	0.01175	27.30	0.00637	27.32	0.01376	27.34	0.02114
27.36	0.02852	27.38	0.03591	27.40	0.04329	27.42	0.03458
27.44	0.02587	27.46	0.01715	27.48	0.00844	27.50	-0.00027
27.52	-0.00898	27.54	-0.00126	27.56	0.00645	27.58	0.01417
27.60	0.02039	27.62	0.02661	27.64	0.03283	27.66	0.03905
27.68	0.04527	27.70	0.03639	27.72	0.02750	27.74	0.01862
27.76	0.00974	27.78	0.00086	27.80	-0.01333	27.82	-0.02752
27.84	-0.04171	27.86	-0.02812	27.88	-0.01453	27.90	-0.00094
27.92	0.01264	27.94	0.02623	27.96	0.01690	27.98	0.00756
28.00	-0.00177	28.02	-0.01111	28.04	-0.02044	28.06	-0.02977
28.08	-0.03911	28.10	-0.02442	28.12	-0.00973	28.14	0.00496
28.16	0.01965	28.18	0.03434	28.20	0.02054	28.22	0.00674
28.24	-0.00706	28.26	-0.02086	28.28	-0.03466	28.30	-0.02663
28.32	-0.01860	28.34	-0.01057	28.36	-0.00254	28.38	-0.00063
28.40	0.00128	28.42	0.00319	28.44	0.00510	28.46	0.00999
28.48	0.01488	28.50	0.00791	28.52	0.00093	28.54	-0.00605
28.56	0.00342	28.58	0.01288	28.60	0.02235	28.62	0.03181
28.64	0.04128	28.66	0.02707	28.68	0.01287	28.70	-0.00134
28.72	-0.01554	28.74	-0.02975	28.76	-0.04395	28.78	-0.03612
28.80	-0.02828	28.82	-0.02044	28.84	-0.01260	28.86	-0.00476
28.88	0.00307	28.90	0.01091	28.92	0.00984	28.94	0.00876
28.96	0.00768	28.98	0.00661	29.00	0.01234	29.02	0.01807
29.04	0.02380	29.06	0.02953	29.08	0.03526	29.10	0.02784
29.12	0.02042	29.14	0.01300	29.16	-0.03415	29.18	-0.00628
29.20	-0.00621	29.22	-0.00615	29.24	-0.00609	29.26	-0.00602
29.28	-0.00596	29.30	-0.00590	29.32	-0.00583	29.34	-0.00577
29.36	-0.00571	29.38	-0.00564	29.40	-0.00558	29.42	-0.00552
29.44	-0.00545	29.46	-0.00539	29.48	-0.00532	29.50	-0.00526
29.52	-0.00520	29.54	-0.00513	29.56	-0.00507	29.58	-0.00501
29.60	-0.00494	29.62	-0.00488	29.64	-0.00482	29.66	-0.00475
29.68	-0.00469	29.70	-0.00463	29.72	-0.00456	29.74	-0.00450
29.76	-0.00444	29.78	-0.00437	29.80	-0.00431	29.82	-0.00425
29.84	-0.00418	29.86	-0.00412	29.88	-0.00406	29.90	-0.00399
29.92	-0.00393	29.94	-0.00387	29.96	-0.00380	29.98	-0.00374
30.00	-0.00368	30.02	-0.00361	30.04	-0.00355	30.06	-0.00349
30.08	-0.00342	30.10	-0.00336	30.12	-0.00330	30.14	-0.00323
30.16	-0.00317	30.18	-0.00311	30.20	-0.00304	30.22	-0.00298
30.24	-0.00292	30.26	-0.00285	30.28	-0.00279	30.30	-0.00273
30.32	-0.00266	30.34	-0.00260	30.36	-0.00254	30.38	-0.00247
30.40	-0.00241	30.42	-0.00235	30.44	-0.00228	30.46	-0.00222
30.48	-0.00216	30.50	-0.00209	30.52	-0.00203	30.54	-0.00197
30.56	-0.00190	30.58	-0.00184	30.60	-0.00178	30.62	-0.00171
30.64	-0.00165	30.66	-0.00158	30.68	-0.00152	30.70	-0.00146

30.72	-0.00139	30.74	-0.00133	30.76	-0.00127	30.78	-0.00120
30.80	-0.00114	30.82	-0.00108	30.84	-0.00101	30.86	-0.00095
30.88	-0.00089	30.90	-0.00082	30.92	-0.00076	30.94	-0.00070
30.96	-0.00063	30.98	-0.00057	31.00	-0.00051	31.02	-0.00044
31.04	-0.00038	31.06	-0.00032	31.08	-0.00025	31.10	-0.00019
31.12	-0.00013	31.14	-0.00006	31.16	0.00000	31.18	0.00000
31.20	0.00000	31.22	0.00000	31.24	0.00000	31.26	0.00000
31.28	0.00000	31.30	0.00000	31.32	0.00000	31.34	0.00000
31.36	0.00000	31.38	0.00000	31.40	0.00000	31.42	0.00000
31.44	0.00000	31.46	0.00000	31.48	0.00000	31.50	0.00000